

Sheffield Hallam University

The applicability of lattice BGK modelling for turbulent hydrodynamics in internal geometrics.

HAMMOND, L. A.

Available from the Sheffield Hallam University Research Archive (SHURA) at:

<http://shura.shu.ac.uk/19750/>

A Sheffield Hallam University thesis

This thesis is protected by copyright which belongs to the author.

The content must not be changed in any way or sold commercially in any format or medium without the formal permission of the author.

When referring to this work, full bibliographic details including the author, title, awarding institution and date of the thesis must be given.

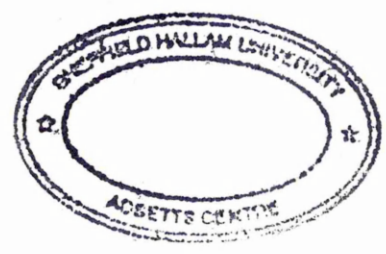
Please visit <http://shura.shu.ac.uk/19750/> and <http://shura.shu.ac.uk/information.html> for further details about copyright and re-use permissions.

SHEFFIELD HALLAM UNIVERSITY
LEARNING CENTRE
CITY CAMPUS, POND STREET
SHEFFIELD S1 1WB.



Fines are charged at 50p per hour

26 FEB 2007 *apm*



ProQuest Number: 10697052

All rights reserved

INFORMATION TO ALL USERS

The quality of this reproduction is dependent upon the quality of the copy submitted.

In the unlikely event that the author did not send a complete manuscript and there are missing pages, these will be noted. Also, if material had to be removed, a note will indicate the deletion.



ProQuest 10697052

Published by ProQuest LLC (2017). Copyright of the Dissertation is held by the Author.

All rights reserved.

This work is protected against unauthorized copying under Title 17, United States Code
Microform Edition © ProQuest LLC.

ProQuest LLC.
789 East Eisenhower Parkway
P.O. Box 1346
Ann Arbor, MI 48106 – 1346

**THE APPLICABILITY OF LATTICE BGK MODELLING
FOR TURBULENT HYDRODYNAMICS IN INTERNAL
GEOMETRICS**

L.A. Hammond

A thesis submitted in partial fulfilment of the
requirements of
Sheffield Hallam University
for the degree of Doctor of Philosophy

2003

Abstract

Traditional approaches to simulating fluid dynamics have focused on spatially and temporally discretised versions of the underlying Navier-Stokes partial differential equations. These approaches form a huge body of work that has evolved over the last century; the modern technique of simulating these systems by numerical approximation is collectively referred to as computational fluid dynamics or CFD. Recently however, new schemes have evolved out of cellular automata and lattice gas approaches which can, under the right circumstances, form efficient and fast alternatives to CFD and which lend themselves to various computational streamlining procedures. These are well represented by the so called lattice Boltzmann and LBGK formalisms — those employed in this work.

In this work the LBGK mono-phase scheme for internal flows is extended, primarily to incorporate models of turbulent flow characteristics, in order to generalise the validity of the schemes for more complex flow geometries and to higher Reynolds numbers. Turbulent flow in infinite aspect ratio ducts is examined in detail. Results sets derived using the extended model are compared quantitatively against theory and experiment. Features of the model are analysed to deduce potential improvements to the scheme and alternatives. Propositions for continued work are discussed in detail.

Before this is done, investigations are carried out on issues of closure for the general LBGK scheme and an improved, adaptable and high order accuracy boundary scheme is developed. For various benchmark geometries, this is qualitatively and quantitatively compared against accepted alternatives. In addition, a central geometric problem of simulating cylindrically symmetric systems on two dimensional Cartesian lattices is addressed. Work is presented on transforming the governing lattice Boltzmann BGK equation, to enable the use of a regular Cartesian grid for performing simulations of flow in pipes. Results for pipe flow are compared to the analytic solution.

Contents

1	Introduction	2
1.1	Front matter	3
1.2	Fundamental context of the work	4
1.3	Work statement and synopsis	9
2	Background science	12
2.1	Introduction and synopsis	13
2.1.1	Fundamental concepts	14
2.2	Continuum mechanics: The equations of motion for a fluid	18
2.2.1	Mass balance	20
2.2.2	Momentum balance	21
2.2.3	Balance equations for incompressible fluids	25
2.2.4	Momentum balance for inviscid fluids	26
2.2.5	The continuum energy equation for a fluid	26
2.3	Statistical mechanics	29
2.3.1	Statistical physics for two essential equations	29
2.3.2	The Liouville equation	32
2.3.3	The Boltzmann equation	38
2.4	Turbulence	45
2.4.1	Some turbulence phenomenology	45
2.4.2	Stability and the transition to turbulence	48
2.4.3	Averaged equations and the closure problem	50
2.4.4	Approaches to turbulence, especially modelling	57
2.5	The lattice Boltzmann method	65
2.5.1	Development of the LBM: a review of the literature	66
2.5.2	Mathematics and details of the scheme	69
2.5.3	Discussion of properties and character of LBM	82
2.6	Flow geometries, simulation domains and forcing	84
2.6.1	Internal flow configurations	85

2.6.2	Some laminar channel flow parameters	96
2.6.3	Driving and constraints of the physical flow	100
2.6.4	Artificial lattice closure devices	105
2.7	Turbulence in simple internal channels	111
2.7.1	Description of channel turbulence and basis for its discussion . . .	112
2.7.2	Boundary layers and turbulence; an overview	118
2.7.3	Analyses of wall induced turbulent velocity profiles in a channel .	121
2.7.4	Analyses of turbulent channel friction data; the Moody curves . .	130
3	Simulation of cylindrical flow on a regular 2D grid	136
3.1	The problem of using a 2D simulation for 3D cylindrical geometry: Intro- duction	137
3.1.1	Cylindrical flow representation	138
3.1.2	General forcing in lattice Boltzmann simulation	139
3.2	Implementing coordinate change in LB by forcing	142
3.2.1	Lattice continuity equation and $h_i^{(1)}$	144
3.2.2	Lattice momentum equation and $h_i^{(2)}$	145
3.2.3	Résumé of axial symmetry forcing issues	148
3.3	Flow in a 3D geometry using a 2D grid: results	150
3.4	Discussion	155
3.5	Synopsis and Conclusions	157
4	An improved lattice closure	159
4.1	Improved lattice closure scheme: Introductory remarks	160
4.1.1	Existing LB closure schemes; a brief review	161
4.2	Six equation system for lattice closure	163
4.2.1	Alternative closure scheme; conception and introduction	163
4.2.2	Lattice closure algorithm	165
4.3	Simulation results for improved BC scheme	171
4.4	Discussion	176
4.5	Synopsis and conclusions	179
5	Application of eddy viscosity model in LBM simulation of turbulent channel flow	181
5.1	Introductory remarks and preview	182
5.1.1	Nature of the novel contribution and synopsis	183
5.1.2	A basis for evaluation of model effectiveness	184

5.2	Models and implementation	191
5.2.1	Eddy viscosity and mixing length in the LBM: a review	191
5.2.2	LB Mixing length model: implementation	194
5.2.3	Turbulent boundary layer implementation	198
5.3	Turbulent channel simulations and results	203
5.3.1	Standard simulation domains implementation of channel geometry	204
5.3.2	Results for wall law bounded channel: flow profiles	206
5.3.3	Results for wall law bounded channel: Moody curves	224
5.4	Discussion	231
5.4.1	Problems solved and lesson learned	232
5.4.2	Dynamics of the turbulence model	234
5.4.3	Analysis of the effect of variable viscosity	235
5.4.4	Other critical points	238
5.5	Synopsis and conclusions	241
6	Summary	242
6.1	Alternatives and future work	243
6.1.1	Turbulence in pipes: bringing our developments together	243
6.1.2	Progression to improved overall scheme	245
6.1.3	Alternatives: self consistent energetics approach	249
6.2	Conclusions	252
6.3	Acknowledgments	254
A	Some mathematical technicalities	255
A.1	General notation and nomenclature	255
A.2	General mathematical prerequisites	257
A.3	Averaging: notation, relations and technicalities	259
A.3.1	Technical aspects	259
A.3.2	Specific case of Reynolds decomposition	263
B	Other snippets of analysis	266
B.1	Obtaining the formula for ω_T by solution of the quadratic, equation 5.15	266
B.1.1	Gradient of the viscosity with relaxation parameter and stress . . .	268

1.1 Front matter

This thesis presents work undertaken by the author as a research student at Sheffield Hallam University over a 36 month period, to October 2001, for the award of Doctor of Philosophy.

The work is sponsored by Rolls–Royce Associates (formerly Rolls–Royce Marine Power) who have a keen interest in the development of modern, alternative approaches to traditional computational fluid dynamics for the simulation of flow in internal geometries. It was carried out under the supervision of members of the (computational) Modelling Group at Sheffield Hallam University, which is jointly provided for by the School of Science and Mathematics and the Materials Research Institute thereof.

Motivation for the work arises in the practical importance of obtaining an accurate description, at various levels of detail, of flows in many and varied fluid systems. The basis for the specific approach taken arises in the interests of members of that group and of the sponsors, in the truly alternative approaches to the problem of simulating fluid systems that have arisen from studies into cellular automata and lattice gases over recent decades. In our case these are Boltzmann type approaches; simulations of discrete particle distributions, as opposed to continuum type equations.

In the following *introductory* sections, opportunity is taken to describe and convey firstly, the industrial, engineering, scientific and socio-economic context of the work; in section 1.2. Secondly, the general content of the thesis, its layout and mode of presentation; section 1.3.

Following the introductory material, a large portion of the thesis is devoted to presentation of *background* material, illuminating the scientific details underpinning the work. It is only after this that the main sections of work are presented. Busy readers, or those familiar with the background of the project are invited to omit these introductory sections if desired.

1.2 Fundamental context of the work

The importance of fluid processes to humanity is a largely unappreciated fact. Fluids, in their various forms, are indeed central to life and to nature. From the air that we breathe and the blood in our bodies, to convection of thermonuclear plasma in the life breathing sun, fluids and their dynamics lie at the heart. Water, in its liquid form, has recently been identified as the single requisite for the existence of life as it is currently understood.

Perhaps as a consequence of such significance and ubiquity, the scientific study of fluids has reached a relatively mature stage. Much effort has been directed to their understanding over the years, especially the latter four centuries. Indeed many of the great natural philosophers such as Archimedes and da Vinci are known to have contemplated the dynamics of fluids. Others still, including mathematicians such as Stokes, Euler and Kolmogorov, have devoted enormous time and effort in the field. Despite this maturity however, there remains much more to be done; some of the most pertinent questions endure unanswered.

In the light of such issues then, it is a sad reality that a knowledge of fluid dynamics is not generally perceived to possess high value. In fact, presently, the general public has little appreciation that such knowledge or understanding might have value, whether it be real and tangible or prospective. It is unfortunate too that the value of advancement in our knowledge is only half heartedly recognised, especially as it is the public who ultimately pay for research activity.

As a small personal effort to counter such a situation, it is hoped that the material discussed in these introductory paragraphs, intended primarily to form a basis for a complete appreciation of the science, might advance a fairer picture of the place, relevance and need for fluid dynamic knowledge in society. That is, by forming a full picture of the social, economic and scientific *context* for this work, interest will be generated, its value demonstrated, and its pursuit thus justified.

To that aim, it is important to have an appreciation of the following two points. Firstly, the ubiquity of fluids and diversity of fluid processes, both human and natural. Secondly, the generality of the science that emerges in the field and its breadth of applicability. In discussing these matters, a feel will be acquired for the level of interest in the subject, held by scientists, industrialists and engineers alike.

Considering the aforementioned ubiquity; the prevalence of fluids and the manifold nature of processes involving, or critically influenced by, their motion. The fluids themselves are commonplace, encompassing liquids, gases and plasmas (the 'fourth state of matter'), but also including species only differentiated in technical ways (as will be demonstrated),

for instance traffic. As regards the processes; these may be heat driven (convective), pressure driven or gravitationally driven. More complex processes are common and include transport processes (movement of variable properties of a fluid with the fluid), mixing, e.g. distribution of contaminants, combustion and other plasma behaviour.

Instances of processes and systems are diverse, arising in fields such as: biology (rheology); vulcanology; planetary science; hydrology and even astronomy. An obvious example being meteorology — the study of atmospheric characteristics and prediction of our weather — which is clearly relevant to everyday life and experience. Less obvious examples are just as significant however. The geomagnetic dynamo for instance — motion of liquid iron in the Earth's core — is believed¹ to be responsible for the Earth's global magnetic compass field. It is now appreciated that without such, and the concomitant protective 'magnetosphere', life on Earth would perish under constant bombardment of high energy solar radiation.

Arguably of greater relevance on a human scale, many *non-natural* systems involve the motion of fluids. Indeed, it could be said that they *all* do, either directly or indirectly in some way. Illustrating the point with a non-obvious example for the unconvinced, consider the creation of modern solid componentry by the injection and subsequent solidification of molten solids in moulds. Such components are essential to virtually every manufacturing process. More apparent industrial and technological examples are as diverse as natural ones. They include: flows around solid bodies (cars, aircraft, shipping); flows through porous media (oil extraction, filters, percolation, wicking); the flow of complex fluids (colloids, suspensions, solutions, multi-phase); reactive flows and combustion; drag reduction and noise reduction. Collectively, the scientific and industrial communities have strong interests in each.

Moving now to the latter point to be highlighted, 'generality'. In the present context, generality refers to the inherent power, aptitude and broad validity, of natural philosophical reasoning and the language of physics. That is, the applicability of our scientific tools and skills to diverse circumstances and within diverse fields.

The principle of generality is perhaps the least appreciated aspect of the physics discipline; it is certainly that most often lost on those working outside the field, hence common misconceptions. Whilst it could also be said, that generality is sometimes not well appreciated even by physicists, most realise that understanding one system allows much to be said in other superficially unrelated fields and that their work can, under said generality, be readily applied elsewhere. Moreover, it could be argued that generality

¹Recent studies provide evidence for presence of 5km fission/fusion reactor at core of Earth; contrary to the established theory [7].

has subtle appeal to practitioners which is often crucial in their adoption of physics as a subject of study, for it belies the primary utility of physics itself.

In the context of this work, generality is what allows us to take a vintage theoretical approach to the modelling and study of *gases* and transform it into a modern, practical tool for the simulation of liquids in real systems. Moreover, generality is the principle that would permit adoption of the *same scheme* for study of other, less obvious flow types. In fact diversification proves viable to: snow in an avalanche; and (amazingly) the collective behaviour of people in rush hour and traffic on motorways. It becomes apparent that the generality attributed to any subject matter, must compound the interest that a physicist has in the field.

A feel for the author's enthusiasm for physical generality — the science's primary beauty — may be apparent at this point. In fact it is easy to extend the point, to include the primary focus of the current work, namely turbulence. The physics that is applied to the study of turbulence is incredibly diverse in nature. As a direct consequence, parallels may be drawn between studies of turbulence and seemingly unrelated sciences, from image recognition (via e.g. wavelet transforms) to prediction and modelling of stock market indices (via traditional statistical analyses).

On a more specific level it is perhaps now pertinent to review more closely the specific circumstances and nature of this work.

As a manufacturer of modern propulsion systems for the aerospace industry and military, most notably marine power plant, the interests of the sponsors of this work is perhaps obvious. Their competitive advantage arises in the efficiency, lifespan, quality, fitness for purpose and cost effectiveness of the engineering solutions they implement. Many of the problems they have to address relate to the flow and energetics of fluids, specifically those contained by so called 'internal' geometries, that is, flows that at least locally have no free surfaces. Important examples include heat exchangers, pumps, turbines and compressors. The prevalence of such systems, in engineering and industry should be pondered for a moment; whereupon the scarcity of industrial processes independent of such technologies must become apparent.

Of utmost practical relevance, to describing flows in these 'real' systems is *turbulence*. Turbulence is one of the most commonly occurring fluid phenomena. Its relative importance in fluid dynamics, cannot be overestimated, especially since the effect it has on global flow properties ranges from highly adverse, to interestingly beneficial, depending on the case in point. Moreover, it is well recognised that most flow realisations — above a certain size or velocity, or in fluid with low viscosity — occur well inside the turbulent regime.

It has been suggested that all aspects of turbulence are ‘contained’ in the Navier–Stokes equations, that is to say that the Navier–Stokes equations fully describe hydrodynamics and turbulence arises merely as a consequence of complexity or uncertainty in the solution. Whilst this is very likely true, a practically useful description for turbulence requires much more than hydrodynamics; despite the practical importance, it has proved a very difficult problem to crack. For these reasons turbulence is one aspect of fluid dynamics that receives a great deal of attention and its study is generally perceived to be of high value and importance.

The problem has been tackled on each of the three conventional fronts: experimental, theoretical and computational; in addition to some hybrid approaches. One aim here, as is perhaps now evident, is computationally to *model* turbulence in a particular context.

Modelling as a strategy uses the physical insights generated over past years of intensive investigation to find inroads on the mathematical problem. Then, depending on the exact nature of the investigation, these are used to generate either exact, statistical or numerical solutions. Owing to the vast complexity of typical systems of interest and the practical requirement for near infinite accuracy, most practical solutions are generated numerically, which necessitates significant use of computational power and efficient algorithms.

‘Computational fluid dynamics’ (CFD) is the name attributed to this pursuit. The work described in this study, whilst similar in nature to CFD, does not directly tackle the fluid dynamical (Navier–Stokes) equations. Instead, it is an indirect approach, made possible under the aforementioned *generality* and arising with physical insights into the parallels between fluid dynamics and the macroscopic emergent behaviour of microdynamical (point particle mechanical) gas systems.

Instantiating the matter of generality, it is now possible to clarify some basic points regarding the approach in this work. The modelling strategy adopted is derived from the lattice gas cellular automata (LGCA), see section 2.5, these in turn being a variant of the more fundamental cellular automata (CA), which were conceived early in the twentieth century. The particular derivative of LGCA is known as the lattice Boltzmann method (LBM) (section 2.5.2) and of that, the Bhatnagar–Gross–Krook (BGK) form (page 73). This is an especially simple gas dynamical model, which amazingly, may be so arranged as to be indistinguishable at the macroscopic level to hydrodynamics.

Specifically, for the purposes of turbulence modelling, the detailed form of the LB scheme is to be altered in such a way as to incorporate those more significant effects that turbulence exerts on the average flow. The model employed is based upon the eddy viscosity concept, as expounded in section 2.4.4. With respect to the many other modelling strategies in existence, this has certainly proved its worth from both practical

and historical perspectives; it is especially simple and therefore an appropriate starting point.

1.3 Work statement and synopsis

A concise statement is now given, describing primary elements of the material to be presented; both as a review for interested readers and a synopsis of the work undertaken. This is integrated with sectional references, so that the layout of the presentation is clarified, thus facilitating targeted reading and general navigation.

The order with which the work is presented in this discourse, does not strictly adhere to that by which it was carried out, nor a clear chronology. In fact most elements of the work ran concurrently over long periods, developments in any one field modifying the efforts made in others. Instead the order of presentation is to a greater extent 'logical', in that during the main thrust of effort toward turbulent channel flow, exploration was necessarily initiated into side issues, as and when they were encountered. Since dependencies between each existed, resolution of these occurred on a logical basis.

Brief preview then, of the thesis composition, starts as follows:

- Chapter 2 provides a sufficient exposition, of each aspect of relevant underlying physics, upon which the scheme itself and our novel developments are based. These aspects fall into two categories, the scientifically general and those specific to the work reported. Treatment of each occurs in such order where possible.

Following the grounding of Chapter 2, Chapters 3 to 5 form the core material to be presented. There, a description is given of individual subjects of investigation, followed by review and analyses of results obtained. An appraisal is made at the time, of the general efficacy and fitness of each idea; these are to be brought together and discussed further in the summary, Chapter 6. Opportunities and ideas for continuation of the work are discussed in Chapter 6 also.

Returning to the preview, the primary results chapters, which are each preceded by a short abstract, are as follows:

- In Chapter 3, the core lattice Boltzmann scheme is augmented by carefully derived forcing terms intended correctly to model flow characteristics that occur in three dimensional, cylindrical geometries, whilst employing a two dimensional Cartesian space discretisation for the simulation. The capacity of the modified scheme for this purpose is then investigated in some detail, based on simulations, and an analysis of errors made.
- Chapter 4 introduces an alternative improved lattice closure scheme, for lattice Boltzmann simulations. The new scheme is based upon simultaneous solution, of non-equilibrium components of link densities propagating onto the lattice, using

the density information propagating off lattice. After firstly deriving the scheme, results on its efficacy and comparisons to analytic solutions are presented for 2 benchmark internal flow configurations. The developments of this section were necessitated as a basis for turbulence studies of the next chapter.

- Chapter 5 describes work on the primary thrust of the project as a whole. A Prandtl mixing length model for channel flow turbulence is adapted for implementation within the lattice Boltzmann framework. This is aimed at the problem of reproducing characteristics of the turbulent flow of simple fluids in internal geometries. Also in this chapter, the improved lattice closure scheme, as developed in chapter 4, is applied to the problem of modelling boundary layer properties at the wall, such as development of sub-grid scale wall layers, and the effect of such on the core channel flow. Results for two main cases, with and without a law of the wall, are thus investigated and compared. Also in this chapter, section 5.4.2 presents an analysis of the aforementioned turbulent channel flow model. This is done to analyse the errors introduced by the model and to search for possible means to correct for these by introducing generalised corrective forcing terms to the LB evolution.

Finally:

- Chapter 6 rounds off the work by an in depth discussion of the results generated so far. This is to include the relative efficacy of each scheme developed, their individual merits and disadvantages, as well as any errors or inaccuracies introduced. Also discussed are alternatives for further work, especially *simultaneous* application of each novel development previously explored, to the case of a simple internal geometry; which would embody an ultimate test of their effectiveness and compatibility together. A deeper, general appraisal of the approach is also made, with respect to it's true alternatives, that is those which differ fundamentally in basis.

Material of relevance for following the work, but not in essence part of the novel developments or results, is presented in the appendixes. Also there, some technical matters are addressed in greater detail:

Appendix A attempts to draw together some of the more pressing mathematical aspects of the work, for definition and clarification. Note that there is not scope to be completely exhaustive here, so some mathematical experience is thereby necessitated.

Appendix A.1 briefly outlines general aspects of the nomenclature employed, extracted from each of the various scientific disciplines employed herein. This is supplemented by appendix A.2 which lists some general mathematical prerequisites which are presumed known in the main body of the thesis.

Appendix A.3 is of particular importance; it deals with specific issues surrounding averaging, which is of fundamental relevance in this work. It introduces notations, the physical meaning associated with the different types of averaging and gives some useful relations which are used regularly throughout other chapters.

Appendix B presents a collection of unrelated topics, too analytically detailed to leave in the main body of text.

Appendix 7 describes some alternative forms of the Liouville equation. Finally, appendix B.1 derives the formula for turbulent relaxation parameter by solving the quadratic given by equation 5.15. Some equivalent forms for this are detailed and aspects of their variation discussed. In particular, a set of derivatives are derived which describe the gradient of the viscosity function, across the typical relaxation parameter/stress domain.

Chapter 2

Background science

2.1 Introduction and synopsis

It is intended that this section of the thesis should provide a solid foundation of relevant knowledge for the interested reader in order to assist pursuit of the work and so that they may gain the maximum insight. Additionally it is hoped that the material presented here will inspire interest in the field, both specific to the work and to the science in general, to stimulate further work and ensure that it will in time be built upon.

The material presented is primarily an overview of the fields and is not intended to be comprehensive. It is not intended either, to form a summary of the material learnt by the author so far, despite the attraction of doing this with respect to completeness. It merely contains material required for the development of the ideas used in the project and to facilitate any continuation.

Before moving to the detailed background presentation, two short asides are taken. Firstly, in the following paragraphs, a brief review is given of the fields that are to be covered and their relevance, so that the busy reader may skip sections of material which they are familiar with and novices may target their weaker areas. After this, in section 2.1.1, the fundamental areas of relevance and scope of the science is discussed.

The detailed background presentation is initiated in **section 2.2** with a summary of ideas from the **continuum theory of fluids** so that the governing equations of hydrodynamics, the so called Navier–Stokes equations, may be derived. These equations are central to any analysis of the flows of interest here. Derivation proceeds by first finding a generic equation that represents all the various forms of the fluid dynamical equations simultaneously, it is then shown how and under what simplifications and limits, this reduces to the more commonly known forms.

Following this, in **section 2.3**, a brief excursion is made into **statistical physics**. There, a review is given of derivations of perhaps the two most important equations of statistical mechanics, the Liouville equation and the Boltzmann equation. These related equations are of high relevance in this work and form fundamental introductory matter in the field.

Section 2.4 deals with various aspects of the phenomenon of **turbulence**. Starting with an overview regarding the phenomena in general the focus moves to the principle equations that govern averaged quantities in the fluid. Eventually, the various means by which the turbulence may be modelled are described and discussed.

Subsequently, **section 2.5** covers the specific modern alternative to CFD which is utilised in this work for the problem of solving for turbulent flow in practically interesting geometries. Primarily this means the **lattice Boltzmann method**, toward which all the novel developments in this work pertain. It will be seen that the lattice Boltzmann

method is the culmination of efforts in diverse fields which are now seen to be equivalent to hydrodynamics.

Finally, in **section 2.6** a brief review is made of **general simulation specific issues**. Geometries of interest to CFD practitioners and engineers are discussed, especially symmetries, coordinate systems and solutions. For these cases the focus then moves to lattice closures, boundary conditions and forcing strategies. Finally characteristics of turbulent boundary layers are discussed and boundary issues of relevance to subsequent work clarified.

2.1.1 Fundamental concepts

As previously stated in the introductory material, the subject of this study is to model global characteristics exhibited by simple fluids during complex motions and subsequently to deduce properties of their average motion. The emphasis falls upon flows in internal geometries; those of interest to us being reviewed in section 2.6. It is necessary however, to further refine other aspects of this specification before moving on. Primarily, it must be emphasised that attention is constrained to so called ‘simple’ fluids, an expansion of what is meant by simple is given next. In addition to this, the nature of the flows considered is restricted to those in a turbulent state, characteristically irregular and apparently random; points relating to this will be addressed subsequently.

Simple fluids

Specifically, with respect to simplicity, the properties that the fluid exhibits and the conditions that the fluid system is subjected to, may be described as ‘conventional’ in that one might expect to encounter such, in everyday experience. This has relevance to various aspects of the study. Firstly, under a *macroscopic* perspective, the fluids considered are characterised by moderate values for density and viscosity parameters, comparable to those of water for instance, hence justification for the term hydrodynamic. Also at the macroscopic level, fluid systems of interest are not of extreme size (smallness) and are not subject to any extremes of temperature or pressure that might invalidate underlying assumptions made during formulation of a relevant mathematical description. This means that no *phase* properties need be considered; boiling, which gives rise to the vapour phase, and freezing which gives rise to solid phase, do not occur. To summarise, only ‘mono-phasic’ systems are dealt with.

This point must be augmented however, as phase character also varies in accordance with *molecular* properties of the fluid, that is at the microscopic level. The primary molecular restriction placed on the fluid is that it be ‘single species’, that is, consisting

of only one type of molecule and, species interfacial effects not being present, unable to separate, coalesce or display other related behaviour.

Molecular *anisotropy* also leads to complex fluid behaviours not considered here. A good modern example of fluids composed of such molecules is liquid crystals. There, anisotropy originates in the shape of the molecules, which are elongated, often substantially, giving rise to a tendency to align amongst themselves and thus form quasi-crystalline states. Anisotropy also arises from dipolar electron distributions which again causes certain packing tendencies in the material. The fluid is deemed to be ‘simple’ at the molecular level in that the molecules themselves can be considered spherically symmetric and they possess no unsymmetric charge distributions.

A subtle yet still important addendum to those points above, of relevance to matters raised in later discussions regarding further work 6.1, is that here molecular motion manifests only translational degrees of freedom, that is molecules considered in this study neither vibrate nor spin.

In fact, formulation of the simulation technique employed in this work (LBGK), is based upon even greater molecular simplification than has been made already. To be precise, it is derived from frictionless point masses, that undergo fully elastic, binary only collisions. Surprisingly, such simplicity does not adversely affect the validity of the approach taken; it will in fact be seen that the scheme possesses greater validity than is required of us to utilise, especially with respect to density and temperature constraints. Aspects such as this and other related matters are discussed where relevant; in particular, the ‘hydrodynamic’ and ‘Boltzmann gas’ limits are covered in the LB section 2.5. Attention now moves from issues regarding the nature of the fluid, to those regarding the nature or type of *flow*.

Turbulent flow

The interests of the author and sponsors is focused on the *turbulent* flow state. This is probably the most typical state that fluids attain in industrial circumstances or those of engineering interest, as well as during natural processes and is therefore of high interest to the scientific community generally. For these reasons, it is unfortunate that turbulent flow is such a complex phenomenon, having proved to be extremely difficult to fully understand or describe mathematically. In fact precious few practically valuable results arise in theoretical investigations unless they are extremely involved in nature. Experimental investigations have proved worthwhile, but are significantly more difficult and costly to carry out and tend not to possess much generality. During the improvement in computational resources that has occurred over recent decades and with the development

of new computational techniques, various *modelling* strategies have become of interest and relevance. It is in this light that the present work adopts a computational modelling approach to the problem of turbulence.

Various methods exist for the solution of flow problems, both turbulent and non-turbulent, each however falls into one of two broad categories. Either the *exact* and instantaneous detail of the flow configuration are to be resolved, or merely the average of these details over some suitable and convenient domain. A prime characteristic of this work is that full resolution of turbulent flow is *not* the goal. Exact detail of space and time dependence in a flow is not automatically valuable, except in some theoretical studies, and is anyway practically unrealisable in many cases. Important flow characteristics tend to depend upon global or average properties, such as the mean velocity field and associated streamlines. Their importance stems from their relevance to calculating global heat and other transfer properties. It is intended that only such *mean* properties are sought.

Most turbulence modelling approaches originate in the CFD realm proper in that they focus on direct numerical implementations of either the governing hydrodynamic equations, traditional turbulence models or both. The modelling strategy here adopts a truly alternative approach, differing significantly at a fundamental level. Despite this, the insights that traditional modelling provides, are still of great utility here.

In fact, this approach chooses not to simulate the Navier–Stokes equations, nor any other continuum or hydrodynamic system. An amazing consequence of generality in this science, means that under the transformation from microscopic to macroscopic perspectives, the Boltzmann equation and its lattice counterpart, are found to be *exactly equivalent* to the Navier–Stokes equations for certain parameterisation ranges. This property is exploited to great effect here, where the (lattice) Boltzmann equation is simulated directly. It is then supplemented with a model for the effects of turbulence and turbulent boundary layers, which has been derived specifically for implementation within the LB framework. In this way, a turbulence model for the cases of interest is developed in a highly alternative fashion. Extra difficulties and problems are introduced compared to CFD, but these turn out to be surmountable and not significantly detrimental. Moreover, modern approaches to simulate the Boltzmann equation are found to be highly efficient and computationally amenable, the LB especially lends itself to algorithmic parallelisation, a point that provided decisive impetus to its original development.

In the rest of this chapter, a detailed exposition is presented, of all relevant background material required to; fully grasp the issues involved in the equivalence and transformation between Boltzmann and Navier–Stokes realms; understand which turbulent properties it is intended be modelled; and how such complex hydrodynamic phenomena may be

2.2 Continuum mechanics: The equations of motion for a fluid

The fluid dynamical equations may be derived by careful consideration of finite volumes within the fluid and the surfaces that bound them. They are essentially balance equations for the mass and the momentum fluxes into and out of these spatial elements. The mass balance equation is known as the ‘continuity equation’ and the simplest form of the momentum equation is known as the Euler equation after the prominent scientist of the eighteenth century — both are derived in the following. The Euler equation describes the time evolution of the velocity field of an inviscid fluid and it may be generalised in such a way as to incorporate more detailed physics such as viscous dissipation, thus giving rise to the Navier-Stokes equation (hereafter NS equation). Alternatively, a generic form for the dynamic equations may first be derived and thereafter reduced to the other widely recognised forms; such is the route taken here.

Equations describing the motion of fluids necessarily involve differential terms, derivation of these being viable by two distinct approaches; it is possible to formulate *integral* relations for a control volume, or to formulate *differential* relations for fluid particles. For simplicity of exposition, the former method is adopted here, though it demands acceptance of a deeper mathematical result¹ not within the scope of this work. Those preferring to follow differential approaches might consider [3] for an easily followed derivation using rectilinear fluid element, or more generally [93, 148].

Making derivations via integral relations necessitates considering volumes of fluid, especially the ‘infinitesimal’ volume element. In this way integral equations are generated at first, which require transformation to their differential counterparts via Gauss’ theorem.

In doing so a slight caveat is required regarding the meaning attached to the word infinitesimal; it is important to clarify the scale of the volume element. Continuum theory regards the behaviour of fluid elements which are, at the scale of flow detail, effectively infinitesimal, but which are supposed still to contain large numbers of elementary particles or molecules. The number of internal particles must be sufficiently high to justify speaking of the so called ‘continuum limit’, where the fluid medium within the finite volume may be considered, in essence continuous, homogeneous and isotropic.

Such an assumption is, perhaps surprisingly, realistic, especially in hydrodynamics where enormous particle numbers and close particle proximity prevail. It is only tested for elements the size of which approaches length scales characteristic of processes by which

¹Gauss’ theorem for transforming surface integrals into volume integrals. See for instance [4, 123].

flow energy is finally dissipated into thermal energy, the so called dissipation length scale ℓ_ϵ . Such small scales are, by default, of negligible importance in typical laminar flow simulations. Unfortunately however, they are of some importance as regards turbulent phenomena, the objective area of this work, for which reason, some discussion of the matter will occasionally be necessitated throughout. The matter is set aside for the moment.

In the following, a volume element is considered which possesses the properties referred to above. It contains many millions of molecules, but is tiny with respect to even the least significant features of the flow. The element is not constrained to have any regular shape and may be arbitrarily bounded. Equations for the balance of both mass and momentum fluxes will be formulated, in and out of the elemental fluid volume V , across its surface S . All comments in the following will be made in the light of figure 2.1, which shows the volumes and surfaces considered.

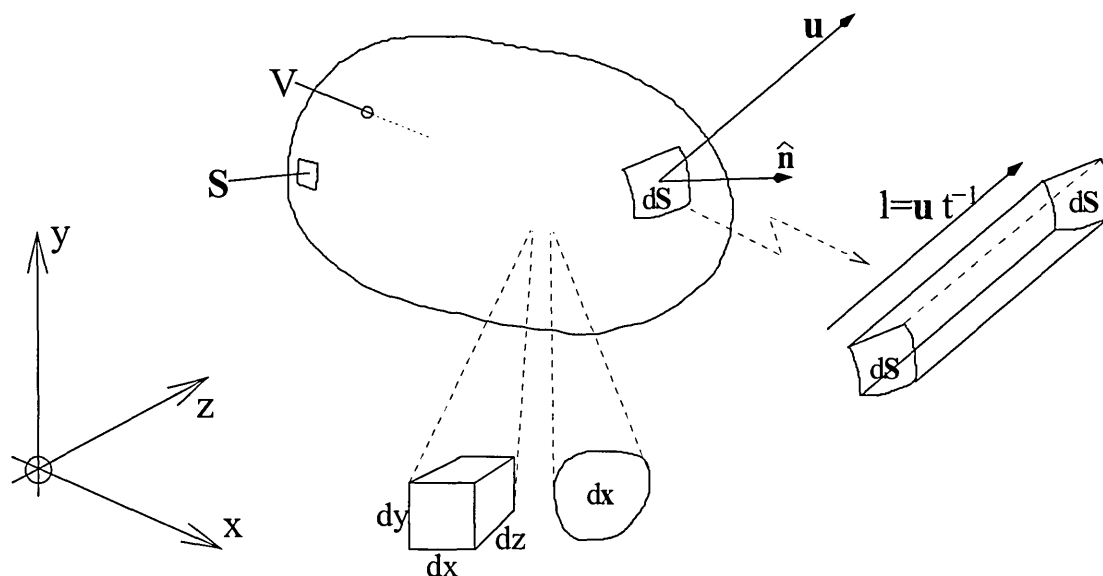


Figure 2.1: Representation of finite arbitrary volume V , with surface (vector) S in Cartesian coordinate system. Also shown are two infinitesimal volumes $dx \, dy \, dz$ and dV . An infinitesimal surface element is shown not to scale: dS . This has unit normal \hat{n} and fluid flow \mathbf{u} across it. The volume of fluid crossing dS in unit time is shown on the right also $(\mathbf{u} \cdot dS)$.

It is also possible, note, to derive an energy balance equation in a similar way to the above. For general isothermal flows however, energy considerations are unimportant, its derivation here is therefore not justified. Instead, in section 2.2.5, the energy balance equation is simply stated; its inclusion is later necessitated during discussions on turbulence energetics.

2.2.1 Mass balance

The mass contained within any arbitrary region will in general depend on the variation of the fluid density there and on its volume. Where density is functionally dependent on both space and time, $\rho(\mathbf{x}, t)$ it is clear that the mass is the integral sum of the product $\rho d\mathbf{x}$ across the entire volume V :

$$M = \int_V \rho(\mathbf{x}, t) d\mathbf{x}. \quad (2.1)$$

Here $d\mathbf{x}$ denotes the elemental volume in space. The temporal variation of the above is given by

$$\frac{dM}{dt} = \int_V \frac{d\rho(\mathbf{x}, t)}{dt} d\mathbf{x}, \quad (2.2)$$

which is the rate of change of mass in the finite volume.

Conservation of mass asserts that this mass change must be balanced by the fluid that flows across the surface \mathbf{S} of the elemental volume, i.e. they must sum to zero. An expression may be obtained for the flux term by considering an elemental area on the surface $d\mathbf{S}$, where the vector notation is a reminder that area is a directed (vector) quantity. The mass flux across this element is proportional to the velocity of the fluid at that point $\mathbf{u}(\mathbf{x}, t)$, the area of the element $d\mathbf{S}$ and the density $\rho(\mathbf{x}, t)$; in fact it is proportional to the product thereof, as may be seen when one considers the dimensions of the flux, $[MT^{-1}]$.

So the flux dM/dt over the infinitesimal surface element is, after dropping the independent variables

$$\left. \frac{dM}{dt} \right|_{\text{element}} = \rho \mathbf{u} \cdot d\mathbf{S} \quad (2.3)$$

and it is apparent that the total mass flux is the integral of this over the entire surface of the arbitrary volume, that is

$$\left. \frac{dM}{dt} \right|_{\text{total}} = \int_S \rho \mathbf{u} \cdot d\mathbf{S}. \quad (2.4)$$

This is a surface integral to which may be applied Gauss' theorem from differential geometry, turning the surface integral into a volume integral² as follows

$$\frac{dM}{dt} = \int_V \nabla \cdot (\rho \mathbf{u}) d\mathbf{x}. \quad (2.5)$$

Summing these two terms, 2.2 and 2.5, to form the balance equation, gives the fol-

²Readers interested in the validity of this may consult books on vector calculus such as [4, 123].

lowing:

$$\int_V \frac{d\rho}{dt} d\mathbf{x} + \int_V \nabla \cdot (\rho \mathbf{u}) d\mathbf{x} = 0. \quad (2.6)$$

which is easily simplified on realising that each integral may refer to the same arbitrary volume. In fact if the volumes are taken to coincide, then the integrands may be collected together to form one integral

$$\int_V \left(\frac{d\rho}{dt} + \nabla \cdot (\rho \mathbf{u}) \right) d\mathbf{x} = 0. \quad (2.7)$$

Subsequently, on noting that the volume V may be arbitrarily chosen, the only way that this expression is non-trivially valid is if the integrand is identically zero at all points, hence the fluid ‘continuity equation’ is arrived at, so named because it is essentially a mass balance equation:

$$\frac{d\rho}{dt} + \nabla \cdot (\rho \mathbf{u}) = 0. \quad (2.8)$$

Various simplifications may be made to the form of the continuity equation, these and its properties with respect to the current work are discussed at a later point. Here, the presentation continues with derivation of the momentum balance equation, which is of paramount importance in the remainder.

2.2.2 Momentum balance

The momentum balance equation may be found by considering the same fluid volume, but this time in contrast looking at momentum fluxes. Momentum contained in the volume is calculated in a similar fashion to that for mass previously, the net *change* in this is then balanced with the total influx and efflux of momentum. Some complicating factors arise, one being the fact that there are more possible contributions to the momentum flux than for mass flux and hence further terms in the balance equation. In fact mass flow may be due to the advection of momentum along with the fluid, it could originate in stress or pressure forces given by the pressure tensor or it may be due to external forces such as electromagnetic or gravity; each contribution requires separate consideration. In addition, tensorial qualities are inadvertently introduced to the equation; a short aside on which is appropriate before proceeding.

In the context of a fluid with a spatio-temporal variation in velocity and density parameters, momentum may be arrived at as the product of the density and the velocity, which effectively gives a momentum density $[ML^{-2}T^{-1}]$. Similarly, a flow of momentum may be given by the product of momentum density $\rho \mathbf{u}$, times the velocity \mathbf{u} , turning the momentum density into a momentum flux per unit area $[ML^{-1}T^{-2}]$. Care must be taken

however, as this in effect creates tensor quantity; the velocity vector appears twice in this product. This more general *direct* case of product between two vectors, means *neither* the dot *or* cross product of the vector with itself; it contains more information than both of these together. In tensor notation, the direct product \mathbf{uu} , is necessarily given by the introduction of a further subscript, giving: $u_\alpha u_\beta$. Note in contrast, the vector product $u_\alpha u_\alpha$ gives the dot product under the implied summation on α .

Having accounted for this, forms for momentum and momentum flux terms are now available and attention must turn to the matter of deriving the individual contributions to the balance equation. For simplicity, external forces are considered no further here; their relevance to the work is not high and they may be introduced easily at later stages. This leaves two other contributions, which are expected to balance with the change in the total momentum over the volume, derived as follows.

The momentum in the volume, here denoted by \mathbf{G} , is given by the integral sum of the momentum density at each point $\rho\mathbf{u}$, over the volume

$$\mathbf{G} = \int_V \rho\mathbf{u}dx, \quad (2.9)$$

the time variation of which is thus given by

$$\frac{d\mathbf{G}}{dt} = \int_V \frac{\partial\rho\mathbf{u}}{\partial t}dx. \quad (2.10)$$

This *total change* in momentum content $d\mathbf{G}/dt$ is physically, or dimensionally, a force; it must balance with net flux of momentum into the volume across its surface, that is the terms must sum to zero. Derivations for the pressure / stress contribution and advection contributions are treated separately and the two are denoted by \mathbf{F}_{pres} and \mathbf{F}_{adv} respectively — both vector quantities with dimensions of force [MLT^{-2}].

The advection term \mathbf{F}_{adv} may be arrived at by summing the dot product of the tensorial momentum flux per unit area term, $\rho\mathbf{uu}$ over the entire bounding surface of the volume as follows

$$\mathbf{F}_{adv} = \int_S \rho\mathbf{uu} \cdot d\mathbf{S}, \quad (2.11)$$

where the integrand is more explicitly given in tensor notation by $\rho u_\alpha u_\beta$.

Similarly for the pressure contribution — ‘general’ pressure being a tensor quantity, herein denoted by sans serif fonts. The pressure force term is given by

$$\mathbf{F}_{pres} = \int_S \mathbf{P} \cdot d\mathbf{S}. \quad (2.12)$$

These contributions summed: $d\mathbf{G}/dt + \mathbf{F}_{adv} + \mathbf{F}_{pres}$, must equate to zero, so the

balance equation reduces to

$$\int_V \frac{\partial \rho \mathbf{u}}{\partial t} dV + \int_S \rho \mathbf{u} \mathbf{u} \cdot d\mathbf{S} + \int_S \mathbf{P} \cdot d\mathbf{S} = 0. \quad (2.13)$$

This untidy *integral* form however, is not easily recognisable, nor is it particularly useful here. To address this, Gauss' divergence theorem is applied once again, as done for the continuity derivation, turning surface integrals into volume integrals. Then, upon recognising that the equation holds for *equal* and *any* volumes V , a more recognisable form for the momentum balance equation may be arrived at:

$$\frac{\partial \rho \mathbf{u}}{\partial t} + \nabla \cdot (\rho \mathbf{u} \mathbf{u}) = -\nabla \cdot \mathbf{P}, \quad (2.14)$$

which, in this highly general form, conceals much detail of the physics of fluids in the nature of the pressure term.

Equation 2.14 is a 'generic' form for the continuum equations of motion of a fluid in the absence of external forcing. It encompasses both the Navier-Stokes and Euler equations, that is viscous and inviscid versions respectively, in their compressible and incompressible forms. Some comments are in order before we may proceed to develop specific, more often quoted variants than 2.14 represents.

Deriving a generic momentum equation in this way leaves unspecified some of the essential physics of fluids such as viscous dissipation of energy, forcing of the flow by net external forces and the like. However, these may be injected as contributory aspects to the form of the momentum flux tensor and the pressure tensor as the level of detail requires it. It is more in keeping with the physics to develop the individual equations in this way, but it is pertinent to point out that other direct derivations are possible, which attain the well known forms in more visible or rigorous ways. A good readable example of the latter approach can be found in the book by Anderson [3]. The starting point there is to consider, at the level of infinitesimal elements, balance equations for the *environment* that the volume element is subject to, explicitly and individually; to that aim it is efficient to consider *regular* volume elements to facilitate the mathematics ($V = \Delta x \Delta y \Delta z \rightarrow dx dy dz$ of figure 2.1). This type of treatment loses some generality and care is required in ascertaining the breadth of validity of equations generated in the light of characteristics of the fluid medium, such as bulk and shear viscosity and whether the fluid is considered Newtonian in its stress / strain characteristics.

Here the presentation moves in the opposite direction. Taking 2.14 as the starting point and inserting the appropriate forms for the pressure and momentum flux tensors, permits simplification of the equation for certain regimes and limits. The various well

known forms are then obtained during simplification. Before this can be done however, the exact detail of the pressure tensor \mathbf{P} needs to be specified; which must appropriately represent additional physics originating therein. Additionally, the momentum flux tensor $\rho\mathbf{u}\mathbf{u}$ may be looked at, to uncover the nature of any simplifications.

Firstly then, the general form for the pressure tensor. Assuming that the fluid exhibits Newtonian³ behaviour, this is found to be⁴

$$\mathbf{P} = \left[p + \left(\frac{2}{3}\eta - \lambda \right) \nabla \cdot \mathbf{u} \right] \mathbf{l} - 2\eta \text{sym}(\nabla \mathbf{u}), \quad (2.15)$$

where η and λ are coefficients of viscous terms, \mathbf{l} is the unit tensor, with components equal to the Kronecker delta $\mathbf{l} = \delta_{\alpha\beta}$ and p is the scalar quantity representing the common notion of pressure. This semi-empirically derived expression for the pressure tensor is used hereafter without further concern, being generally accepted as adequate for the Newtonian case. λ Represents *bulk* viscosity, that is the constant of proportionality between compressive or tensile stresses applied to the fluid element and the strain that it exhibits (in any given direction) — fluid isotropy is assumed. η Represents the *shear* viscosity of the fluid, equivalent to λ but for shear stresses.

Secondly, the momentum flux tensor, $\rho\mathbf{u}\mathbf{u}$. Term two of equation 2.14 consists of the divergence operator, acting on both \mathbf{u} the velocity and ρ the density of the fluid. It is the divergence of a triple product, $\partial_\beta \rho u_\alpha u_\beta$ to which may be applied the product rule of differentiation in the usual way: successively to parts of the product. The initial choice of partitioning of the product proves to be unimportant, leaving, in tensor notation:

$$\partial_\beta \rho u_\alpha u_\beta = \rho u_\alpha \partial_\beta u_\beta + \rho u_\beta \partial_\beta u_\alpha + u_\alpha u_\beta \partial_\beta \rho. \quad (2.16)$$

After substitution and rearrangement, this has the effect of giving 2.14 an extra non-linear contribution on the left-hand side. Its detailed form then appears as follows

$$\frac{\partial \rho \mathbf{u}}{\partial t} + \rho(\mathbf{u} \cdot \nabla)\mathbf{u} + \mathbf{u}(\nabla \cdot \rho \mathbf{u}) = -\nabla \cdot \left(\left[p + \left(\frac{2}{3}\eta - \lambda \right) \nabla \cdot \mathbf{u} \right] \mathbf{l} - 2\eta \text{sym}(\nabla \mathbf{u}) \right), \quad (2.17)$$

where the third term on the LHS, is terms one and three of RHS of 2.16, in a condensed form⁵.

Following the above it is now possible to make refinements to equation 2.14, honing

³Newtonian character asserts that the functional form of the strain exhibited by the fluid under stress — stress being proportional to only first order contributions to fluid velocity gradients — is simple linear proportionality.

⁴A derivation of this form for the pressure tensor can be found in [66] where the 81 potential components of the general rank 3 tensor are vastly reduced.

⁵This is conventionally done to group terms which go to zero under incompressibility.

it toward recognisable target forms.

2.2.3 Balance equations for incompressible fluids

In the first instance, to obtain the fluid dynamical equations in the limit of fluid incompressibility, it is ensured that variation of density with independent parameters is negligibly small; that is, $\partial_t \rho$ and $\partial_\alpha \rho$ are set to zero. Invariance of the density parameter, ρ , in both continuity and momentum balance equations (2.8 and 2.14), then permits its factoring from all differential operators and subsequent dividing out, which is sufficient to ensure that it then appears only on the RHS of equations. There, by dividing the viscous coefficients, it forms the so defined *kinematic* viscous coefficients: $\nu = \eta/\rho$ and $\nu' = \lambda/\rho$, being the kinematic shear and kinematic bulk viscosities respectively.

A great simplification to the *mass* balance, or continuity equation, 2.8, emerges as a consequence of the above. Since there is no time variation in the density, it now takes the form:

$$\nabla \cdot \mathbf{u} = 0, \quad (2.18)$$

which says that, for an incompressible fluid there is no divergence in the velocity field.

Simplifications to the *momentum* equation arise in parallel with the above; their application leads to the so called ‘incompressible Navier–Stokes’ equation:

$$\frac{\partial \mathbf{u}}{\partial t} + (\mathbf{u} \cdot \nabla) \mathbf{u} = -\frac{1}{\rho} \nabla p + \nu \nabla^2 \mathbf{u}, \quad (2.19)$$

which is the most crucial continuum equation as regards this work. It describes the motion of Newtonian fluids under the commonly applied assumption of negligible variation in fluid density. It may very usefully be expressed in tensor form as follows

$$\partial_t u_\alpha + u_\beta \partial_\beta u_\alpha = -\frac{1}{\rho} \partial_\alpha p + \nu \partial_\beta \partial_\beta u_\alpha, \quad (2.20)$$

which will be more commonly utilised.

This is the continuum momentum equation that the LB model of later chapters aims to recover as macroscopics for its *hydrodynamic* regime. In essence, the final form of *macroscopic* conservation equations, as arise through the Chapman–Enskog expansion of the lattice Boltzmann equation, must be identified with the likes of equation 2.20 and for the LB equation to be pronounced a sufficient hydrodynamic model, equivalence of the two must be demonstrated. This procedure, which is at the heart of the LB method, is followed in section 2.5.2, page 76.

2.2.4 Momentum balance for inviscid fluids

To obtain the *inviscid* form of 2.14, that is the Euler equation, it is required that no account be taken of dissipation of momentum into thermal energy. This is equivalent to specifying viscosity parameters of the pressure tensor to be zero. Terms therein, which represent viscosity, are therefore assumed to tend to the value zero in advance.

As can be seen, if viscosity coefficients are allowed to tend to zero $\eta, \lambda \rightarrow 0$, describing an infinitely ‘mobile’ fluid, or a fluid with no viscous dissipation of momentum transfer, then the pressure tensor reduces to the far simpler form $\mathbf{P} = p\mathbf{l}$. The divergence of this (RHS of equations) is then simply the gradient of the scalar pressure field⁶.

The following form for the *compressible* Euler equation is thus arrived at:

$$\frac{\partial \rho \mathbf{u}}{\partial t} + \nabla \cdot (\rho \mathbf{u} \mathbf{u}) = -\nabla p, \quad (2.21)$$

In a similar way to equation 2.19, equation 2.21 may be rephrased in tensor form to give the following

$$\partial_t \rho u_\alpha + \partial_\beta \rho u_\alpha u_\beta = -\partial_\alpha p. \quad (2.22)$$

Further, *incompressible* versions of the above Euler equation may be formulated, following the same approach for the momentum flux tensor, which gives rise to

$$\frac{\partial \mathbf{u}}{\partial t} + (\mathbf{u} \cdot \nabla) \mathbf{u} = -\frac{1}{\rho} \nabla p. \quad (2.23)$$

2.2.5 The continuum energy equation for a fluid

In a similar manner to that discussed above, equations may be generated describing the energetics of fluids under the continuum assumption. These are as follows:

$$\rho \frac{\partial E}{\partial t} + \rho (\mathbf{u} \cdot \nabla) E = -\mathbf{P} : \nabla \mathbf{u} - \nabla \cdot \mathbf{q}, \quad (2.24)$$

in ‘vector’ notation, with the following tensor equivalent:

$$\rho \partial_t E + \rho u_\alpha \partial_\alpha E = -P_{\alpha\beta} \partial_\beta u_\alpha - \partial_\alpha q_\alpha. \quad (2.25)$$

Here, E is the total non-kinetic energy, excluding potential due to external fields; \mathbf{q} is the energy flux vector field, see for instance McQuarrie [93], which is usually assumed to

⁶Note that $p\mathbf{l} = p\delta_{\alpha\beta}$, so that $\partial_\beta \mathbf{P} = \partial_\beta p \delta_{\alpha\beta} = \partial_\alpha p$ by the summation convention, which is simply ∇p .

be given by a simple relation such as Fick’s law:

$$\mathbf{q} = -\lambda \nabla T, \quad (2.26)$$

where T is the temperature and λ the thermal conductivity coefficient.

The primary equations derived previously: mass balance 2.8; momentum balance 2.14; taken with the above energy balance, 2.24, are a system of non-linear partial differential equations which are widely supposed to correctly describe all fluid flow phenomena at all but the microscale. As a consequence of this they are said to ‘contain’ even turbulence. This point is open to debate, but it arises in the ability of the equations to model many levels of fluid behaviour in a way which has been corroborated experimentally and with some degree of accuracy. The momentum equation, with appropriate substitution for the pressure tensor (equation 2.15) is often called the Navier–Stokes (NS) equation. It has been known since the work of Navier, [97], of 1823! Stokes, working separately, is credited for its development despite the fact that his work appeared much later [130,131]. The plural Navier–Stokes *equations*, either refers to the vector nature of the equations, or is a misnomer loosely referring to the fluid dynamical equations.

For some simple flow geometries, analytical solutions for the velocity field have been found which have also been verified experimentally. However these instances are few and far between owing to the complex nature of such equations and their general intractability. Indeed for the vast majority of flow geometries, the NS equations are presently insoluble and even some of the deeper mathematical questions regarding solubility, such as existence or uniqueness of solution, are as yet unanswered (see Frisch [45] and texts on dynamical systems theory [6,8]). For this reason, most attempts to obtain the solution velocity field nowadays, are carried out numerically using appropriately formulated finite difference versions of the continuous equations.

Finite difference schemes discretise the governing equations both spatially and temporally onto an underlying grid (not necessarily regular) by truncating Taylor expansions for differentials to a specific order of accuracy. This allows efficient calculation of flow variables and time updating by computer algorithms; they are generically referred to as computational fluid dynamics (CFD) ‘solvers’.

It is possible however, to model the behaviour of a fluid (i.e. the Navier–Stokes equations) without directly tackling a NS numerical scheme. Such is the approach adopted in the main body of this work. Section 2.5 of the background material details how this is possible. In brief preview, a mathematical ‘creature’ is created (refined form of cellular automata (CA)), that is not a fluid, but which is endowed with just enough basic properties of fluids, to ensure that on mathematically ‘zooming out’ from idealised micro-scale

basis to the macro-scale, the observable and quantifiable attributes of the system assume essentially fluid dynamical character. Before going on to discuss this modelling scheme, it is timely to review some of the underlying statistical mechanics upon which it is based; this is discussed next. It is recommended that a good feel for the approach then be obtained, by reviewing section 2.5, before moving on to the main presentation of new results.

2.3 Statistical mechanics

The mathematics and ‘language’ of this thesis, is based centrally upon that pertaining to descriptions of random or complex systems. Randomness in the conventional sense may arise as a direct consequence of complexity, as even simple systems exhibit seemingly random behaviour if they are very large, have strong internal interactions (non-linearity) or if the observation timescale is relatively large. Randomness also arises in other ways — some processes are stochastic at core level. Both cases of system, may only be described, or have their characteristics inferred, in a statistical sense. The field of mathematical physics developed for such purposes is collectively referred to as statistical physics.

This branch of physics has seen a huge investment of effort over the years. Various subdivisions exist within the field, primarily reflecting the age and nature of the physics. For instance, it may be subdivided into classical and quantum descriptions and further into mechanical (deterministic) and, say, true stochastic systems.

Statistical *mechanics* is a term loosely relating to statistical descriptions of mechanical systems. Traditionally the systems are models developed for molecular level (microscopic) dynamics, usually in gases. The field envelopes a huge proportion of the great physics done around the end of the nineteenth / beginning of the twentieth century and provides the formal mathematical framework to which this work belongs. In essence it is the global (macroscopic) physics, of classical particle dynamics and interactions at the atomic scale. For the purposes of background to the work herein, this is encapsulated in the Boltzmann equation.

To present a full review of such a body of understanding, is not within the scope of this work. Hence material presented in the following is intended simply as a ‘taster’, of a small but representative selection of the more crucial topics. Good standard texts on the subject include [18, 19, 66, 93, 117].

2.3.1 Statistical physics for two essential equations

In order to fully understand and appreciate the material upon which this work is based it is advisable to develop a solid, practical knowledge, of the formalism and scope of the *Boltzmann equation*, which is of fundamental relevance. This equation may be derived in more or less physically intuitive ways. Rigorous derivation of the Boltzmann equation requires working within the Liouville formalism, the development of a knowledge of which is facilitated by observing derivation of the Liouville equation; hence the following section, 2.3.2. Both the Boltzmann equation and the Liouville equation describe simple models of gas systems — the dynamical evolution of a great number of idealised particles.

In a subsequent section 2.3.3, a comparatively intuitive Boltzmann derivation is followed. Parallels between the two formalisms will be discussed, in order to enhance the understanding that is sought. Before that however, some elementary topics from the statistical physics literature are described. This is to provide the necessary conceptual framework for the analyses. In addition, it is intended to clarify general points and technicalities such as notation, scope, assumptions and limitations of the methods employed.

A definition and discussion of phase space

Derivation and basis of the Liouville formalism depend upon the notion of *phase space*. For some readers this concept may require definition before headway is possible, hence the current discussion. Readers who are familiar with the concept of phase space should freely omit the following paragraphs.

Phase space is a theoretical construct which could be considered as a generalisation of the familiar Euclidian space — denoted \mathcal{R}^3 — which surrounds us. In \mathcal{R}^3 a unique *point* of that space may be exactly specified by stating its *coordinates*; three numbers, quantifying the distance in space that the point is at, along three mutually perpendicular or *orthogonal* axes, from an arbitrary space *origin* point. Mathematically then, the position of a point in the three dimensional Euclidian space is an ‘ordered triplet’, consisting of three scalar components with respect to three orthogonal axes. This idea is readily extended to any dimensional space, say n -D, by stating an ordered n -tuple of coordinates specifying a generalised idea of point in the n -dimensional space. Many examples of this exist, the mere inclusion of time creates the conceptually familiar idea of a ‘point in space-time’. It is a powerful tool however, and is of great use here.

Unfortunately phase space comes in two ‘flavours’, confusing the matter slightly, as will be seen. It may readily be accepted for instance, that the position and velocity of a particle, consisting of three spatial and three velocity components, may be taken together to construct a new six dimensional space. There, a point specifies exactly the position *and* velocity of a particle *simultaneously*. It provides an intermediate space, to a basis for Boltzmann’s *velocity distribution* (phase) space of the next section, 2.3.3. Alternatively, a parallel construction of arguably higher use and merit may be devised, involving position and *momentum* for the particles. This is more in keeping with the accepted notion of phase space, because momentum based analyses arise naturally in quantum mechanical and Hamiltonian analyses. That aside, it is apparent that the three velocity vector components of a particle v_i , $i = \{1, 2, 3\}$ may be considered *equivalent* as coordinates to the particles’ traditional position coordinates x_i in that they specify a vector quantity exactly, with respect to some known orthogonal system of axes. The

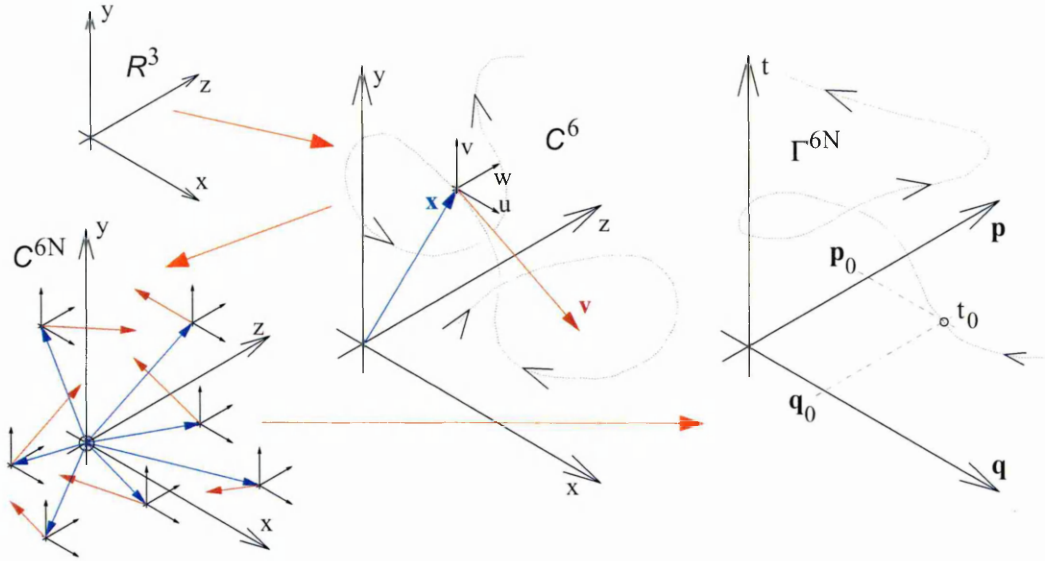


Figure 2.2: Generalisation of Cartesian space, via three stages, to the phase space. Following the arrows: from \mathcal{R}^3 to the six dimensional ‘configuration’ space of Boltzmann (x, y, z, u, v, w) , here denoted C^6 ; then, incorporating *all particles’* positions (blue vectors) and their velocities (red vectors) in a congruent physical space, denoted C^{6N} ; finally, true phase space, where all coordinates are equivalent except time, denoted Γ^{6N} . Note that in phase space momenta are used instead of velocities; also that in the diagram all coordinates are confined to the (\mathbf{p}, \mathbf{q}) plane and *time* is represented in the vertical axis.

same may be said for momentum coordinates.

Extending the idea one step further still, leads to an heuristic definition for the phase space. Following Gibbs [47], not just the six dimensions of a *single* particle’s position and momentum are included, but the six vector components for *all* the particles in the system of particles which constitutes the gas. For N particles this leaves a $6N$ dimensional vector, which is an ordered $6N$ -tuple, specifying a point in the $6N$ dimensional phase space. This *exactly* specifies the dynamic state of the whole system of particles at any one instant.

The phase space is often denoted by Γ and the point within it, variously by, for instance, (\mathbf{p}, \mathbf{q}) in the momentum-position formalism. This is a condensed ‘vector-style’ notation; the bold type is used to highlight the two $3N$ dimensional sub-space vectors⁷ in Γ . Notation for the coordinates of a Γ -space point is then as follows⁸

$$(\mathbf{p}, \mathbf{q}) = (p_x^{(1)}, p_y^{(1)}, p_z^{(1)}, q_x^{(1)}, q_y^{(1)}, q_z^{(1)}, p_x^{(2)} \dots p_\alpha^{(n)}, q_\alpha^{(n)} \dots q_z^{(N)}). \quad (2.27)$$

Here and in the following, the suffix $\alpha = \{x, y, z\}$ denotes spatial components and superfix

⁷This generalised notation is fine until one adopts consistent generalised forms for the various vector differential operators; div, grad, curl and ∇^2 etc. where some care is then due; see equation 2.36, item 6 of appendix A.2.

⁸See appendix on mathematical technicalities; A.2, item 5.

(n) is a particle label such that $n = \{n \in \mathcal{N} | n \leq N\}$; \mathcal{N} being the set of natural numbers.

Note that the trajectory of such a point, describes simultaneously, the exact dynamical evolution of all particles in the system under consideration (neglecting collisions for now). As will be seen, the Liouville equation describes the dynamical evolution of this point in a statistical sense; alternatively it describes the probable evolution and thus the behaviour, en mass, of the system.

It is pertinent to note at this stage that the definition of Γ provided here is lacking in some respects owing to its relative simplicity. Complicating factors exist, omitted here for brevity of exposition. For instance it is explicitly assumed that the dynamical state of the system is given by the $6N$ dynamical variables for position and velocity of particles and therefore that no degeneracy occurs for other modes of kinetic motion. So there can be no vibrational or rotational components to the energy and motion of particles, implying that they must be spherically symmetric and internally homogeneous. Our adopted system therefore is highly idealised in nature and forms a first approximation to real fluid behaviour.

In addition to this some very subtle assumptions are being made about the nature and density of the system, since if a particle has finite size then some subsets of the phase space are effectively excluded from occupation, as no two particles can occupy the same, or overlapping areas of real space. Other subtleties exist which are discussed as they arise, but they do not greatly alter the fact that the Γ -space concept is extremely useful for the mathematical description of complex dynamical systems.

2.3.2 The Liouville equation

The Liouville equation is widely regarded as the most fundamental equation in statistical physics. It belies descriptions of a wide range of physical systems, made within the statistical framework. It also provides the link between statistical properties of phase space and the real macroscopic phenomena that is observed and can be measured. What's more, it has validity in both the classical and quantum formalisms.

For this reason alone, inclusion of its derivation here may be warranted, however the argument is more powerful than that owing to the fact that the Liouville equation may be employed in rigorous derivation of the Boltzmann equation — which is of great importance in this work — and since the *language* of the Liouville derivation is used to arrive at many of the powerful statements of kinetic theory.

The Liouville equation derived

In the absence of collisions, or equivalently, for the case of true ‘point’ particles, equations of motion describing the motion of gas particles in the system are already in place. They are simply Newton’s second law applied to each particle, which gives rise to differential equations for each particle trajectory and, consequently, the evolution of the entire system. In the Hamiltonian formalism, Newton’s laws are expressed in terms of positions and conjugate momenta. For a system of N particles with three degrees of freedom, they are:

$$\dot{p}_\alpha^{(n)} = \frac{\partial H}{\partial q_\alpha^{(n)}} , \quad \dot{q}_\alpha^{(n)} = \frac{\partial H}{\partial p_\alpha^{(n)}} , \text{ for } \alpha = x, y, z \text{ and } n = 1, 2, \dots, 3N . \quad (2.28)$$

In principle it is possible to integrate this set of ODEs to obtain the functional form of $p_\alpha^{(n)}(t)$ and $q_\alpha^{(n)}(t)$ for all particles. However this is practically impossible for all but the simplest systems. The reasons for this impossibility lie in more than one factor; but primarily in that, to find an exact trajectory we need to specify an exact start point, say $(\mathbf{p}_0, \mathbf{q}_0)$ at time $t = t_0$. Knowing this ‘initial condition’ would permit determination of all constants of integration in the aforementioned integration. However, such data can never really be *known*, not least because their mere specification requires infinite accuracy.

On account of such *uncertainty* in data, it becomes logical to think in terms of a statistical framework. It seems plausible to determine a *likelihood* of the system being in a specific state at t_0 , or alternatively a probability distribution for initial state occupancy. This line of attack proves incredibly useful, partly because it bridges the gap between the theoretical and the practical, but importantly because for any specific set of state variables describing a whole system, a virtually infinite number of phase points are consistent.

This suggests the introduction of an ensemble of systems, in the traditional sense of statistical mechanics. Consider an ensemble consisting of N_S isolated systems⁹ (technically, the *micro-canonical ensemble*). The exact dynamical state of each system is given by a point in Γ and the ensemble appears as a ‘cloud’ of such points. To this cloud it is useful and fair to associate a density (number density), which, in the limit of infinite N_S may non-rigorously be regarded as having a value at all points, that is may be regarded a continuous function on phase space. Having dispensed with some mathematical pitfalls at this point, the idea is readily pursued.

A probability distribution function is defined, denoted $P(\mathbf{p}, \mathbf{q}, t)$, for the probable

⁹Note the distinction between number of particles N and number of systems in the ensemble N_S .

occupancy of states in Γ -space. Note that P is normalised as follows:

$$\int_{\Gamma} P(\mathbf{p}, \mathbf{q}, t) d\mathbf{p}d\mathbf{q} = 1, \quad (2.29)$$

that is, there are no regions for the state to occupy that aren't in Γ . Alternatively that the state is in Γ with probability certainty. The said number density of particles is then the product: $N_S P(\mathbf{p}, \mathbf{q}, t)$, that is the number of systems times the local probability distribution. In saying such, the following are assumed: firstly, that all areas of Γ are equally relevant; secondly, there is equal theoretical, or 'a priori', state occupancy probability. These are subtle but important points of relevance to establishing the validity of statements made within the Liouville, and to some extent Boltzmann, formalisms.

Now, since the motion of points in Γ is given by deterministic equations, noting also that the effect of *collisions* is *not* considered in the Liouville analysis¹⁰, it follows that an evolution equation for the distribution of systems in the ensemble may be derived. Hence if the distribution at $t = t_0$ is known, namely $P(\mathbf{p}_0, \mathbf{q}_0, t_0)$, it is possible to predict $P(\mathbf{p}, \mathbf{q}, t)$ at subsequent times. This is also equivalent to writing an equation of motion for the probability distribution in Γ -space. The Liouville equation is that equation.

Derivation here, of the Liouville equation, follows closely that given in [93] (p. 402 (also p. 118)) and is similar to those less rigorous presentations of other texts, such as [18, 66, 117]. The treatment is closely analogous to derivation of the continuity equation 2.8 of fluid dynamics, to which the reader is referred 2.2.1.

Consider now, an elemental volume in the phase space, denoted $d\mathbf{p}d\mathbf{q}$, where it is understood the 'bold' vector-style notation¹¹ merely hints at the two underlying $3N$ dimensional phase sub-spaces. Similarly, consider some finite arbitrary region in Γ , the volume of which being denoted V_T ; note that in terms of volumetric magnitude: $V_T \gg d\mathbf{p}d\mathbf{q}$. In general the number of phase points within the volume V_T will be proportional to the size of V_T but not to its shape. The number, denoted N_{V_T} is in fact the integral sum of the number density function over V_T , i.e.

$$N_{V_T} = N_S \int_{V_T} P(\mathbf{p}, \mathbf{q}, t) d\mathbf{p}d\mathbf{q}. \quad (2.30)$$

¹⁰It is this point which degrades the practical utility of the Liouville equation and distinguishes it from the Boltzmann equation. Such (important) matters are discussed as the Boltzmann equation is derived, 2.3.3.

¹¹Here $d\mathbf{p}d\mathbf{q}$ represents the product $dp_x^{(1)} dp_y^{(1)} dp_z^{(1)} dq_x^{(1)} \dots dp_x^{(2)} \dots dp_x^{(n)}, dq_x^{(n)} \dots dq_z^{(N)}$. Also often denoted $d^{3N}p d^{3N}q$. Again, see appendix on mathematical technicalities A.2, item 4.

This will in general vary with time, following the variation of P , giving

$$\frac{dN_{V_T}}{dt} = N_S \int_{V_T} \frac{dP}{dt} d\mathbf{p}d\mathbf{q}, \quad (2.31)$$

where the dependency notation is now dropped for brevity. This represents the net change in the number of phase points *within* V_T at any time.

Next consider the *flux* of phase points across the surface S of the volume as individual system ensembles evolve. Drawing analogy with aspects of the continuity equation derivation, the ensemble of phase points may be considered a fluid, but with density P . The motion of this fluid is the *velocity field in* Γ ; that is the time derivative of each coordinate, at every point, both coordinate types (momentum and position) having equivalent status. Defining this generalised velocity as the time derivative of (\mathbf{p}, \mathbf{q}) , here denoted \mathbf{u}_Γ :

$$\begin{aligned} \mathbf{u}_\Gamma &= (\dot{\mathbf{p}}, \dot{\mathbf{q}}) \\ &= (\dot{p}_x^{(1)}, \dot{p}_y^{(1)}, \dot{p}_z^{(1)}, \dot{q}_x^{(1)} \dots \dot{p}_x^{(2)} \dots \dot{p}_\alpha^{(n)} \dot{q}_\alpha^{(n)} \dots \dot{q}_z^{(N)}) \\ &= (\partial_t p_x^{(1)}, \partial_t p_y^{(1)}, \partial_t p_z^{(1)}, \partial_t q_x^{(1)} \dots \partial_t p_x^{(2)} \dots \partial_t p_\alpha^{(n)} \partial_t q_\alpha^{(n)} \dots \partial_t q_z^{(N)}), \end{aligned} \quad (2.32)$$

it is thus possible to derive an expression for the rate of flux of phase points across the volume surface. In the usual way the familiar ‘mass density equals mass over volume’ may be used, but adapted to ‘(surface elemental) number *flux* equals (local) number density times (local) volume-*rate*’. Here the volume-rate is the usual dot product of local velocity \mathbf{u}_Γ and elemental surface area, denoted $d\mathbf{S}$. Since the local number density is $N_S P(\mathbf{p}, \mathbf{q})$, this gives rise to

$$\left. \frac{dN_{V_F}}{dt} \right|_{\text{element}} = -N_S P \mathbf{u}_\Gamma \cdot d\mathbf{S}, \quad (2.33)$$

where the negative sign indicates outward flux for positive velocity. The total flux is then (in the absence of collisions), simply the integral over the entire surface S :

$$\frac{dN_{V_F}}{dt} = -N_S \int_S P \mathbf{u}_\Gamma \cdot d\mathbf{S}. \quad (2.34)$$

Again, as for equation 2.4, a (generalised) form of Gauss’ theorem may be applied to this result and transform the ‘*hypersurface*’ integral into a volume integral¹² giving

$$\frac{dN_{V_F}}{dt} = -N_S \int_{V_F} \nabla_\Gamma \cdot (P \mathbf{u}_\Gamma) d\mathbf{p}d\mathbf{q}, \quad (2.35)$$

¹²See mathematical technicalities, A.2, item 8

where it is understood that the divergence and ‘velocity’ \mathbf{u} terms’ subscript, Γ , denotes generalised forms of divergence and velocity for phase space vectors. That is that \mathbf{u}_Γ represents the phase space velocity and ∇_Γ the divergence operator in Γ -space; given by

$$\nabla_\Gamma \equiv \sum_{n=1}^N \left(\sum_{i=1}^3 \frac{\partial}{\partial p_i^{(n)}} + \sum_{i=1}^3 \frac{\partial}{\partial q_i^{(n)}} \right). \quad (2.36)$$

Here the terminology means that the sum over the set $i = 1, 2, 3$ actually denotes summation over spatial components x, y, z of $\dot{\mathbf{p}}^{(n)}$ and $\dot{\mathbf{q}}^{(n)}$ respectively for any particle n .

Now, each possible phase point represents a potential state of the system and as such they may neither be created or destroyed. For this reason, if the two phase space volumes coincide, $V_T = V_F = V$, then the two terms 2.31 and 2.35 derived above must be equal: $dN_{V_T}/dt = dN_{V_F}/dt$, alternatively their difference is zero, or the net influx and efflux of phase points within V_F must be zero:

$$N_S \int_{V_T} \frac{dP}{dt} d\mathbf{p}d\mathbf{q} + N_S \int_{V_F} \nabla_\Gamma \cdot (P\mathbf{u}_\Gamma) d\mathbf{p}d\mathbf{q} = 0. \quad (2.37)$$

The case of coincidental volumes, $V_T = V_F$, allows combination of terms to form one integral. Moreover, the relation 2.37 is valid for *arbitrary* choice of volume V ; hence, since the integral is always zero for arbitrary V , the integrand must be zero over all regions as corollary. The implication being analogous to that for the continuity equation 2.8:

$$\frac{dP}{dt} + \nabla_\Gamma \cdot (P\mathbf{u}_\Gamma) = 0. \quad (2.38)$$

This is the Liouville equation in its most concise form¹³; some discussion on it now follows. Most comments are necessarily quite theoretical in nature; compare the following with those for the Boltzmann equation of pages 42 on.

The Liouville equation, 2.38, describes the motion of the system phase state (point) in the theoretical phase space Γ . It also describes the nature of the probability density and in that respect is similar to the continuity equation 2.8 of fluid dynamics. This allows quite simple interpretational alternatives to the equation to be stated (see Gibbs’ original works and [47]): 1) the Jacobean determinant, for transformation of coordinates in Γ , is unity; 2) the density of phase points is conserved along a system trajectory, because volume is similarly conserved; 3) equivalently, the phase space ‘fluid’ is incompressible; 4) phase space trajectories do not cross. Refer to figure 2.3 for diagrammatic representation. It is

¹³There exists many ways of expressing this equation, each having specific advantages and disadvantages, dependent on the context; see appendix 7 herein. See also [93] for Hamiltonian forms and the ‘Liouville operator’.

not trivial to attain good understanding of these equivalent statements, for this reason the interested reader is referred to the general literature, say [47, 66]. Finally, an important theorem on phase space assures us that the system will always return arbitrarily close to its start point if given enough time. This is the Poincaré recurrence theorem, [105], mentioned in the following discussion on the Boltzmann equation.

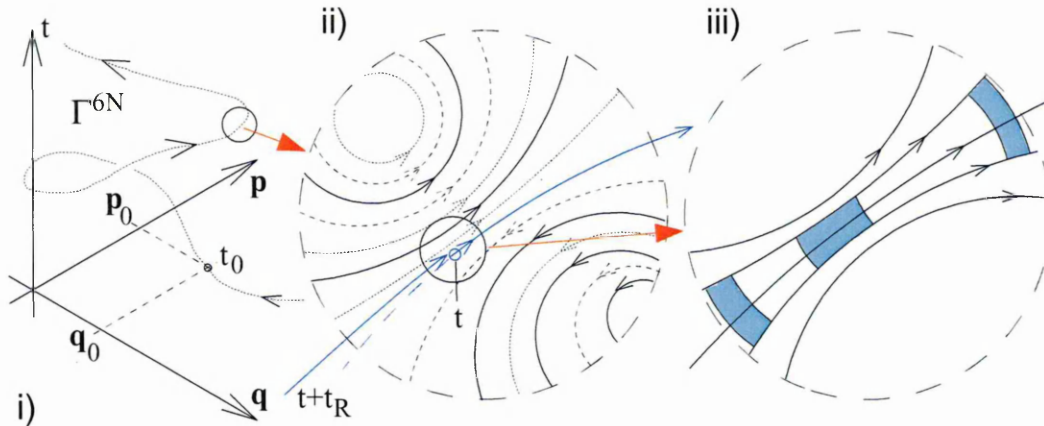


Figure 2.3: Aspects of the nature of phase space. Part i) is representation of phase space itself, with the evolution of a phase point over time (motion). Part ii) represents a portion of Γ , highlighting that phase trajectories cannot cross, no matter how complex their actual topology. The motion highlighted blue demonstrates the Poincaré recursion theorem: the system will always return arbitrarily close to its original state after the recursion time, here denoted t_R . Part iii) represents the various Liouville conservations along a system motion. The coloured volume, whilst changing shape, preserves both its volume and the density of phase trajectories inside.

Note that the Liouville equation does *not* incorporate the effect of collisions between particles. By assuming that the particles are point like, it is also implicitly assumed that they have zero collision cross-section and therefore don't collide. In this respect the Liouville equation is purely Newtonian, deterministic and effectively reversible: a system phase space trajectory, could equally well be followed in either direction — the evolution is deterministic and one to one. This is the primary way in which it differs from Boltzmann's result, which imposes a preferred direction of time.

Boltzmann's result, 2.49, to follow, can be thought of as a realisation of Liouville's more theoretic counterpart, and collision processes aside, may be derived from it. The importance of the two is acknowledged in fields as diverse as astrophysics, plasma physics and fusion, gas kinetics, many body systems, combustion and, most relevantly here, even hydrodynamics.

2.3.3 The Boltzmann equation

No exposition may be made, of the modern *lattice Boltzmann theory* or the material upon which it is based, without first setting the historical and physical context that the LB formalism occupies. The lattice Boltzmann scheme, as its name suggests, is a modern discrete parallel to its more theoretically interesting counterpart, the Boltzmann equation. Ludvig Boltzmann [1844–1906] developed the equation that bears his name, during the nineteenth century (see for instance [14]), at a time when all physics was ‘classical’. It is within this framework that the theory possesses most of its validity.

Boltzmann’s approach focused squarely upon gases, but it transpires that his work is a valid explanation and description for more general condensed matter, namely fluids. Specifically, he considered the case of simple gas molecules, undergoing binary only collisions; the meaning of such terms is expanded upon in the following. Primarily, they possess no capability for storing energy to rotational or vibrational degrees of freedom, nor mechanism by which the energy associated with translational degrees of freedom may be dissipated. This simplification is concomitant to underlying assumptions that the particles are spherically symmetric and possess no internal structure. Here the focus is on single species, monatomic gases.

Note the loose, interchangeable use of the words molecule and particle. What is meant is a point like entity, resembling an atom in that it is considered a ‘fundamentally indivisible part’. Generalisation to multiple species or to molecules with internal degrees of freedom is relatively simple in all respects except notation; the former being carried out in most relevant texts. See for instance [18, 19, 66, 93] for good general treatments.

What Boltzmann generated was a statistical description of dynamic processes at a molecular level, which, crucially, took account of collision processes. In bringing in this increased realism in the particle physics, over that of the Liouville equation, he turned theoretical utility into practical validity. Central to the picture is the concept of the ‘velocity distribution function’, the dependent solution variable of the Boltzmann equation, which is to be defined and further described next.

Notation and basis

The essence of Boltzmann’s analysis is an attempt to determine global and macroscopic properties or behaviour of an assembly of a great many modelled particles undergoing microscopic dynamical processes. The work draws heavily from that great monument of knowledge known broadly as statistical physics. For a full discussion of Boltzmann gas kinetics, see for example [18, 19, 66, 93], or any similar text.

Boltzmann firstly creates a formalism for describing the states that such a system may

occupy, the so called ‘velocity distribution function’, $f(\mathbf{x}, \mathbf{v}, t)$. This is a *single particle distribution function* for state occupation in configuration space; equivalent to a particle probability density¹⁴, over positions in the range $[\mathbf{x}, \mathbf{x} + d\mathbf{x}]$ and velocities in the range $[\mathbf{v}, \mathbf{v} + d\mathbf{v}]$ at time t . The velocity distribution is therefore only superficially similar to the probability density $P(\mathbf{p}, \mathbf{q}, t)$ of the Liouville derivation; note that the ‘space’ of the Boltzmann distribution is a ‘configuration’ space, as opposed to the phase space — see \mathcal{C}^6 of figure 2.2. It also differs in that there is no reflection of Γ -space’s multi-particle nature¹⁵, only ‘a’ (singular) position and motion define the dimensionality — the space is *six* dimensional.

The Liouville probability distribution P , automatically, by its definition, took account of the many individual particles in the system. In that way it is a form of multi-particle distribution function, equivalent for instance to the product¹⁶ of single particle distributions, let’s call $P_1^{(n)}$ say, one for each particle, n :

$$P(\mathbf{p}, \mathbf{q}, t) \equiv \prod_n P_1^{(n)}(p_x, p_y, p_z, q_x, q_y, q_z, t), \text{ for: } 1 \leq n \leq N. \quad (2.39)$$

where N is the number of particles. The single particle distributions exist over overlapping or *congruent* six dimensional spaces, $(p_x, p_y, p_z, q_x, q_y, q_z)$. Boltzmann’s distribution function can be interpreted heuristically as just one of these, for an arbitrary particle, n^* . So, in effect, it is $P(\mathbf{p}, \mathbf{q}, t)$ integrated or averaged over $N - 1$ coordinates of (\mathbf{p}, \mathbf{q}) as follows:

$$f(\mathbf{x}, \mathbf{v}, t) \equiv P_1^{(n^*)}(p_x, p_y, p_z, q_x, q_y, q_z, t), \quad (2.40)$$

where (q_x, q_y, q_z) is effectively the same as (x, y, z) .

The following moments of the velocity distribution function are initially defined¹⁷

$$\int_{\mathcal{S}_C} f(\mathbf{x}, \mathbf{v}, t) d\mathbf{x}d\mathbf{v} = M, \quad (2.41)$$

where \mathcal{S}_C is the entire accessible configuration space; contrast with normalisation of P ,

¹⁴Note the density *at a point* is zero; similarly, the expected number of particles with position, \mathbf{x} and velocity, \mathbf{v} is zero — the point has zero measure.

¹⁵In addition to common usage of velocity, \mathbf{v} , over momentum, \mathbf{p} .

¹⁶Probability of combination of individual *independent* events is the product of individual probabilities, note. See equation 2.39.

¹⁷Note that some presentations use different definition for f . Here we follow Cercignani [18], in which f is a ‘mass distribution’ function.

equation 2.29. Also:

$$\int_{\mathcal{S}_V} f(\mathbf{x}, \mathbf{v}, t) d\mathbf{v} = \rho(\mathbf{x}, t), \quad (2.42)$$

$$\int_{\mathcal{S}_V} f(\mathbf{x}, \mathbf{v}, t) \mathbf{v} d\mathbf{v} = \rho(\mathbf{x}, t) \mathbf{v}(\mathbf{x}, t), \quad (2.43)$$

where \mathcal{S}_V the entire velocity space. Here, M is the total mass of gas, $\rho(\mathbf{x}, t)$ is its local density. Later, other moments are used that further indicate the nature of f .

Derivation

By considering fluxes and balance equations for the velocity distribution function, the Boltzmann equation may be derived in a way very similar to: that for the Liouville equation, in section 2.3.2; and that for the mass continuity equation of fluid dynamics, section 2.2.1. Hence it is perhaps not surprising that, when the macroscopic behaviour of the microscopic Boltzmann formalism is investigated, fluid dynamical properties are arrived at; there is some underlying similarity or truth behind it all.

Here, for purposes of indicating equivalencies between derivation approaches, it is helpful to follow an alternative route. This method may just as effectively be applied to continuity or Liouville derivation, the latter case however, would generate some notational complexity, obscuring the point. Here the reduced dimensionality of the configuration space is more amenable and makes the formal arguments more transparent.

Crucially the effect of collisions is invoked; the beauty of which only becomes apparent upon further analyses. These will be discussed here briefly in the comments, page 42 on. Also crucially, the Boltzmann equation addresses the case of *dilute* gases. In a dilute gas, molecules are taken to spend large periods of time between collisions. Moreover, collisions between three or more particles are considered extremely rare and therefore negligible in their effect. The specific domain of validity is known as the Boltzmann gas limit (BGL), which is discussed further in later the comments, page 42.

Under these circumstances the state of the gas relates more closely to the singlet particle distribution — hence the applicable definition of f , given previously: page 38 on. Moreover, whilst f represents probability, it also, for a finite volume, $dx d\mathbf{v}$ say, represents particles. So, in the absence of collisions, the mass density field at some configuration space point (\mathbf{x}, \mathbf{v}) , namely $f(\mathbf{x}, \mathbf{v}, t)$, is expected to evolve entirely deterministically according to simple dynamics.

In fact the mass density function at the evolved point, consists exactly of the evolved particles from the initial point, i.e. they are the same. Positions change from \mathbf{x} to $\mathbf{x} + \Delta_t \mathbf{v}$ (old position, plus velocity times time duration); similarly velocities change according to

the acceleration: $\mathbf{v} \rightarrow \mathbf{v} + \Delta_t \mathbf{X}$, where X is force per unit mass; and time increments by Δ_t . Hence

$$f(\mathbf{x} + \Delta_t \mathbf{v}, \mathbf{v} + \Delta_t \mathbf{X}, t + \Delta_t) = f(\mathbf{x}, \mathbf{v}, t), \quad (2.44)$$

in the absence of collisions.

The RHS of equation 2.44 is readily identified as the result of Taylor expanding the function f , but in the higher (six) dimensional space. Carefully establishing appropriate gradient terms for this space allows the velocity distribution function f to be expanded as follows:

$$f(\mathbf{x} + \Delta_t \mathbf{v}, \mathbf{v} + \Delta_t \mathbf{X}, t + \Delta_t) = [1 + \Delta_t \partial_t + \Delta_t (\mathbf{v} \cdot \nabla) + \Delta_t (\mathbf{X} \cdot \nabla_{\mathbf{v}})] f(\mathbf{x}, \mathbf{v}, t), \quad (2.45)$$

where, to accuracy of order Δ_t , $\mathcal{O}(\Delta_t^2)$ terms are ignored. Note that the forcing term dot product $\mathbf{X} \cdot \nabla_{\mathbf{v}}$ is between the forcing vector, \mathbf{X} and gradients with respect to velocity coordinates, $(\partial_{v_x}, \partial_{v_y}, \partial_{v_z})$, hence the del operator subscript \mathbf{v} .

Combining equations 2.44 and 2.45, with Δ_t set to unity and incorporating a book-keeping term, say $\partial f / \partial t|_{\text{coll}}$, to account for the effect of collisions, gives

$$\frac{\partial f}{\partial t} + (\mathbf{v} \cdot \nabla) f + (\mathbf{X} \cdot \nabla_{\mathbf{v}}) f = \frac{\partial f}{\partial t} \Big|_{\text{coll}}. \quad (2.46)$$

In essence this is the Boltzmann equation. It has LHS which is effectively a substantive derivative, but with forcing term also (third on LHS); the RHS is an undefined collision operator. So far, the RHS collision term $\partial f / \partial t|_{\text{coll}}$ merely *accounts for* the net effect of mass scattered both into and out of the stream from (\mathbf{x}, \mathbf{v}) to $(\mathbf{x} + \Delta_t \mathbf{v}, \mathbf{v} + \Delta_t \mathbf{X})$ due to collisions. As yet no physics has gone in to specify its nature.

Rigorous microdynamical analyses of collision processes give rise to collision terms necessarily dependent upon the *two* particle distribution function f_2 — obviously the chance and nature of collision depends on the chances of the two particles being in the right place at the right time. This gives rise to an ‘open’ and therefore insoluble system (two particle distribution depends upon three and so on). However it is possible to express f_2 in terms of f_1 ($f_1 = f$ note) as the combined probability of two individual independent events (i.e. the product of probabilities for the two occurrences):

$$P_{2N}^{(2)}(\mathbf{p}, \mathbf{q}, \mathbf{p}_*, \mathbf{q}_*, t) = P_N^{(1)}(\mathbf{p}, \mathbf{q}, t) P_N^{(1)}(\mathbf{p}_*, \mathbf{q}_*, t), \quad (2.47)$$

where $*$ denotes the second particle and which, for $f_1 \equiv f$, translates to

$$f_2 = f f_*. \quad (2.48)$$

Again, see appendix A for notations and meanings.

This is the nature of Boltzmann's 'molecular chaos' assumption, often called the 'stosszahlansatz'. It effectively says there is no correlation¹⁸ between the two particles velocities *before* any collision and crucially defines the range of validity of the ensuing Boltzmann equation. Validity of the assumption weakens as the density of the system increases, as in reality, some correlation does exist.

Here, the detailed form of Boltzmann's collision term is not investigated further. It is arrived at by considering scattering cross sections and angles for two body collisions and bears only minor relevance to the aim here. Instead Boltzmann's eventual result is merely stated, as follows:

$$\frac{\partial f}{\partial t} + (\mathbf{v} \cdot \nabla) f = \frac{\sigma^2}{m} \iint (f' f'_* - f f_*) |\mathbf{v}_r \cdot \mathbf{n}| d\mathbf{n} d\mathbf{v}_* . \quad (2.49)$$

Here, m is particle mass, σ is the particle scattering cross section, \mathbf{n} is a unit vector meaning that integration occurs over all directions (strictly here \mathbf{n} varies over one hemisphere), and \mathbf{v}_r is the two particle's relative velocity as follows:

$$\mathbf{v}_r = \mathbf{v} - \mathbf{v}_* . \quad (2.50)$$

Other distribution terms, (f 's), are distinguished: according to which particle (second one denoted by subscript *); and by pre- and post-collision velocities (latter primed), given as follows:

$$\begin{aligned} f' &= f(\mathbf{x}, \mathbf{v}', t), & \text{where: } \mathbf{v}' &= \mathbf{v} - \mathbf{n}(\mathbf{n} \cdot \mathbf{v}_r), \\ f'_* &= f(\mathbf{x}_*, \mathbf{v}'_*, t), & \text{where: } \mathbf{v}'_* &= \mathbf{v}_* + \mathbf{n}(\mathbf{n} \cdot \mathbf{v}_r), \\ f_* &= f(\mathbf{x}_*, \mathbf{v}_*, t). \end{aligned} \quad (2.51)$$

In equation 2.49, external forcing terms have been neglected. Note also that integration is over velocity of the second particle. The collision term, RHS of equation 2.49, is often abbreviated to $Q(f', f)$.

Comments

Equation 2.49 is the Boltzmann equation in its well known form. At a fundamental level it expresses simple continuity arguments and balances for a system of elastic spheres in a

¹⁸Here correlation applies between velocities of two particles approaching a collision. In real fluids, liquids especially, to which the Boltzmann formalism possesses some validity, there is in fact finite correlation on a local scale.

manner entirely analogous to the mass and momentum balance equations of continuum fluid dynamics. It is an *integro*-differential equation, describing the evolution of the velocity distribution function. A quick review reveals two primary aspects to its nature: the LHS is analogous to a substantive derivative in continuum theory, which describes the convection and advection of an idealised gas; whereas the RHS integral, $Q(f, f')$, is a specific representation of particle collision effects for Boltzmann's hard elastic sphere model.

It is the latter of the two contributions — incorporation of realistic, but complex, particle collision effects within the gas — that makes the Boltzmann equation valid for classes of real fluids; without this it would possess little practical value. Moreover, therein lies its intractability.

The most fundamental corollaries of Boltzmann's collision arise with the molecular chaos ansatz, the weakest but most significant aspect of the derivation. By invoking the stosszahlansatz, Boltzmann introduced *non-determinism* by the back door. This not only diversifies away from Newtonian mechanics and predictability, significantly, it introduces the '*arrow of time*'. Up to this point the (Liouville) dynamics are entirely reversible — invariant under time reversal — and regions of Γ map, one to one, in either direction, to other regions of Γ . Now, the randomness encapsulated in the stosszahlansatz meant the following:

- The dynamics are irreversible — mappings under time translation, in phase or configuration space, are no longer one to one.
- A functional of the velocity distribution function — namely H — is found to only ever change by decreasing; this is the famous H-theorem.
- The functional H reveals the existence of equilibrium states and that the system will continuously evolve toward these.
- H also provides a means to find equilibrium states, thus facilitating demonstration that the equilibrium is Maxwellian.
- H can be associated with an ever increasing entropy — hence physical interpretation of irreversibility and the arrow of time.
- Interesting theoretical corollaries emerge, revitalising philosophical debate on the meaning of entropy, reversibility and the recurrence time:
 - Loschmidt's initial objection [85–87] regarding the existence of at least one motion for which H would increase — the reverse motion.

- Zermelo’s paradox, see for example [154–156], which bases its argument on the Poincaré recursion theorem [105], that a system must eventually return arbitrarily close to its original configuration. See figure 2.3.

The greatness of Boltzmann’s work was not realised until much later. Note for instance that at the time, even the ‘atomistic’ nature of matter — a cornerstone of modern physics, which has since only been *adapted* by quantum mechanics — was not yet accepted! Depressed by the lack of faith in his work, even hostility toward his ideas, and for unclear personal reasons, Boltzmann took his own life in 1906. The poignancy of this tragic outcome becomes more acute when viewed retrospectively; it was not long after that that atomistic physics was accepted and Boltzmann’s work took its founding place for a whole new discipline.

Most of the objections (which were quite scathing) were not rigorously resolved until years later, in the works of the Ehrenfests [39] and later still Smoluchowski [126]. The latter of these painted our modern picture of the ‘reality’ of phase space; it also effectively redefined what is meant by equilibrium and highlighted the role of ‘non-equilibrium fluctuations’.

Diversifications of Boltzmann’s gas kinetic models were developed and analysed in ensuing years. However, in terms of balance between breadth of validity and depth of realism, equation 2.49 and its variants will always rank highly. In that respect, some regard the Boltzmann equation as one of the most important equations of classical physics, though this point of view has been described as exaggerated by others. Whatever the stance taken, it is true that the equation has stood the test of time, unaltered from its original form, being as valid today as it ever was. That it has stood such a test is largely due to its simplicity of reasoning, hand in hand with its practical utility.

For further modern reading on the Boltzmann equation, including: means to approach its solution, various theoretical and practical issues and its: range of validity, weaknesses and strengths, there can be few better works than Cercignani’s [18]. Therein close reference is made to the current literature too. Furthermore, a small but significant proportion of Boltzmann’s own work has been published — translated to English — and is currently still available, see Brush [14].

Limitations and scope of gas models are briefly discussed in section 2.5, where the context is more in keeping with this work. In particular, the scope of discretised dynamical gas models *of liquids* — the LB — is emphasised.

2.4 Turbulence

The general intractability that turbulence has presented to theorists over the past century or so has given rise to the development of some spectacularly creative and diverse schemes aimed toward understanding and predicting the primary characteristics of typical turbulent flows. These schemes, some elegant others artless in their general approach, exemplify some of the best creativity originating in the field of science. Progress has however proved grueling, and nowadays, especially with the explosion in availability and performance of computational hardware, much effort is directed toward either modelling turbulent flow characteristics, or directly simulating the flow (DNS), usually with some form of small scale cut-off mechanism incorporated (e.g. large eddy simulations (LES) or sub-grid scale (SGS) models).

Here is not the place to present a review of the vast literature that has appeared on this subject over the years, it is too diverse in origin and range of validity. Instead, the intention is to build a solid knowledge base and framework of reference material, upon and around which much of the subsequent discussion will be based.

The presentation starts with a brief review of some core turbulence phenomenology, to include: Reynolds number and transition and flow similarity. Any detailed treatment should ideally consider: the energy budget and cascade, some dimensional analysis, vortex dynamics and other heuristic theories; unfortunately, here there is not the scope. Instead, the discussion moves on to describe central issues regarding transition to turbulence and how the turbulent fluctuations are sustained. Beyond that, the focus moves to the so called Reynolds decomposition; an early and important analysis which leads to the Reynolds averaged Navier–Stokes equations. This material is of great relevance to the work described later. Finally a brief review is provided of the commonly encountered modelling strategies; again, this material is of great relevance in subsequent chapters.

2.4.1 Some turbulence phenomenology

This section presents a small selection of material frequently encountered during studies on turbulence. It includes both aspects of the nature of turbulence itself and some conventions regarding the framework within in which it is commonly viewed and described. Treated firstly is what must be the single most useful parameter used in fluid dynamics — an unavoidable aspect of the phenomenology — the Reynolds number. Strictly speaking this might be more appropriately defined in later sections, say 2.7 page 111, in the context of *complete flow realisations*, that is ‘fluid, plus geometry, plus flow forcing’. However, it is included here by necessity, as a consequence of its fundamental descriptive

utility.

Reynolds number and transition to turbulence

The Reynolds number is a dimensionless grouping of basic fluid and flow parameters, which describes and parameterises the level to which a flow is ‘driven’ or subjected. First utilised in founding works by Reynolds, initiated in 1883 [115] (and up to [116]), it is used as a means to fairly compare the physical state of a flow between different regimes and scenarios.

It is constructed from length ℓ , velocity V and viscosity ν parameters, which have dimensions: $[L]$; $[LT^{-1}]$ and $[L^{-2}T^{-1}]$ respectively, the latter being the kinematic viscosity (η/ρ). These combine as follows:

$$Re = \frac{\ell V}{\nu}, \quad (2.52)$$

to give the dimensionless Reynolds number. Other definitions may be made depending on the context.

Typically the mean flow velocity is used, hence the capitalisation. Length parameters may be arbitrarily chosen, but must be consistent if direct comparison of distinctly different flow types is required. For the case of simple channel geometries, as utilised in this work, a measure of the channel width is all that is required. Some care is required however and the issue is addressed properly in the section on hydraulic radius, see page 97. Pre-empting that to be specific, the channel hydraulic diameter, \varnothing_h , is typically used for the length parameter ℓ .

It is only in the context of Reynolds number that *similarity* between flows may be considered; see ‘similarity principle’ in the next section, page 47. Similarity may be defined between flows, over ranges of Re , after realising that flows generated for various forcings and geometries may be considered equivalent if their Reynolds numbers are equal.

Just as importantly, the Reynolds number describes the point around which transition between laminar to flow turbulent regimes occurs. A brief discussion of the mathematics of transition is provided in a later section herein, 2.4.2. When driving conditions in a laminar flow mean the Reynolds number approaches certain value Re_{cr} , the laminar nature of flow spontaneously degenerates into apparent random motion superimposed onto an altered mean — this being a primary finding of Reynolds’ early papers [115,116]. A brief aside is now taken to illustrate the utility of the Reynolds number in that context.

In his famous experiments, of flow gradually constrained into a long and regular glass tube, complete with an injected dye trace, [115,116], Reynolds observed the following:

- For low driving conditions (Re) the flow is ‘laminar’ — fluid flows in continuous

annular layers which slip over each other; shear does not change between layers, giving a parabolic profile.

- At some level of forcing, now denoted Re_{cr} , spontaneous disruptions of the laminar nature emerge intermittently.
- Any higher level of forcing generates a fully turbulent flow state — complex, apparently random motion, imposed over a distinct average profile.
- Illuminating the turbulent flow state by electrical discharge reveals the complex nature of the sinuous motion.
- Improving the isolation of the apparatus and thereby decreasing perturbations on the flow enables higher Reynolds number to be reached in the laminar state, before transition.
- Finally, there appears to be no basis to suggest that transition *must occur* at any Re ; decreasing disturbances always led to higher transition — a modern day point of contention.

See any good fluid dynamics / mechanics text.

The point at which transition is initiated is thereafter denoted the critical Reynolds number, Re_{cr} . Below that point the flow is laminar and stable; above it, infinitesimal flow perturbations are amplified through non-linear terms of the Navier–Stokes equations and the flow exhibits instability of one form or another. See section 2.4.2.

Flow similarity principle

Note that ‘similarity’ in the sense it is to be defined in the following, is applicable in the context of both turbulent and non-turbulent flow; however, it is strictly only valid in incompressible fluids. It may be arrived at by observing symmetries in the equations of motion for the fluid. However, it is also an apparent feature of (laminar) flows suggested under even casual observation.

The similarity principle says that there is only one parameter which describes a flow for any particular configuration of flow boundaries, no matter what their size. That parameter is the Reynolds number; the dimensionless grouping of the earlier section, page 46. As a consequence, flows in the same shaped geometry are similar (and described as so) if their Reynolds numbers coincide, even when their size, velocity or viscosity differ.

The implication that ‘all / total’ size has no bearing on a flow realisation is more precisely a reference to scale and it is the *scale invariance symmetry* of the underlying

Navier–Stokes equations which lies at the heart. This will not be detailed further here, those interested might refer to say [45].

Experimental investigations demonstrate its validity for both laminar and turbulent flows. In the former it is visible in streamlines; in the latter it is only true and therefore only observable in a statistical sense. That is, turbulence actually breaks some of the symmetries, but taking suitably long term averages of measured properties reveal that, especially at high (limiting) Reynolds number, the averaged values possess equivalent symmetries.

It can be proved in more advanced theoretical studies how symmetries are restored in a statistical sense. In that respect the book by Frisch [45] is an especially good starting reference.

In a common practical sense, the similarity principle has as corollary, that bodies of equivalent shape have the same ‘drag coefficient’ no matter what their size. Drag coefficient — being defined in essence to utilise this point — is therefore an ideal parameterisation, of the shape (form) or design quality of a body, with respect to efficiency of movement through a fluid.

2.4.2 Stability and the transition to turbulence

The following few pages provide a brief mathematical description of the onset of turbulence. This is of interest partly because it illustrates an important tool in the physicist’s arsenal for investigating complex systems; namely perturbation approaches and spectral analyses. Some comments in later chapters assume a degree of familiarity with such concepts.

Not every solution of the equations of motion, even if exact, can occur in nature. Natural flows must obey the governing equations but also be stable.

Stability of a flow means that any inevitable perturbations that occur as a natural feature of real systems, must have a tendency to decay in magnitude over time. When there is a converse tendency for these perturbations to grow over time the flow is said to be (absolutely) unstable.

Adopting the notation $\mathbf{v}'(\mathbf{x}, t)$, for a small perturbation on the steady solution, $\mathbf{v}_0(\mathbf{x})$, to the fluid dynamic equations, implies the velocity decomposition:

$$\mathbf{v} = \mathbf{v}_0(\mathbf{x}) + \mathbf{v}'(\mathbf{x}, t), \quad (2.53)$$

where, note, $\mathbf{v}_0(\mathbf{x})$ has no time dependence by definition. Similarly for the pressure, set

$$p = p_0(\mathbf{x}) + p'(\mathbf{x}, t). \quad (2.54)$$

Upon substitution of equations 2.53 and 2.54 into the governing Navier–Stokes equation, 2.19, a *soluble* equation for the velocity perturbations is generated. This is made possible on appeal to the fact that $\mathbf{v}_0(\mathbf{x})$ and $p_0(\mathbf{x})$ are ‘known’ functions, which themselves satisfy the Navier–Stokes equation:

$$(\mathbf{v}_0 \cdot \nabla)\mathbf{v}_0 = -\frac{1}{\rho}\nabla p_0 + \nu\nabla^2\mathbf{v}_0. \quad (2.55)$$

Also, since the quadratic terms in \mathbf{v}' generated in the substitution are negligible, under the presumption that the perturbation is small. The following is derived:

$$\partial_t\mathbf{v}' + (\mathbf{v}_0 \cdot \nabla)\mathbf{v}' + (\mathbf{v}' \cdot \nabla)\mathbf{v}_0 = -\frac{1}{\rho}\nabla p' + \nu\nabla^2\mathbf{v}'. \quad (2.56)$$

Here the independence of \mathbf{v}_0 with time has nullified a $\partial_t\mathbf{v}_0$ term (continuity equation).

This PDE for $\mathbf{v}'(\mathbf{x}, t)$ is seen to be *linear*, in contrast to the usual Navier–Stokes equation (also non-parabolic), with coefficients which are ‘known’ functions of \mathbf{x} and not t . The general solution of such may be written as a sum of solutions in which $\mathbf{v}'(\mathbf{x}, t)$ depends on time as $e^{-i\omega t}$:

$$\mathbf{v}'(\mathbf{x}, t) \approx \sum_{\omega \in \Omega} A_\omega(t) f_\omega(\mathbf{x}), \quad A_\omega(t) \approx (\text{constant})e^{-i\omega t}. \quad (2.57)$$

The discrete (p indexed) $\omega \in \Omega$ therein, are determined by solving equation 2.56 with appropriate boundary conditions (the particular solution). They are in general complex:

$$\omega = \omega_p + i\gamma_p. \quad (2.58)$$

Now, the crucial term in this analysis is:

$$A_\omega(t) \approx (\text{constant})e^{-i\omega t}; \quad (2.59)$$

from equation 2.57, part two. This, dependent on the values taken by ω and on the index p , can represent either:

- A damped oscillation, where γ_p is negative;
- A non-oscillating, monotonically increasing or decreasing, function where γ_p is zero.

This case is of little interest here as we have already assumed the fluctuating velocity term to be composed of oscillatory contributions.

- An unstable and therefore increasing oscillation, where γ_p is positive. This case is crucial, as it describes a spectral mode which is (once initiated) increasing in time.

Bearing the above points in mind, then stable laminar flow must consist of $\gamma_p = 0$ for all possible ω_p (all p). However, consider the effect of increasingly exciting the flow; such as occurs when conditions such as forcing, velocity and shear stresses are increased, or when viscosity (the damping mechanism) is reduced.

As the Reynolds number increases and additional modes are excited, eventually it will reach a critical value $Re = Re_{cr}$ the ‘critical Reynolds number’ at which point a mode is excited where ω_p is negative. From that instant, as modes couple to modes, each of which may at any time have the property $\omega_p < 0$, the flow exhibits gross instability and may be described as in a turbulent state. Such ‘blow up’ — see Frisch [45] — describes the onset of turbulence well¹⁹.

In the following section, reference will be made to a decomposition of the velocity and pressure fields which is superficially similar to this, but where the *net* effect of the $A_\omega f_\omega$ terms accumulate to form a single contribution. The fluctuating term there is supposed to be stochastic and, in general, is not of small magnitude; in contrast to assumptions for the true perturbation \mathbf{v}' . Care must be taken to not blur the distinction between the two.

2.4.3 Averaged equations and the closure problem

Reynolds, in his now antique work on the subject [115, 116], revealed the nature of the beast to some extent. His approach took as basis a decomposition of the velocity field into the sum of two distinct contributions, suggesting that \mathbf{u} be comprised of the mean flow, plus a fluctuating part representing the effect of the turbulent eddies. In the following discussion, the following decomposition notation is used²⁰

$$\mathbf{u}(\mathbf{x}, t) = \mathbf{U}(\mathbf{x}) + \tilde{\mathbf{u}}(\mathbf{x}, t). \quad (2.60)$$

Hence, the velocity field is assumed to consist of the sum of an average term, \mathbf{U} , and fluctuating term or perturbation $\tilde{\mathbf{u}}$ ²¹. Importantly, note that the velocity average term

¹⁹Note, the basis for the above analysis was taken from Landau and Lifschitz [81] which is a recognised classic of the literature.

²⁰Note, the notation here does not conform to any work thus far cited. Discussion of this and summary of notations is provided in appendix A.3.1, page 260.

²¹Note that the perturbations here need not be small, as is required in strict perturbation expansions.

\mathbf{U} , is spatially but not temporally dependent, representing a point average over time; in contrast, other contributions vary with both space and time. The nature of the averaging is of great relevance to the analysis, a matter addressed in more detail elsewhere, A.3.

Reynolds substituted the velocity sum 2.60, into the governing equations of the velocity field, namely the continuity 2.18 and Navier-Stokes equations 2.20; an analysis which is followed here. Firstly, an analogous decomposition is adopted for the pressure p , into average and fluctuating components, as follows:

$$p = P + \tilde{p}. \quad (2.61)$$

Upon substitution and, after expanding all products, the following is derived, in tensor form

$$\begin{aligned} & \partial_t U_\alpha + \partial_t \tilde{u}_\alpha + U_\beta \partial_\beta U_\alpha + U_\beta \partial_\beta \tilde{u}_\alpha + \tilde{u}_\beta \partial_\beta U_\alpha + \tilde{u}_\beta \partial_\beta \tilde{u}_\alpha \\ = & -\frac{1}{\rho} \partial_\alpha P - \frac{1}{\rho} \partial_\alpha \tilde{p} + \nu \partial_\beta \partial_\beta U_\alpha + \nu \partial_\beta \partial_\beta \tilde{u}_\alpha, \end{aligned} \quad (2.62)$$

where dependencies (spatial and temporal) have been dropped for brevity. Here, it is implicitly assumed that there is no variation of fluid density: $\tilde{\rho} = 0$, or $\partial_{(\alpha \text{ or } t)} \rho = 0$; that is, equation 2.62 is applicable only to incompressible fluids, which assumption permits further simplification in the following.

The aim is to now take a statistical average of equation 2.62, over a suitable time domain and in accordance with restrictions arising in the light of our particular aim. Such are discussed further in the appendix A.3.1. There are well established rules applying to averaging of the type employed here, these are listed in the appendix also, from page 262.

In taking the average, it is important to bring out the fact that simplification (of 2.62) depends critically on the dependencies that each variable has. Note that mean quantities are spatially variant, but not temporally, $U_\alpha(x_\alpha)$, whereas fluctuating quantities vary with both space and time, $\tilde{u}_\alpha(x_\alpha, t)$. This is important since, whether ensemble or time averaging is employed, expectations are made at each point in space; hence at any point, mean quantities (e.g. U_α) and their derivatives, are constant with respect to the averaging and may be factored out.

Equation 2.62 may be further simplified in the light of applying the Reynolds decomposition to the continuity equation. Since continuity in incompressible fluids amounts to $\nabla \cdot \mathbf{u} = 0$, then (in tensor notation):

$$\partial_\alpha U_\alpha + \partial_\alpha \tilde{u}_\alpha = 0, \quad (2.63)$$

which on averaging gives, see operator identities A.18 and A.20:

$$\partial_\alpha U_\alpha + \partial_\alpha \langle \tilde{u}_\alpha \rangle = 0, \quad (2.64)$$

where angular braces, $\langle \cdot \rangle$, denote averaging (expectation operator). Now, since

$$\langle \tilde{u}_\alpha \rangle = 0, \quad (2.65)$$

(defining property of stochastic variable, 1) it is deduced that both the mean flow *and*, by direct corollary, the turbulent fluctuations, are incompressible:

$$\partial_\alpha U_\alpha = 0 \quad , \quad \partial_\alpha \tilde{u}_\alpha = 0. \quad (2.66)$$

In this way and in accordance with appendix A.3.2, page 264, the following averaged equation is derived:

$$\partial_t U_\alpha + U_\beta \partial_\beta U_\alpha + \langle \tilde{u}_\beta \partial_\beta \tilde{u}_\alpha \rangle = -\frac{1}{\rho} \partial_\alpha P + \nu \partial_\beta \partial_\beta U_\alpha, \quad (2.67)$$

applicable to incompressible fluids. Note that this is *exactly* the Navier–Stokes equation, but for *averaged* dependent variables (velocity field and pressure) and with the caveat that there appears a new term (term 3, LHS) which consists entirely of fluctuating parameters. Note that under the averaging, the time derivative strictly disappears, see the appendix A.3.2; here it survives, for later purposes, under the finite time averaging applied.

Equation 2.67 relates *mean* quantities; that is to say, all the terms in it are resultant of the averaging process, except term 2 which is an ‘unresolved’ mean of some fluctuating velocity terms. Term 2 is, however, totally analogous to the others in that it represents a transport of mean momentum (strictly per unit volume), that arises in the contribution of fluctuating components to the velocity.

Equation 2.67 may be written in a form to highlight the role of stresses. Stress terms appear under the simple divergence operator; here ∂_β . On noting that the ‘mean strain rate’ $S_{\alpha\beta}$, is defined conventionally as²²

$$S_{\alpha\beta} = \frac{1}{2} \left(\frac{\partial U_\beta}{\partial x_\alpha} + \frac{\partial U_\alpha}{\partial x_\beta} \right), \quad (2.68)$$

²²Note that $S_{\alpha\beta}$, the symmetric part of the general tensor $\partial_\alpha U_\beta$, is often denoted $D_{\alpha\beta}$ on account of its interpretation as a ‘deformation’ tensor. Both names will be used interchangeably. The anti-symmetric part: $(\partial_\beta U_\alpha - \partial_\alpha U_\beta)/2$ defines *vorticity*, that is, ‘rotation without deformation’ and is often seen as $\frac{1}{2} \Omega_\gamma \varepsilon_{\alpha\beta\gamma}$, where $\Omega_\gamma = \partial_\beta U_\alpha \varepsilon_{\alpha\beta\gamma}$. $\varepsilon_{\alpha\beta\gamma}$ being the Levi-Civita third rank tensor, see page 259.

it is apparent that the last term of equation 2.67 is just $\nu\partial_\beta(2S_{\alpha\beta}-\partial_\alpha U_\beta)$. This, on noting that the order of ('adjacent') differential operators may be swapped, is just $2\nu\partial_\beta S_{\alpha\beta}$, as under incompressibility the latter term is zero ($\partial_\alpha \text{div}U = 0$). Hence it is possible to put equation 2.67 in the following form:

$$\partial_t U_\alpha + U_\beta \partial_\beta U_\alpha + \langle \tilde{u}_\beta \partial_\beta \tilde{u}_\alpha \rangle = \frac{1}{\rho} \partial_\beta \Sigma_{\alpha\beta}, \quad (2.69)$$

where the mean pressure P terms and the mean strain rate terms $S_{\alpha\beta}$ (both stress) are subsumed into a new collection of stresses defined by

$$\Sigma_{\alpha\beta} = -P\delta_{\alpha\beta} + 2\nu\rho S_{\alpha\beta}. \quad (2.70)$$

This procedure may be taken a step further by manipulating the crucial fluctuations term. Invoking the product rule for term 2 of the LHS implies:

$$\langle \tilde{u}_\beta \partial_\beta \tilde{u}_\alpha \rangle = \langle \partial_\beta \tilde{u}_\alpha \tilde{u}_\beta \rangle - \langle \tilde{u}_\alpha \partial_\beta \tilde{u}_\beta \rangle, \quad (2.71)$$

the latter RHS term of which is zero by further application of the continuity conditions (2.66). This then implies:

$$\langle \tilde{u}_\beta \partial_\beta \tilde{u}_\alpha \rangle = \langle \partial_\beta \tilde{u}_\alpha \tilde{u}_\beta \rangle, \quad (2.72)$$

allowing equation 2.69 to be recast in such a way as to highlight the interpretation of term 2 as *another* form of stress²³:

$$\partial_t U_\alpha + U_\beta \partial_\beta U_\alpha = \frac{1}{\rho} \partial_\beta (\Sigma_{\alpha\beta} - \rho \langle \tilde{u}_\alpha \tilde{u}_\beta \rangle). \quad (2.73)$$

Finally, note that the *total* mean stress may be defined as

$$T_{\alpha\beta} = -P\delta_{\alpha\beta} + 2\nu\rho S_{\alpha\beta} - \rho \langle \tilde{u}_\alpha \tilde{u}_\beta \rangle, \quad (2.74)$$

which, logically, is equivalent to

$$T_{\alpha\beta} = \Sigma_{\alpha\beta} - \rho \langle \tilde{u}_\alpha \tilde{u}_\beta \rangle. \quad (2.75)$$

This contains all terms upon which the divergence operator acts, hence its interpretation as total stress.

The contribution, $\rho \langle \tilde{u}_\alpha \tilde{u}_\beta \rangle$, of turbulent motion to the total mean stress, is usually

²³After applying relation A.20 of page 263, the RHS of 2.72 is observed to be of divergence operator / operand form. See also, for example, Tennekes and Lumley [139] for a demonstration of this.

denoted by $\tau_{\alpha\beta}$ and is called the Reynolds stress tensor in honour of the theorist who first noted it. Equation 2.73 itself is known as the Reynolds averaged Navier–Stokes equation, or the Reynolds momentum equation.

Some points on the nature of the Reynolds averaged momentum equation and its stress terms are now discussed.

- **Correlations.** The second term in RHS of 2.75 is of paramount importance in work on turbulence. It determines the effect that the turbulent fluctuations have on the *mean* flow. Under the statistical definition of the random variable $\tilde{\mathbf{u}}$ it is apparent that the term $\langle \tilde{u}_\alpha \tilde{u}_\beta \rangle$ there is the *point correlation tensor* between \tilde{u}_α and \tilde{u}_β .

The traditionally defined *correlation coefficient* is the ratio of this to the square root of the product of the two variances:

$$c_{\alpha\beta} \equiv \frac{\langle \tilde{u}_\alpha \tilde{u}_\beta \rangle}{\sqrt{\langle \tilde{u}_\alpha^2 \rangle \langle \tilde{u}_\beta^2 \rangle}}, \quad (2.76)$$

where, note, the Einstein summation convention does not apply. Obviously $c_{\alpha\beta}$ varies between -1 and 1, the two extremes indicating perfect correlation and anti-correlation respectively. $c_{\alpha\beta} = 0$ means no correlation.

For the case of the two fluctuations read at two differing points, the correlation tensor is vector dependent on distance:

$$R_{\alpha\beta}(\mathbf{r}) \equiv \langle \tilde{u}_\alpha(\mathbf{x}, t) \tilde{u}_\beta(\mathbf{x} + \mathbf{r}, t) \rangle. \quad (2.77)$$

In the Reynolds decomposition the (point) correlation tensor occurs adjacent to the (assumed invariant) density coefficient, where it is then known as the Reynolds stress, $\tau_{\alpha\beta}$.

With respect to the magnitude of the correlation and therefore the Reynolds stress,

$$\tau_{\alpha\beta} = -\rho \langle \tilde{u}_\alpha \tilde{u}_\beta \rangle \begin{cases} = 0 & \text{where } \tilde{u}_\alpha \text{ and } \tilde{u}_\beta \text{ are not correlated,} \\ \neq 0 & \text{where } \tilde{u}_\alpha \text{ and } \tilde{u}_\beta \text{ are correlated.} \end{cases} \quad (2.78)$$

In general, and especially in turbulent flow, $\tau_{\alpha\beta} \neq 0$ and correlation exists. In fact the magnitude of the term is relatively large and the net effect of turbulence on the mean flow is significant.

- **Closure problem.** It is apparent that decomposing the velocity and pressure fields

into contributions of differing types but at ever decreasing scales seems at first to be soundly based. The process introduces terms (correlations here) in increasing power, that is higher order non-linearities. Unfortunately however, with respect to turbulence, it not possible to argue that such terms may be considered small, as one would in a perturbation expansion. In fact generally the turbulent correlation tensor plays a significant, if not dominant, role. Repeating the process with ever smaller corrections just leads to higher order correlated terms appearing in the equations. Such is a manifestation of the so called *closure problem*; a characteristic of all non-linear systems, of which turbulence is a prime example.

The Reynolds stress tensor then warrants a direct attack, of which the eddy viscosity / mixing length approach, to be discussed later this section 2.4.4, is an early and still important example. See page 58 on.

- **Relation to mixing length** The process of deriving Reynolds averaged Navier–Stokes equations is of heightened relevance here because similar manipulations are used in the very early stages of mixing length analyses.

The mixing length analyses of Prandtl, von Kármán and Millikan (for citations, see next paragraphs) all are based upon dimensional arguments and simple physical reasoning on an equation for the energy of the turbulence— specifically for the channel, a differential equation equivalent to 2.126. This equation is derived as a specific geometrical form of the more general ‘turbulent energy budget’ which is of central importance; see equation 2.83

The turbulent energy budget is derived, in a way similar to the Reynolds averaged Navier–Stokes, by multiplying the Navier–Stokes equations by \bar{u}_α , taking the time average and subtracting the energy equation for the mean flow (similarly derived). Details of this can be found in e.g. Tennekes and Lumley [139]; also see page 56. Note, the energy budget can be derived via alternate means; see Frisch, [45], where a Fourier analysis is performed scale by scale on the turbulent fluctuations.

Foremost for the interests of modelling, Reynolds’ work hints at parallels between the usual viscous stress terms and characteristics of the turbulence. This was first realised by Boussinesq [15] as long ago as 1877, which led him to invoke the now ubiquitous concept of *eddy viscosity*, see the later section of page 58. Over ensuing decades the eddy viscosity idea was built upon by the likes of Prandtl [107], Taylor [137] and von Kármán [142, 143] with the aim of turbulence modelling in mind. Their more fundamental turbulence modelling schemes successfully exploited the eddy viscosity insight; they constitute the tool through which the early inroads on modelling were made, retaining a high degree of

credibility even today. Partly for this reason and partly due to technical suitability, the work presented here utilises this idea from the outset.

Dynamical energy equations

Another prime use for the Reynolds averaged Navier–Stokes equations is in deriving dynamical energy equations, for which they compromise the start point. For such purposes the stress $\sigma_{\alpha\beta}$, may, in a similar fashion to velocity 2.60 and pressure 2.61, be decomposed as

$$\sigma_{\alpha\beta} = \Sigma_{\alpha\beta} + \tilde{\sigma}_{\alpha\beta}, \quad (2.79)$$

with the *fluctuating stress tensor* taken to be

$$\tilde{\sigma}_{\alpha\beta} = -\tilde{p}\delta_{\alpha\beta} + 2\nu\tilde{s}_{\alpha\beta}, \quad (2.80)$$

and with the fluctuating strain rate (not necessarily conventionally) taken as

$$\tilde{s}_{\alpha\beta} = \frac{1}{2} \left(\frac{\partial \tilde{u}_\beta}{\partial x_\alpha} + \frac{\partial \tilde{u}_\alpha}{\partial x_\beta} \right). \quad (2.81)$$

All these relations will be referred to occasionally elsewhere.

To derive dynamical energy equations then, firstly consider equation 2.73 multiplied by the mean velocity, U_α . After some manipulation (mainly generalised product rule) it is possible to obtain the dynamical equation describing the *mean flow energy*, $U_\alpha^2/2$. In tensor notation it appears as follows:

$$\rho U_\beta \partial_\beta \left(\frac{1}{2} U_\alpha U_\alpha \right) = \partial_\beta (\Sigma_{\alpha\beta} U_\alpha - \rho \langle \tilde{u}_\alpha \tilde{u}_\beta \rangle U_\alpha) - \Sigma_{\alpha\beta} S_{\alpha\beta} - \rho \langle \tilde{u}_\alpha \tilde{u}_\beta \rangle S_{\alpha\beta}, \quad (2.82)$$

where as previously defined $\Sigma_{\alpha\beta} = -P\delta_{\alpha\beta} + 2\nu S_{\alpha\beta}$.

Alternatively, if equation 2.73 is multiplied by the fluctuating velocity, \tilde{u}_α , then, after taking the time average, and subtraction of the aforementioned equation for the mean flow energy 2.82, it is possible to rearrange and obtain the dynamical equation describing: *mean kinetic energy of turbulent velocity fluctuations*, $\langle \tilde{u}_\alpha^2 \rangle / 2$. In practice the latter process is considerably more involved, but is very important as regards the energetics of turbulence as it amounts to derivation of the so called *turbulent energy budget*:

$$\begin{aligned} U_\beta \partial_\beta \left(\frac{1}{2} \langle \tilde{u}_\alpha \tilde{u}_\alpha \rangle \right) = & - \partial_\beta \left(\frac{1}{\rho} \langle \tilde{u}_\beta \tilde{p} \rangle + \frac{1}{2} \langle \tilde{u}_\alpha \tilde{u}_\alpha \tilde{u}_\beta \rangle - 2\nu \langle \tilde{u}_\alpha \tilde{s}_{\alpha\beta} \rangle \right) \\ & - \langle \tilde{u}_\alpha \tilde{u}_\beta \rangle S_{\alpha\beta} - 2\nu \langle \tilde{s}_{\alpha\beta} \tilde{s}_{\alpha\beta} \rangle. \end{aligned} \quad (2.83)$$

Both equation 2.82 and 2.83 are crucial for our understanding of turbulence. They describe production, dissipation and transfer of energy between its various elements. This is a matter to which attention will return.

2.4.4 Approaches to turbulence, especially modelling

Conventional means of arriving at a representation of turbulent characteristics are diverse and numerous. Broadly however, they fall within the three usual categories: experimental, where data measured in real flows are collected; theoretical, which offers very diverse strategies; or computational, where traditional CFD is used, either with or without some form of turbulence model. Here some general points are mentioned emphasising the context of internal channel geometries.

Experimental work investigating flow in simple channels has been in evidence for decades, see later sections 2.7 and 5.1.2. It demonstrates some consistency between results of activities of the various groups, especially true toward the limit of high Reynolds number. Bearing in mind the simplicity of such conduits, it might be argued that experimental work on such might be considered complete, in that little may be gained from further work except perhaps increases in accuracy. In the light of the various empirically derived inferences based on such work, see for instance those of sections 2.7 and 5.1.2, this argument is strengthened. At a practical level anyway, further experimental investigations, on even simple channels, are: generally expensive (cost of equipment); often time consuming (building sufficient driving apparatus, measurement systems and the physical channel etc.); very case specific; and difficult to further extend or generalise quantitatively. Moreover, discrepancies do exist between results of various experimental groups, a matter which is far from fully understood. With no precise consensus engineers often turn to the other two alternatives, namely CFD or theory.

Theoretic approaches to practical turbulence problems suffer a similar range of potential inadequacies. They are: possibly limited or unsuccessful in their power and scope; difficult to validate without invoking additional experiments or models; and technically relatively complex. They may also come to fruition over longer timescales. Moreover, owing to complexity, theoretic studies are usually carried out within the academic community, as the theory involved may be highly intractable, consequently the work is often not exploited as vigorously and might be either too general or too specific to be of great practical use. Various theoretical approaches to turbulence are described in brief in the latter parts of this section, pages 63 to 64.

Computational methods are fast gaining in popularity at present. Researchers now have easy access to increasingly better computational resources, meaning improved speed

and accuracy along with improved algorithmic efficiency, improved applicability and scope and improved validation. Essentially, computational methods generate increasingly trusted results, relatively quickly and at low cost.

Obviously a computational modelling stance is adopted in this work, the LBGK alternative to CFD being exploited for the purpose. Results so generated are to be compared and judged with respect to those of the diverse earlier studies just mentioned. Identification is therefore required of any consensus between these, which is treated in another section, 2.7. In the ensuing section a deeper review is given of the computational modelling approach, specific to current purposes.

Turbulence modelling

Boussinesq's eddy viscosity insight [15] mentioned in section 2.4.3, draws an analogy between the normal microscopic collisional interpretation of viscosity, which is the only 'real' viscous process in hydrodynamics, and a generalised form which appears to be manifest in typical turbulent flow. Essentially the net effect of the complex swirling hierarchy of eddies, may be regarded as another means by which momentum is transferred in the flow, the effect of such on the average velocity being represented by the Reynolds stresses, $\tau_{\alpha\beta}$, in equation 2.74. The Reynolds stress term can be seen as equivalent to, and is dimensionally the same as, the microscopic viscous stress term that precedes it: $2\nu S_{\alpha\beta}$. This suggests guessing a relationship between $\tau_{\alpha\beta}$ and $S_{\alpha\beta}$ as a modelling strategy. Boussinesq assumed a linear relationship, thus modelling turbulence by introducing the 'eddy', 'apparent' or 'turbulence' viscosity, ν_T :

$$T_{\alpha\beta} = -P\delta_{\alpha\beta} + (2\nu + \nu_T)S_{\alpha\beta}. \quad (2.84)$$

which is, of course, equivalent to the turbulent velocity correlations modelled as follows

$$\tau_{\alpha\beta} \equiv -\rho\langle\tilde{u}_\alpha\tilde{u}_\beta\rangle \equiv \nu_T S_{\alpha\beta} = \nu_T \left(\frac{\partial U_\alpha}{\partial x_\beta} + \frac{\partial U_\beta}{\partial x_\alpha} \right). \quad (2.85)$$

More concisely, if less tersely, the eddy viscosity is often referred to as the 'turbulent exchange coefficient for momentum', this name being more indicative of its origin.

Many turbulence models employ the concept of eddy viscosity to some extent. The difference between them arises primarily in the way that we assign the value of the modified viscosity, ν_T , which must be assigned for the model to be of any practical use. Probably the most common of these involves the characterisation of a length scale over which properties of the turbulence are supposed to 'prevail'. This is conventionally known as the mixing length hypothesis, which leads to 'mixing length models'.

These are usually attributed to Prandtl, but Taylor reached a similar state of reasoning independently (may have published earlier). In the body of this work, a mixing length approach is taken to the problem of modelling effects of turbulence on mean character of a flow. For this reason the following analysis and that of 5.2.2 are presented, to introduce the mixing length and the various subtleties and ideas involved.

Mixing length hypothesis, model and limitations

The mixing length model may be arrived at via two distinct routes, as will be demonstrated. The originator, Prandtl, attempted to quantify transfer of momentum in a turbulent fluid in a way analogous to that used for derivation of molecular viscosity, that is by taking a gas kinetic approach. In his early work (of 1925) [107], Prandtl was required to invoke the concept of a length scale over which turbulence is assumed to prevail (the mixing length); heuristically the argument goes as follows.

Consider a ‘planar turbulent shear’ flow along direction x , where the mean velocity $U_x(y)$, invariant with x and z , is sheared over y ; shear $\partial_y U_x$ is positive and decreasing, say, due to the presence of a boundary (these are conventional planar shear coordinates). Then envisage that the fluid is composed of fluid particles flowing in distinct layers and that a property of the flow might, under turbulent fluctuations, be transported between layers, that is along y , intact. At some definite distance, the properties of the particle are assumed to have finally but suddenly mixed, so that a differential in the property is imparted to that layer. The dubious nature of this proposition is understood, but is deliberately extended: Suppose now that shear is constant between layers (they are sufficiently close with respect to mean velocity gradient); moreover, that this applies to all relevant particles arriving in any layer. A position is then reached from which may be derived a gradient / diffusion model of turbulent mixing. The property Prandtl was interested in of course is the turbulent momentum flux, so the working proceeds by finding the momentum differential imparted by each particle, translating this to a flux by it’s product with the local velocity and finally quantifying the average effect over the particles.

Firstly, a particle changing between layers to some reference layer at $y = y_0$, from one Δy away, will have a *momentum* differential ΔM_V (per unit volume, hence V suffix) according to

$$\Delta M_V = \rho[U_x(y_0) - U_x(y_0 - \Delta y) + \tilde{u}_x(y_0, t) - \tilde{u}_x(y_0 - \Delta y, t - \Delta t)], \quad (2.86)$$

after the Reynolds decomposition. Preempting a following step, it is apparent that

differences between the random fluctuations may be expected to be zero if averaged over all particles arriving at the plane $y = y_0$ ²⁴. The other (first two) terms may then be taken as the first order approximation to gradient in U_y . That is

$$\Delta M_V = \rho \Delta y \frac{\partial U_x}{\partial y}. \quad (2.87)$$

This is supposed to hold for all particles arriving in the plane y_0 (from either direction); hence, denoting each particle by index i , the distance it has traveled as Δy_i , then for each particle arriving in the plane, the momentum differential per unit volume is:

$$\Delta M_{V_i} = \rho \Delta y_i \frac{\partial U_x}{\partial y}. \quad (2.88)$$

In the usual way (see continuum mechanics section 2.2.2), the *flux* per unit area and time of this momentum differential is derived from product of the above (2.88) with the velocity associated with fluid particle i , which shall here be denoted u_{y_i} . Hence, indicating the new quantity by the suffix *At*, the differential *per unit area and time* is:

$$\Delta M_{At_i} = \rho \Delta y_i \frac{\partial U_x}{\partial y} u_{y_i}, \quad (2.89)$$

this being applicable to each particle i . Taking an expectation of this gives the desired turbulent momentum transfer quantity and invokes the statistical properties of fluid particle velocities u_{y_i} and initial positions $y_0 - \Delta y_i$. The turbulent momentum flux for this particular flow configuration consists of only a xy component and, with respect to prior analyses, is denoted τ_{xy} ; that is, $\langle \Delta M_{At_i} \rangle = \tau_{xy}$. Hence

$$\langle \Delta M_{At_i} \rangle = \tau_{xy} = \rho \frac{\partial U_x}{\partial y} \langle u_{y_i} \Delta y_i \rangle. \quad (2.90)$$

In Prandtl's analysis no explicit averaging in 2.90 need be undertaken. Instead, he hypothesised that

$$\langle u_{y_i} \Delta y_i \rangle \equiv c u'_y \ell_{\text{mix}}, \quad \text{where } u'_y = \sqrt{\langle u_y^2 \rangle}, \quad (2.91)$$

which implies

$$\tau_{xy} = \rho c u'_y \ell_{\text{mix}} \frac{\partial U_x}{\partial y}, \quad (2.92)$$

where c is an undetermined constant. Also, by virtue of our definition of turbulent

²⁴This amounts to another accepted weakness of the analysis.

exchange coefficient for momentum, equation 2.85, the eddy viscosity must be:

$$\nu_T = c u'_y \ell_{\text{mix}}. \quad (2.93)$$

These three equations are the essence of Prandtl's mixing length hypothesis. All statistical properties are subsumed into the RMS velocity term, u'_y ; the distances traveled Δy_i are assumed then to be represented by one length scale, that being the mixing length ℓ_{mix} . Reference to any text on kinetic theory demonstrates that such is directly analogous to the fact that kinematic viscosity is the product of RMS molecular velocity and particle mean free path.

In practice Prandtl went further by means of an additional assumption to approximate the velocity scale. Specifically, he assumed that transverse and axial components of the velocity were roughly the same, i.e. $u_x \approx u_y$; equivalently, that good correlation exists between u_x and u_y . These arguments permit the following

$$u'_y \approx \ell_{\text{mix}} \left| \frac{\partial U_x}{\partial y} \right|. \quad (2.94)$$

See for instance Hinze [65], or Tennekes and Lumley [139] for details. This gives rise to the familiar

$$\tau_{xy} = \rho \kappa^2 \ell_{\text{mix}}^2 \frac{\partial U_x}{\partial y} \left| \frac{\partial U_x}{\partial y} \right|, \quad (2.95)$$

and, importantly here:

$$\nu_T = \kappa^2 \ell_{\text{mix}}^2 \left| \frac{\partial U_x}{\partial y} \right|. \quad (2.96)$$

The latter two equations may readily be generalised to:

$$\tau_{\alpha\beta} = \rho \kappa^2 \ell_{\text{mix}}^2 \frac{\partial U_x}{\partial y} |S_{\alpha\beta}|, \text{ and } \nu_T = \kappa^2 \ell_{\text{mix}}^2 |S_{\alpha\beta}|, \quad (2.97)$$

for purposes of later chapters herein.

In retrospect it is evident that specification of ℓ_{mix} is a 'supplementary' matter, in that it is the assumptions made prior to that point which are of greatest relevance. In fact modelling is relatively insensitive to the way mixing length is quantified and diverse ways to allocate its value exist. This is not to diminish the value of Prandtl's ideas, which despite their flimsy basis, continue to be of general value in both analyses and simulations alike. It seems that weaknesses of the model must in some way cancel each other out.

Modern perspectives show that a relationship of the form of equation 2.92 is little more than a dimensional necessity of Prandtl's assumptions; again see [139] "The gradi-

ent transport fallacy” p.47, for a good explanation of this. More interestingly, modern statistical analyses enable the length scale arrived at, whichever means is followed, to be related to definite and physically tangible attributes of turbulence itself.

Of the many and diverse means by which ℓ_{mix} may be assigned, von Kármán in particular worked on alternatives [140]. His work met with frustrated success, however, and the whole concept never gained anymore credibility than that with which it began. In this work, approaches to this aspect of the modelling are described at a more appropriate point; page 197, regarding implementation. In particular, lattice Boltzmann implementation of a mixing length model, as is employed later, gives rise to further differences and subtleties; discussion of these points is also left to the relevant section, 5.2.

Other modelling strategies

From the perspective of traditional CFD, the turbulence model of this work may be seen as an instance of sub-grid model, where turbulence behaviour over scales smaller than that of the grid are modelled, to derive their effect on the main flow features. Such sub-grid scale (SGS) models are common in the turbulence literature.

Another commonly seen modelling strategy is the large eddy simulation (LES). Here, in a way very similar to SGS models, only a selective portion of the larger scale (significant) features of the flow are resolved. Picking scales in this way is most usefully expressed in the ‘spectral’ context, where variation of the instantaneous velocity field is viewed from its Fourier space perspective. Then concentrating efforts so as to resolve only features on a scale larger than some threshold, is equivalent to filtering out high frequencies in the spectrum. SGS and LES amount to averaging out, or filtering, features above a certain cut-off frequency.

Since modelling the Reynolds averaged Navier–Stokes equation in a way that retains a time derivative term (equation 2.67 and comments thereafter) *in lattice Boltzmann*, strictly requires definition of a ‘filtered density’, see especially Hou *et al.* [68] on this technicality. Similarly, since in LB some averaging is implicit in the nature of the densities. Then SGS and LES may be considered particularly appropriate approaches for turbulence modelling within the LB framework. This is because the filtering or averaging mentioned may be arranged to ‘match up’ to that required for the turbulence modelling.

Other turbulence modelling approaches are commonly utilised in CFD. These are almost all significantly more refined than the simple mixing length idea, focusing on energetics and deriving differential equations for solution along side the purely hydrodynamic. They are generally classified ‘non-algebraic’ and in accordance with the number and type of differential equations; namely, one, two and multi-equation models. For a

good general discussion of turbulence modelling see Launder and Spalding [82]. Some of these schemes are extremely successful, especially in specific applications where each may be more appropriate or suitable. In diversity of application however, their advantage is eroded.

Despite the fact that complexity and relative specialisation effectively preclude, for a first attempt on the problem, the use of advanced energy equation models, some discussion of such has appeared in the literature. Succi, Amati and Benzi for instance [132], describe a basis for implementing a k - ϵ model by introducing two other node distributions to represent mean turbulent kinetic energy and its dissipation respectively. Teixeira also describes a k - ϵ model [138], though it is formulated in an entirely different way and could be described as a hybrid LB CFD scheme. k - ϵ is the prime example of a so called two equation turbulence model. A ‘true’ LB k - ϵ implementation, in the sense of [132], is probably the next logical step in terms of model, with which to build on the studies carried out here. This is reviewed in the discussion of further work, 6.1.

Overview of turbulence theory

Various theoretic approaches to turbulence are now briefly mentioned. Primarily because they may yield interesting consequences for the modelling fraternity; that is, further clues as to how turbulence properties might be invoked in a modelled flow. In no particular order:

Vortex dynamics is a whole field dedicated to describing turbulence, by treating the eddies as of central significance. **Vortex stretching** is the modern focus of attention in that it best describes the observed fact that vortices with their axis aligned along the direction of mean shear are best at communicating or transferring energy between scales of motion.

Functional and diagrammatic approaches may be regarded as encompassing a vast and varied subset of turbulence research, to include: ‘closure equations’, e.g. Kraichnan’s direct interaction approximation (DIA) and derivatives; ‘field theoretic’ methods and ‘diagrammatic’ methods. They focus on statistical properties of the spectrum and distributions of turbulence quantities.

Multi-scale methods, to include the most well known, the renormalisation group (RNG), which is borrowed from quantum field theory.

Dynamical systems research (non-linear) has elided some results, despite it being a high abstraction approach.

Intermittency is another aspect of the phenomenology of turbulence which warrants explicit mention, partly due to the attention it received. This is the term used to de-

scribe the fact that some random functions are not self-similar at all points and in fact show ‘bursts’ in their behaviour. Intermittency, dependent on one’s perspective, may be regarded as manifestation of the beast itself (turbulence) at either cause or symptomatic level.

Dimensional analyses tend to be very simple and have been particularly successful, yielding many of the significant early results. In fact, the mixing length model may be derived entirely on dimensional grounds. Little further ground is made on this front these days.

Spectral methods focus on results which may be obtained by treating turbulence from a functional perspective and observing its spectrum. Much of this work is well established and is covered in the texts.

Wavelet analyses form the logical modern extension to spectral methods. Here, the spectral decomposition is with respect to both space and scale using ‘wavelets’, analysing functions which consist of ‘packets’ of the underlying trigonometric ones. See Farge [41] for a recent and definitive addition to the literature. Extension of the idea might be possible to direction (and in some way to time dependence?).

A good review and introduction to the whole set, along with a historical perspective, can be found in Frisch, [45].

2.5 The lattice Boltzmann method

The lattice Boltzmann method (LB / LBM) is an indirect, discrete gas kinetic approach to fluid dynamical modelling. It is derived from the lattice gas cellular automata (LGCA) and is made possible under physical equivalence of the emergent macroscopic behaviour exhibited by simple microscopic gas dynamical models and macroscopic hydrodynamics. As such it is the perfect example of generality in physics (see introductory material 1.2).

The term ‘lattice Boltzmann’ derives from the fact that the underlying equation is a discrete analogue to the famous Boltzmann equation (BE), 2.49. This was derived in the latter part of the nineteenth century and is covered in some detail in section 2.3.3. The term lattice is commonly used to denote simple space discretisation, but historically, approaches to solve the BE numerically have targeted discretisation of the velocity variable. This gives rise to discrete ordinate methods or discrete velocity models (DVM) along with other forms of finite difference schemes (various simple finite differences in space and / or time). Examples of the former go back years, especially many works of A.B. Huang around the late sixties, too numerous to cite. Of the latter, see M. Kac, T.E. Broadwell and Gatignol; they include some of the precursors to the LGCA of recent decades. Discretisation in the lattice Boltzmann however, is performed on all independent variables: space, time and velocity; setting it apart from other more extensively studied variants. This is in common with LGCA.

Boltzmann arrived at his equation by considering fluxes and balance conditions for the so called ‘velocity distribution function’ $f(\mathbf{x}, \mathbf{v}, t)$; a statistical density of particles, $0 \leq f \leq 1$, having positions in the range $[\mathbf{x}, \mathbf{x} + d\mathbf{x}]$ and velocities in the range $[\mathbf{v}, \mathbf{v} + d\mathbf{v}]$ at time t . In the LBM, the continuous nature of the independent variables \mathbf{x} and \mathbf{v} is dispensed with for purposes of reduction in complexity. Hence the distribution function is written, for example, as: $f_i(\mathbf{x}^*, t^*)$, where the subscript i , denotes velocity vector in a discrete, finite set: $i \in (0, 1, 2, \dots, q)$ and where the superscript $*$, denotes discretisation of lattice position or time. q is the number of non-zero velocity values. Commonly the star $*$ is omitted as no confusion arises.

Discrete Boltzmann formalisms are employed in limits of validity where the microdynamical processes that are described by the Boltzmann equation, reveal Navier-Stokes hydrodynamic behaviour at a macroscopic level. That is, using the LBM, hydrodynamic ‘modes’ (momentum, density) which are governed by continuum equations are *modelled*. As mentioned in section 2.3.3, the BE is strictly only valid in the Boltzmann gas limit (BGL); this will be discussed in the following, where it relates to the LB.

In the following, for the purposes of later chapters, the exact nature of the LB scheme will be examined in some detail. Means to augment it should become apparent from the

presentation, but they will be highlighted where important, as later in this work some are exploited, as fundamental aspects of the primary novel developments.

In addition to the above, as an illustrative and pedagogical tool, the nature of other more traditional approaches to the problem of modelling fluids will be addressed also. Interested readers, keen to find out more, are referred to the literature, as illuminated in the following initial section 2.5.1.

2.5.1 Development of the LBM: a review of the literature

The following is intended to form an introductory overview of the literature pertaining to the lattice Boltzmann method. The purpose is merely to form a basis for further exploration, not to give an all encompassing review.

Starting at the LGCA stage, around the mid-eighties, Frisch, Hasslacher and Pomeau [44] extend the scope of early ‘lattice gases’, from simple square lattices, which had been around since a series of papers by Hardy, Pazzis and Pomeau [55–57], to the triangular lattice, with hexagonal node neighbourhood. The original square lattice gases suffered from a lack of rotational symmetry, owing to the simplicity of the underlying lattice. In developing a hexagonal LG, Frisch, Hasslacher and Pomeau effectively bestowed rotational invariance on the LG and, in so doing, provided a first working model for LG hydrodynamics, now commonly known as the FHP model. This original hexagonal scheme was shortly afterward extended to the three dimensions. This had to be done by invoking the use of a four dimensional lattice [35, 152] (and later [43, 60, 120]) as, it turns out, no three dimensional lattice has the required rotational invariance properties, a matter addressed at about the same time by Wolfram [152]. He was working independently on deeper geometric and mathematical aspects of LGCA, including lattice basis types and their symmetries and describes the requirement for a four dimensional lattice comprehensively.

During the next year, 1987, an important review paper appeared [43] which thoroughly summarised the then state of the art. Therein, mention is first publicised of the simplified collision rules for a Boltzmann gas and of the averaging procedure which renders LGCA lattice Boltzmann. The stage was set for further development and for a shift of focus.

It is of value at this point to take a short aside to highlight the marvelous quantum leap embodied in the newly improved LGCA. From one perspective, the FHP model is an incredibly simple model of a gas, where: particle velocity may only take one of *six*²⁵

²⁵Seven velocities exist if the rest particle (zero velocity) is included.

values; time and space are partitioned into a coarse set of manageable chunks; particle presence in any of these being represented merely by 0 or 1 on the lattice; only six basic types of collision are possible; and, evolution of system state is expressed in a *three term* expression. From another perspective, the viewpoint of bits in a computer: the entire system is represented by a Boolean field; no floating point operations occur during system evolution, only memory exchanges; tables may be set up to assist mappings. Whatever the viewpoint, the fact that *hydrodynamics* emerges as the macroscopic equations of the system, is a superb example of generality in physics, as expounded in the introductory discourse 1.2. The interested reader is referred to any of the three main texts: [119, 121, 135] for a fuller exposition of the state of affairs in the LGCA world.

Returning to the main thread, the first true *lattice Boltzmann* paper was Mc Namara and Zanetti [92], which addressed one of the problems that FHP and its derivatives suffer from, namely ‘statistical noise’. In this context, statistical noise is the inherent fluctuation and ‘bittiness’ (discrete nature) of the underlying LGCA dependent variable, the Boolean node occupancy field. In simple terms, noise in the LB is removed by *pre*-averaging the Boolean field; in contrast to the *post*-averaging that had to be carried out during extraction of macrodynamics from LGCA. It is entirely analogous to what is done whilst making the transition from the exact microdynamics of the Newtonian viewpoint on gas kinetics, to the probabilistic and distributional perspective of the Liouville formalism²⁶.

Averaging of this kind is over an ensemble and, in moving to work with averaged quantities, some of the technical attributes of the LGCA are lost, which precipitates limitations to the method further down the line. See e.g. [135] and later discussions, section 6.1.

This by no means represents the end product, however, Mc Namara and Zanetti’s work dealt with just one of the array of problems LGCA faced. It retains most LGCA features, especially with respect to the collision. Collision in LGCA, whilst simple, nevertheless permits multiple body interactions, which is to be contrasted with Boltzmann’s collision integral, 2.49. At about the same time, Higuera and Jimenez [62] published a paper in which a simplified Boltzmann collision is implicitly assumed. Again, the averaging procedure of the LGCA is circumvented, thus removing problems of statistical fluctuations.

At this point the scheme is in essence a velocity-vector discrete Boltzmann equation, having velocity (link) dependent relaxation parameter. The earlier work however still referred to the underlying LG in order to generate their collision form, whereas the

²⁶Strictly, with the explicit involvement of collisions preserved, direct transition to the Boltzmann (BBGKY) formalism.

latter adopts a linearised form for the collision, thereafter known as the linearised lattice Boltzmann (LLB). This is used in further development of the scheme, but it is at this point that some advantages of the original LG are lost (unconditional stability). Higuera and Succi [63] apply the new scheme to flow past a circular cylinder in the same year, thus establishing the efficacy of the new scheme. Various other papers follow, perhaps most notably [61] which gives a more practical fluid dynamical perspective.

In 1991 Chen *et al.* [20] apply and extend the LBM for the simulation of magnetohydrodynamics. This paper is the first to mention the ‘single relaxation parameter’ simplification, which was to become known by the acronym LBGK (for lattice Bhatnagar-Gross-Krook), although the connection to the work of Bhatnagar, Gross and Krook [10] of 1954, is not made until later (see [112]). In the same year, a development of the scheme is proposed by Koelman [74], which takes terms only up to second order in the Mach number to solve the problem of lack of Galilean invariance and velocity dependent pressures. This matter is something which is worked on extensively in subsequent papers.

Also in 1991 the first review of lattice Boltzmann scheme appears [133], though it was to be followed by a more comprehensive paper by Benzi, Succi and Vergassola [9]. The latter is a good review candidate to form the basis for study of the early LB development.

Two important papers then appear in 1992, both addressing the issues of lack of Galilean invariance and velocity dependent pressures (equivalently equation of state). It is not clear as to how these differ from or extend the previous work on the matter by Koelman; all three papers cite similar advances. In Qian, d’Humières and Lallemand [112] the term LBGK is introduced for the single relaxation parameter model used in [20]. In Chen, Chen and Matthaeus [21] the same matter is seemingly independently discussed and the phrase pressure corrected LBE (PCLBE) is introduced to refer to the way in which the velocity dependence of the equation of state is removed. Qian and d’Humières work, [112] provides a good illustrative example, of the two dimensional, nine velocity (D2Q9) LBGK model. It is analysed and presented in detail in (the appendix of) a later work by Hou *et al.* [69]. The model presented later, 2.5.2, follows these papers in spirit at least. They complete the picture for the main steps in the evolution of the core LBGK scheme — that adapted and further extended in this work.

Subsequent papers of importance include those that set the scheme on a rigorous footing: Abe [1] and He and Luo [58] independently suggest a means to go directly from the Boltzmann equation to the lattice Boltzmann equation, effectively circumventing the laborious and cloudy steps of the Chapman–Enskog expansion and proving their equivalence. Ziegler [157] is the first to discuss LB boundary conditions explicitly. Sterling and Chen [129] provide a stability analysis. He *et al.* [59] and Zou, Hou and Doolen [161]

provide analytic solutions for flows in simple internal configurations.

A clear presentation of the traditional Chapman–Enskog expansion, which takes one from Boltzmann equation to Navier–Stokes equations, is provided in an appendix to Hou *et al.* [69].

Various modern critiques exist, L.S. Luo in particular has been vocal in promoting a more careful and rigorous approach. Recent papers of unusual interest include: Luo [90] where thermohydrodynamic LB is discussed from a theoretic perspective and existence of a H-theorem is debated (should be read alongside Chen and Teixeira [27] of the same issue); also on the theme of thermally self-consistent LB see for example Boghosian and Coveney [13] and Vahala *et al.* [146].

A good review article is provided in Chen and Doolen [22], which comprehensively brings the many issues of LBM usage into one up to date discussion. In addition there are now books on the subject. The first was by Rothman and Zaleski, *Lattice Gas Automata*, [121]. A more recent example is provided by Succi, *The Lattice Boltzmann Equation*, [135].

Papers regarding the employment of modified LB schemes specifically to incorporate or model the effects of turbulence are not mentioned at this point. Instead they appear, for the purpose of greater clarity of exposition, in the relevant section 5.2.1 of chapter 5.

Attention now proceeds to the main body of this section, a detailed exposition of the LB scheme itself.

2.5.2 Mathematics and details of the scheme

This section details the lattice Boltzmann scheme. The intention is not to be all encompassing nor rigorous; there is no need and the scope of this work does not permit. Also, importantly, the presentation is not ‘systematic’ as others attempt to be, in that it doesn’t start at one end and work to the other, that is from microscopic to macroscopic or vice versa. Instead it is intended to provide just an overview of the main aspects and attributes of LBM; characteristics which distinguish it from either hydrodynamics or other gas kinetic models.

Attributes are discussed under the headings: the velocity distribution function and its moments; the lattice; lattice evolution and the lattice Boltzmann equation; finally lattice Boltzmann equation macrodynamics. Following that a short digression, page 82, puts the whole into its scientific context.

The velocity distribution function and its moments

Boltzmann's continuous 'velocity distribution function' is approximated by a very simple discrete set of densities for each discrete point on the lattice. The discrete velocity values are indexed by subscript i , where $i \in [0, 1, 2, \dots, q]$, q being the finite number of non-zero velocity values. Hence the LB velocity distribution function is often written $f_i(\mathbf{x}^*, t^*)$, $0 \leq f_i \leq 1$; this notation adapts Boltzmann's traditional name f for the density. Here superscript $*$ on the space variable \mathbf{x} denotes space discretisation onto the lattice (treated next), similarly for time. Commonly the star $*$ is omitted as no confusion arises.

Various summations may be sought, in close analogy with integrals of the continuous Boltzmann case: integrating over space as follows:

$$\int_X f(\mathbf{x}, t) d\mathbf{x} = m, \text{ has LB equivalent: } \sum_{\mathbf{x}^* \in X} f_i(\mathbf{x}^*, t^*) = m, \quad (2.98)$$

giving m , the total mass of fluid. Here X denotes the entire fluid domain of interest; summation is over all nodes on the lattice. Dependency notation is dropped hereafter, except where explicitly necessary. Note that Boltzmann's integrals over velocity—moments of the distribution in the statistical sense—have lattice equivalents as follows:

$$\begin{aligned} \int_V f dv &= \rho \equiv \sum_i f_i = \rho, \\ \int_V f \mathbf{v} dv &= \rho \mathbf{v} \equiv \sum_i f_i \mathbf{c}_{i\alpha} = \rho u_\alpha. \end{aligned} \quad (2.99)$$

Moments such as these are used in definition of the macroscopic observables of the LB scheme. Hence the former equation gives the macroscopic fluid density whilst the latter gives momentum density.

Higher moments occur and are engineered so as to recover hydrodynamic macroscopics when a Chapman–Enskog expansion is performed on the LB scheme; this and other important matters are discussed in relation to macroscopics, at page 76.

Equilibrium. It can be shown (see for instance Cercignani [18] for the continuous case) that if an equilibrium solution exists for the Boltzmann equation it may only depend functionally upon so called 'collision invariants'. Clearly these are quantities which are unaffected under the entropy increasing effect of the collision operator (RHSs of both BE and LBE). It may also be shown that only five *elementary* collision invariants exist and that these are: the scalar ρ ; the three components of velocity v_α ; and the square of the velocity magnitude $v_\alpha v_\alpha$, which equate loosely to mass, momentum and energy. Following the Chapman–Enskog expansion generates lattice dependent constraints on

the relative influence of these terms (Lagrangian multipliers in the continuous case), it is then possible to use these and other information to further specify the form of $f_i^{(0)}$. Picking then, the simplest form of equilibrium distribution function that has the required properties, gives the following commonly utilised form for $f_i^{(0)}$ (often written \bar{f}_i):

$$f_i^{(0)}(\rho, \mathbf{v}) = w_i \rho \left[1 + \frac{\mathbf{v} \cdot \mathbf{c}_i}{c_s^2} - \frac{v^2}{2c_s^2} + \frac{(\mathbf{v} \cdot \mathbf{c}_i)^2}{2c_s^4} \right]. \quad (2.100)$$

In equation 2.100, the values w_i are ‘weights’ with values: 4/9 for the rest velocity ($i = 0$); 1/9 for ‘square’ link velocity (i even); and 1/36 for diagonal velocities (i odd), respectively. The c_s parameter is the velocity of sound on the D2Q9 lattice, which takes the value $1/\sqrt{3}$.

A defining solubility prerequisite of the LB scheme — see later section on Chapman–Enskog expansion, page 76 — is arrangement for the following to be valid for the *equilibrium portion* $f_i^{(0)}$ of the full distribution function:

$$\begin{aligned} \rho &= \sum_i f_i^{(0)}, \\ \rho v_\alpha &= \sum_i f_i^{(0)} c_{i\alpha}. \end{aligned} \quad (2.101)$$

These apply in addition to the similar full f_i moment summations of equations 2.99.

The lattice

The continuous nature of the independent variables is dispensed with for purposes of reduction in complexity and to render the problem numerically soluble. Space is discretised onto a regular lattice, $\mathbf{x} \rightarrow \mathbf{x}^*$, which is to be described by information on a corresponding array of ‘nodes’. Time is partitioned into discrete steps, $t \rightarrow t^*$. Velocity is discretised in such a way that in ‘unit time’, or one time step, information propagates in precise inter-nodal increments *between nodes* on the lattice, that is, the set of velocity vectors coincides with the set of simple lattice translation vectors.

The form of space discretisation and hence the nature of the velocities depends upon the chosen lattice type. Two and three dimensional lattices exist in various forms. The basic ‘shape’ may be square, ‘triangular’, hexagonal, etc. but must tessellate²⁷ over the entire fluid domain. Symmetries, it turns out, are critical in establishing correct macrodynamic behaviour of the scheme, see [43], these place the most severe restriction on the set of possible lattices. Certain rotational symmetries are necessary to ensure

²⁷Pack together indefinitely leaving no interstitial space.

rotational invariance at macroscopic level; first established in [44]. Various lattice types are appropriate for the purpose and are utilised extensively. For in depth treatments of other lattices see LB texts [119,121,135]; for a detailed mathematical perspective on lattices and symmetries see [152].

Lattice types are often referred to by an abbreviation consisting of the dimensionality D and the number of links or velocities Q . Here the focus is restricted to just two dimensions and a square lattice is utilised on account of its adequacy and simplicity. Under the aforementioned naming convention, the lattice of interest here is referred to as the D2Q9; this is shown schematically in figure 2.4.

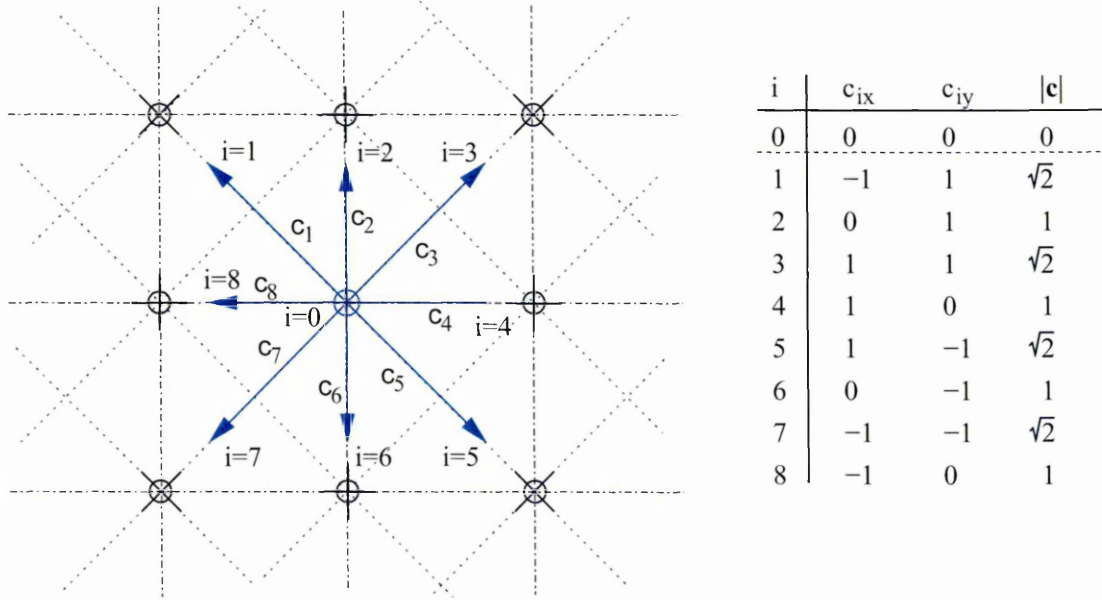


Figure 2.4: Representation of the lattice (dotted and dashed lines) and densities on a node (blue arrows). Nearest neighbours are shown as ‘plus signs’ on a circle, \oplus , whereas next nearest are crosses on a circle, \otimes . The table shows velocity components by link index i ; units are lattice constant times reciprocal time step. Final column gives the relative magnitude of velocity with respect to the basic distance / time units. First row is the zero velocity.

Note that whilst the D2Q9 lattice consists of a two dimensional, square array of nodes, it is more complex than early HPP models [56]: the velocity set includes vectors along links between nearest *and next nearest* node neighbours. Each ‘node’ has four nearest neighbours and four next nearest neighbours; nearest neighbours occur along ‘square’ links, whereas next nearest are found along diagonals. Again, see figure 2.4.

Discrete velocity is denoted by \mathbf{c}_i , or, in tensor notation $c_{i\alpha}$. Since velocity vectors are intended to coincide with basic lattice translation vectors, the i subscript not only specifies velocity direction and magnitude, it also indexes links between lattice nodes, hence the loose association in terminology: link \equiv velocity. In the D2Q9 then $0 \leq i \leq 8$. Labelling is chosen arbitrarily to be as in figure 2.4. Components of discrete velocity

vectors are as set out in the table of that figure. Inclusion of a zero or rest velocity, $c_{0\alpha} = 0_\alpha$, completes the set and is necessary to take care of some deeper technical issues regarding the form of the equilibrium distribution and stability of the scheme — especially in thermal models [2, 13, 104, 129]. Relative velocity magnitudes are seen to be 0, 1 and $\sqrt{2}$ for zero link ($i = 0$), ‘square’ links ($i = 2, 4, 6, 8$) and diagonals ($i = 1, 3, 5, 7$) respectively.

Lattice evolution and the lattice Boltzmann equation

The lattice update is known as evolution, it consists of two main steps — for the bulk at least — streaming and collision, denoted here by \mathcal{S} and \mathcal{C} respectively. An alternative name for the stream operator is propagation, which is used frequently herein. These two aspects of evolution are analogous to advection (streaming) and collision of the continuous Boltzmann approach, hence most of the complexity of the modelled system — especially its non-linearity — resides in the collision.

In the previous section 2.5.1, mention is made of the various simplifications that have been applied to the form of the collision term, during development of the LBM. Firstly, in [62], the collision is rendered quasi-linear; then, reference to underlying microdynamics is removed, in [64]; finally the collision matrix is diagonalised in [20, 74, 112]. This latter form is referred to as the BGK LB, or LBGK. Only the LBGK model is to be discussed here. The collision operator in such circumstances takes the form of a simple *relaxation*; the top relation of the following:

$$\begin{aligned}
 \mathcal{C} : \quad f_i^\dagger(\mathbf{x}, t) &= f_i(\mathbf{x}, t) - \omega[f_i(\mathbf{x}, t) - \bar{f}_i(\mathbf{v}, \rho)], \\
 \mathcal{S} : \quad f_i(\mathbf{x} + \Delta_t \mathbf{c}_i, t + \Delta_t) &= f_i^\dagger(\mathbf{x}, t), \\
 \mathcal{E} &= \mathcal{C} \circ \mathcal{S}.
 \end{aligned} \tag{2.102}$$

Here \mathcal{E} represents the full lattice evolution operation and \circ denotes functional composition. The relaxation parameter in this case is ω , Δ_t represents the discrete time interval. Also, the post-collide field is denoted by f^\dagger and the *local* equilibrium distribution function, as calculated from local macroscopic variables, by \bar{f}_i .

An alternative and much more common way of expressing lattice evolution is with the ‘evolution equation’:

$$f_i(\mathbf{x} + \Delta_t \mathbf{c}_i, t + \Delta_t) = f_i(\mathbf{x}, t) - \omega[f_i(\mathbf{x}, t) - \bar{f}_i(\mathbf{v}, \rho)]. \tag{2.103}$$

This equation is visibly similar in nature to Boltzmann’s continuous precursor 2.46. Most

of equation 2.103, LHS ‘advective’ derivative terms directly analogous to the those of the Boltzmann equation, may be derived upon first order Taylor expansion of the velocity distribution function. The RHS represents the LBGK collision.

So the evolution equation is essentially a finite difference relaxation scheme for the continuous Boltzmann equation. It has in fact been proved that the Boltzmann and lattice Boltzmann equations are precisely equal under certain limiting conditions [1, 58]; equivalently, that discretisation of the BE gives rise to the basic LBE model. It has also apparent that the BE is continuous limit of discretisation of the LBE. The aforementioned works are quite recent but have now been generalised to include gases with a non-ideal equation of state [89].

Graphical representation of lattice evolution is presented over subsequent pages for illustration — figures 2.5, 2.6 and 2.7. Therein the same section of lattice, which includes

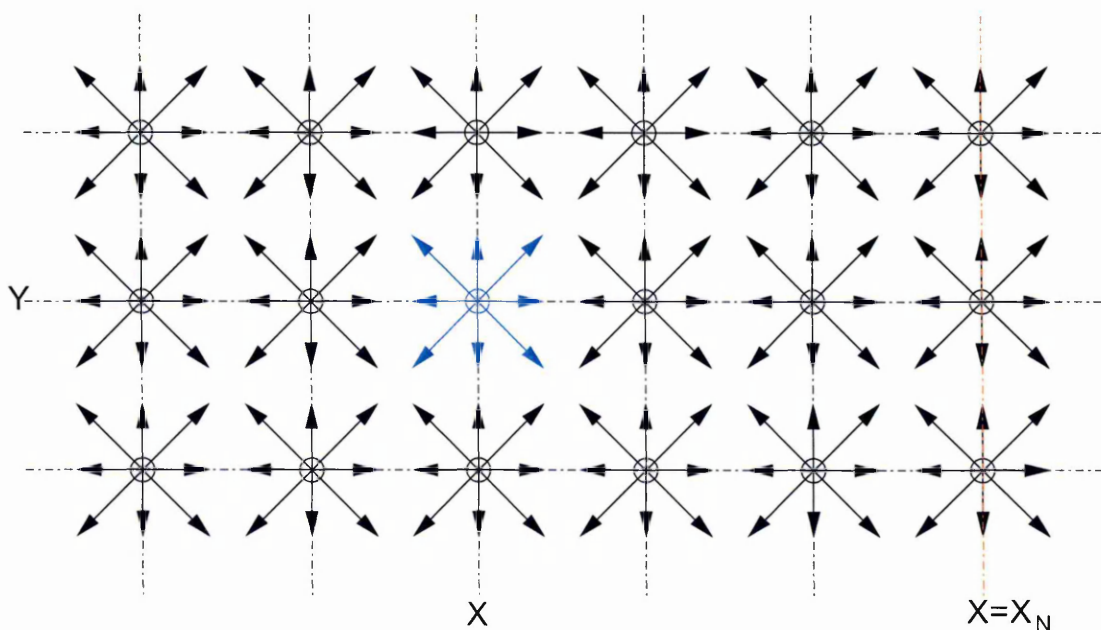


Figure 2.5: Representation of lattice at some arbitrary initial point. The square lattice is represented by dot-dash lines, densities (by velocity) are represented by arrows oriented in respective lattice directions. All initial values are assumed known. One set of node densities, at location (X, Y) , is highlighted in blue; evolution of this information is to be followed over the next figures, 2.6 & 2.7. A section of lattice boundary is included, highlighted red, for later discussion.

a section of boundary at right, is shown at three distinct evolutionary stages. The first and last stages, figures 2.5 and 2.7 respectively, are *equivalent* stages, in that they both contain post collide density values, f^i . They are not equal however, as there is a full time step difference. The middle stage, figure 2.6, contains post stream information.

With respect to the set of boundary nodes, included for illustration and later reference, note that during the stream operation, no information is available to populate inward

pointing velocity density values at the boundary (highlighted as red circles on links), figure 2.6; such is the nature of the lattice closure problem. Lattice closure is addressed in manifold ways, see sections 2.6.3 and 2.6.4. As an important aspect of results presented here, chapter 4 details a new and useful way to achieve closure to second order accuracy.

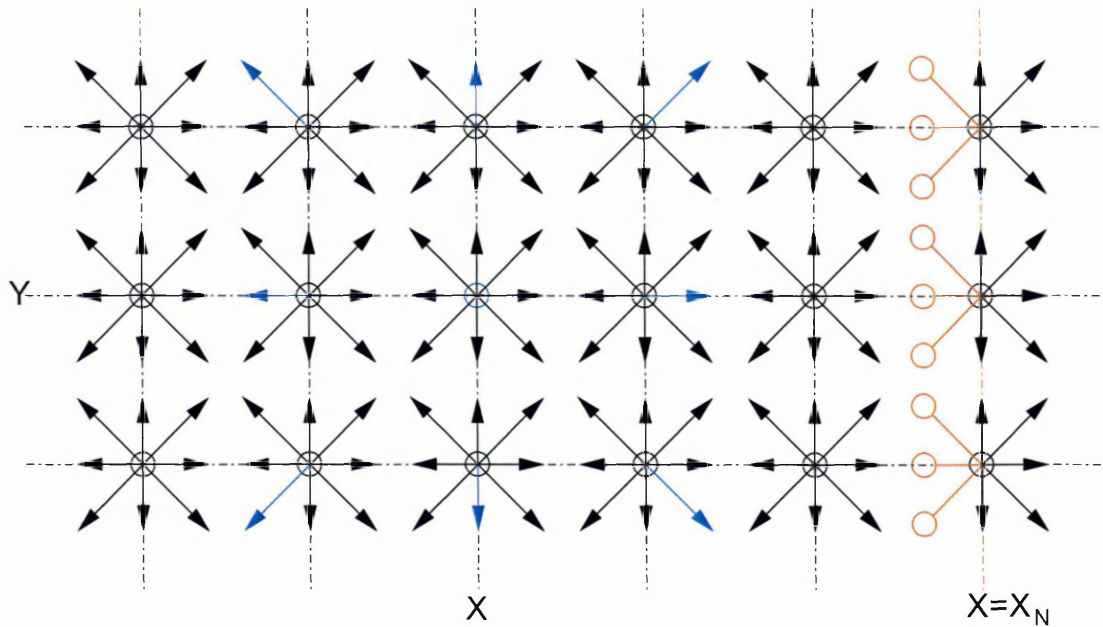


Figure 2.6: Representation of the lattice after a propagate step. Highlighted densities have moved (propagated) to neighbouring nodes as shown (other data propagate similarly), zero velocity stays put. Density values at the boundary, left undefined under propagation operator, are denoted by dark red circles on link.

Salient features of the LB scheme, are as follows: the primary ‘working’ variable is a discrete velocity distribution function for modelled fluid particles; no detail of the microscopic dynamics, collisions etc. is retained in the scheme, just their global or overall character; moments of the distribution define macroscopic observables; the collision operation is affected by simple ‘relaxation’ of the density distribution toward a *local* equilibrium; the equilibrium itself is calculated entirely locally; all calculations are highly local, rendering the scheme a good candidate for computational parallelisation; the streaming operator provides advective terms by rearranging the density distribution amongst neighbouring nodes; finally, evolution, \mathcal{E} , operates on the density field over the whole lattice and is defined to ensure that correct conservation occurs for macroscopic observables (i.e. some of the low order raw moments of the distribution) and so that, to a given order of accuracy, no spurious invariant quantities [43] occur in the derived macroscopics. Ultimately, the macroscopics of this system are proven to be exactly those of hydrodynamics — an amazing fact considering the seemingly disparate nature of the two systems.

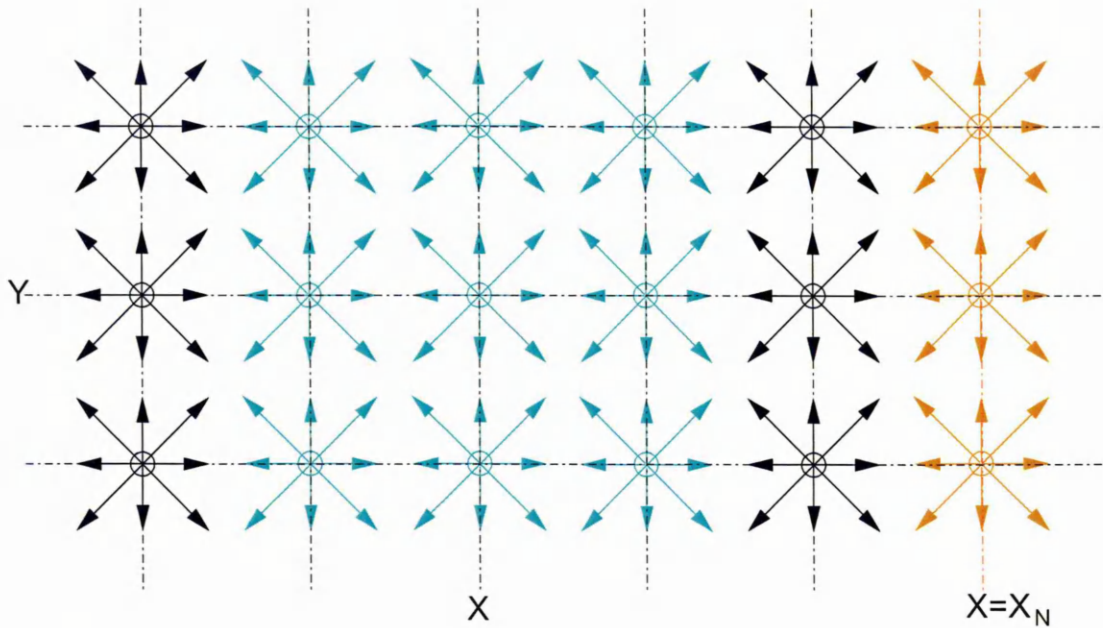


Figure 2.7: Post collide lattice representation, this is equivalent to data of figure 2.5. All nodes have been relaxed to a local equilibrium calculated using information in figure 2.6 (based upon post propagate information). Hence information from node (X, Y) has now influenced all new density values at neighbouring sites, denoted cyan. *Lack* of information at the boundary has likewise influenced densities local to the boundary, denoted brown.

Lattice Boltzmann equation macrodynamics

The LB scheme described over previous sections stands in its own right; it is one eminently suitable for parallel computation and is evidently simple. Its primary utility, however, has yet to be demonstrated. In particular, as a model for hydrodynamics, various important matters have yet to be indicated. The basis for this entire work is the fact that the LB scheme recovers hydrodynamics as its macroscopic behaviour; mathematical evidence for this has yet to be provided, however. The purpose of this section is to provide such and in so doing indicate how parameters involved in LB simulations are related to macroscopic variables of the modelled fluid.

As mentioned previously, certain primary macroscopic variables arise as basic properties (moments) of the velocity distribution function f_i ; these are already established, see equations 2.99 and 2.101. Other important variables have yet to be defined. Perhaps the most important example is the lattice fluid viscosity — the only variable which is purely characteristic of the fluid and not the flow. A clear method to assign its value might not immediately be apparent.

The way in which macroscopic properties of the microscopic gas model are conventionally found is, in direct analogy to that for basic parameters, to develop further moments. Moreover, *relations* between them must be found in order that physical (fluid) coun-

terparts may be identified. Crucially, developing these relations necessitates expansion of the governing *equation*. Hence, it is not just the solution function f_i which must be expanded, but the evolution equation itself. Conventionally, on account of its efficacy, this is achieved by performing a so called ‘Chapman–Enskog expansion’.

Chapman and Enskog’s analysis is one of successive approximation. It is a form of Hilbert expansion [18], but differs in that the equations themselves are expanded in addition to the dependent variable. Their work was a significant breakthrough in the field of gas kinetics and is routinely studied in continuous gas kinetics even today. An original source of reference for the *continuous* Boltzmann case may be found in Chapman and Cowling [19]; see also later texts such as Cercignani [18] and Liboff [84].

Here, in an attempt to derive the *lattice* fluid’s macrodynamics from the evolution equation (2.102, or 2.103), a discrete analogue of the original Chapman–Enskog expansion must be followed. Full derivation of hydrodynamics requires this be followed for each specific lattice type; it is in so doing that many important foibles and nuances of the LB scheme arise.

The full Chapman–Enskog expansion however, is rather long winded and mathematically delicate; moreover, some founding assumptions are nothing less than flaky. Following the Chapman–Enskog expansion in detail therefore cannot be justified, however, it is essential that some of its more significant aspects be treated here.

It is suggested that interested readers satisfy themselves of its general validity at least once, for one lattice of interest, but then stop at that. The reason for the suggestion is that recent additions to the literature demonstrate that the transition from micro to macro scales can be carried out other ways, [1, 58]. Moreover, in an as yet unpublished pre-print by D.J. Holdych *et al.* [67], it is shown to be possible from a much more mathematical / computational stance. A good recent exposition to follow, specifically for the D2Q9 case of relevance here, may be found as an appendix to [69].

Chapman–Enskog expansion in brief: A first characteristic presumption of the analysis is a decomposition of the distribution function into a hierarchy of contributions at distinct orders. The purpose of performing such an *expansion* of f_i is to invoke qualities and attributes of scale and relative influence, so that more complex behaviour can be introduced and tracked. Next the equations themselves must be similarly expanded, so that successive approximations can be found for the systems macroscopics.

The former has already been done note, in that equilibrium $f_i^{(0)}$ and non-equilibrium $f_i - f_i^{(0)}$ components to the distribution have been defined. Further detail in behaviour and, therefore, realism arises as the expansion is developed, *up to a point*. Over devel-

oping the expansion merely introduces complexity with which no practical reality can be identified.

The full distribution function then is supposed, at first approximation, to be composed of an *equilibrium* component $f_i^{(0)}$ (oft denoted \bar{f}_i) which, at better approximation, is found in summation with further contributions of successively lesser physical relevance, as follows:

$$f_i = f_i^{(0)} + \epsilon f_i^{(1)} + \epsilon^2 f_i^{(2)} + \epsilon^3 f_i^{(3)} \dots \quad (2.104)$$

Here ϵ is the *expansion parameter* and the $f_i^{(n)}$, where $n \geq 1$, are non-equilibrium distributional components.

Note that a particular attribute of the LBGK comes into effect at this point. When moving from quasi-linear LB to linearised and BGK models, aspects of the underlying collisions (which were incorporated into the scattering matrix) are lost. To recoup these (which are collision conservation laws) the same summation laws must henceforth be assumed of the equilibrium distribution function, as are applied to the full distribution function. That is:

$$\begin{aligned} \sum_i f_i^{(0)} &= \rho \\ \sum_i f_i^{(0)} c_{i\alpha} &= \rho v_\alpha \end{aligned} \quad (2.105)$$

Compare to equations 2.99. Which also implies that summations for non-equilibrium portions $f_i^{(1)}$ and higher be zero in addition²⁸. Hence, by way of equations 2.99:

$$\sum_i f_i^{(n)} \Delta_i = 0 \quad n > 0, \quad (2.106)$$

where $\Delta_i = 1, c_{ix}$ or c_{iy} is intended to condense notation for zeroth and first moments.

Prosecution of the Chapman–Enskog expansion then appears to follow either of two distinct paths, dependent on how the expansion parameter is treated and hence how the decrease in significance of terms is invoked; the end result being equivalent.

In one, the expansion parameter is treated as a kind of arbitrary, bookkeeping, scale identification parameter, which in the end, is set to unity (and hence disappears). In this case the $f_i^{(n)}$ are interpreted as having progressively lesser significance with n .

In the other, possibly more physically self consistent route, the expansion parameter is identified with a real, dimensionless, physical attribute of the system which may be

²⁸Note this really implies that $\sum_i \sum_n$ like moments are zero, for $n \geq 1$. But, to the order to which f_i is usually expanded, this only affects the first non-equilibrium portion; see equation 2.106.

assumed small; hence the significance of terms depends on its power ϵ^n . Equivalence of the two seems to be achieved by, in the latter case, imposing extra constraints on the subsequently expanded *evolution* equation, as will be seen; though no direct demonstration or proof of this has been unearthed by this author.

Texts adopting the former approach include Liboff [84], whose concise and direct style indicates, in addition to his great understanding, his unwillingness to get bogged down by technicalities. Those following the latter, more careful approach, include Cercignani [18]. Note that both examples discuss only the continuous case; upon which the discrete case is built, but from which it differs significantly. Hence, presumably, the source of much mathematical opacity and confusion on the matter; sediment in the muddy Chapman–Enskog waters.

The latter ‘physical’ approach takes the expansion parameter, ϵ , to be the Knudsen number (ratio of mean free path to a typical length scale in the flow):

$$\epsilon \equiv Kn = \frac{\ell_{\text{mfp}}}{\ell_i} \quad (2.107)$$

where i denotes integral scale. The Knudsen number then varies over the range $0 \leq Kn \leq \infty$, but is always small. High Kn (relatively speaking, still less than one) corresponds to a rarefied gas (few molecular interactions), whereas as $Kn \rightarrow 0$ corresponds to a dense gas and the hydrodynamic limit.

Moving to the next stages of the Chapman–Enskog expansion now; ‘expansion’ of the *evolution equation* proper (as opposed to the distribution). This seen to be a more or less intuitive process, consisting initially of a simple Taylor expansion of equation 2.103, to the first few orders of the expansion parameter ϵ . To achieve this necessitates expanding the independent variables, as follows:

$$\begin{aligned} x &= \epsilon^{-1}x_1 \\ t &= \epsilon^{-1}t_1 + \epsilon^{-2}t_2, \end{aligned} \quad (2.108)$$

where only the first lowest order terms are deemed of relevance to achieve the near equilibrium dynamics of interest.

It is slightly worrying that the decomposition assumed for time goes to an inconsistent order, but the aim here is to truncate time expansion into (only) *two* scales. They being to represent dynamics on ‘fast’ and ‘slow’ timescales. No such need arises in the spatial domain.

The former of equations 2.108 is easily rearranged to give an expression for the spatial

derivative operator:

$$\partial_x = \epsilon \partial_{x_1}. \quad (2.109)$$

Application of similar reasoning, but to the case of temporal derivative operator, requires a dubious extension to another power in ϵ . However, it is not unreasonable to assume that:

$$\partial_t = \epsilon \partial_{t_1} + \epsilon^2 \partial_{t_2}, \quad (2.110)$$

from which point, the advective (stream) operator may be written:

$$D_t = \epsilon \partial_{t_1} + \epsilon^2 \partial_{t_2} + \epsilon v_\alpha \partial_{x_1 \alpha} + \epsilon^2 v_\alpha v_\beta \partial_{x_1 \alpha} \partial_{x_1 \beta} + \dots, \quad (2.111)$$

at second order and in vector form.

Using the differential operators so derived, it is possible to construct the desired evolution equation expansion. This is not shown here as subsequent Chapman–Enskog expansion stages involve an intricate substitution of the expanded distribution function 2.104 and consequent simplification of the set of expressions so derived. Equation 3.7 of a future chapter, 3, provides an indicative view on this start point; it has traditional forcing terms included also. The treatment from there instantiates a specific route through the expansion mathematics and is presented in greater detail than here.

In pursuit of the expansion from here (simplification, collection and identification of terms on equivalent orders in ϵ), extra care seems to be necessary when following the physical approach. Then the expanded equations are best rearranged into an ‘operator’ form with one side arranged to be zero. Thus, as the operator is expanded, zero equalities may be imposed on the set of equations at each individual magnitude in ϵ . To see this see the book by the originator himself: Chapman and Cowling [19]; recently reprinted for the purpose. These ‘extra’ constraints, engineered to exert desired influence on the outcome, permits factoring of the expansion parameter at each level; equivalent to its removal by being set to unity when done the other way.

Such ‘engineering’ is sufficient to permit solving for the macrodynamical equations. The Chapman–Enskog expansion proceeds by collecting terms in like powers of the expansion parameter; reducing these by simplification; back substituting between orders etc. Some of which is demonstrated in later chapters, especially 3.2 where specific forcing terms are incorporated to the process and are followed through.

Simplifications alluded to previously depend especially on particular properties of the underlying lattice. For instance that all zeroth order moments over the lattice velocity

basis sum to zero:

$$\sum_i \Delta_i = 0, \quad (2.112)$$

where the notation is in keeping with equation 2.106.

The requirement for isotropy and Galilean invariance in derived macroscopics imposes further restrictions on the possible unknowns and thereby permit further refinement. These will not be discussed further here as whole publications have been devoted to such finer details in the literature. Galilean invariance for instance is discussed in [79, 113].

The end result is a set of equations representing macroscopics at various orders of approximation or detail. These were found to be so similar to hydrodynamics that it could not be ignored and a process of term ‘identification’ follows; most of which is relatively obvious.

Viscosity arises when considering $\mathcal{O}(\epsilon^2)$ terms in the expanded equations. After dividing out ϵ , a pre-multiplier of $\rho(\partial_\alpha v_\beta + \partial_\beta v_\alpha)/2$ within the divergence terms of the RHS appears at the next order as:

$$\frac{2\tau - 1}{6} \epsilon, \quad (2.113)$$

and hence may be identified (by reference to the momentum balance equation 2.14) as the kinematic viscosity ν . Since the relaxation time $\tau = 1/\omega$, the previous may also be written

$$\nu = \frac{1}{6} \left(\frac{2}{\omega} - 1 \right) \epsilon, \quad (2.114)$$

where the expansion parameter, ϵ , is (usually, dependent on the approach taken to the expansion, as mentioned in earlier discussions, pages 78 on) set to unity. Note that the positivity requirement of viscosity, $\nu \geq 0$, then gives rise to domains: $\tau \geq 0.5$ for τ ; and $0 \leq \omega \leq 2$ for ω , respectively.

As regards higher moments of the distribution (which are almost exclusively second moments only), a few other points warrant mention. Most notably that, in combination with the choice of equilibrium distribution function, 2.100, equations 2.101, after the Chapman–Enskog expansion, give rise to a non-viscous pressure tensor of the form:

$$\Pi_{\alpha\beta}^{(0)} = \sum_i f_i^{(0)} c_{i\alpha} c_{i\beta} = \frac{1}{3} \rho \delta_{\alpha\beta} + \rho v_\alpha v_\beta. \quad (2.115)$$

All symbols have their usual meaning [69, 112].

With respect to second velocity moments of the *non-equilibrium* distribution $f_i^{(n)}$, in contrast to first order moments given by equation 2.106, these are *not* zero. In particular,

it can be shown from the Chapman–Enskog analysis that:

$$\sum_i f_i^{(1)} c_{i\alpha} c_{i\beta} = -2c_s^2 \rho \tau S_{\alpha\beta}, \quad (2.116)$$

where $S_{\alpha\beta}$ is the rate of strain. Note that since $S_{\alpha\beta}$ is symmetric, equations 2.106 and 2.116 provide six equations constraining the $f_i^{(1)}$'s and thereby a possible way to close the lattice. These equations then are central to the method described in chapter 4. Moreover, in that they provide a means to introduce shear to possible algorithmic extensions of the core scheme, equation 2.116 is also of considerable relevance to turbulence model implementation — specifically for a law of the wall.

Other higher moments exist, certain of which are identifiable with additional macroscopic, as will be seen in later chapters (5).

2.5.3 Discussion of properties and character of LBM

Limits of validity arise in two ways. Firstly, the approximation of continuous differentials by difference type equivalents and the underlying discretisation necessarily introduces error at the level of truncation in the associated Taylor expansion. Hence the term various ‘orders’ of accuracy is used. Secondly errors arise in assumptions made in the formulation of the underlying BE, these may rigorously and explicitly be deduced if one works through the derivation of the LBM from its LGCA origins. In Boltzmann’s more physically transparent continuous formulation, it is apparent that they primarily relate to particle interaction aspects as follows:

Perhaps most importantly, Boltzmann’s molecular chaos ‘stosszahlansatz’ is assumed implicitly [14]. This essentially means that there is no correlation between particle velocities pre-collision, or that no account is taken of such.

Additionally, our system is assumed to occupy the low Mach number regime, that is $M \ll 1$, where the Mach number M defined by the ratio $M = U/u$, is much less than unity. Hence mean flow speeds U representative of the large scale character are small with respect to the mean of individual *particle* or molecular speeds u , (alternatively the velocity of sound).

Finally, the Boltzmann equation and hence all derivative methodologies, assume that the density of the medium is sufficiently rarefied that only binary collisions occur between gas particles. Strictly, the Boltzmann gas limit (BGL) is considered: For particle scattering cross-section σ , and particle number n , individual values tend as follows: $n \rightarrow \infty$, $\sigma \rightarrow 0$, with the products $n\sigma^2$ and $n\sigma^3$ remaining finite. Note that the *ideal gas* limit has $n\sigma^2$ remaining finite with $n\sigma^3 \rightarrow 0$, i.e. the effective volume of particles is zero, whereas

the BGL has both products remaining finite: $n\sigma^3 \rightarrow b > 0$ meaning that the mean free path is finite. As such the BGL represents a more realistic class of gas model than ideal gases.

Macroscopic hydrodynamic equations are traditionally derived from the lattice Boltzmann equation by performing a Chapman-Enskog expansion (CEE). The CEE procedure is well known amongst practitioners of traditional kinetic methods for the continuous case, the discrete case requires subtle modification, but is in essence the same. It is rather convoluted and fussy to perform and a description does not fall within the scope of this report. It has recently been shown that hydrodynamics may be arrived at from the discrete BE via other routes [1, 58] which now sets the LBM on a yet more rigorous footing.

Limitations and scope of the LBM are discussed, where relevant, throughout subsequent chapters.

2.6 Flow geometries, simulation domains and forcing

Typical industrial systems consist of basic components which may be quite generally utilised over a wide range of differing systems. They in turn are typically composed of just a few commonly occurring elements; obviously those of interest here relate to fluid dynamical processes. The basic elements which go to make up such systems might be categorised as either active or passive. Active elements are in general quite application specific, such as pumps, meters, switches (valves) and the like. Passive elements might include reservoirs of various kinds, connections, junctions as well as more complex types such as heat exchangers. Whatever the taxonomy, it is clear that elements such as connectors: pipes, ducts and their junctions, say, occur very commonly; moreover their properties and impression on the flow inside will, over the entire system, be of great significance. Attention therefore is often focused on these two geometric types: pipes and ducts.

Most flow systems consist, at least in part, of these forms of conduit. Moreover, under simplifications of modellers, more complex systems may be modelled purely as configurations of variously proportioned channels. System elements such as these therefore, form the practical basis for the investigations undertaken in this work — whilst simple in nature, complex behaviour they nevertheless exhibit. Their discussion needs to be set in a rigorously clear perspective. Such is the purpose of this penultimate section of background material, which addresses a mixed bag of geometric and channel configurational issues.

In the following it will become apparent that pipes and ducts differ only subtly. Pipes will be considered cylindrical channels, whereas ducts are considered channels with rectangular cross section. The words pipe and duct, whilst denoting configurations distinct in nature, will often be used interchangeably with reference to the channel. This occurs primarily as a descriptive convenience; symmetries about centre are more obvious in the pipe representation — centre line is at radius $r = 0$ for instance — whereas commonality with the simulation domain is more obviously expressed from a Cartesian perspective. No confusion should arise. Similarly there should be no confusion over other technicalities of the nomenclature. For instance, the phrases ‘flow geometry’ or simply ‘geometry’ are commonly used throughout this work as another loose reference to the actual physical configuration that constrains fluid flow.

The presentation begins with a relatively detailed review of laminar flows in the three internal geometries which are of most interest; section 2.6.1. This is followed by an overview of some important physical parameterisations commonly applied to simple channels; section 2.6.2. In section 2.6.3, a brief aside is taken to consider the various physical

boundary conditions that will be encountered. Therein, at page 101, such are translated into the context of the simulation lattice and the various lattice closure schemes. Finally, in section 2.6.4 more practically amenable means to induce or drive fluid motion are discussed — especially forcing schemes for translationally invariant flows, at page 108.

2.6.1 Internal flow configurations

Attention in this work is focused on so called ‘internal’ flow geometries. For the present purpose, these may be defined as ones that are wholly occupied by a single phase of fluid; in this case a liquid. Equivalent definitions are: that there are no surfaces to the fluid, either to gas phases or to other liquid species; alternatively, that only solid walls, or boundaries consisting of the primary fluid undergoing flow, delimit the systems of interest.

Real instances of such systems are ubiquitous; see section 1.2 and 5.1 for the practical context. Most interest falls upon two main practical cases: pipes and ducts, description of which initiates the following discourse. Types other than such channels are considered however, including plane Couette (shear) flow and the lid driven cavity (LDC), but these are of interest for their theoretic utility (analytic solutions) and they do not possess much practical relevance.

The purpose of these discussions, specific to internal geometries, is to deal with geometric technicalities regarding dimensionality, coordinate systems, coordinate representations, symmetries and descriptive conventions. Such matters are to be clarified and defined, in order to enable precise and unambiguous specification of investigations carried out in later chapters.

Channel flow geometries: pipes and ducts

Channel flow is a three dimensional modelling problem. Commonly however, in simulations and theory, this dimensionality is reduced to two dimensions, by postulating that the flow is invariant with one coordinate, that is along one direction in space. Physical equivalents to such simplified systems are: *duct* channels, *infinitely deep* in a direction perpendicular to the flow direction; or, cylindrically symmetric *pipe* channels. Primary flow configurations considered in this study fall into these categories. An alternative statement of this reduction in dimensionality is that the fluid is constrained to move in only two dimensions. Practical realisations of this idealised flow can be approximated in experiments.

Ducts and pipes are represented by coordinate systems (x, y) and, nominally, (r, z) , respectively. The two instances are described diagrammatically in figure 2.8, parts i)

and ii). Obviously both these systems are symmetric about their centre lines, a property which may be exploited in simulations. The pipe however, has differing centre line symmetry in that it is *axial* and, to highlight such differences, extra mention is made of it in the next sub-section. Features common to both pipes and ducts are discussed here.

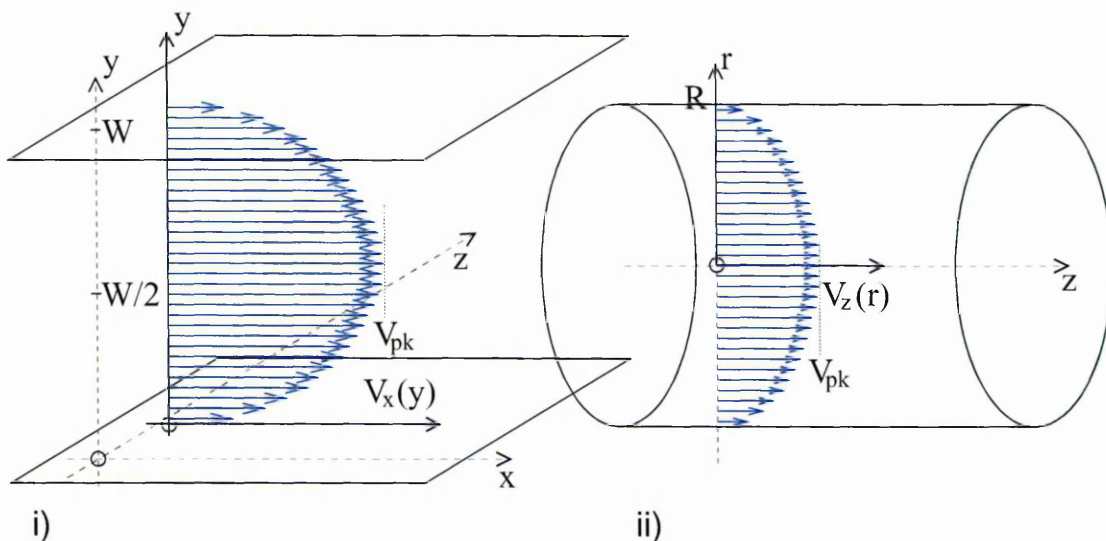


Figure 2.8: Two types of translationally invariant channel. Representations of the flow profiles generated under forcing F_x are included for illustration only. i) Infinitely deep duct flow, translationally invariant with x . ii) Pipe or axially symmetric flow, translationally invariant with z . The $r = 0$ line represents the pipe axis. Pipe flow is discussed in the next section (page 89), where it is explained that, due to increased cylindrical friction over the duct case, the profile magnitude shows a reduction by a factor of two.

Further reduction in the complexity of such channels may be afforded upon realising that, during a theoretical analysis, one would likely consider the case of a channel with infinite length in the along stream direction. This is practically of interest regarding any system with large aspect ratio²⁹. In such cases the channel is said to be ‘translationally invariant’, both along channel and with the flow.

Translationally invariant channels are effectively a one dimensional modelling problem. Implementation of such geometries, at the level of simulation domain, is made by imposing periodic boundaries at appropriate lattice edge nodes. Details of this and other lattice closure issues are discussed at page 101.

Analytic solutions, for the cross channel profile of velocity, are easily found for translationally invariant flow. Since a good working knowledge of such is required in following chapters, derivation of solutions are now provided and properties of these discussed.

Under said invariance and steady state conditions, the Cartesian form of the governing Navier–Stokes equations reduce to the following parabolic forms, for $\alpha = x$ and $\alpha = y$

²⁹Aspect ratio in this respect refers to the ratio of length to width, L/W , for the channel.

respectively:

$$0 = -\frac{1}{\rho}\partial_x p + \nu\partial_{yy}v_x, \quad (2.117)$$

$$0 = -\frac{1}{\rho}\partial_y p. \quad (2.118)$$

As usual, incompressibility is assumed. Components x and y refer to directions ‘cross’ channel and ‘along’ channel respectively. At this point, by considering Cartesian equations, application is now restricted to the duct geometry; pipe equivalents are considered in the next sub-section.

A solution to this equation is readily derived. Note that equation 2.118 essentially asserts that pressure p can only depend upon x (hence $\partial_x p \rightarrow dp/dx$ in equation 2.117). Note also that the latter RHS term of equation 2.117 can not depend upon x , as $v_x(y)$ is assumed under translational invariance. Hence neither does the former RHS term depend upon x and it may be regarded as constant, allowing simple integration of 2.117 to give:

$$v_x(y) = -\frac{1}{2\eta}\frac{dp}{dx}y^2 + c_1y + c_2, \quad (2.119)$$

where p is now known to depend only on x . This is the general solution which is particularised under application of the BCs.

Various BC formulations may be applied for the same essential situation. Taking the geometry to be as in figure 2.8 part i), $0 \leq y \leq W$, no slip wall conditions are:

$$\begin{aligned} v_x(y=0) = 0 &\implies c_2 = 0, \\ v_x(y=W) = 0 &\implies c_1 = \frac{W}{2\eta}\frac{dp}{dx}, \end{aligned} \quad (2.120)$$

giving

$$v_x(y) = -\frac{1}{2\eta}\frac{dp}{dx}(Wy - y^2), \quad (2.121)$$

for channel width W . Note that by convention a positive pressure gradient gives rise to negative flow and vice versa; hence the minus sign. Exemplary parabolic flow profiles representing this solution are provided in figure 2.9 part i).

The cross channel mean velocity, hereafter denoted V , may be obtained by simple integration of equation 2.121 over the interval $[0, W]$ and subsequent division by the width:

$$V = \frac{1}{W}\int_0^W v_x(y) dy = -\frac{1}{2\eta W}\frac{dp}{dx}\left[\frac{Wy^2}{2} - \frac{y^3}{3}\right]_0^W, \quad (2.122)$$

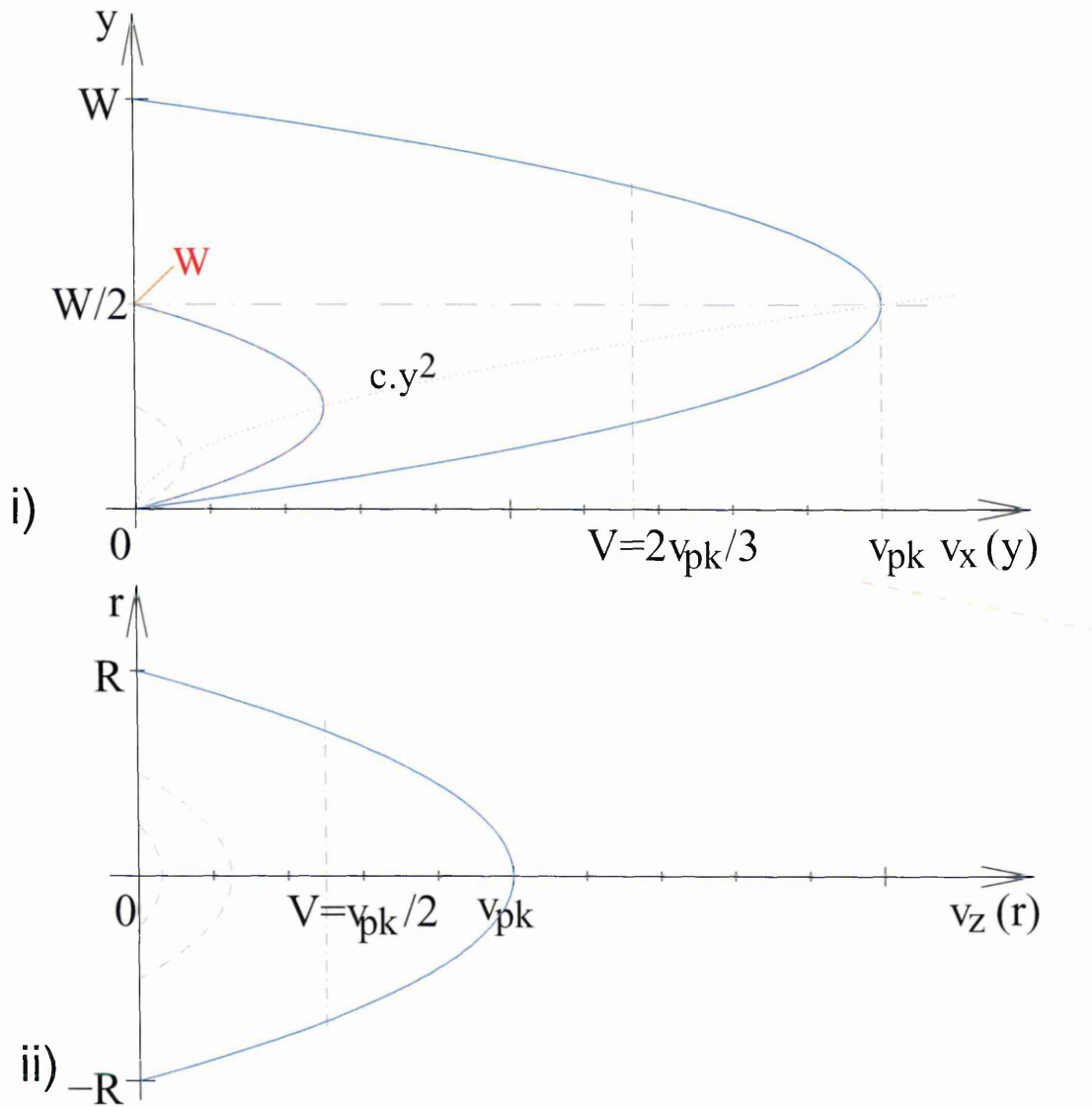


Figure 2.9: Exemplary parabolic flow profiles for laminar (Poiseuille) flow in simple channels. Part i) is $v_x(y)$ in planar geometry (laminar duct flow). Part ii) shows $v_z(r)$ for cylindrical geometry (laminar pipe flow). Solid blue profiles have equivalent *linear* sizes, i.e. $W = 2R$. Peak velocity is denoted v_{pk} (at duct centre line); mean velocity is denoted capital V — note relative magnitudes. Dashed blue profiles are for halved channel sizes, revealing square dependence of peak velocity in both cases (dotted line (top) is equation of v_{pk}). Dot-dash lines are constructions. Dashed red lines represent equivalents to solid blue, but for case of equal hydraulic diameter to that of opposite graph (e.g. red W equals R of part ii)).

to give

$$V = -\frac{dp}{dx} \frac{W^2}{12\eta}, \text{ which implies } \frac{dp}{dx} = -\frac{12V\eta}{W^2}. \quad (2.123)$$

Hence a one dimensional steady state laminar velocity profile is parabolic, as follows:

$$v_x(y) = \frac{6V}{W^2}(Wy - y^2). \quad (2.124)$$

The central, peak velocity, v_{pk} , occurs at the point $y = W/2$ and is given by

$$v_{pk} = \frac{3V}{2}. \quad (2.125)$$

See any good fluid dynamics texts, such as [73, 81]. Equation 2.124 is essentially the equation for a parabola which passes through the origin $y = 0$, intersects the x axis at W and has peak velocity v_{pk} .

Note that for any given forcing scenario, that is dp/dx and viscosity η are known and constant, the velocity profile magnitude and hence peak and mean channel velocities, go as the square of the channel width. Note also that, for the idealised (infinitely deep) duct geometry, the peak velocity is always 3/2 times the mean velocity; which coefficient is to be compared to equivalents for the pipe flow. Laminar pipe flow equivalents, including steady state solution profile, are provided in the next sub-section. Some comments on the results derived here, are also made there, comparatively.

Axially symmetric channels: pipes

An axially symmetric geometry, in the context of this work, is one for which the three dimensions that describe the flow space, may be reduced to two for the simulation space, where there is no flow variation with angular dependence around some characteristic axis. This situation is shown schematically in figure 2.8 part ii) and in figure 2.9 part ii) which represent ‘pipe flow’.

Such a configuration may be represented in more than one way. Here, the (x, y) coordinates of the page are transposed to (z, r) in order to highlight the cylindrical nature. Strictly, a section of the pipe is considered which is distant from either of its ends, pipe length runs with the z -direction, the axis appears horizontally along the centre line of the diagram, flow occurs parallel to this (conventionally, though arbitrarily, from left to right).

Under the applied translational independence (body forcing too therefore), flow is additionally constrained to be invariant with z , thus leaving only radial r and temporal t independent variables: $\mathbf{v}(\mathbf{x}, t) \mapsto v_z(r, t)$. Hence, as with other work on channels herein,

the simulation domain may be rendered spatially one dimensional.

Analytic solutions, for the cross channel profile of velocity at steady state, arise from cylindrical Navier–Stokes equations which reduce to the form:

$$0 = -\frac{1}{\rho}\partial_z p + \frac{\nu}{r}\partial_r r\partial_r v_\alpha. \quad (2.126)$$

Here, the subscript α represents (z, r) ; components z and r refer to directions ‘along’ channel and ‘radial’ respectively.

A solution to this equation is readily derived by following a similar procedure as that for the duct case (previous sub-section, page 87). Taking the geometry to be as in figure 2.8 part ii), hence $-R \leq r \leq +R$, no slip wall conditions: $v_z(r = \pm R) = 0$, give

$$v_z(r) = -\frac{1}{4\eta}\frac{dp}{dz}(R^2 - r^2), \quad (2.127)$$

as the solution steady state velocity profile in a pipe. Exemplary parabolic flow profiles from this solution are given in figure 2.9, part ii).

Proceeding to the mean velocity, which is important for ‘global’ flow characterisation, care must be exercised as this is *not* possible by simple integration with respect to r (over $-R$ to R). To do such a ‘Cartesian integration’ does not account for the fact that increasing fluid volume is associated with locations an increasing distance r from centre line.

It is possible to find the peak velocity however, which occurs at $r = 0$:

$$v_{\text{pk}} = -\frac{1}{4\eta}\frac{dp}{dz}R^2 \quad (2.128)$$

and which, on re-substituting into equation 2.127, gives the flow profile in terms of the peak as follows

$$v_z(r) = v_{\text{pk}}\left(1 - \frac{r^2}{R^2}\right), \quad (2.129)$$

for laminar *pipe* flow. This may be used to find the mean (and mean in terms of the peak) effectively through a coordinate change, by relating the volumetric flow rate to velocity. The mean in terms of total volumetric flow is given by

$$V = \frac{Q}{A} = \frac{Q}{\pi R^2}, \quad (2.130)$$

where A is the cross sectional area of the pipe and Q the full flow rate. Invoking the ‘weighting’ of a small change in Q by r , consider the area of an elemental annular ring,

centered on the axis and located at r :

$$dQ = 2\pi r \, dr \cdot v_z(r), \quad (2.131)$$

where the thickness of the element is dr . This quantity is seen to be a volume of fluid per second (volumetric flow rate) if one observes the dimensions, $[L^3T^{-1}]$. The integration may now be made and thus the mean related to the peak, via Q . Integrating equation 2.131, with $v_z(r)$ substituted from equation 2.129:

$$Q = 2\pi v_{\text{pk}} \int_0^R r \left(1 - \frac{r^2}{R^2}\right) dr = \frac{\pi v_{\text{pk}} R^2}{2}, \quad (2.132)$$

which, on using equation 2.130, gives the peak in terms of the mean for laminar pipe flow as:

$$v_{\text{pk}} = 2V, \quad (2.133)$$

after some rearrangement. Further manipulations also reveal

$$\frac{dp}{dz} = -\frac{8\eta V}{R^2}. \quad (2.134)$$

It is apparent from the above, that flow in an axially symmetric channel geometry, is superficially identical to that in duct geometries, but that subtle differences exist. Both profiles are parabolic, a fact which arises with the underlying nature of the reduced Navier–Stokes equations. However, magnitudes of the velocity profiles differ, which has consequences for the relative mean velocities, volumetric flow rates and derived friction coefficients.

Summarising these differences:

- The flow profile magnitude in a pipe, associated with a certain driving pressure dp/dx and viscosity η , will at all points be exactly half that of the duct; compare equations 2.121 and 2.127, with R set to $W/2$.
- The *mean* flow velocity is exactly two thirds of the *peak* velocity for the duct, which compares to the mean being precisely half that of the peak in the pipe.

These points also mean that the volumetric flow *per unit area*, driven by certain pressure gradient, will be a factor 4 times lower for pipe flow than the infinitely deep duct. Though it is not likely that such practical and ideal flow configurations will ever need to be compared in the same light, the reader needs to be aware of these features in this work, because of the focus on these two geometries.

Features such as these, reflected in profile magnitudes on the figures 2.8 and 2.9, must be recovered by the model introduced in chapter 3. The model developed there successfully enables simulation of an axially symmetric system, directly on a regular Cartesian grid, by use of appropriate forcing terms in the LB evolution. Forcing in general, is discussed as a basis for such a scheme in section 2.6.4, at page 108 on.

The aforementioned qualities arise, physically, under the shearing influence imposed by the domain walls. Essentially, ratios of shear inducing area and flow cross sectional area differ by a factor of two between cases, demonstrated as follows. Wetted area³⁰, $A_W = 2\pi R\ell$ for the pipe (circumference times length) and $A_W = 2(d + W)\ell$ for the duct, d being the duct ‘depth’. Cross sectional areas are: $A = \pi R^2$ for the pipe and $A = Wd$ in the duct. Ratios of these are: $2\pi R\ell/\pi R^2$ for the pipe and $2d\ell/dW$ for the duct (strictly in the limit as duct depth d approaches infinity: W in the numerator may then be ignored). On making their domain sizes equivalent: $R = W/2$, the ratio for the pipe evaluates to twice that of the duct, at $4\ell/W$. So, equivalently, shear surfaces in the pipe act on a higher proportion of the fluid mass because friction induced shearing area scales with R^2 .

Combine this with the respective geometric qualities, which further affects total flow rate. The ‘weighting’ effect by an r factor, when integrating over radial position, mean that central, high flow areas, make lesser contributions to the overall volumetric flow. The net effect, is that friction induced shear on the flow, by the walls, is effectively four times higher in the pipe geometry.

Simple shear flow geometries: Couette flow

Shear occurs in all flow configurations where solid walls exist. Walls impose no slip velocity conditions on the fluid in contact; that is, the difference in velocity between fluid immediately adjacent to the wall and the wall is zero. This is a commonly accepted standard, utilised in virtually all flow simulations.

The amount of shear induced in a fluid, under specific flow conditions, is related directly to the fluid viscosity. Simple shear flows are of added interest therefore, because they provide a means to calculate fluid viscosities.

Pure shear flows are practically difficult to realise, but by clever design of the flow configuration it is possible to do so. Idealised embodiment of such, may be investigated in the theoretical and numerical frameworks, if it is arranged for the dimensions of the configuration to be sufficiently extreme as to ‘iron out’ geometric problems. This way it is

³⁰Owing to translational invariance, channel lengths may be factored out and it is possible to consider instead ‘wetted perimeters’, p_w , though this is not necessary.

possible to induce nearly ideal shear flow and, moreover, flow for which analytic solution is possible. The arrangement is commonly described as ‘counter rotating cylinders’ and is known eponymously as Couette flow; it is shown schematically in figure 2.10.

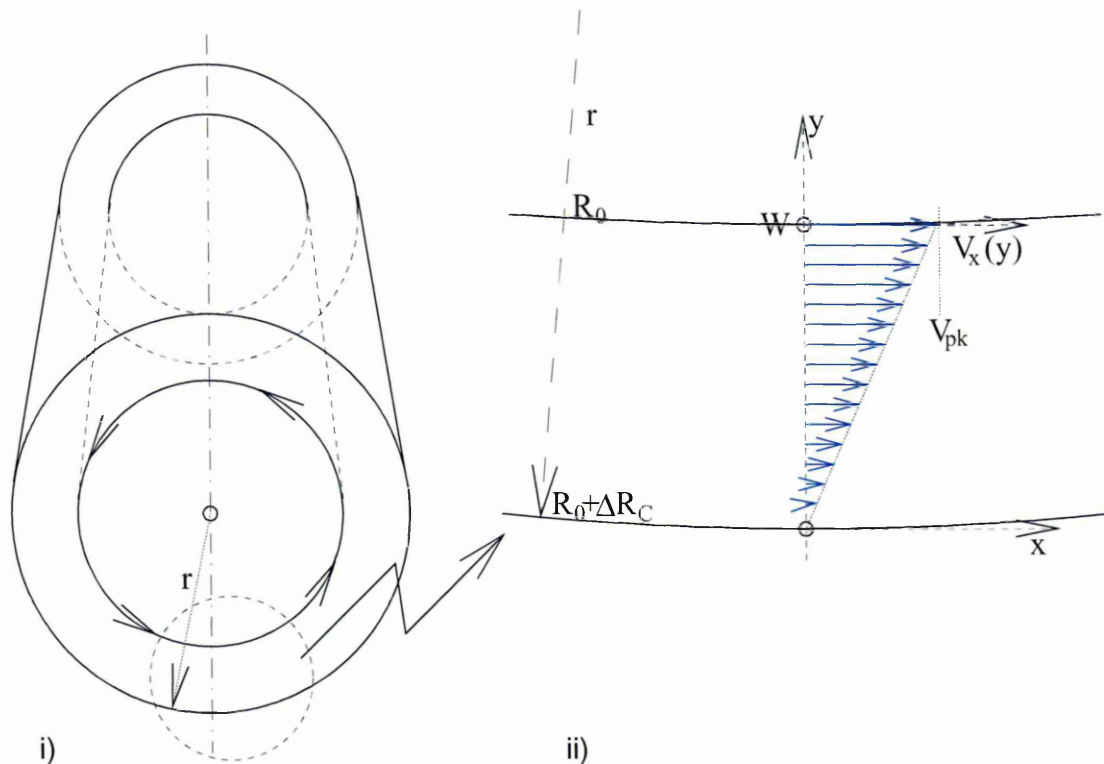


Figure 2.10: Experimental implementation of a ‘pure shear’ flow. The arrangement gives rise to ‘Couette’ flow. Simulations and analytic solutions arise from the idealised case represented in figure 2.11.

Computationally this configuration may be approximated under certain limiting conditions. Primarily, curvature of the flow domain is rendered negligible if the fluid zone occupies a very thin range of radii ΔR_C , at great distance off axis R_0 : $R_0 \leq r \leq R_0 + \Delta R_C$; $R \rightarrow 0$; $R_0 \rightarrow \infty$. This idealised representation of Couette flow is alluded to in figure 2.10 part ii) and its absolute limiting case shown in figure 2.11. The latter conveys how the experimental arrangement is implemented in a computational framework.

The aforementioned constraints are equivalent to infinite length in the simulation domain, or alternatively, translational invariance, which may be implemented in the usual way if certain restrictions on the way flow is induced are adhered to. Periodic BCs are imposed to bound the flow in the ‘infinite’ direction (see later in this section, page 105) and fluid motion is driven by the use of body forcing (again, see later, page 108), thus rendering the flow domain translationally invariant. Translational invariance may itself be exploited in an alternative derivation of an analytic solution, which is summarised next.

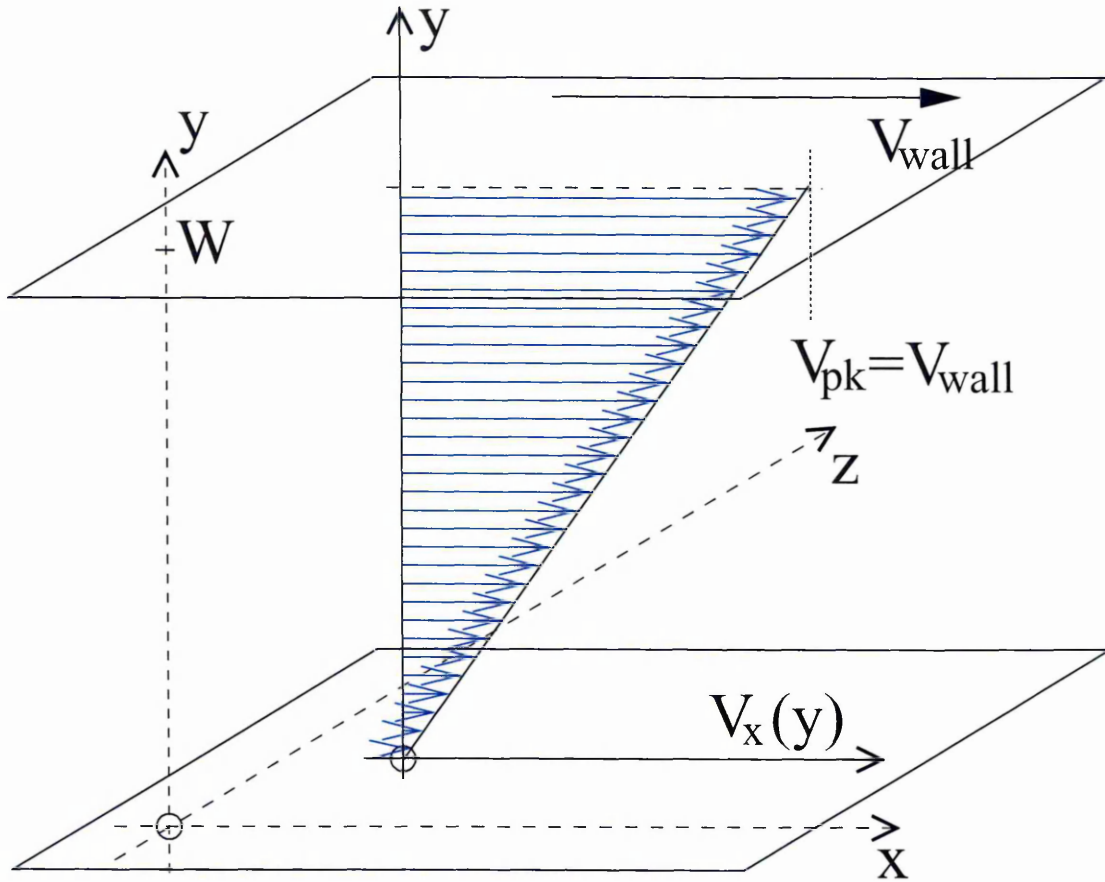


Figure 2.11: Computational domain for ‘pure shear’, or Couette flow; the ‘top’ wall in this case is driven at speed $v_x = v_{\text{wall}}$. Illustration of a steady state velocity profile is also shown for the case of laminar flow.

Variations on the theme of Couette flow centre on time variation of velocity of the driven wall. Of particular interest here is the so called impulsively driven Couette flow, where the driven wall starts impulsively from rest at some point $t = 0^+$ and accelerates to wall velocity, v_{wall} instantaneously. Obviously this is not feasible practically, but it is of interest herein because, again, an analytic solution may be found; derivation of this now follows.

Consider the geometry presented in figure 2.11. Fluid is constrained to lie between the two planes at $y = 0$ and $y = W$. Under invariance, the governing incompressible Navier-Stokes equations reduce to a one dimensional diffusion equation with inhomogeneous boundary conditions. The upper surface is impulsively started at $t = 0^+$ to velocity $v_x(y = W) = v_{\text{wall}}$, $v_y(y = W) = 0$ (in lattice units). Seeking a solution in the form of a steady state with separable transient yields:

$$v_x(y, t) = \frac{v_{\text{wall}}}{W} y + \frac{2v_{\text{wall}}}{\pi} \sum_m \frac{(-1)^m}{m} \sin\left(\frac{m\pi y}{W}\right) \times e^{-m^2\pi^2\bar{t}}, \quad \bar{t} = \frac{\nu t}{W^2}. \quad (2.135)$$

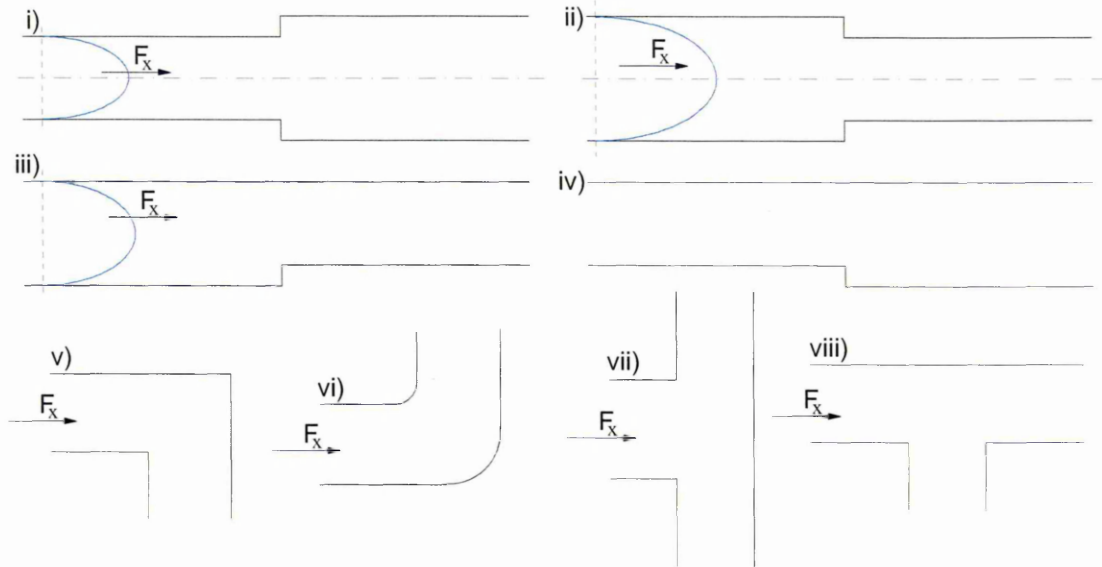


Figure 2.12: Examples of other geometries, discussed especially regarding further work. i) Sudden expansion. ii) Sudden constriction. iii) Front facing step. iv) Back facing step. v) and vi) Bends. vii) and viii) Tee junctions.

Here \bar{t} represents a *dimensionless* time parameter allowing direct comparison between analytic and measured profiles. Plots of the behaviour of this solution are provided in section 4.3 and the nature and efficacy of the improved boundary scheme is discussed in that light.

Other, more complex geometries

Other internal flow configurations are of great practical interest but, whilst very simple, most represent increased complexity over simple channels. Instances include bends, junctions, constrictions and expansions. Most are pretty self explanatory in nature, but simple representations of each are provided in figure 2.12 to remove any ambiguities. Further detail is provided when mention necessitates it.

One other configuration however, which commonly occurs and is routinely studied on account of its simplicity in some respects, is not so self explanatory. A brief description therefore follows, for the purposes of completeness and general context with respect to the literature and validation of the core LB code.

The ‘lid driven cavity’ (LDC) is of interest because it is a fully internal and purely shear driven case. Under this arrangement there are no flow BCs, no imposed pressure gradients and, in the absence of gravity, which is typically neglected, there are no body force terms.

A schematic of the lid driven cavity is shown in figure 2.13. Important characteristics

it possesses are that the flow is: entirely enclosed by solid boundaries; and, forced by friction generated shear at the moving wall. This has the control advantage of removing the need for flow, or von Neumann, closure conditions completely; a significant enhancement of simplicity, at the expense only of practical utility.

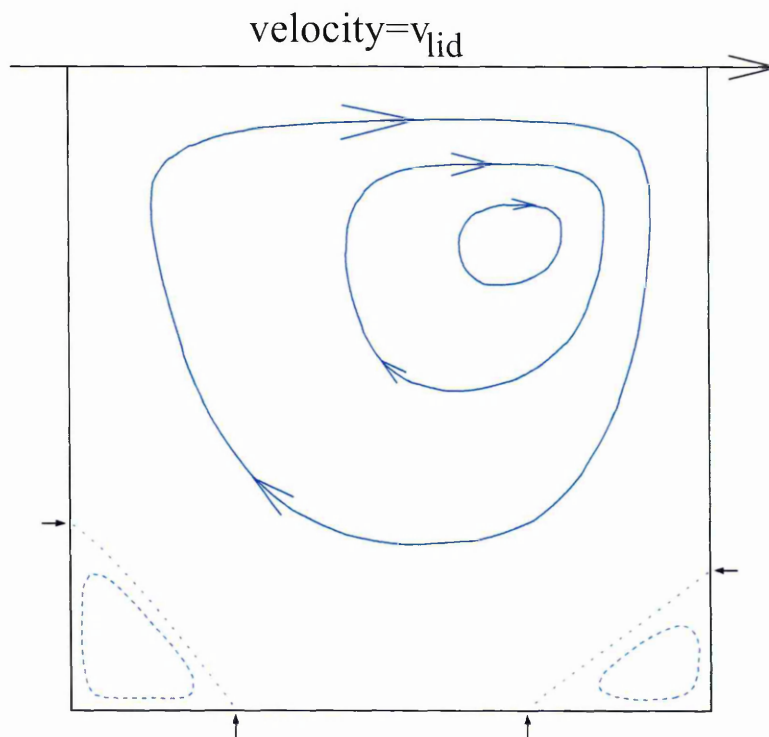


Figure 2.13: The lid driven cavity (LDC) and representative streamlines. Streamline arrows illustrate magnitudes. Small re-circulations, as occur at high Reynolds number, are shown in appropriate corners (dashed lines). Lines of zero velocity are shown dotted and their contact points with the wall marked. Re-circulations have very low velocity magnitude relative to primary circulation.

A large amount of detailed work has been published on the LDC configuration [69,94]. This enables easy validation of flow characteristics for the purposes of checking code writing. For exemplary references on LBGK applied to the LDC see: Miller [94]; and Hou *et al.* [69]. In the current work the LDC was used simply to validate the core LB scheme, prior to any scientific investigations and is not included here.

2.6.2 Some laminar channel flow parameters

The following two brief asides define important parameters which will be used widely in the remainder of this work. Whilst their derivation is not necessary, presentation here is given in a derivational context to increase their appreciation. In a following section 2.7, some of the concepts introduced will be utilised in definition of further useful flow parameters, most notably the friction coefficient.

Hydraulic radius / diameter

For the case of circular conduit there exists a logical length scale with which to parameterise channel size. The pipe diameter is used, which allows simple calculation of other flow parameters such as Reynolds number, page 46, and friction factors (to follow, page 116). However, for the case of non-circular conduits, a logical choice for length parameterisation is not so obvious. A convention is required for a length parameterisation that somehow relates fundamentally to the actual size of the channel.

The ‘*hydraulic radius*’ is defined for this purpose, thus generalising the idea of radius to non-circular, arbitrary cross section channels. It is arrived at through a commonly occurring relation between flow cross sectional area A and ‘wetted perimeter’ of the channel p_w , neither of which refer to distances along the flow. In fact the hydraulic radius is simply the ratio thereof:

$$R_h = \frac{A}{p_w}. \quad (2.136)$$

Note however that the nomenclature is somewhat misleading: the actual length parameter used, ℓ_g say, is always four times the hydraulic radius:

$$\ell_g = 4R_h. \quad (2.137)$$

Subscript g denotes the geometry. The factor four is intended to ‘calibrate’ the definition in order to give the diameter in pipe flow cases: for circular cross section, the length parameter used amounts to four times πR^2 over $2\pi R$, which is, note,

$$\ell_g = 2R = \varnothing, \quad (2.138)$$

that is (logically) *twice* the actual radius — the diameter. But the nomenclature then suggests a diameter which is four times a radius! (by $\varnothing = 4R_h$). A hydraulic diameter might just as well be defined instead, say $\varnothing_h = 4A/p_w$, which some treatments do and is used here (then, for the pipe, $\varnothing_h = \varnothing$). However, to keep in concert with standard treatment, the fundamental parameter is the ratio of area to perimeter, R_h .

For the case of ‘infinitely deep’ duct (of depth d), to which much of the work herein refers, the hydraulic radius is similarly A over p_w ; which is dW , over $2(d+W)$. Hence, on noting that as d tends to infinity the W in p_w becomes negligible and may be dropped, d conveniently cancels to give a hydraulic diameter:

$$\varnothing_h = 2W. \quad (2.139)$$

Hence the hydraulic diameter of a duct channel is twice the duct width. Moreover, it is twice that of a pipe, at least where W is taken to be $2R$.

The hydraulic diameter is used as the primary length parameterisation of a geometry for the purposes of calculating Reynolds number and friction factors. It is useful in that it effectively captures geometric subtleties such as that which gives rise to duct flow profiles with twice the magnitude of equivalently driven pipes. To see this consider the Reynolds number, $Re = \varnothing_h V / \nu$, where for the pipe $\varnothing_h = 2R$ and for the duct $\varnothing_h = 2W$. On noting that $W = 2R$, then all else being equal, that is at the same Re , flow profile magnitude U must be a factor of two lower in the pipe — which it is.

Wall shear stress and viscosity

Pressure drop occurring along laminar flow in simple conduits, arises with viscous friction forces exerted on the fluid by the static wall. As fluid elements impinge on their neighbours, which in general will have differing velocities, it is obvious that some of the velocity information will be communicated in the process — faster regions speed up slower ones and vice versa. Assuming the accepted paradigm of zero velocity differential between wall and immediately adjacent fluid, the net effect of this communication is to impede flow, as viscous induced shear transmits retardation forces into the bulk of the fluid.

The nature of flow, especially whether it is turbulent or laminar, has a great influence on the relative effect of this process. Importantly, it is accepted that in the case of *turbulent flow* a mechanism of this sort exists, but it differs in that it is *barely dependent on viscous effects*. So conversely, quantifying just how much a flow is impeded by the wall under specified flow conditions gives a good indication of flow character. In a subsequent section, 2.7.1, this matter is explored further, with the intention of parameterising pressure drops and friction effects for the turbulent case.

The primary factor of concern turns out to be the shear stress due to the mean fluid flow at the wall. This *wall shear stress* — a pressure in that it is a force over an area, dimensions $[ML^{-1}T^{-2}]$ — is typically denoted τ_w , a convention adopted herein. No confusion should arise between this and either the LB relaxation parameter, or the Reynolds stress tensor.

To quantify it consider the idealised case of laminar flow in a regular channel situated in space, that is free from gravity. The pressure differential between two points will be entirely due to resistive friction forces exerted on the fluid by the walls. Working in terms of forces, wall shear stress τ_w being a pressure note, a simple balance equation may be drawn up. Force terms due to pressure are given by the sum over both points, of the

product of pressure and flow cross sectional area, A : $PA + (P + \Delta P)A$ where $A = \pi R^2$ for the pipe, $A = dW$ for the duct and ΔP represents the pressure differential. This expression must sum to zero with that for friction forces; that being: $\tau_w A_w$ where area A_w is the wetted area of wall, that is $2\pi R\Delta x$ for the pipe and $2(d + W)\Delta x$ for the duct, where the two points are Δx apart. Observing the limit as Δ tends to zero, also (as done above) as $d \rightarrow \infty$, gives

$$\frac{dP}{dx} = -\frac{4\tau_w}{\mathcal{O}_h}, \quad (2.140)$$

for both pipe and duct. Obviously this can be interpreted by it's inverse, as a relation for the stress in terms of the pressure gradient.

Shear stresses exhibited in a laminar flow, may be directly related to the viscosity — that most important property of the *fluid*. Typically, an idealised shear flow situation is considered; the flow between two parallel planes for instance, where there is finite velocity difference between the two along some direction in the plane — similar in principal to Couette flow. Despite the fact that the fluid in such an arrangement continuously deforms, it nevertheless exerts a constant viscous induced friction force between the planes which, for uniform sliding motion, exactly balances the external force producing the motion.

In such cases the velocity gradient in the fluid is constant and proportional to the plane velocity differential. Moreover, the shear force per unit area, τ is proportional to the velocity gradient — often known as the rate of shear dv/dy . The constant of proportionality is deemed a property of the fluid and in the Newtonian approximation — which holds strong for almost all flows — it is known as the viscosity; the 'Newtonian coefficient of viscosity, for that fluid, η . Commonly it is divided by the fluid density to give the kinematic viscosity, $\nu = \eta/\rho$.

Hence the relation

$$\tau = \nu\rho\frac{dv}{dy}, \quad (2.141)$$

arises for laminar shear flow. This may be derived in other ways, it being in essence Newton's second law applied to layers in the fluid.

It is useful for later purposes to evaluate this expression for shear stress *at the wall*, τ_w . Using equation 2.124 for the analytic flow profile in a duct, it is possible to differentiate to find the gradient:

$$\frac{dv}{dy} = \frac{6V}{W} - \frac{12Vy}{W^2}, \quad (2.142)$$

which at the wall ($y = 0$) evaluates to $6V/W$, V being the mean velocity. Substituting

this into equation 2.141 gives a wall shear stress as follows:

$$\tau_w = \nu\rho \frac{6V}{W}. \quad (2.143)$$

The shear stress τ can then be shown to be a linear function of distance into the channel, taking the value τ_w at the wall and reaching zero at mid channel. In fact, in ducts:

$$\tau = \tau_w \frac{y}{W/2}. \quad (2.144)$$

This being applicable for laminar pipe flow too; in that case however, distance into the channel is given by r/R and the wall shear stress by:

$$\tau_w = \nu\rho \frac{4V}{R}. \quad (2.145)$$

Finally it is possible to take aforementioned values for τ_w and use these in equation 2.140 to relate pressure gradients to mean velocity, viscosity and channel width. This relation is known as ‘Poiseuille’s equation for laminar flow in [channels]’. It is quoted here for the more frequently observed pipe case:

$$\frac{dP}{dx} = -\frac{32\nu\rho V}{\phi_h^2}, \quad (2.146)$$

and may be obtained by direct solution of the Navier–Stokes equations with appropriate BCs and simplifications. It demonstrates that the pressure gradient is constant along the channel and, logically, negative for positive flow. This equation will be used later as an intermediary to gain an expression generalising the friction factor of a turbulent flow to the laminar case, equation 2.189.

2.6.3 Driving and constraints of the physical flow

Any flow is effectively defined by its boundaries. When a physical flow is studied, investigators usually break the problem into domains of behaviour over which there is a hierarchy of relevance and importance, these are then observed separately to some extent. Usually there is a region of great interest where specific questions arise and outside which assumptions are made; a whole system might be studied as a collection of such units. Importantly, there is almost always a region of lesser interest outside the primary focus, for which simplified conditions are presumed to hold. The conditions there are embodied in *boundary conditions* for the domain of interest.

To facilitate understanding, validation, or advancement of the current work, it is im-

portant to clarify matters pertaining to the boundary implementations employed. These are related either directly or indirectly to physical equivalents in the real flow. Efforts are made in the following to evaluate and review available boundary schemes and in so doing elucidate those issues which are specific to a scheme such as LB. Motivation to do so stems, in part, from a need to prepare groundwork for what is one of the primary novel developments advanced in this thesis, namely, an efficient and transparent means to generate *second order accurate* boundary conditions; work presented in detail in chapter 4.

Boundary conditions and simulation closure

The boundary conditions that it is required be implemented in these studies are physically identical to those encountered in CFD. Typical parameters on which BCs might be defined are velocity, pressure and flux conditions at various levels of simulation complexity. For each parameter, either its value may be specified at the boundary, or the derivative thereof — occasionally some combination. The former are known as Dirichlet conditions, the others as von Neumann and Robin or mixed conditions respectively.

Any physicist involved in modelling, would surely agree on the high degree of influence imposed by boundary conditions, on solution accuracy over the domain under consideration (be it numerical or general). It is merely representative of the common observation that ‘the devil is in the detail’. LB is certainly no exception in that regard.

Computationally, specification of BCs reduces to a matter of *lattice closure*. Next, the diverse ways to achieve *LB* lattice closure are described; those employed in this work are indicated and a discussion is provided of the salient features of each. Details of *improved* boundary conditions for the LBM, along with their limitations or inadequacies, are covered more thoroughly in chapter 4. Comments in the following make appeal to figure 2.14, which shows simulation domains for the three commonly employed flow modelling strategies.

A retrospective view of the literature reveals that boundary condition implementations for lattice Boltzmann have been inspired by equivalents formulated for lattice gases; see for instance [48, 124, 157]. Moreover, they require only minor modification in order to function sufficiently well. Gradually however, inadequacies of adopting this approach have surfaced, especially during increasingly complex investigations and more quantitatively focused studies. Subsequent efforts to address this issue by improving boundary schemes soon became frequent additions to the literature. Development of a *universally* acceptable closure scheme for LB has not occurred however, probably due to the varied nature of phenomena to which the LBM is routinely applied. As many authors focus on

these, which include: multi-phase fluids, porous media, suspensions and diffusive walls for example — for which the LB is eminently suitable — widely differing constraints are placed on boundary implementation. A universal scheme therefore is probably neither realistically attainable, nor desirable even; progress has appeared ad hoc as a consequence.

Flow inlets and outlets. These strictly *open* or *flux BCs* constitute flow boundaries on the lattice and a means to induce flow. Practical implementation turns out to be rather more convoluted than would first appear. The reason for this is that flow implies velocity, which not only implies velocity distribution, but *specific to the LB* pressure and density also, as the three are inextricably linked.

Density is the primary working variable of the LB, in contrast to traditional CFD which work with velocities directly. In LB velocity arises as the first moment of the density distribution and pressure only through identification of terms in the derived macroscopics. This state of affairs imposes a certain equation of state on the lattice fluid:

$$p = \rho T \quad , \quad \text{where} \quad T = c_s^2 \quad , \quad (2.147)$$

which is simply the ideal gas equation $PV = nRT$. Pressure therefore, is a ‘complexified’ parameter, see e.g. [135]. This tenuous wording is intended to pick out the fact that it remains essentially simple, but as a characteristic of the LB, it becomes tied through an equation of state, to density and temperature variables.

Various contradictions then arise in that either the pressure distribution or inward and out bound velocity profiles should be an *emergent* characteristic of the simulation; setting these could therefore be regarded as ‘fixing’ or influencing the solution. In addition, if an approximate profile is selected for input and output, a section of lattice and associated computational resources must be set aside to allow this to evolve to the natural form.

As a consequence, application of pressure BCs in order to drive a simulation is slightly more involved than CFD. Ways to get round this exist, but no need to do so arises here, as very simple alternative closures are available. These are brought together later, page 105 under the heading ‘artificial lattice closure devices’. Other aspects of the physical flow are easier to deal with at lattice level:

Velocity boundary conditions. These are probably the most commonly applied within any fluid dynamical simulation; perhaps due to the fact it subsumes the zero velocity, ‘no slip’ condition, which is universally presumed for solid walls. Note that a velocity BC may be considered an instance of the above flow BC, but a subtle difference is evident: a wall, or region of fluid, may be moving at specified velocity, but crucially the

normal flow component at the interface between the two might be zero. Hence what is meant here might be more succinctly, if verbosely, termed **(impermeable) interfacial** boundary conditions; which may be moving or static but over which there is no fluid flux.

Such may be modelled in two ways: either a von Neumann condition with zero normal component, or, since all *relative* components of the velocity vector where fluid and wall contact are assumed to disappear, a no slip condition on a moving wall. No difference between the two is felt by the fluid and they are completely interchangeable; hence in LB the most convenient is chosen

No flow velocity BCs, especially the no slip condition, are very simple to implement at first order accuracy in LB simulations, they are discussed in the next subsection. Higher order accuracy is non-trivial and various methods have been proposed. These are discussed in greater detail in section 4.1. This work utilises simple no slip Dirichlet BCs on velocity at the boundary almost exclusively.

‘Forcing’ conditions. This refers to the fact that flow may be induced by external force fields, such as electromagnetic or more likely gravitation. Forcing in the usual sense, i.e. by pressure differential, is as mentioned previously, slightly complicated in LB. Precisely what is meant here, is invoking a tendency to flow by application of forcing terms direct to fluid particles. In LB this is achieved quite simply by the addition of a directional forcing term in the lattice evolution equation. It is effectively a link dependent density reallocation, symmetric about the down stream axis and asymmetric across it. This mode of applying a force permits various possibilities for lattice closure, most particularly the so called artificial closures, to be discussed at page 105.

No slip velocity (Dirichlet) boundary conditions

Fundamental aspects of LB closure are common between schemes and are found to be quite simple, centering on matters such as conservation and balance. For closures intended to realistically portray solid interfaces, mass must be conserved in the closure and velocity must tend to zero if it is to appear consistent with the widely accepted no slip condition.

One BC contender has been very routinely applied for such purposes, to the point of becoming a standard in some respects; that is the **‘bounce back’** method. Bounce back is the simplest possible means to achieve zero velocity BC for a general flow configuration. It is this algorithmic simplicity which promotes its use, but which also leads to inadequacies as will be seen. The term bounce back is indicative of origins with the Boolean particle field of the LGCA. Individual particles impinging on a boundary undergo simple velocity

reversal in a sort of wall collision step. A no slip boundary condition automatically emerges in the wall region (not necessarily on it) and necessary mass balance conditions and the like are met at a stroke. In LB the equivalent, velocity ‘population’ is replaced by discrete velocity distribution, but simple manipulations such as reversal may be made just as easily. No floating point operations are required, only memory re-assignments.

Early flow simulations employing LBM schemes made use of bounce back boundary conditions [48, 74]. In these works, the emphasis naturally fell on extending the range of applicability or phenomena to which the LB could legitimately be applied. Technicalities of implementation such as boundary conditions were, quite rightly, not high on the agenda. Later, more demanding applications highlighted weaknesses. Initial detailed analyses directly addressing such include Ziegler [157] and Skordos [124], though papers such as [83] and [29] addressed LG boundaries at an earlier time.

Ziegler, in his very readable paper [157], compares two FHP-II schemes: traditional bounce back and the ‘re-interpreted’ bounce back³¹, along with a third suggested scheme which brings the LB collision step onto the wall nodes. He shows that in reality bounce back fixes the no slip condition at a point approximately half way between the bulk node and the wall node. Equivalently, it might be argued that the bounce back scheme enforces a finite ‘slip velocity’ at the wall. The distinction is blurred and it is equally valid to adopt either point of view.

This and many subsequent papers demonstrate that bounce back is only first order accurate. Because of this, it essentially degrades the second order accurate core scheme in the region of the wall; an effect which then propagates into the bulk. It is pertinent to note however, that for less rigorous studies of ‘bulk’ fluid behaviour, the bounce back scheme is still widely utilised and accepted. The degradation in performance is often of lesser relevance than its great implementational simplicity, a perspective especially visible in situations where the boundaries are either complex and high accuracy flow field is not of prime importance, or they are extensive, where the relative magnitude of error is reduced by increasing the size of the lattice— its ‘resolution’. Examples of the former include simulations of flow through porous media in [134]. All practitioners adopt the latter approach to reduce error, when it is possible to do so.

Other common boundary condition closure schemes

Variations exist of the bounce back scheme, for which various names have been proposed, including modified bounce back and enhanced bounce back. In one, the exact location of

³¹Hereafter the re-interpreted bounce back is referred to as bounce back on the link (BBL) [147] and Ziegler’s suggested scheme is known as ‘modified’ bounce back, see for example [59].

the zero wall velocity point (which almost never occurs exactly at the wall) is determined and allowed to fall between lattice nodes; in others a slip velocity is implemented at the wall to negate attendant failings of the simple bounce back scheme. In another, a fraction of the density is made to bounce back ‘specularly’, i.e. reflect. This ‘bounce back fraction’ method may be used to impose free slip BCs. Simple bounce back and the bounce back fraction scheme have been implemented in this work at one point or another.

During discussions in the following chapters, bounce back will, in part due to its historical acceptance, frequently be used as the yardstick by which to judge other methods by.

Other essentially first order accurate schemes, for implementing zero velocity conditions, include the so called ‘equilibrium forcing’. There f_i incoming to the bulk are assigned the equilibrium value $\bar{f}_i(\mathbf{v}, \rho)$ associated with the velocity of the wall at that point, usually zero, and a mass balance condition.

In addition to the aforementioned closure schemes, which are all first order accurate, various simple alternatives exist which effectively impose second order accurate boundary conditions. These are discussed in section 4.1, where the topic of the chapter is a novel addition to the set. During discussions in the following chapters, bounce back will, in part due to its historical acceptance, frequently be used as the yardstick by which to judge other methods by.

2.6.4 Artificial lattice closure devices

Periodic boundary conditions: Ubiquitous in many diverse fields, for extremely simple closure of simulation domains without introducing complications, these perhaps require little explanation. In direct analogy with theoretic attempt to avoid explicit BCs, this computational equivalent has at heart the idea that space can somehow be ‘wrapped around’, through some extra dimension, before being reconnected to itself by its opposite edges. This is directly equivalent to taking a finite region of space and ‘tiling’ it, to cover all space, so that edges need not be considered. The process may be carried out on any of the independent (usually spatial) dimensions.

A lattice equivalent to this is easily implemented upon recognising that the space re-connection manifests itself as a simple mapping of information between memory addresses in the computer. For lattice Boltzmann simulations information propagating off lattice at one edge, is used to populate a specific, opposite, set of on propagating unknown information at the opposite domain edge. Information should propagate in a way indistinguishable from there being exact copies of the simulation domain tiled in direct

adjacency.

Importantly for this work, it must be realised that such a device rules out the possibility of any differential in properties along the direction rendered periodic. Crucially, any pressure gradient is ruled out, which leaves a minor problem concerning the way that the flow is driven; forcing can no longer be related to the physical attributes of the system and must therefore be imposed artificially. This is not an insurmountable or difficult problem however. Methods to get round it invoke a hypothetical ‘body force’, which acts on the fluid in a manner similar to gravity — everywhere equally (homogeneously). With such a driving mechanism applied, the resultant, oft desirable lack of variation in any particular direction, is conventionally termed ‘translational invariance’; in summary, the dimensional complexity of the problem is reduced by one for each invariance. See figure 2.14 part i).

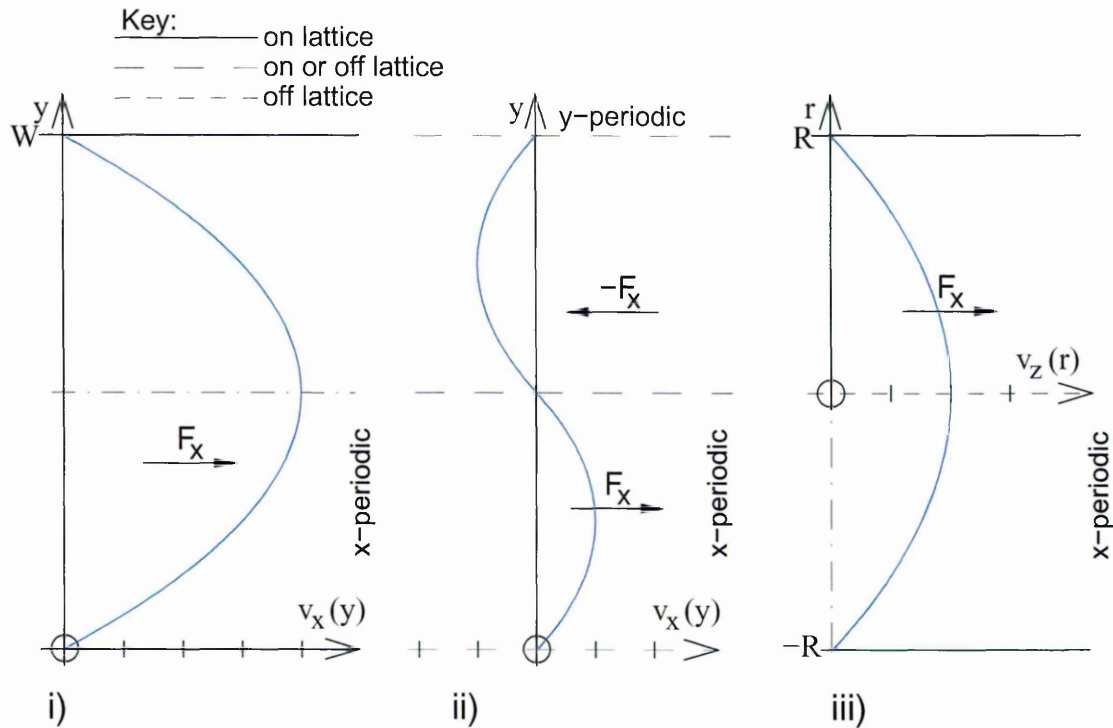


Figure 2.14: Computational domains for three types of translationally invariant channel and representations of the flow profiles generated under forcing F_x . i) shows normal forcing and Dirichlet BCs; ii) is *contra-forced*, walls may be on or off lattice; iii) is the axially symmetric geometry, referred to on page 89, where the $r = 0$ line must lie off lattice, and which due to increased cylindrical friction, shows an expected reduction by a factor two in the velocity magnitude.

In these studies translational invariance is utilised widely, for its simplicity and the computational reduction afforded as the dimensionality is reduced. Implementation of the crucial body force is described in the next subsection, from page 108 on.

Contra-forcing: Periodic BCs previously discussed permit other bounding possibilities. Contra-forcing, also referred to as square wave forcing, is another widely used contrivance for closure of very simple computational domains. The name is obviously misleading, it is more a devious means to implement second order accurate, zero velocity BCs than a forcing scheme per se. Moreover, it is really the symmetry of the system of interest which is exploited for the purpose.

Originally proposed in the early stages of the development of LGCA by Kadanoff *et al.* [71]. They utilised the idea as another means to implement lattice gas closure and hence compute LG shear viscosity via Poiseuille flow. Contra-forcing uses the fact that when simulation domains are ‘tiled’ in a given direction, i.e. extra ‘ghost’ copies of the lattice are placed in direct adjacency, neighbouring lattices may have *exactly opposite* forcing conditions applied.

Briefly, for a simulation domain which is fully periodic, that is in both x and y directions, the forcing is split into two halves parallel to the direction of flow, each of which is forced in opposition. In this sense contra-forcing is a forcing scheme, see diagram ii) of figure 2.14. In doing so however, a boundary of zero velocity necessarily emerges between the two forcing zones, on account only of the symmetry. That is the primary utility of the idea. A no slip, zero velocity BC, will always be obtained in this way, simply due to the symmetry of the information content, however in this work, the following more efficient version is used instead.

Truncated contra-forcing: This is a variation on the basic idea, which recognises and makes further appeal to the underlying symmetric basis. It depends upon the fact that, under the symmetry that is utilised to impose the ghost lattice, there is no difference, in terms of node density *information*, between information fluxes in each direction across the interface between forcing. Hence, important unknown information propagating *onto* the real lattice, which it is desired be found, is precisely a reflected image of that information propagating off lattice, onto the ghost lattice.

The sole requirement, for complete removal of the ghost lattice, is an algorithmic step which observes off propagating density values and rearranges them by a link transformation (strictly a rotation in space) to assign the on propagating unknowns. Notably, this scheme also endows all wall nodes with bulk properties. Here it is used in simulations of parabolic flows in the simple channels of chapter 3.

Periodic BCs, translational invariance and body forcing

Simulations presented in this work take advantage of the fact that a pressure driven channel is exactly equivalent to one that's translationally invariant; that is, bounded periodically in the direction of forcing and with the device of body forcing utilised in order to drive the fluid. Earlier discussions of channels (section 2.6.1) are not based upon a translational invariance assumption, however, all results derived there turn out to be valid. Further details on the translationally invariant channel, especially regarding the forcing, are now given.

Flow may be initiated in the absence of a pressure gradient by invoking a hypothetical body force on the fluid uniformly at all points. This may be demonstrated to be exactly equivalent to a pressure driven flow and forcing parameters may be calibrated mathematically to a pressure equivalent. Crucially this enables the simulation domains to be implemented periodically in the along stream direction and hence one dimensional. For all channel geometry work undertaken in this project, such a simulation 'trick' has been employed; representations of commonly seen configurations are presented in figure 2.14. Once reduced in this way, periodicity has removed the need to close the simulation domain in the along stream direction with a *physically* derived model, that is with 'open', or flux BCs; the closure is thus greatly simplified.

Typically the forcing consists of simple additive terms incorporated into the lattice evolution equation, as follows:

$$f_i(\mathbf{x} + \mathbf{c}_i, t) = f_i(\mathbf{x}, t) - \omega[f_i(\mathbf{x}, t) - \bar{f}_i(\mathbf{v}, \rho)] + F_i. \quad (2.148)$$

where Δ_t of equation 2.103 has been set to unity. Therein, body forcing terms F_i must obey the mass continuity condition

$$\sum_i F_i = 0, \quad (2.149)$$

which is easy to arrange. Forcing then arises in the first moment of the evolution equation, embodied in the term \mathcal{G} , where, it can be shown:

$$\mathcal{G} = \sum_i F_i c_{ix}, \quad (2.150)$$

for x-direction forcing. The relation

$$\frac{\partial p}{\partial x} = \frac{\mathcal{G}}{3}, \quad (2.151)$$

then arises from identifications in the resultant macroscopics. This forcing scheme is used widely in this work.

Three obvious means do derive consistent F_i are readily apparent. For illustration only, consider flow in the x -direction, with link labelling as shown in figure 2.4.

- A fixed proportion, P_ρ say, of the mean density ρ_0 can be added to links 3,4 and 5, whilst simultaneously subtracted from links 1,8 and 7 respectively. In this case the best single figure to represent forcing magnitude is the density fraction P_ρ , as it scales effect with simulation density and reminds one of the fact that the amount redistributed must be small for stability: the effect of the collision operator must be sufficiently strong in relation, to ‘erase’ the added forcing information when at equilibrium.
- A very similar method to the above, generates additive terms which are ‘weighted’ in accordance with the equilibrium distribution link weights, w_i . The benefit of this is possibly to allow slightly increased forcing: weighting the forcing terms presumably makes their effect consistent with the underlying lattice and therefore less liable to reach an instability threshold. Though evident during simulations, no direct proof of this has been uncovered by the author, however.
- Even more consistent would be to determine how a uniformly translating equilibrium for specified velocity differs from the static equilibrium and use the difference itself as the a basis for forcing terms. In effect

$$F_i = \bar{f}_i(\mathbf{v}_f, \rho) - \bar{f}_i(\mathbf{0}, \rho). \quad (2.152)$$

This has the lattice consistency built in and permits single (vector) parameter forcing quantification, \mathbf{v}_f . Care must still be taken to ensure that the lattice is not over forced by making the forcing parameter too high, as the usual stability limitations apply. It is of interest to consider how this velocity based forcing parameterisation might be mathematically linked to the forcing terms, i.e. *acceleration*, it is intended to invoke³².

These various forms of forcing have all been utilised in this work at some stage or another. No distinction need be drawn in that the net effect may be quantified in the

³²Some work on this was carried out by the author for constrained flows. It was established that simulation velocity tends exponentially toward some attenuated proportion of the value \mathbf{v}_f in the presence of boundaries. No exact, usable mathematical relation was established however, between profile velocity and that (velocity) used to specify F_i .

forcing parameter \mathcal{G} , which may be related to the pressure gradient via identification in the macroscopic equations.

The present means to induce flow (body forcing) also suggests ways in which the macroscopic nature of an LB simulation may be manipulated to yield useful results. Incorporation of artificial forcing terms is a commonly applied means to introduce useful physics in the continuous counterpart to LB, i.e. kinetic theory. Much rigorous work has been done on the validity and appropriateness of such an approach, which has established its wide acceptance. Here, the method is successfully applied in chapter 3 to the problem of enabling cylindrical simulations to be performed on a flat Cartesian grid.

2.7 Turbulence in simple internal channels

Important *global* characteristics of fluid systems depend upon the precise nature and fine detail of the flow inside. Heat transfer between wall and fluid is governed by local velocity gradients; overall pressure drop in a system depends critically on the nature of the flow, consequently so does volumetric flow rate; mixing of the flow is enhanced by complex or random flow, whether it be between species, mixing of phases or transport of heat. In a typical industrial system, such behaviours usually epitomise the ones which it is intended the system exploit and to aid the process of design, it is of value to gain quantitative information on how they contribute.

In a turbulent flow, which is the most commonly occurring flow state, all global flow variables differ significantly from those of the theoretic laminar counterpart. It is the precise form of such changes to mean flow characteristics that this work attempts to address, specifically for the case of *isothermal channel turbulence*. A brief excursion is therefore now taken, to review the known physics associated with turbulence in channels and to carefully indicate any differences with the laminar counterpart. This is so that discussions of later chapters may be made within an appropriately defined framework.

In those later investigations, changes to the global character of the flow are most evident in the shape of the mean velocity profile. Consequently, the profile of mean velocity in particular becomes a prime target of investigations. It describes the averaged detail well and other global characteristics such as volumetric flow rate, friction and drag are derived from it. Since the latter of these arise in wall effects, it is necessary to focus on the effect exerted by the wall, via the so called boundary layers, on the turbulence and mean flow.

The discussion begins with a review of some general properties of turbulent boundary layers. After this, the most important and relevant aspects of the problem are discussed in the light of quantitative results from both theory and experiment. This is to provide the foundation material for assessment of results generated later. As will be seen, it is here broken down into three primary elements; namely, boundary layers, flow profiles and Moody curves. These are discussed in the context of both pipes and ducts, though mainly pipes for which more material exists. Specific results of direct relevance to the infinite depth duct studies of chapter 5 are developed therein.

Application of the LBGK scheme in such circumstances and results so generated form the primary material of this work; they are presented and discussed in chapter 5. Further application of the models proposed, but to the cylindrically symmetric case, are discussed in relation to further work, 6.1.

2.7.1 Description of channel turbulence and basis for its discussion

The state to which a particular flow is driven is parameterised by the dimensionless group of variables known as the Reynolds number, defined on page 46. With respect to the Reynolds number it is evident that a flow may exist in one of two primary states: laminar or turbulent; transition between such realms occurs around a certain level of driving, denoted by the critical Reynolds number, Re_{cr} . Below the critical Reynolds number there are *laminar* flow conditions and it is possible, where the channel is translationally invariant, to arrive at an analytic solution for the velocity profile. Equation 2.121 describes this profile — a parabola — and a normalised solution is represented in figure 2.9. At higher Reynolds number however, flow has undergone transition to the turbulent state, inducing dramatic change in the flow nature.

Under such turbulent conditions, there exist additional mechanisms by which momentum and energy are distributed, augmenting those explicitly accounted for in the Navier–Stokes equation. They have the effect of changing both the detailed nature of the flow and important net flow characteristics. Though the flow detail is extremely complex and can't practically be resolved on account of the superimposed random component of motion over the mean, large scale or global properties can still be deduced. This is because the fine detail of turbulence, although important, has a net effect which is in some way an average over the the fluctuations and which is the same amongst the whole class of turbulent flows — the similarity principle again 2.4.1.

As mentioned earlier, the mean velocity profile most adequately illuminates the global properties of isothermal channel turbulence. It is well known however, that no *precise* analytic form exists for this profile shape, or even a universally acceptable qualitative description — such summarises the problem from an engineering perspective. Any discussion of such then is rendered somewhat qualitative, as will be seen. Moreover, though experimental results on pipe flow are well established and frequently utilised, quantitative data applicable to the duct flow case is a rarer commodity. Strictly the former is not a valid basis for discussion of the results of later chapters, which pertain to the infinitely deep duct channel. For this reason points specific to the Cartesian channel realisation are carefully highlighted.

Exemplary turbulent flow profiles are shown in figure 2.15 obtained from pipe data. For comparison, equivalent laminar flow profiles are also given for the Reynolds number in question. Though quoted data are consistent with equal Reynolds numbers, it is important to appreciate that a laminar flow realisation may be physically impossible at

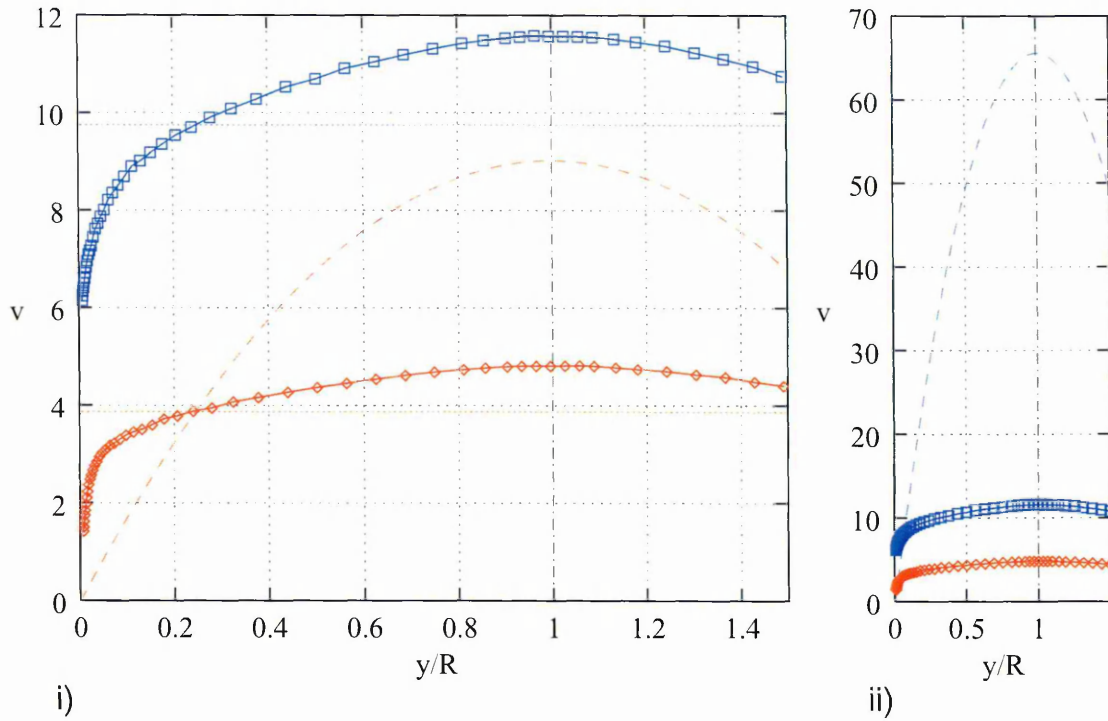


Figure 2.15: Part i) Exemplary turbulent velocity profiles $v_x(y)$ in a pipe at two Reynolds number: red diamonds \diamond are experimental data for $Re = 31,577$; blue squares \square are for much higher Reynolds number, $Re = 230,460$. Also shown are theoretical laminar profiles, calculated for consistent Reynolds numbers (by colour) — dashed lines — and an indication of the turbulent mean velocity— dotted. Part ii) is the same but with higher v range to demonstrate increasing relative scale of laminar profile with increasing Re . Lines cross in part i) coincidentally. Mean in pipe has higher weight at edge, note.

such driving levels (a contentious point in itself³³). What is shown in the laminar profiles of figure 2.15, are Reynolds number specific data calculated using analytic expressions of section 2.6.1 (equation 2.124).

Obviously distinct differences exist between the two, which it is intended the simulations capture both qualitatively and, to some extent quantitatively, as mentioned. A detailed statement of the main features is provided as introduction to the main studies of chapter 5. Such are not discussed further here, instead quantitative relations are to be described, in order to provide an exact framework for their analysis.

Before proceeding, it is pertinent to review some fundamental aspects of the physics of turbulence in channels and how such is best described. Initially it is necessary to review aspects of dimensional analysis and to define some dimensionless groups, which are commonly utilised (to follow). Much discussion of results will centre around a these and a few simple flow dependents such as friction coefficient, shear stress, mean velocity and

³³Deducing that the onset of turbulence might be restrained in decreasingly perturbed initial states implies physical peculiarities, most notably frictionless flow, at high Reynolds number. See equation 2.189, or consider a forward projection of the laminar branch of the Moody chart 2.18.

friction velocity; these may be constructed most simply from the dimensionless groups. A fundamental feature of quantitative channel turbulence studies is the Moody chart, which relates friction factor to dimensionless Reynolds number. This is discussed also.

Dimensional aspects

It has been identified in retrospect that much of the conclusions of early works on turbulence generally, which includes that in channels, can be deduced by alternative paths based on dimensional analyses. Certain major results are a good example of this. For example the highly relevant mixing length form for the modelled Reynolds stress may be derived dimensionally, equation 2.97. Similarly and more spectacularly the equation for the spectrum of turbulence in the inertial sub-range, otherwise known as the Kolmogorov spectrum, see [45, 75, 139]. Dimensional arguments are standard tools in the arsenal of physicists, they derive criteria and suggest suitable forms for both parameters and their relationships. In essence, by appeal to the dimensions of the fundamental variables and some quite simplistic reasoning, it is possible to derive quite general insights and understanding.

Here, the simple but nevertheless very useful end of the spectrum is described, primarily consisting of *normalisations*, that is reduction to the open interval [0,1] of the range of a parameter by expressing it as a ratio with some other parameter of like dimension, usually the peak value. In a later section, page 122, dimensional analysis is used ‘predictively’ to ascertain the form of flow profiles.

Normalising data, essentially scaling it, enables better comparison between data sets and the identification of underlying features therein, characteristic of the physics and not our interpretational limitations. Basic variables and their combinations are highlighted, against which it is useful to normalise.

Any coordinate notation may be utilised. Here, for convenience of comparison between results of the various approaches, a hybrid Cartesian / cylindrical combination is employed. This is common. In the following, x is the along stream direction and y the distance across channel: $y = 0$ at one boundary and $y = W$ at the other, where W is the channel width.

Once the physical notion of greater fluid ‘weight’ for increasing $|r|$ is fully appreciated, Cartesian y and cylindrical r may, to highlight their equivalence as spatial parameters, be related by:

$$\begin{aligned} y &\equiv r + R & , & & 0 \leq y \leq W , \\ r &\equiv y - W/2 & , & & -R \leq r \leq R , \end{aligned} \tag{2.153}$$

without risk of erroneous interpretation or confusion. Channel widths in both systems are related by $W = 2R$ (note hydraulic diameters: $\varnothing_h = 2R = 2W$ however). So whilst normalisations may thus be carried out with respect to W or R , it is obvious that to highlight flow *symmetry* and to enable direct comparison, $R = W/2$ is the better choice. Hence y/R ‘location across channel’ is often seen as a spatial parameterisation when distances off the wall and into a channel are considered. This, by 2.153, is a simpler equivalent to $r/R + 1$.

Once the dependence of profile magnitude on parameters such as channel width, forcing and geometry is understood, section 2.6.1, it often makes sense to work in terms of normalised profiles. Various normalisations are possible: measured velocities are commonly divided by the central peak value, v/v_{pk} , to give data over the domain $[0, 1]$, thus enabling easy comparison of shape. Others commonly appearing however, refer to a new, dimensional and non-fundamental parameter, defined with dimensional reduction in mind. It is introduced to encompass a collection of parameters that appear frequently in analyses of channel flow, whether turbulent or laminar, and to highlight their role. The **friction velocity**, v_τ :

$$v_\tau = \sqrt{\frac{\tau_w}{\rho}}, \quad (2.154)$$

is so named on account of its velocity dimensions $[LT^{-1}]$ (it is often denoted v^*). Note that friction velocity incorporates attributes of the *whole flow* — the geometry, fluid and forcing — through the wall shear τ_w , see equation 2.140. It enables alternative normalisations of velocity data. In particular, the **dimensionless velocity**, v^+ , is given by:

$$v^+ = \frac{v}{v_\tau}, \quad (2.155)$$

which is effectively the velocity normalised to the friction velocity. Dimensionless velocity therefore, like v_τ , possesses qualities of the whole flow configuration.

Often seen also are normalisations of ‘shifted velocity data’. The ‘velocity defect’ may be defined as³⁴

$$\frac{v_{\text{pk}} - v}{v_\tau}, \quad (2.156)$$

which is the difference between peak velocity at channel centre and point means, normalised to the friction velocity. Importantly here, this is used by Goldstein in [50], see section 5.1.2, in a semi-empirical relation for the velocity profile *between planes*.

Finally, returning to spatial variables, the **dimensionless ‘location’**, y^+ , is given

³⁴Other definitions exist depending on the approach, see for instance equations 2.171 and 2.183.

by:

$$y^+ = \frac{v_\tau y}{\nu}, \quad (2.157)$$

which also incorporates attributes of the whole fluid/flow configuration.

This latter dimensionless location is particularly useful. It permits a universally valid quantification of locations of interfaces between the various layers near a wall; as demonstrated in section 2.7.2. Most of its utility however, is derived in the fact that it is a Reynolds number in disguise — note the similarity with equation 2.52. As a Reynolds number which is dependent on distance into the channel, it parameterises the proclivity to turbulent behaviour as one moves away from the attenuating effect of a boundary. It then seems logical that there might be a laminar layer in close proximity to the wall, Prandtl's accepted assumption, again see section 2.7.2.

With these in mind it is possible to generate the following useful relations:

$$\begin{aligned} v_\tau &= V \sqrt{\frac{f_F}{2}}, \\ v^+ &= \frac{v/V}{f_F/2}, \\ y^+ &= \frac{yRe}{2R} \sqrt{\frac{f_F}{2}}, \end{aligned} \quad (2.158)$$

and for the laminar flow, using the first of 2.158 and equation 2.189:

$$v_\tau = V \sqrt{\frac{8}{Re}}. \quad (2.159)$$

All of which are used occasionally in manipulations of later chapters.

The friction factor

Well established studies of turbulent flows indicate that friction losses are proportional to both the area of contact between fluid and wall and to the fluid kinetic energy per unit volume. The former of these will be denoted A_w and the latter is taken in the usual way to be $\rho V^2/2$, where V is the mean velocity. Surprisingly, the viscosity of a turbulent fluid affects little sway over friction based energy losses, the dependency being negligible to a few orders of magnitude. This demonstrates the seriousness of turbulence practically: otherwise dominant viscous effects are overwhelmed and the problem reduces to one of flow rather than fluid.

The origin of viscosity as a fluid parameter is as a constant of proportionality quantifying the extent to which shear forces applied to a fluid manifest themselves as velocity gradient in the flow. An equivalent parameter to this is needed for the turbulent flow

where viscosity does not appear. Such is the basis for the friction coefficient. More specifically it is the *retardation* of the flow which it intends to [quantify/capture], as the concept of velocity gradient is somewhat meaningless in turbulence.

In section 2.6.2 (page 98), the shear exhibited in a (laminar) flow is described as proportional to applied forcing and the constant of proportionality defined as viscosity, equation 2.141. Here, observed resistive shear forces F are, as previously mentioned, proportional to the area over which it is felt, A_w , and the kinetic energy, thus:

$$F \propto \frac{\rho V^2}{2} A_w = f \frac{\rho V^2}{2} A_w, \quad (2.160)$$

where the constant of proportionality f has been named the friction coefficient, or friction factor.

Note that the wall shear stress τ_w is just the pressure term F/A_w , hence, on employing equation 2.140 to relate this to the pressure gradient and hydraulic diameter, the *Fanning* friction factor may be defined:

$$f_F = -\frac{dp}{dx} \frac{\varnothing_h}{2\rho V^2}. \quad (2.161)$$

This is just one of various definitions however. That of originated by Darcy is perhaps most commonly seen [12, 30], being used by Blasius and by Moody for the Moody charts in [96]. The Blasius friction factor is just four times Fanning's:

$$f_B = 4f_F, \quad (2.162)$$

and is also known as the Darcy–Weisbach friction factor, $f_{DW} = f_B$.

The friction factor is important generally, but is especially so here in relation to studies of later chapters. This is because it facilitates quantification of global flow characteristics such as pressure drop, mean and hence volumetric flow. It encompasses and summarises all complex behaviours of turbulence which tend to impede the flow and is particularly ‘tangible’ in the case of simple channel geometries. This has perhaps become acknowledged gradually, as engineers solve design problems by reducing a problem to simpler questions for which reliable answers may be found by reference to standard sources of information. One such source is the Moody chart, which is used and referred to extensively in these studies. Presentation of friction data and the Moody chart are discussed in section 2.7.4.

2.7.2 Boundary layers and turbulence; an overview

It is observed in many areas of the study of fluids, that the nature of boundary layers is of utmost importance when determining *global* properties of a flow. Turbulent flow is no exception in that regard, indeed the matter is perhaps especially crucial. It will be seen that the practical value of a flow study or simulation, hinges crucially on appropriate boundary layer incorporation.

Some examples make the practical importance of boundary layers apparent and the need for their correct implementation hopefully clear:

- Consider for instance the mixing of fluid that occurs in turbulent eddies and the consequential increase this has on its heat transfer properties. Bear in mind that efficient thermal energy conversion in heat exchangers is arguably one of the most valuable engineering battlegrounds faced at present. The effects of turbulence are known *not* to extend right down to the wall, instead there is a laminar layer near the wall serving to ‘insulate’ or buffer the wall from turbulence. Knowledge of this is therefore of crucial importance in typical energy transfer processes.
- Consider also the flow over a wing; an engineering study of classic importance in aerodynamics. The thickness³⁵ of the boundary layer determines the ‘form’, or profile drag, that the wing exhibits and hence its efficiency. Perhaps oddly, the thickness of the wing boundary layer is lower in the turbulent case; a feature visible from later results herein. Knowledge of this fact led in the past to the introduction of boundary layer turbulators in aerodynamics, an important but simple improvement to wing design.

It may be argued that flow character is defined *entirely* by its constraining boundaries and that correct inclusion of these is therefore *essential* in simulations for accuracy of results; a point deduced widely and which is generally accepted. Certainly, the presence of flow boundaries is the differentiating property between so called ‘free’ flow, and ‘constrained’ flows, such as those occurring in the internal geometries of this work. In this work boundary layers created by opposing walls of the channel extend influence toward, meet and overlap in, the centre of the channel. The presence of boundaries in such situations thus becomes the essential feature in our simulations and in the strategy to be employed. To the point that, a concerted effort is made to develop a scheme that

³⁵Definition of boundary layer ‘thickness’ — a parameterisation of the extent of its effect — is highly arbitrary. Note the diminishing effect of a wall goes to zero only in the limit of infinite distance, being strictly finite at all other points.

correctly implements a wall model for the case of turbulent flow. This is the subject of a whole later chapter 5.

The turbulent boundary layer

In the proximity of a wall, it is obvious that the wall must passively exert some influence on the flow. The effect is expected to be most notable near to the wall, becoming less significant as the distance to the wall increases. A point may be arbitrarily defined at which the effect of a wall is negligible, this gives rise to the concept of a boundary layer. The boundary layer then, could be defined as a region of fluid where the properties of the flow are determined largely by boundary effects.

For laminar flow, the presence of a boundary generates a simple friction induced shear, or gradient in the flow velocity, where the relative component between the two tends toward zero as the wall is approached. Traditional assumptions require that this *actually* vanishes at the wall, i.e. that their relative velocity is zero. This requirement is borne out experimentally and theoretically for a huge class of flows, including turbulent.

Boundary layers in turbulent flows are very different to the simple shears that characterise the laminar equivalent and are much more complex in nature. It is still expected that the relative velocity of the wall and fluid will tend to zero as the wall is approached, but the way in which this occurs is vastly different, a matter of significance here. In fact, some idea of the nature and complexities of the turbulent boundary layer must be gained in order that appropriate means to model these regions may be arrived at.

A representation of the near wall region, in turbulent flow is provided in figure 2.16; much of the discussion centers on this. The basis for figure 2.16 is both analytical and experimental and in so far as it is heuristic, it is generally accepted as appropriate by both disciplines. Its analytic basis will become clear in the following. Similarly, with respect to the results of dimensionally based analyses of the next section, figure 2.17 (page 129) represents the same information as figure 2.16 but expressed in the analytically more appropriate dimensionless variables.

It can be seen that the turbulent boundary layer is conventionally divided into distinguishable sub-layers. Two of the better treatments on the subject of the various layers, as seen by the author, are to be found in Knudsen and Katz [73] and especially Tennekes and Lumley [139].

Dimensionless location, y^+ , of the previous section, page 116, is conventionally used to quantify the distances from the wall of interfaces between the various layers. These are found to be quite universal, which adds credence to the notion of relatively distinct layers. Hence, in terms of y^+ the layers are as follows:

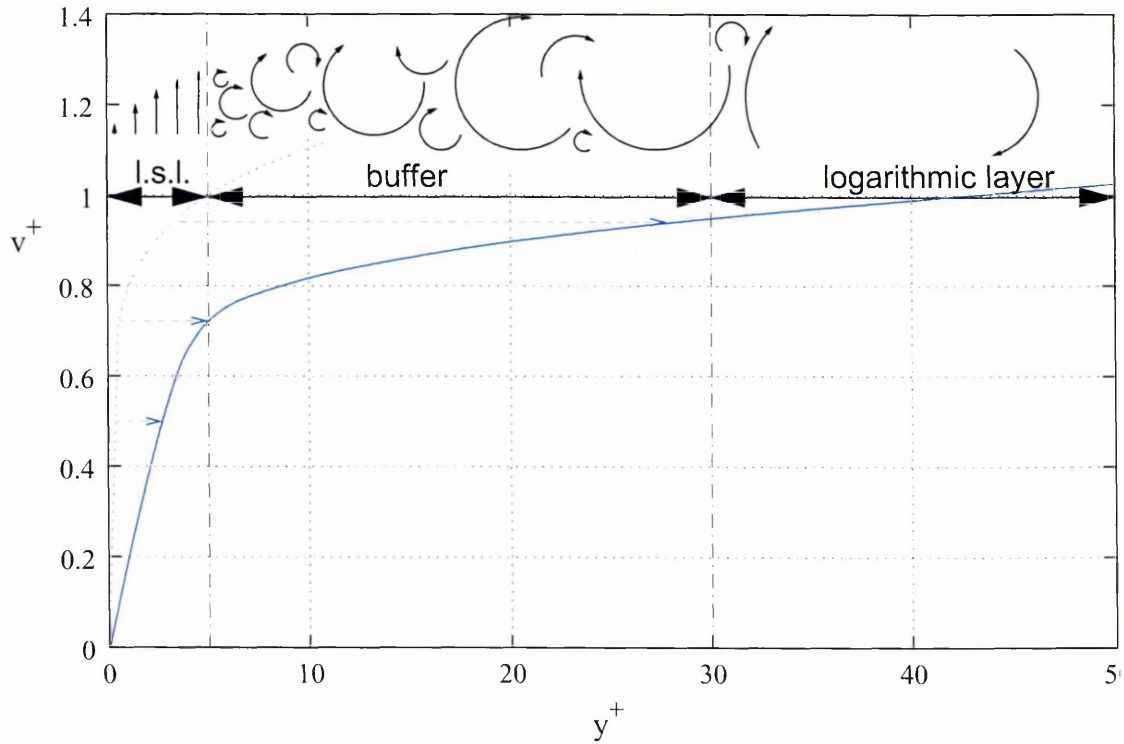


Figure 2.16: The subdivision of the turbulent boundary layer into at least three distinguishable sub-layers. Shown for illustrative purposes only is the seventh power law (dotted blue line) stretched (indicated by blue arrows) as the near wall region is magnified. Also represented (above) are qualitative changes that occur as one moves away from the wall, with y^+ . Closest to the wall is the supposed laminar sub-layer, $0 \leq y^+ \leq 5$. There flow profile varies as $u^+ = y^+$. Next out is the overlap zone, which ‘buffers’ the laminar sub-layer from the wild fluctuations of the turbulence—the buffer layer, $5 \leq y^+ \leq 30$. Further into the bulk, for $30 \leq y^+$, there is the logarithmic layer.

- The range $0 \leq y^+ \leq 5$ defines the laminar sub-layer.
- Above that, $5 \leq y^+ \leq 30$ delineates the overlap or buffer region.
- Further in, $30 \leq y^+ \leq 500$, there is the turbulence dominated logarithmic layer.
- Finally around the channel centre, $500 \leq y^+$, there is fully developed core turbulence.

Note that limits of the buffer layer, and therefore between all layers, are quite vague. The character of the laminar sub-layer is clear in that viscous forces dominate; similarly for the core turbulence, where inertia forces dominate. The buffer layer is often called the overlap region because both forces play a role and determine the shape of the mean flow profile. More details on the nature of the layers is provided in the following sections.

This breakdown of the turbulent boundary layer is not derived as part of a single coherent picture of the wall layer, as may be expected. Instead it has been arrived at in a very ad hoc fashion by diverse contributions, both experimental and theoretical, that have arisen over a long period of time. It is largely heuristic in design and empirical in quantification, but is generally accepted as physically quite accurate. The purpose here is not to question the validity of the information contained in figure 2.16, but to ensure that some of the accepted features of this situation, are emergent in our simulations as result of implementation of wall models designed for the purpose.

2.7.3 Analyses of wall induced turbulent velocity profiles in a channel

Much analytic work has been carried out on the wall layers, leading to some important and useful insights. To review these, either rigorous or hand-waving approaches might be followed. Whilst it would be nice and in keeping to rigorously develop some of the ideas, the context (and space) dictates this to be unnecessary. For that reason the presentation here is heuristic and follows dimensional arguments, initially at least.

Prandtl, in [106], speculated that there must be a layer in close proximity to the wall which manifests no turbulent character. This became perhaps the most widely accepted postulate in the turbulence literature. His hunch was based upon the simple expectation that, under the no slip assumption, *approaching* the wall the fluid velocity must itself tend to that of the wall. Also that, any circulatory nature or eddies in the flow can not be bigger than the region in which they exist, which necessarily approaches zero as the wall is neared. Moreover, and importantly, he postulated that, with the effect of turbulence

decreasing, at some indefinite point near the wall viscous forces must overwhelm those of the turbulence, this giving rise to a laminar flow layer in contact with the wall.

Since experimental investigations are very difficult so close to the wall, it took years for direct evidence for this to emerge. Now, the idea of the viscous sub-layer, as it is known, is well accepted. At the time progress was made by careful *predictive* dimensional analyses, based upon Prandtl's assumptions and experimentally verified knowledge of flow 'scales'. These are discussed from page 122.

Before that, another known result of the time was used by Prandtl to derive an initial expression for the near wall velocity profile. He used the Blasius friction law [11], section 2.7.1, page 133. The work [108] led to the so called power law distribution, or seventh power law:

Power law velocity distribution for turbulence in pipes

Using Blasius' relation, 2.192, and substituting for friction factor using equation 2.160, rearranged in terms of kinetic energy and wall shear, gives:

$$\frac{2\tau_w}{\rho V^2} = 0.079 \left(\frac{\varnothing_h V}{\nu} \right)^{-\frac{1}{4}} . \quad (2.163)$$

This, rearranged for the mean velocity, where all other parameters are constant, is of the form:

$$V \propto R^{1/7} , \quad (2.164)$$

note the indices. From this may be derived an equivalent for the peak velocity and a similar expression for velocity in terms of distance y from the wall. Combination of these then gives rise to

$$\frac{v}{v_{pk}} = c \left(\frac{y}{R} \right)^{\frac{1}{7}} , \quad (2.165)$$

which is (Prandtl's) so called (seventh) power law [108] for the turbulent velocity distribution in a pipe. It expresses the velocity distribution in terms of dimensionless units, velocity and distance are normalised to the peak and radius respectively. It is accurate over the range for which Blasius' friction law is valid, that is over: $3000 \leq Re \leq 10^5$. Note also that, it being a pipe flow result, relations so generated are not necessarily applicable to duct geometries.

Scales, dimensional analyses and the law of the wall

Any discussion of internal turbulence hinges critically on the matter of scale. It is instructive to consider simple systems. Obviously, the infinitely deep duct, with streamwise

translational invariance, is a problem reduced to a one dimensional form — at least at the level of mean velocity. Conventionally y (equivalent to $r + R$, for $-R \leq r \leq R$) denotes the cross stream location, see 2.6.1, and all variation occurs with this.

With respect to the y direction, distances which might be considered for scales include the: hydraulic diameter, channel width, pipe radius and half channel width. However, none of these can be used to illuminate boundary layer detail. Even the boundary layer thickness δ , is not available, as most developed flows have sufficiently thick boundary layers for those on opposite sides to meet and overlap in the centre. In fact the only *macroscopic* length scale of relevance practically is the distance to the nearest wall; i.e. y . Indeed, this is how the mixing length is related to y .

In that light, some dimensional analysis is now followed; just one of the various possible perspectives on the matter. Note, for a relevant treatment see Knudsen and Katz [73]; alternatively, ‘Buckingham’s theorem’ in the definitive work by Buckingham [16].

In an attempt to describe boundary layer features, Prandtl built on his mixing length postulates for the near wall region [109]. Firstly, under the assumption that flow near a wall doesn’t depend on parameters describing the distant features, it is plausible to take the mean to depend functionally as follows

$$U_x = f(y, \rho, \mu_0, \tau_{\text{wall}}), \quad (2.166)$$

that is, only on location, density, viscosity and wall shear. Next, anticipating a dimensionless form for the profile, in the sense of velocity in terms of location, appropriate scaling factors by which to rationalise velocity and location are sought. That is, groupings of the various fundamental variables in the RHS of 2.166 are found, which have dimensions of velocity [LT^{-1}] and distance [L] respectively. In fact only two occur, one for each:

$$\sqrt{\frac{\tau_{\text{wall}}}{\rho}} \quad \text{and} \quad \frac{\mu_0}{\rho} \sqrt{\frac{\rho}{\tau_{\text{wall}}}} = \frac{\nu_0}{u_\tau}. \quad (2.167)$$

Denoting these by u_τ (hence last term above) and y_f the earlier definitions 2.154 and 2.157 are arrived at from the ratios:

$$\frac{U_x}{u_\tau} \equiv u^+ \quad \text{and} \quad \frac{y}{y_f} \equiv y^+ = \frac{u_\tau y}{\nu_0}. \quad (2.168)$$

Once these dimensional scaling factors are found, Buckingham’s theorem permits the functional relationship f of equation 2.166 to be restated as:

$$u^+ = F(y^+), \quad (2.169)$$

that is, some other function F between the dimensionless variables. Equation 2.169 is known as the *law of the wall*; from it can easily be derived various quantitative expressions describing the near wall distribution of velocity.

Outside the near wall region, in the so called ‘core turbulence’, more dimensional analysis yields:

$$U_x = g(y, \rho, \delta, \tau_{\text{wall}}), \quad (2.170)$$

where, note, μ_0 is replaced by δ . From this the *velocity defect law* is derived:

$$u^+ = G\left(\frac{y}{\delta}\right), \text{ which implies: } \frac{U_x - U_{\text{pk}}}{u_\tau} = G\left(\frac{y}{\delta}\right). \quad (2.171)$$

Where both g and G represent some, as yet unknown, functional dependence. The term $U_x - U_{\text{pk}}$ is often referred to as the *velocity deficit* (similar to the wake function of section 5.3.2).

In later sections, further use will be made of the velocity defect law; it will be discussed at the time. For now, the better known ‘near wall’ (that is, *law of the wall*) velocity distributions are to be derived (or stated). This is done for pipe flow, despite the fact that simulations of later chapters 5 focus on the duct geometry. The reason for this is the ‘universal’ nature of flow solutions, in that similarity permits their use on a qualitative basis at least, possibly quantitatively, as will be seen.

At least two types of form are possible for F , related to the nature of assumptions invoked. Primarily, these are distinguished in the context of shear assumptions. In the first of following sections, page 124, the case of constant shear in the viscous sub-layer is dealt with. All subsequent sections, from page 125 to page 128, deal with various results derived for the case of nearly constant turbulent shear dictated by the mixing length hypothesis.

Linear velocity distribution for viscous sub-layer

In the viscosity dominated viscous sub-layer, shear flow is assumed to be governed by a laminar like relation of the form 2.141. If τ_{xy} (τ of equation 2.141) is assumed constant, then it must take the value it takes at the wall, that being τ_w . Rearrangement and integration then yields

$$U_x = \frac{\tau_w y}{\mu_0} + c. \quad (2.172)$$

Under the boundary condition that velocity is zero where $y = 0$, the constant evaluates to zero, hence

$$U_x = \frac{\tau_w y}{\rho \nu_0}. \quad (2.173)$$

which, on introducing the friction velocity, u_τ , 2.154 may be rearranged in terms of dimensionless variables (from $\tau_w/\rho = u_\tau^2$, 2.141). The result is:

$$u^+ = y^+ . \quad (2.174)$$

The range of y^+ over which this linear relation holds is so close to the wall that it is practically difficult to verify. Nevertheless it is an accepted result, now validated. Validity extends as far as $y^+ = 5$ *at the most*, beyond which turbulent momentum transfer processes are sufficiently strong to cause departure from the purely viscous. Turbulent forces are not seen to dominate however, until $y^+ \approx 30$, hence the layer $5 \leq y^+ \leq 30$ becoming known as the overlap layer. The viscous sub-layer profile appears as a curve when plotted semi-logarithmically; see region *I* of figure 2.17.

Logarithmic velocity distribution for turbulence in pipes

After working on his mixing length theory, page 59, Prandtl [110] used it to derive a law for the turbulent velocity distribution near a boundary. It can be shown to be directly equivalent to a conclusion arising from dimensional analysis. It is known as the ‘logarithmic velocity distribution’ [110] and is important here for later chapters.

For the laminar sub-layer and overlap (buffer) regions nearest the wall, it is at least plausible to employ the linear shear stress relation 2.144 of section 2.6.2, to quantify what is actually τ_{xy} in terms of the wall shear stress τ_w . Equation 2.95 for the turbulent shear in terms of mixing length may then be written:

$$\tau_w \frac{y}{W/2} = \rho \kappa^2 \ell_{\text{mix}}^2 \frac{\partial U_x}{\partial y} \left| \frac{\partial U_x}{\partial y} \right|. \quad (2.175)$$

Since the laminar sub-layer and overlap regions are very narrow with respect to a typical flow, the ratio $2y/W$, which translates to r/R for pipes, is very near to unity. Setting it to one, by way of an assumption, permits rearrangement to:

$$\sqrt{\frac{\tau_w}{\rho}} = \kappa \ell_{\text{mix}} \frac{\partial U_x}{\partial y}, \quad (2.176)$$

in which the LHS is conventionally denoted v_τ after the dimensionless ‘friction velocity’ of page 115. Also by way of an assumption, in the near wall region there is supposed to be only one relevant and applicable length scale, that being the distance to the nearest wall; it is this that the mixing length means to quantify. Hence, in the near wall region

$\ell_{\text{mix}} = y$. Such reasoning gives to the integrable equation:

$$\partial U_x = \frac{v_\tau}{\kappa} \frac{1}{y} \partial y, \quad (2.177)$$

with solution

$$U_x = \frac{v_\tau}{\kappa} \ln y + c. \quad (2.178)$$

The constant of integration, c , remains to be specified.

This is the logarithmic distribution of mean velocity, valid for the near wall region where viscous forces are negligible, behaviour being dominated by turbulent momentum transfer and a geometric mixing length. Whilst this derivation *chooses* features strictly applicable only to either the laminar sub-layer or the turbulence and is in that respect quite flimsy, it nevertheless yields a very accurate description for a very large section of the velocity profile, which consequently is known as the logarithmic layer. It is a valid *approximation* however, to the whole of a wall induced turbulent shear. Though in reality significant deviation is observed for the laminar sub-layer and in the core turbulence. Again, see figure 2.17.

Prandtl's turbulent distribution in pipes

Is found from integration of equation 2.178 with the boundary condition that peak velocity occurs at channel centre line:

$$U_x = U_{\text{pk}} + \frac{1}{\kappa} u_\tau \ln \frac{y}{R}. \quad (2.179)$$

This is found to match experimental data very well [73], despite the fact that it overestimates velocity at the centre line (and therefore the cross channel mean) because, as a strictly increasing wall model, it has a sharp peak (ogive form) there, with gradient discontinuity.

Turbulent velocity in pipes due to von Kármán

von Kármán, in [142] and [143], arrived at a similar result to equation 2.178, via his similarity theory. It may be arrived by the 'differential equations method' of dimensional analysis, that is by assuming ν_T to be a function of $\partial_y U_x$ and $\partial_y \partial_y U_x$, that is first and second order gradients in the mean velocity. It is

$$U_x = U_{\text{pk}} + \frac{1}{\kappa} u_\tau \left[\ln \left(1 - \sqrt{\frac{r}{R}} \right) + \sqrt{\frac{r}{R}} \right]. \quad (2.180)$$

His analysis also gives rise to other forms for the eddy viscosity:

$$\nu_T = \frac{\kappa^2 (\partial U_x / \partial y)^3}{(\partial^2 U_x / \partial y^2)^2}, \quad (2.181)$$

and the mixing length:

$$\ell_{\text{mVK}} = \frac{\kappa (\partial U_x / \partial y)}{\partial^2 U_x / \partial y^2}. \quad (2.182)$$

These were comparatively unsuccessful in application, however, being less accurate than Prandtl's simpler version. Moreover, on a practical level, it is apparent that 2.182 gives infinite eddy viscosity at 'shear inflections', that is where $\partial_y \partial_y U_x = 0$. Both jets and wakes manifest such inflections.

Wang's turbulent distribution in pipes

Wang, in a later work, [149], derived another empirical form for the profile:

$$\begin{aligned} u^+ = \frac{U_x}{u_\tau} &= \frac{U_{\text{pk}}}{u_\tau} - \frac{1}{\kappa} \left(\ln \frac{1 + \sqrt{\frac{r}{R}}}{1 - \sqrt{\frac{r}{R}}} - 2 \tan^{-1} \sqrt{\frac{r}{R}} \right. \\ &- 0.572 \ln \frac{\frac{r}{R} + 1.75 \sqrt{\frac{r}{R}} + 1.53}{\frac{r}{R} - 1.75 \sqrt{\frac{r}{R}} + 1.53} \\ &\left. + 1.14 \tan^{-1} \frac{1.75 \sqrt{\frac{r}{R}}}{1.53 - \frac{r}{R}} \right). \end{aligned} \quad (2.183)$$

Obviously this is more complex than earlier counterparts, but it is found to have much higher accuracy at high Reynolds number.

The Universal velocity distribution for turbulence in pipes

Using Prandtl's turbulent velocity distribution of a previous section, equation 2.179, it is possible to derive a further and more general form of velocity distribution. This is known as 'universal' because it is made compatible with both the law of the wall 2.169 *and* the velocity defect law 2.171. See von Kármán [141] or Millikan [95].

It depends upon the following working assumptions: Firstly that the viscous layers and turbulent layers are distinct. Secondly that shear is constant through the laminar layer. Third, there are only viscous forces there. Finally that the relation so derived is valid for *all* pipes of all sizes and is therefore an absolute constant. It is not derived here on account of space and context. Instead, it is quoted in various forms corresponding to its diverse application:

For **smooth pipes**:

$$u^+ = \frac{1}{\kappa} \ln y^+ + B, \quad (2.184)$$

Empirically derived values for the constants κ and B were frequent additions to the literature. A good review of the earlier ones is to be found in [73]. It is seen that values for κ , which is since [142] known as the von Kármán constant, arise over the range $0.38 \leq \kappa \leq 0.41$, with $\kappa = 0.4$ the accepted figure matching most data. See e.g. Nikuradse [99]. It has been mooted that this value is too high on account of the fact that real simulations are not carried out at high enough Reynolds number and that a better value then should be more like $\kappa = 0.3$. Note that since it is often the reciprocal which occurs, the coefficient $2.5 = 1/\kappa$ is regularly seen.

B in sense of 2.184 and typical texts, say [148, 150], is usually given the value of 5, or another in the range $4.4 \leq B \leq 5.85$.

A cursory look at equations 2.178 and 2.184 reveal their equivalence as respectively, dimensional and dimensionless forms, for the same physics; being related by a simple multiplicative factor which maps c to B and vice versa.

Various extension of this work have been done, most importantly to the case of non-smooth pipes. Where the pipe relative surface roughness is defined by the ratio of typical amplitude e to pipe radius R the following arises for **rough pipes**:

$$\frac{V}{v_\tau} = 2.5 \ln \frac{R}{e} + 4.75. \quad (2.185)$$

See [73] for further references. Similarly, the following combined expression may be derived for **general pipes**:

$$v^+ = 2.5 \ln \frac{y}{R} + 3.75 + \frac{\bar{V}}{v_\tau}. \quad (2.186)$$

As expressed in terms of the cross channel mean velocity \bar{V} , equation 2.186 does not incorporate relative roughness and therefore demonstrates that the *profile shape* is unaffected by surface roughness in any way except magnitude; good evidence to suggest internal turbulence mechanisms are independent of the boundary.

Consequential description of the turbulent boundary layer

The following comments are made in respect to figure 2.17, which is a direct equivalent to figure 2.16, but in dimensionless independent variables.

Starting at the innermost, the location dependent Reynolds number, y^+ , is less than unity for a region very close to the wall. There, viscous processes are expected to dominate and the zone is known therefore as the viscous sub-layer. As a consequence of viscosity, the flow is effectively laminar in nature, which leads to a linear form for the law of the wall, equation 2.174. This region is conventionally deemed to extend to $y^+ = 5$, but some

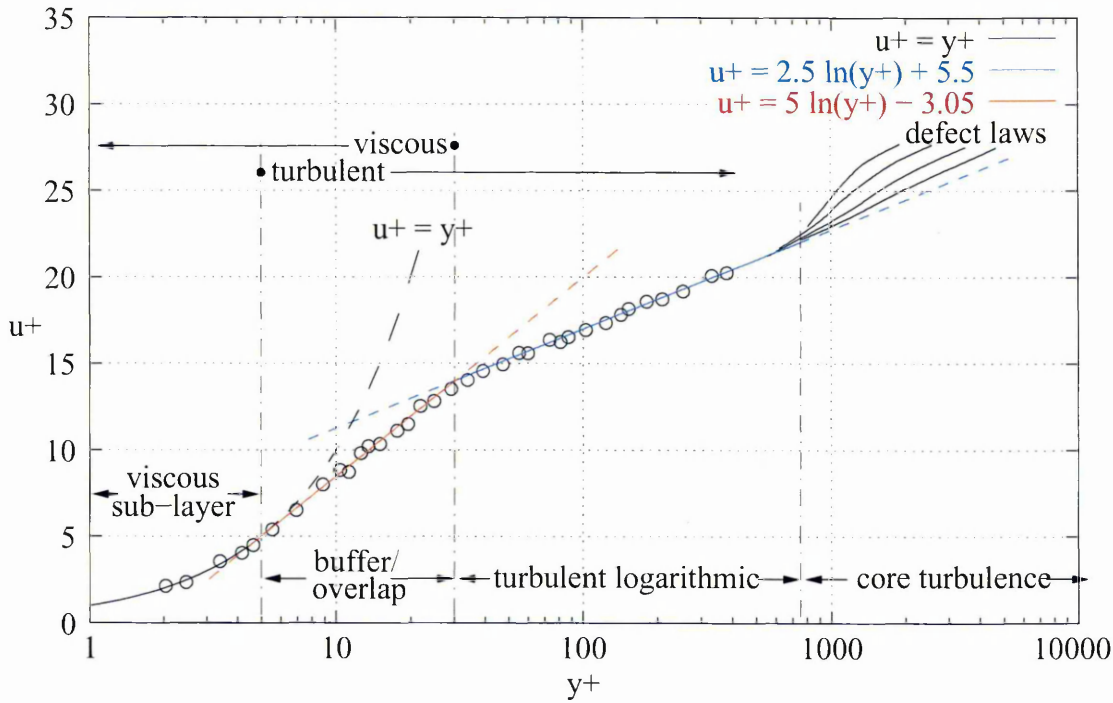


Figure 2.17: Analytically derived turbulent mean profile of velocity in the near wall region and consequential subdivision of the turbulent boundary layer. Note, the the seventh power law 2.165 is not comparable on this plot as it is not derived dimensionally. From wall out: the laminar sub-layer, $0 \leq y^+ \leq 5$, profile varies as $u^+ = y^+$; next, the overlap zone or ‘buffer’ layer, $5 \leq y^+ \leq 30$, shown using relation 2.187; further out, the fully turbulent logarithmic layer $30 \leq y^+ \leq 500$, given by, say, equation 2.184; lastly the ‘core’ turbulence, $500 \leq y^+$, described by velocity defect laws. Data points (circles) are illustrative only.

studies define the overlap region as extending from say $y^+ = 3$ and up.

Further into the channel, the overlap region is defined as that where owing to the proximity of the wall, any the eddies are necessarily small and the relative isolation from the bulk means viscous and turbulent processes have comparable effect. This layer is conventionally deemed to reside in the y^+ range: $5 \leq y^+ \leq 30$.

Further out there is a region where turbulent momentum transfer is dominant and viscous effects are negligible. This leads to a logarithmic turbulent mean velocity profile — for which various forms have been derived — named therefore the logarithmic layer. The logarithmic profiles however, turn out to be very good approximation to behaviour across the entire half channel. This is despite the rather flimsy nature of both the mixing length hypothesis, upon which most analyses have been based, and the piecwise manner in which it is dealt with.

Finally, ‘beyond’ any direct effect from the wall, there is ‘core’, inertia dominated turbulent flow. There the velocity defect law holds. Deviation in the core region (the defect) is variable, dependent on the type of boundary layer and specifics of its environment. Little attention will be directed to this region in the current studies. A set of

examples of such are indicated in the figure 2.17, however; for illustration only.

With respect to the overlap, or buffer layer, where no semi-analytic form for the profile exists, it was found that data could still be modelled by a logarithmic curve. In [143], using data of Reichardt and Reichardt and Schuh [114] which extend over $1.5 \lesssim y^+ \lesssim 300$ and thus cover the entire overlap layer, von Kármán showed that the expression:

$$v^+ = 5.00 \ln y^+ - 3.05, \quad (2.187)$$

was a good empirical fit, at least for the range $5 \leq y^+ \leq 30$.

Later, in the context of improvements to the universal velocity distribution, Deissler, by neglecting the effect of kinematic viscosity, derived an inverse relationship, [31]:

$$y^+ = \frac{1}{n} \frac{\int_0^{nu^+} e^{-(nu^+)^2/2} d(nu^+)}{e^{-(nu^+)^2/2}}, \quad (2.188)$$

which was hardly altered by a subsequent analysis [33]. The value of n was established empirically as 0.109. Equation 2.188 provides an excellent fit for both smooth and rough pipes over the reduced range $5 \leq y^+ \leq 26$.

2.7.4 Analyses of turbulent channel friction data; the Moody curves

The discussion now turns to the other primary form of data which will be of interest in these studies, that is friction data. In section 2.7.1 the friction coefficient, or friction factor, is defined. It turns out that quantification of the retardative effect of walls in a flow is best done in terms of the dimensionless parameters of Reynolds number and friction coefficient. A presentation of observed friction behaviour in terms of flow forcing etc. is highly illustrative of the problem of flow in internal geometries. Collections of such data are often grouped to form the curves of a ‘Moody chart’; which arises as follows.

The Moody chart

Essentially the Moody chart for flow in channels is a plot of friction coefficient against Reynolds number. Owing to the great breadth of turbulence characteristics assembled therein, general properties of the Moody chart will be referred to extensively in later chapters; an illustration is therefore provided in figure 2.18, to which the reader is referred. Observe the vague similarities between a Moody chart and phase diagrams of condensed matter physics. Here the ‘phases’ are fluid *flow* behaviours; in the figure delineated by dot–dash lines. Variants on the theme occur; in particular here \log_{10} axes are employed.

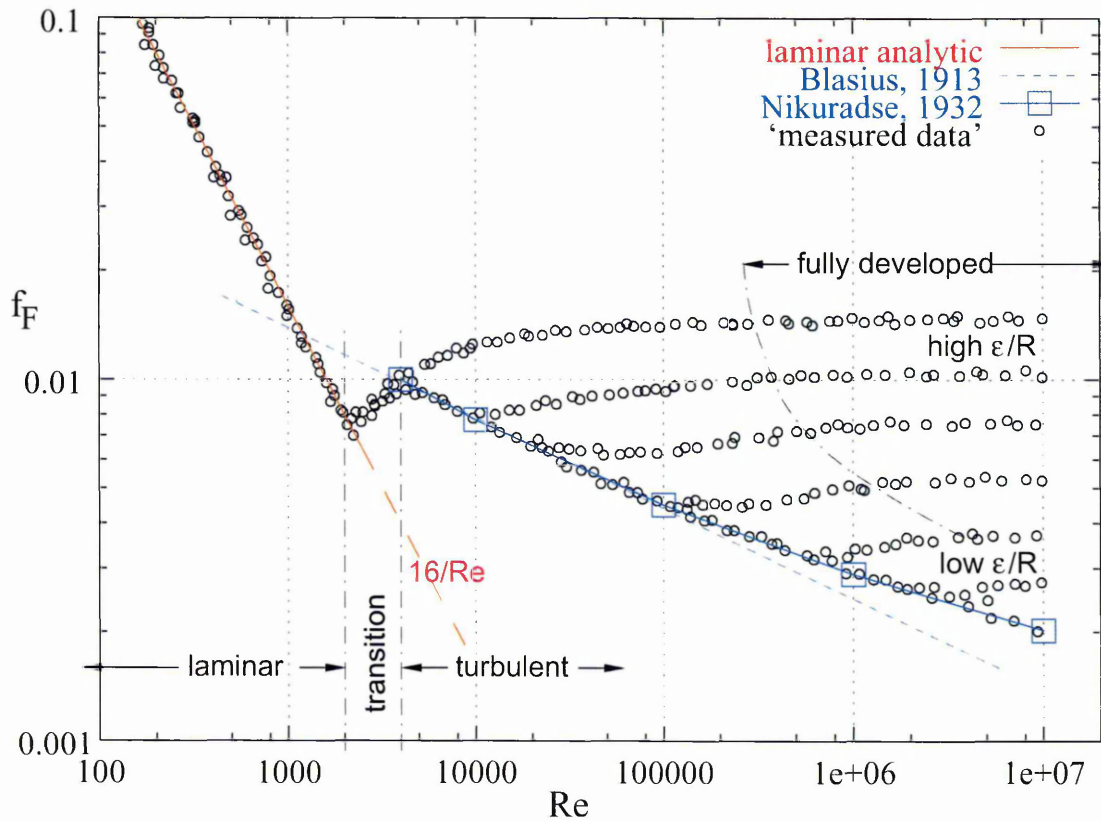


Figure 2.18: Example Moody chart for cylindrical geometry, i.e. pipe flow, using Fanning friction factor. Transition between laminar and turbulent regimes occurs around Reynolds number $Re_{cr} \approx 2000$. Below Re_{cr} laminar flow data follow the analytic straight line solution 2.189. Above transition data possess dependence on qualities of the wall, especially roughness (ϵ/R), which gives rise to a continuous set of branches. Semi-empirical relations for turbulence in infinitely smooth pipes are also shown (blue): the Blasius equation 2.192, dashed; and Nikuradse's relation 2.193 mentioned later, page 134, solid and squares. Only in the flat high Re tail is the turbulence supposed fully developed. Data 'points' are illustrative only.

Data in the plot fall, at first sight, into three distinct regions, which summarise all three manifestations of flow: laminar, transition and turbulent — hence its utility. At low Reynolds number the flow is laminar and friction factor dependence³⁶ is linear and negative, this is the straight line section of figure 2.18, up to Reynolds number around 2000. For Reynolds number above that (strictly $Re \geq Re_{cr} = 2300$) there is a poorly defined region characterised by a jump in the coefficient of friction and by high scatter in experimental data. At higher Re still the flow is turbulent, though not necessarily ‘fully developed’. There, more complex features are visible in the chart, especially:

- An underlying theoretic trend: the ‘Blasius friction law’, equation 2.192, discussed in the next section and denoted by the dashed blue line.
- A superior equivalent to the above; in particular, Nikuradse’s relation [99], equation 2.193, also in the next section, page 134 (many similar exist), which is valid over a greater range of Re .
- Branching at higher Reynolds number, dependent on the pipe roughness.
- A poorly understood rise after the dip in each branch.
- Finally, a ‘flat tail’ at high Re , which is very dependent on pipe roughness³⁷. This is the only region of the chart which is supposed to represent fully developed channel turbulence.

Recall that friction factor is essentially equivalent to viscosity and is strictly therefore a turbulence parameter (earlier this section). Well it is nevertheless possible to derive consistent values for the laminar flow regime. To do this take equation 2.146 for laminar flow (in pipes) and substitute for $-dp/dx$ from rearrangement of equation 2.161. On simplifying, $\nu/V\varnothing_h = 1/Re$ note, the following are arrived at:

$$f_F = \frac{16}{Re}, \quad (2.189)$$

or in terms of the Blasius / Darcy–Weisbach friction factor,

$$f_{DW} = f_B = \frac{64}{Re}, \quad (2.190)$$

³⁶See next paragraphs which extend the friction factor into the context of a laminar flow.

³⁷The internal surface quality is discussed later, in section 5.4 and 6.1 in relation to extensions and further work. It is defined here, as is usual, by the ratio of typical roughness amplitude to pipe radius, ε/R

which relate f to Re . On a \log_{10} scale this is a straight line:

$$\log f_{\text{F}} = \log 16 - \log(Re), \quad (2.191)$$

with gradient -1 and ‘intercept’ (with the $\log(Re = 1000)$ line) of about $10^{-1.8}$, or 0.016 (for Fanning f_{F}). Such is the straight line, laminar portion of the Moody chart 2.18.

Friction laws

Over the years, much data has been generated on wall induced friction in turbulent channels and various workers have attempted to model data with various empirical relations. Some, in addition, have tried to build descriptive relations from first principles. Both have met with some success, to the point that engineers have well established means at their disposal, with which to solve pipe specification problems.

The well known of these are briefly reviewed in the following paragraphs. This is both to further illuminate relevant turbulent behaviour and to provide quantitative data with which to compare results generated by modelling in chapter 5. The discussion indicates relations presented visually in figure 2.19, which consists of friction relation data for just the turbulent portion of the Moody chart, i.e. $Re > Re_{\text{cr}}$.

The **Blasius friction law** was the first analytic expression to correlate friction coefficient versus Reynolds number, thereby elucidating various results under discussion at the time. Blasius worked on numerous variants of his ‘Blasius equation’ problem, generating a range of differing friction laws: in 1908 on turbulent flow past a plate; in 1911 the first such study on pipes, for Reynolds number in the range $4000 \leq Re \leq 10^5$; and most importantly in 1913 [11] where he assembled his results with those of other authors to suggest a relation valid for a wider range of Reynolds number:

$$f_{\text{B}} = 0.079Re^{-1/4}, \quad (2.192)$$

which is valid from $Re = 3 \times 10^3$ to 10^5 . It is this result which Prandtl first used to calculate velocity distributions across the channel, see page 122. It strictly approximates the smooth wall branch of the Moody curve only.

So much information and physics is contained in the Moody chart that the recovery of only a small fraction will be sufficient to voice an optimistic stance on the efficacy of the LB mixing length model invoked in chapter 5. Such matters are addressed nearer the time in section 5.1.2 and in the discussion section 5.4.

Nikuradse, in extending the range of Reynolds number over which turbulence in pipes had been investigated, obtained an empirical relation, which modelled data he had gath-

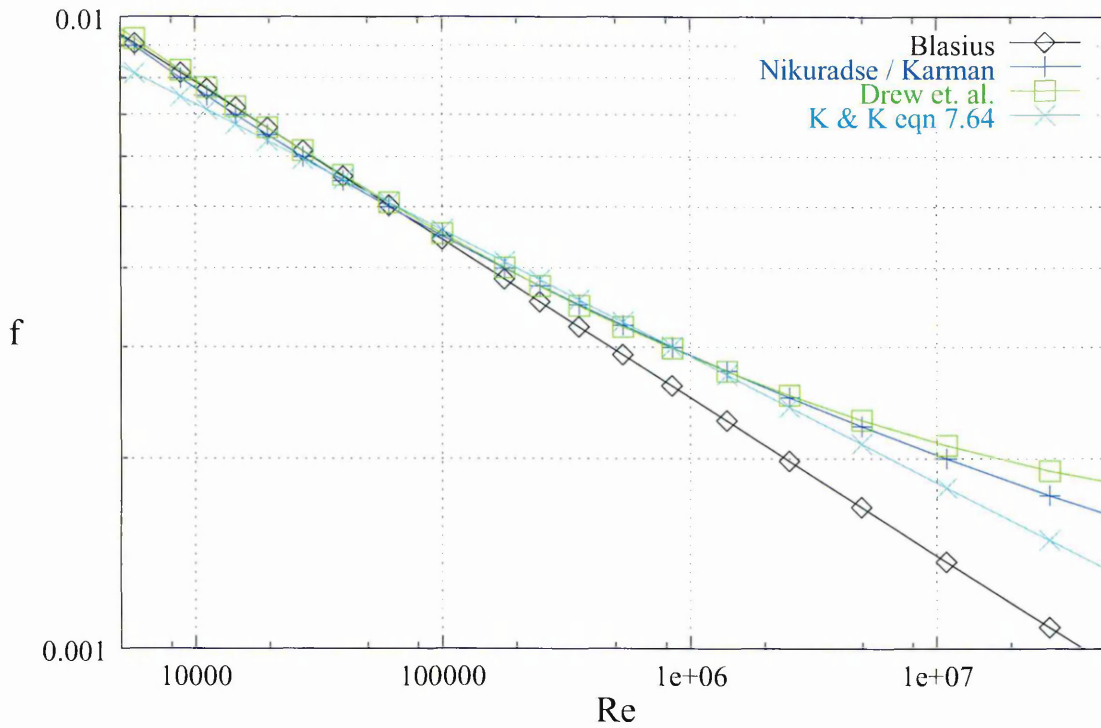


Figure 2.19: Comparison between the various friction laws mentioned. The Blasius data arise in equation 2.192. The second plot, in blue, are consistent with two sources: the relation arrived at empirically by Nikuradse [99], equation 2.193; and that derived theoretically by von Kármán [142], as discussed, page 134. Data in green arise through the relation 2.194, derived by Drew *et al.* [36]. Finally, the data for the last curve, in light blue were obtained from another relation in Knudsen and Katz [73], see equation 2.195. Compare these empirical matches and theoretical curves to those of figure 2.18.

ered and matched that of other workers very well, [99]:

$$\frac{1}{\sqrt{f_B}} = 4 \log(Re \sqrt{f_B}) - 0.4. \quad (2.193)$$

His data were collected over the range $4 \times 10^3 \leq Re \leq 3.24 \times 10^6$ making it, at the time, a most comprehensive study. Moreover, its good statistical fit to the data, for the entire range considered, make it an accepted standard for finding friction factors in smooth tubes even today. Unfortunately, as an inverse relation, friction data cannot easily be calculated for any particular Reynolds number.

Many equivalents to this relation may be found, not least that of von Kármán [142], who derived theoretically a very similar form for equation 2.193. It was identical in all respects except values for coefficients in the RHS; these were 4.06 and 0.6 respectively. A further empirical relation of this kind was obtained by Drew *et al.* [36]:

$$f = 0.0014 + 0.125Re^{-0.32}, \quad (2.194)$$

which is used extensively. Last to be mentioned here, Knudsen and Katz [73] cite the following

$$f = 0.046Re^{-0.2}, \quad (2.195)$$

which they state is derived from a relation used in heat transfer calculations.

In chapter 5, results discussed earlier this section are used in two ways: the empirical relations for both flow profiles, 2.165 to 2.188, and Moody curves, 2.192 and 2.193 to 2.195, are used as yardsticks by which data derived in our simulations can be evaluated.

Despite the fact that experimental results have been in evidence a long time, inconsistencies do exist and these have boosted efforts to derive truly analytic equivalents to the empirical friction relations (in addition for flow profiles and the like). Contemporary treatments are not of relevance to this work however, for which the reader is referred to the general turbulence literature.

Interpretation of friction characteristics of flow in pipes and channels is usually practically biased. On a grander and more phenomenological level however, the various processes at work, by which Moody curve gradient is reduced, may be seen as the necessary natural mechanisms to curtail any ‘peculiar’ physical behaviour at extremes. Specifically, the expectation that the fluid experience ever decreasing dependence of retardative forcing on flow kinetic energy, see defining relation for friction coefficient, equation 2.160, whilst *increasing forcing* (and thereby *velocity* contribution to Reynolds number), contradicts common sense, or some energetically motivated paradigmatic presumption. To see this note that, extrapolating such a situation to its logical limit would mean that, once set in motion, a fluid flowing at near infinite Reynolds number would experience virtually zero friction and would hence tend to continue in motion indefinitely.

Chapter 3

Simulation of cylindrical flow on a regular 2D grid

By inserting position and time dependent ‘source’ or ‘forcing’ terms into the microscopic evolution equation of a lattice Boltzmann fluid and treating the generalised scheme within the usual Chapman–Enskog methodology, the emergent dynamics of the lattice fluid are demonstrably and usefully transformed. The method of adjustment is demonstrated by implementing the cylindrical polar coordinate form of the continuity and momentum equations on a rectangular lattice and generating results for pipe flow. With straightforward systematic adjustment of the simulation, the approach here produces results in excellent agreement with theory.

3.1 The problem of using a 2D simulation for 3D cylindrical geometry: Introduction

This chapter details implementation, application and analysis, of an adaptation of lattice Boltzmann forcing scheme aimed at recovering, in the lattice fluid’s macroscopics, characteristics of flow in a geometry other than the Cartesian space of the simulation domain. Specifically, for the sake of definiteness, a forcing strategy is considered that targets recovery of macroscopic equations identifiable with cylindrical polar coordinate forms of both Navier–Stokes and continuity equations. In so doing it is demonstrated how the form of the macroscopic equations, describing the lattice fluid, can be usefully adjusted by adding variable source terms to the microscopic momentum density evolution equation.

Adapting the lattice Boltzmann scheme, by the use of forcing, is a relatively straightforward and commonplace operation. Indeed, all flow simulations necessarily involve such modification simply to drive the flow. Here, the forcing is more complex. It is intended to account for the fact that one cannot simply use a 2D Cartesian simulation domain to represent flow in other 2D geometries.

Consider flow in a pipe or cylinder; a common and important flow realisation. This is inherently three dimensional in nature, but where there is flow invariance around the geometric axis, that is ‘cylindrically symmetry’, only two coordinate axes are required as a basis for flow characterisation. Traditional coordinate representation consists of ϕ , r and z ; these then reduce to just r and z , where invariance is with ϕ , around the axis, r is radial coordinate and z is distance along the pipe. Under such circumstances, it is tempting to assume that the two axes of the 2D lattice Boltzmann simulation, x and y , may be used simply to represent r and z directly. To do so would not be correct, however.

The problem in this instance, with using such a ‘flattened’ simulation space to represent a three dimensional configuration, is that the volume of fluid associated with any

point on the 2D grid *increases* as one moves radially outward from the geometric axis.

At first glance this may seem to be relatively innocuous, but not so. In fact comparing two appropriate 2D geometries, channel flow and pipe flow say, it readily becomes clear that the relative effect on the fluid, of friction imposed by the domain walls, is much higher for the cylindrical case. To illustrate this, compare the ratio of wetted perimeter to flow cross sectional area for the two cases. On one hand, the numerator is twice the channel depth, on the other it is the cylindrical circumference¹. It emerges that the flow profile magnitude for the cylindrical case will be exactly half that for the infinitely deep duct; a subtle point to a computational physicist, but one of some obviousness to fluid dynamicists.

What this demonstrates, is that the 2D lattice Boltzmann scheme used herein, which models a geometry invariant with the third dimension, is, in its unmodified form, not capable of resolving such geometric or coordinate transformation issues. It would be of great value if a modification could be found that rendered the LB scheme capable of reproducing this and related detail. Such is the matter addressed in the current chapter.

In the remainder of this section, further detail on the specific nature of these investigations is presented: the particular geometry of interest is discussed and a coordinate transformation specified in section 3.1.1; an appropriate form of the transformed equations is also set out in section 3.1.1; and a discussion of forcing in general is presented in section 3.1.2, as a basis for subsequent development and analysis. Section 3.2, proceeds to focus on the particular problem detailed earlier, forming the main technical content of the chapter: equations are derived specifying particular forcing terms for the case in point. Implementation of a test bench for the scheme so devised is detailed in section 3.3. There also, results of the various simulations are presented. Section 3.4 discusses, in the light of these results, the strategy's efficacy and utility, together with suggestions for further work. Finally, in section 3.5, conclusions are drawn and a synopsis of results given.

3.1.1 Cylindrical flow representation

Consider the problem of the laminar flow of an incompressible, isotropic liquid, in internal geometry, with rotational symmetry around the z -axis. The azimuthal velocity in such a configuration, v_ϕ , and ϕ coordinate derivatives, vanish from the incompressible Navier–Stokes and continuity equations, [81]. The remaining radial and axial velocities v_r and

¹Strictly this has to be done for the limit as channel depth, d , approaches infinity. The result $2\pi R\ell/\pi R^2$ is obtained for the cylinder, $2d\ell/dW$ for the duct. Under $R = W/2$, the latter evaluates to *twice* the value for the cylinder, at $4\ell/W$.

v_z and pressure P satisfy three equations in the two spatial coordinates z and r . On making the replacements:

$$\begin{aligned}(z, r) &\rightarrow (x, y), \\ (v_z, v_r) &\rightarrow (v_x, v_y),\end{aligned}\tag{3.1}$$

a pseudo-Cartesian representation of pipe flow is obtained:

$$\partial_x v_x + \partial_y v_y = -\frac{v_y}{y},\tag{3.2}$$

$$\frac{Dv_x}{Dt} = -\frac{1}{\rho}\partial_x P + \nu\nabla^2 v_x + \nu\frac{1}{y}\partial_y v_x,\tag{3.3}$$

$$\frac{Dv_y}{Dt} = -\frac{1}{\rho}\partial_y P + \nu\nabla^2 v_y + \nu\frac{1}{y}\left(\partial_y v_y - \frac{v_y}{y}\right).\tag{3.4}$$

The last terms on the right hand side of equations 3.2 to 3.4 are hence forward designated ‘non-rectangular’.

It can be shown that equations 3.2 to 3.4 may be obtained from a lattice Boltzmann scheme simulating incompressible flow, with the following macroscopic equations for the two unknown quantities v_x and v_y :

$$\partial_t \rho + \partial_x \rho v_x + \partial_y \rho v_y = -\frac{1}{y}\rho v_y,\tag{3.5}$$

$$\frac{D\rho v_\alpha}{Dt} + \partial_\alpha P - \nu\nabla^2 \rho v_\alpha = \frac{\nu}{y}\partial_y \rho v_\alpha - \frac{\nu\rho v_y}{y^2}\delta_{\alpha y},\tag{3.6}$$

where $\alpha = x, y$ and the usual summation convention applies.

The RHS terms in continuity and momentum equations, 3.5 and 3.6, arise from the particular way in which the simulation has been adapted from cylindrical polar coordinates and *not* from external, physical accelerations impressed upon the fluid.

3.1.2 General forcing in lattice Boltzmann simulation

The strategy discussed in this chapter aims to augment the normal lattice evolution process with an algorithmic step intended to invoke properties of radially varying flow volume and fluid mass in the lattice fluid. Such properties are represented by the RHS terms of equations 3.5 and 3.6.

There are in fact very few ways in which behaviour of the LBGK scheme can strongly be influenced for such purposes. The lattice may be modified, but this removes a great deal of the beauty of the LB; it might prove useful to modify the relaxation parameter

spatially, but it is unclear as to whether this could ever produce the right physics. The most obvious line of attack is to devise suitable ‘external’ forcing terms. Forcing of any kind is easily implemented in the LB, so long as simple constraints such as mass conservation are met at the same time.

In reality forcing is a necessary element of any practical simulation, those presented here being no exception in that regard. The reason for this is simply that in some way equilibrium must be broken so that flow is initiated. In this chapter and elsewhere in this work, so called ‘body forcing’ is utilised for this purpose, hence it is discussed in the introductory section 2.6.4. However, to exemplify the general concept of forcing and since it occurs essentially ‘tied in’ to the strategy here, it makes a good case study, so a brief aside is now taken to discuss.

The idea in body forcing the lattice fluid is to impart a force that replaces or simulates the configurational reality of pressure gradient which drives most flows. It is achieved quite simply by, at an appropriate stage in the lattice evolution, adjusting the distribution of density among the links of forced nodes according to a simple algorithm. This is done in such a way to meet required conservations, but also to deliberately ‘break’ others. Body forcing conserves mass but not momentum; the whole purpose is to impart momentum to the fluid in a similar fashion to how a pressure gradient would.

Practically, forcing is implemented simply by subtracting mass symmetrically from links on one side of the node and adding it symmetrically to links on the opposite side. The quantities redistributed this way are called forcing terms, herein denoted h_i . Such adjustment amounts to a modified collision step and is therefore to be performed with equivalent timing as for collision.

For the current purpose, of adjusting the simulation so as to model the effect of greater fluid mass and volume as one moves radially out from the central axis, a more complex forcing algorithm is required. In fact the previously mentioned body forcing is ‘static’ in the sense that the parameters used to implement the forcing, are calculated only once, that being when the simulation pressure gradient is specified. In a way similar to body forcing, the new *axial symmetry* forcing terms are to be implemented by a simple addition of link dependent density terms. In contrast however, these now depend algorithmically on parameters such as the node distance from pipe axis and radial gradients of flow velocity, that is, the forcing terms in this case are dependent on the geometry and the emerging flow character.

Here and in the paper, [52], the two types of forcing are in fact calculated and implemented simultaneously, using now space dependent and dynamic contributions at order ϵ and ϵ^2 , denoted $h_i^{(1)}$ and $h_i^{(2)}$ respectively. The discussion now moves on to this issue,

3.2 Implementing coordinate change in LB by forcing

The macrodynamics of equations 3.5 to 3.6 are sought for the case of a two dimensional, nine velocity (D2Q9) lattice Bhatnagar–Gross–Krook fluid [112], which is to be modified. Note, however, this analysis will generalise directly to any particular LB scheme. Common lattice Boltzmann notation, consistent with that of the rest of this work, is employed.

With the intention of driving the lattice fluid toward a non-uniform momentum distribution, a *spatial and velocity dependent* microscopic term $h_i(\mathbf{r}, t)$ is incorporated into the evolution equation for the lattice fluid’s momentum distribution, thereby adjusting it as follows:

$$f_i(\mathbf{r} + \epsilon\Delta_t\mathbf{c}_i, t + \epsilon\Delta_t) = f_i(\mathbf{r}, t) + \frac{1}{\tau}[f_i^{(0)}(\mathbf{v}, \rho) - f_i(\mathbf{r}, t)] + h_i(\mathbf{r}, t). \quad (3.7)$$

Here Δ_t is the explicit time step, ϵ the Chapman–Enskog expansion parameter (Knudsen number) and all other terms have their usual meaning. For purposes of extracting the dynamics of this modified scheme 3.7 a Chapman–Enskog type expansion is performed, with the h_i , like the f_i , expanded in powers of ϵ . Bearing in mind that, in the corresponding unadjusted LBGK scheme [112], the $\epsilon^n f_i^{(n)}$, $n > 0$ are the cause of *departures* from equilibrium, h_i are then taken to be at least $\mathcal{O}(\epsilon)$:

$$h_i = \epsilon h_i^{(1)} + \epsilon^2 h_i^{(2)} + \epsilon^3 h_i^{(3)} + \dots, \quad (3.8)$$

where, it is emphasised, there is no ‘equilibrium’ $\mathcal{O}(\epsilon^0)$ h_i term.

It is natural to take the lead term $\epsilon h_i^{(1)}$ to be zeroth order in velocity gradients (this ensures consistency with several previous LB applications in which the lattice fluid is body forced by a spatially uniform pressure gradient; see, for example, [88] and the references therein). Accordingly $h_i^{(1)}$ is taken to be zeroth order in gradient quantities, and $h_i^{(2)}$ to contain any first order gradients in macroscopic observables ρ, \mathbf{v} ; so, in general $h_i^{(n)}$ contains $(n - 1)$ th order gradients in ρ and \mathbf{v} .

The question now is to determine the $h_i^{(n)}$ that give equations 3.5 and 3.6 in a consistent fashion. From a Chapman–Enskog type expansion of the Taylor expanded evolution equation 3.7 (after Hou *et al.* [69]), the result:

$$(\partial_{i0} + c_{i\gamma}\partial_\gamma)f_i^{(0)} = -\frac{1}{\tau}f_i^{(1)} + h_i^{(1)}, \quad (3.9)$$

is obtained at $\mathcal{O}(\epsilon)$; and at $\mathcal{O}(\epsilon^2)$:

$$\partial_{t1} f_i^{(0)} + (\partial_{t0} + c_{i\gamma} \partial_\gamma) \left(1 - \frac{1}{2\tau}\right) f_i^{(1)} = -\frac{1}{\tau} f_i^{(2)} + h_i^{(2)}. \quad (3.10)$$

In deriving the macroscopic dynamics, it is usual to substitute for $f_i^{(1)}$ in equation 3.10 using equation 3.9, which gives

$$\partial_{t1} f_i^{(0)} + (\partial_{t0} + c_{i\gamma} \partial_\gamma) \left(1 - \frac{1}{2\tau}\right) \left[-\tau(\partial_{t0} + c_{i\delta} \partial_\delta) f_i^{(0)} + \tau h_i^{(1)}\right] = -\frac{1}{\tau} f_i^{(2)} + h_i^{(2)}. \quad (3.11)$$

Equations 3.9 to 3.11 are *not* then used to relate $f_i^{(n)}$ to the $h_i^{(n)}$, as might be expected. Rather, the problem is partitioned in such a way as to recover the RHS (LHS) terms in target equations 3.5 and 3.6 from the $h_i^{(n)}$ ($f_i^{(n)}$) independently.

Defining $\Delta_{i\alpha}$ to be equal to $c_{i\alpha}$ and 1, moments may be taken of equations 3.9 and 3.11, setting for the $f_i^{(n)}$:

$$\partial_{t0} \sum_i f_i^{(0)}(\mathbf{v}, \rho) \Delta_{i\alpha} + c_{i\gamma} \partial_\gamma \sum_i f_i^{(0)}(\mathbf{v}, \rho) \Delta_{i\alpha} = -\frac{1}{\tau} \sum_i f_i^{(1)} \Delta_{i\alpha} \quad (3.12)$$

$$\sum_i \left[\partial_{t1} + \left(\frac{1}{2} - \tau\right) (\partial_{t0} + c_{i\gamma} \partial_\gamma)^2 \right] f_i^{(0)}(\mathbf{v}, \rho) \Delta_{i\alpha} = -\frac{1}{\tau} \sum_i f_i^{(2)} \Delta_{i\alpha}, \quad (3.13)$$

where

$$\Delta_{i\alpha} = c_{i\alpha}, 1. \quad (3.14)$$

This, taken with the usual constraints:

$$\begin{aligned} \sum_i f_i^{(0)}(\mathbf{v}, \rho) &= \rho \\ \sum_i f_i^{(0)}(\mathbf{v}, \rho) c_{i\alpha} &= \rho v_\alpha \\ \sum_i f_i^{(0)}(\mathbf{v}, \rho) c_{i\alpha} c_{i\beta} &= \rho \delta_{\alpha\beta} / c_s^2 + \rho v_\alpha v_\beta, \end{aligned} \quad (3.15)$$

corresponds to the unadjusted isothermal LBGK scheme [112, 158]. Such is then used without further modification to recover the usual LHS terms in the model's macrodynamics (equations 3.5 and 3.6).

Implicitly, therefore, the corresponding moments of the h_i :

$$-\sum_i h_i^{(1)} \Delta_{i\alpha}, \quad (3.16)$$

$$\tau \left(1 - \frac{1}{2\tau}\right) \sum_i (\partial_{t0} + c_{i\gamma} \partial_\gamma) h_i^{(1)} \Delta_{i\alpha} - \sum_i h_i^{(2)} \Delta_{i\alpha}. \quad (3.17)$$

must be used to generate the new ‘target’ terms in the lattice continuity and momentum equations — for present purposes, terms of the RHSs of equations 3.5 and 3.6. Note that expressions 3.16 and 3.17 relate to $\mathcal{O}(\epsilon)$ and $\mathcal{O}(\epsilon^2)$ respectively. Care must therefore be exercised; as is evident from expressions 3.16 and 3.17, the choice of $h_i^{(1)}$ must influence the form of $h_i^{(2)}$ and so forth.

For the particular application of pipe flow, a form for the $h_i^{(1)}$ will first be selected that yields the desired modification of the lattice continuity equation 3.5, in addition to appropriate body forcing; this is done in section 3.2.1. Thereafter the $h_i^{(2)}$ will be determined from the chosen $h_i^{(1)}$ and from the target modification to the lattice fluid’s momentum equations 3.6, section 3.2.2.

3.2.1 Lattice continuity equation and $h_i^{(1)}$

Modifications to the lattice continuity equation, resulting from the inclusion of forcing terms $h_i^{(1)}$ and $h_i^{(2)}$ into the lattice evolution equation, are now considered. Taking equation 3.9 and summing over all i , the following is obtained at $\mathcal{O}(\epsilon)$:

$$\partial_{t0} \rho + \partial_\beta \rho v_\beta = \sum_i h_i^{(1)}. \quad (3.18)$$

With the target dynamics of equations 3.5 and 3.6 in mind, the following selection of $h_i^{(1)}$ emerges:

$$h_i^{(1)} \equiv w_i \left(\mathcal{G} c_{ix} - \frac{\rho v_y}{y} \right), \quad (3.19)$$

where \mathcal{G} is a position and time independent parameter for the forcing magnitude and where w_i takes on the usual D2Q9 values, section 2.5.2, page 71. With this choice for $h_i^{(1)}$, the RHS of equation 3.18 takes the desired form:

$$\sum_i h_i^{(1)} = \sum_i w_i \left(\mathcal{G} c_{ix} - \frac{\rho v_y}{y} \right) = \mathcal{G} \sum_i w_i c_{ix} - \frac{\rho v_y}{y} \sum_i w_i = -\frac{\rho v_y}{y}. \quad (3.20)$$

Proceeding to $\mathcal{O}(\epsilon^2)$ now. Summing on i in equation 3.11 the expression

$$\tau \left(1 - \frac{1}{2\tau}\right) \left[\partial_{t0} \sum_i h_i^{(1)} + \partial_\gamma \sum_i h_i^{(1)} c_{i\gamma} \right] - \sum_i h_i^{(2)} \quad (3.21)$$

is obtained, in the LHS of the lattice continuity equation. This, with the target dynamics

in view, should vanish. Using equations 3.19 and 3.20 therefore leads to

$$\sum_i h_i^{(2)} = \left(\tau - \frac{1}{2} \right) \left[\partial_{t_0} \sum_i w_i \left(\mathcal{G} c_{ix} - \frac{\rho v_y}{y} \right) + \partial_\gamma \sum_i w_i \left(\mathcal{G} c_{ix} - \frac{\rho v_y}{y} \right) c_{i\gamma} \right], \quad (3.22)$$

which, since \mathcal{G} is constant in space and time, becomes

$$\sum_i h_i^{(2)} = \left(\tau - \frac{1}{2} \right) \left[\partial_{t_0} \sum_i \left(-w_i \frac{\rho v_y}{y} \right) + 0 \right]. \quad (3.23)$$

Hence a condition on the $h_i^{(2)}$ arises:

$$\sum_i h_i^{(2)} = \left(\frac{1}{2} - \tau \right) \frac{1}{y} \partial_{t_0} \rho v_y, \quad (3.24)$$

further consideration of which is postponed to the next section.

3.2.2 Lattice momentum equation and $h_i^{(2)}$

With an appropriately modified continuity equation secured, attention now falls upon the lattice Euler equation. This should gain a term at $\mathcal{O}(\epsilon)$ by the choice of $h_i^{(1)}$ (equation 3.19). To see this, equation 3.9 is multiplied by \mathbf{c}_i and summed over i , yielding:

$$\partial_{t_0} \rho v_\alpha + \partial_\beta \Pi_{\alpha\beta}^{(0)} = \sum_i h_i^{(1)} c_{i\alpha}, \quad (3.25)$$

which, by invoking the previous selection of $h_i^{(1)}$, namely equation 3.19, gives

$$\partial_{t_0} \rho v_\alpha + \partial_\beta \Pi_{\alpha\beta}^{(0)} = \mathcal{G} \sum_i w_i c_{ix} c_{i\alpha} - \frac{\rho v_y}{y} \sum_i w_i c_{i\alpha} = \frac{1}{3} \mathcal{G} \delta_{\alpha x}. \quad (3.26)$$

Here, the standard D2Q9 result: $\sum_i w_i c_{i\alpha} c_{i\beta} = \delta_{\alpha\beta}/3$; and the fact that first order moments of the lattice link set are zero, have been employed.

Clearly the lattice fluid's Euler equation has gained a body force density term. Such is widely used to mimic the effect of a *spatially uniform* body force (pressure gradient) impressed throughout the lattice fluid:

$$\begin{aligned} \partial_{t_0} \rho v_x &= -\partial_\beta \Pi_{x\beta}^{(0)} + \frac{1}{3} \mathcal{G}, \quad \text{for } \alpha = x \\ \partial_{t_0} \rho v_y &= -\partial_\beta \Pi_{y\beta}^{(0)}, \quad \text{for } \alpha = y \end{aligned} \quad (3.27)$$

wherein, for $\alpha = y$, the \mathcal{G} term has no effect reflecting conditions of the chosen geometry.

The equilibrium momentum flux tensor, however:

$$\Pi_{\alpha\beta}^{(0)} \equiv -\frac{1}{3}\rho\delta_{\alpha\beta} + \rho v_\alpha v_\beta \quad (3.28)$$

still contains pressure gradient terms $\rho\delta_{\alpha\beta}/3$, it is emphasised. Using the latter of equations 3.27 then, condition 3.24 on the $h_i^{(2)}$ can be recast as follows

$$\sum_i h_i^{(2)} = \left(\frac{1}{2} - \tau\right) \frac{1}{y} \partial_{t0} \rho v_y = -\left(\frac{1}{2} - \tau\right) \frac{1}{y} \partial_\beta \Pi_{y\beta}^{(0)} \quad (3.29)$$

and substituting for $\Pi_{\alpha\beta}^{(0)}$, equation 3.28, this becomes:

$$\begin{aligned} \sum_i h_i^{(2)} &= \left(\tau - \frac{1}{2}\right) \frac{1}{y} \partial_\beta \left(-\frac{1}{3}\rho\delta_{y\beta} + \rho v_\beta v_y\right) \\ &= \left(\tau - \frac{1}{2}\right) \frac{1}{y} \left[-\frac{1}{3}\partial_y \rho + \partial_\beta \rho v_\beta v_y\right] \\ &= \frac{3\nu(\tau)}{y} \left[-\frac{1}{3}\partial_y \rho + \partial_\beta \rho v_\beta v_y\right], \end{aligned} \quad (3.30)$$

the last line of which invokes the standard LB identification between kinematic viscosity and relaxation parameter: $\nu(\tau) = (2\tau - 1)/6$, see section 2.5.2 and [112].

Considering $\mathcal{O}(\epsilon^2)$ now, equation 3.11 is multiplied by \mathbf{c}_i and summed over i to obtain the new terms generated by the forcing. Since the usual Navier–Stokes macroscopic terms arise in this process, it is possible, since they equate, to cancel them out leaving only new terms; these may then be grouped in the RHS of the lattice Navier–Stokes equation:

$$\sum_i h_i^{(2)} c_{i\alpha} - \tau \left(1 - \frac{1}{2\tau}\right) \left[\partial_{t0} \sum_i h_i^{(1)} c_{i\alpha} + \partial_\gamma \sum_i h_i^{(1)} c_{i\alpha} c_{i\gamma}\right]. \quad (3.31)$$

Simplification of this expression is possible through the time independence:

$$\partial_{t0} \sum_i h_i^{(1)} c_{i\alpha} = \partial_{t0} (\mathcal{G}\delta_{\alpha x}/3) = 0. \quad (3.32)$$

Also, expression 3.19 is now used for $h_i^{(1)}$, the first term of which is seen to be zero because it is an odd moment of the lattice basis. This permits the following reduction:

$$\begin{aligned} &= \sum_i h_i^{(2)} c_{i\alpha} - \left(\tau - \frac{1}{2}\right) \left[0 + 0 + \partial_\gamma \left(-\frac{\rho v_y}{y}\right) \sum_i w_i c_{i\alpha} c_{i\gamma}\right] \\ &= \sum_i h_i^{(2)} c_{i\alpha} - \frac{1}{3} \left(\tau - \frac{1}{2}\right) \partial_\alpha \left(-\frac{\rho v_y}{y}\right), \end{aligned} \quad (3.33)$$

where again, the identity $\sum_i w_i c_{i\alpha} c_{i\beta} = \delta_{\alpha\beta}/3$ (a standard D2Q9 result) has been employed. Finally, the usual identification of lattice fluid (kinematic) viscosity, $\nu(\tau) = (2\tau - 1)/6$, leaves:

$$\sum_i h_i^{(2)} c_{i\alpha} + \nu(\tau) \partial_\alpha \left(\frac{\rho v_y}{y} \right). \quad (3.34)$$

This expression, 3.34, is the one required to supply additional target terms to match those in the RHS of the Navier–Stokes equation, 3.6.

Taking those terms required of the forcing strategy, as appear in the RHS of the macroscopics 3.6 and equating them to those arising as a consequence of the introduction of forcing, 3.34, provides:

$$\sum_i h_i^{(2)} c_{i\alpha} + \nu \partial_\alpha \left(\frac{\rho v_y}{y} \right) = \frac{\nu}{y} \left(\partial_y \rho v_\alpha - \frac{1}{y} \rho v_y \delta_{\alpha y} \right). \quad (3.35)$$

This must be done if the scheme is to successfully model cylindrical geometries. On rearranging, the above becomes

$$\sum_i h_i^{(2)} c_{i\alpha} = \nu \left[\frac{1}{y} \partial_y \rho v_\alpha - \frac{1}{y^2} \delta_{\alpha y} \rho v_y - \partial_\alpha \left(\frac{\rho v_y}{y} \right) \right], \quad (3.36)$$

which by the product rule, is equivalent to

$$\nu \left[\frac{1}{y} \partial_y \rho v_\alpha - \frac{1}{y^2} \delta_{\alpha y} \rho v_y - \frac{1}{y} \partial_\alpha \rho v_y - \rho v_y \partial_\alpha \frac{1}{y} \right]. \quad (3.37)$$

Simplification proceeds on noting that, for both $\alpha = x$ and y , each of terms 2 and 4 in the RHS contributes zero², leaving:

$$\sum_i h_i^{(2)} c_{i\alpha} = \nu \left[\frac{1}{y} \partial_y \rho v_\alpha - \frac{1}{y} \partial_\alpha \rho v_y \right]. \quad (3.38)$$

From equations 3.30 and 3.38 expressions for the moments of the $h_i^{(2)}$ are thus as follows

$$\sum_i h_i^{(2)} = \frac{3\nu}{y} \left[-\frac{1}{3} \partial_y \rho + \partial_\beta \rho v_\beta v_y \right], \quad (3.39)$$

$$\sum_i h_i^{(2)} c_{i\alpha} = \frac{\nu}{y} (\partial_y \rho v_\alpha - \partial_\alpha \rho v_y), \quad (3.40)$$

where, note, the RHS of the latter is equivalent to $\nu \nabla \times (\rho \mathbf{v})|_{\hat{x}/y}$.

In seeking a form for $h_i^{(2)}$ that satisfies the above two conditions simultaneously, it is

²For $\alpha = x$, terms 2 and 4 are zero: $\delta_{\alpha=xy} = 0$ and $\partial_{\alpha=x} 1/y = 0$; whereas for $\alpha = y$, term 4, $\partial_{\alpha=y} 1/y$, equals $-1/y^2$ hence canceling term 2.

apparent that their respective RHSs must both contribute on the same basis. With this in mind, and the fact that the RHSs are link independent, it is logical at first to postulate that $h_i^{(2)}$ consists of a sum of the form

$$h_i^{(2)} = k_{0i}R_0 + k_{1i}R_1, \quad (3.41)$$

where R_0 and R_1 denote RHSs of the zeroth and first order moments respectively (equations 3.39 and 3.40) and where k_{0i} and k_{1i} are undetermined constants that are probably link i dependent. For this case the essence of equations 3.39 and 3.40 can then be summarised as

$$\sum_i k_{0i} = 1 \quad , \quad \sum_i k_{1i} = 0, \quad (3.42)$$

$$\sum_i k_{0i}c_{i\alpha} = 0 \quad , \quad \sum_i k_{1i}c_{i\alpha} = 1. \quad (3.43)$$

The question then is, what (simple) constants k_{0i} and k_{1i} have these properties.

It is immediately apparent that the usual link weight factor w_i will alone suffice for k_{0i} ; its weight sums over i to unity and its first (odd) lattice moment is zero. (Any link independent coefficient may also be applied to this).

The case of k_{1i} seems ‘similar’ but is at odds with the usual w_i moment. Inspection of equation 3.40 suggests division of the RHS by $c_{i\alpha}$ factor. Avoiding this however, but noting that this would be equivalent to an odd moment, (-1^{th}), suggests an appropriate choice for k_{1i} . Obtain an odd moment in the latter of 3.42 and even in the latter of 3.43 by making $k_{1i} = c_{i\beta}$. Hence one simple and satisfactory choice of the $\mathcal{O}(\epsilon^2)$ forcing term is:

$$h_i^{(2)} = 3w_i \frac{\nu}{y} \epsilon^2 \left[\left(-\frac{1}{3} \partial_y \rho + \partial_\beta \rho v_\beta v_y \right) + (\partial_y \rho v_\beta - \partial_\beta \rho v_y) c_{i\beta} \right], \quad (3.44)$$

to which the usual β summation convention applies.

3.2.3 Résumé of axial symmetry forcing issues

In summary, to recover lattice fluid macrodynamics equivalent to pipe flow, whilst using a regular square lattice under a uniform applied pressure gradient, forcing terms (equation 3.8) are required to be of the form:

$$\begin{aligned} h_i^{(1)} &= w_i \left(\mathcal{G}c_{ix} - \frac{\rho v_y}{y} \right), \\ h_i^{(2)} &= w_i \frac{3\nu}{y} \left(-\partial_y \frac{\rho}{3} + \partial_x \rho v_x v_y + \partial_y \rho v_y v_y + \partial_y \rho v_x c_{ix} - \partial_x \rho v_y c_{ix} \right). \end{aligned} \quad (3.45)$$

This scheme incorporates terms, $w_i \mathcal{G}_{c_{ix}}$, representing the commonly applied body forcing condition.

For purposes of performing the simulations described in this section, the gradient terms in 3.45 are evaluated using discrete difference approximations, evaluated from lattice macroscopics using second order accurate expressions. Note however, that stresses and higher order fluxes, such as appear in 3.45, can be computed more in the spirit of lattice Boltzmann method and without recourse to such finite differences. This is possible using appropriate higher order moments of f_i , see equation 2.116, thereby avoiding the problems of instability, dissipation and numerical inefficiency which finite difference schemes introduce.

Attention now proceeds to specific simulation details and to a presentation of the results so obtained.

3.3 Flow in a 3D geometry using a 2D grid: results

In this section, results are discussed from a test bench simulation of forced flow in an infinitely long circular pipe, driven by a uniform pressure gradient (effective body force density) parallel with the pipe axis. The intention is to correctly account for the differential in fluid properties, that occurs as one moves radially out, in the two dimensional representation, from the central axis of a three dimensional cylindrically symmetric system. The general idea is reviewed in section 2.6.1, pages 85 and 89 of this report and earlier in this chapter, 3.1.

Figure 3.1 is a schematic of the computational domain used to simulate the configuration. Discrete lattice coordinates will here be represented with integers X and Y ; X represents distance along the pipe in the direction of flow and Y represents cross channel distance. All the results reported relate to eventual steady state velocity distribution on the lattice. The lattice is initialised globally with node density $\rho = 1.0$. Convergence to steady state was checked by monitoring the time development of the lattice velocity field residuals, as will be seen.

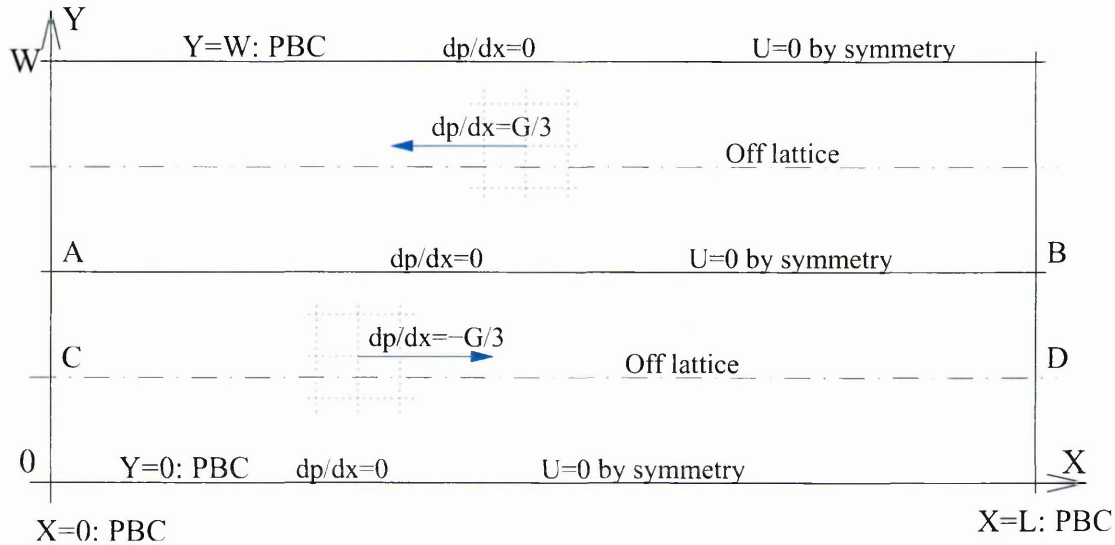


Figure 3.1: Schematic of the test bench implementation of uniform contra-forced pipe flow, sections 2.6.3 and 2.6.4. Blue arrows indicate forcing: below (above) line AB the lattice fluid is body forced toward the right (left). Note that negative dp/dx gives rise to positive flow. Duct axes (broken lines) should be located off lattice, which can be achieved by appropriate positioning of the periodic boundaries, that prevail between left and right, and between top and bottom, of the lattice.

To bound the flow in the X direction, periodic boundaries were installed along vertical lines $X = 0$ and $X = L$. The issue of ‘horizontal’ boundaries shall be returned to shortly. Flow was forced (see below) parallel to the X direction. Thus the overall algorithm is translationally invariant along the horizontal. Under such circumstances it is possible

to make the lattice length L conveniently small, thereby avoiding any axial lattice fluid density gradient, which might otherwise lead to compressibility error [151].

Consider the half of the simulation below the horizontal line connecting A and B . Here fluid was induced to flow in the direction from A to B by use of a positive body force constant \mathcal{G} , corresponding to an applied pressure gradient of $-\mathcal{G}/3$, $\mathcal{G} > 0$, equation 3.27. For this region of the lattice, the pipe axis is the broken line connecting C with D corresponding to $y = 0$. Since certain forcing terms in equations 3.45 refer to the reciprocal of y (distance from pipe axis), care must be exercised to avoid any singularity. Accordingly, line CD should be located off lattice, which can be achieved by appropriate positioning of the horizontal no slip lattice boundaries.

The general problem of terminating an LB lattice, so as to impose a no slip condition on the lattice fluid velocity field, is unsolved. However, a number of methods that closely mimic the effect of friction on the flow have been devised; for a discussion see section 2.6 and references therein. Here the symmetry of this particular problem can be exploited, by ‘contra-forcing’; again see sections 2.6.3 and 2.6.4. In fact periodic boundary conditions were also applied, along the lines $Y = 0$ and $Y = W$, with the upper layer of lattice fluid (above the line connecting A with B) forced in reverse, by use of a subtracted body force constant $-\mathcal{G}$, for $Y > W/2$, corresponding to positive pressure gradient $-3dp/dx$ ($\mathcal{G} > 0$ remember). This of course, has the effect of forcing the top fluid layer toward the left. Where the two lattice fluids contact, in the lines $Y = 0$ (equivalent to the periodic image line $Y = W$) and $Y = W/2$, a zero of velocity (no slip boundary) must, on general grounds, occur. Two opposing parabolic flow profiles are thus established for a range of values of LBGK collision parameter (lattice fluid kinematic viscosity).

Figure 3.2 shows the variation of axial velocity v_x , with position Y , in the lower half of the simulation lattice (below line AB in figure 3.1). As a result of the particular flow forcing strategy and lattice closure, the resulting flow profile is exactly parabolic, with on lattice zeros of velocity in the lines $Y = 0$ and $Y = W/2$.

The Darcy–Weisbach friction factor, equivalent to Blasius’, defined through the usual relationship:

$$\frac{dP}{dx} = f_{\text{DW}} \frac{1}{\varnothing_h} \frac{1}{2} \rho V^2. \quad (3.46)$$

where \varnothing_h is the hydraulic diameter (the physical diameter \varnothing for a circular pipe) and V the average velocity (half the peak velocity), was measured over the full range of LBGK collision parameter $1/\tau$. Figure 3.3 shows f_{DW} expressed as a ratio with F , the analytical value for a fully developed laminar pipe flow:

$$F = \frac{64}{Re}, \quad Re = \frac{Vd}{\nu}. \quad (3.47)$$

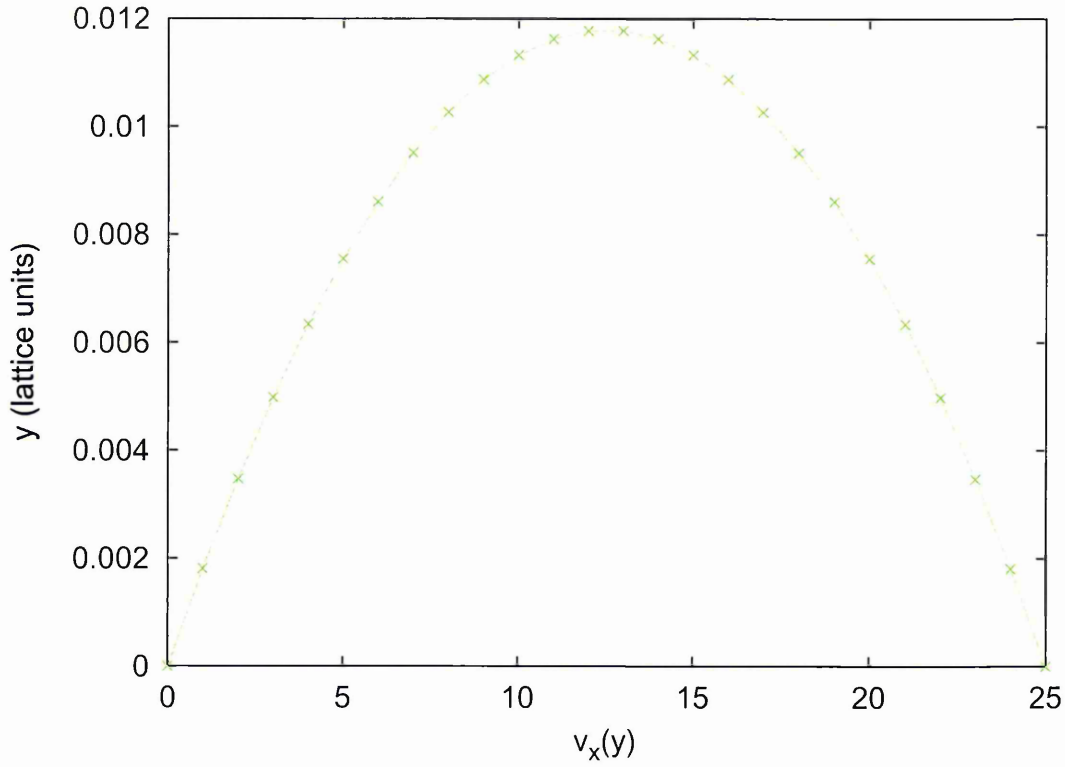


Figure 3.2: Variation of steady state axial velocity $v_x(Y)$ across the lower half of the simulation lattice (below line AB in figure 1). As a result of the particular forcing strategy employed the resulting flow profile is exactly parabolic with on lattice zeros of velocity in the lines $Y = 0$ and $Y = W/2$.

The data presented in figure 3.3 correspond to a Reynolds number $Re = 10$, which was kept constant by varying the simulation pressure gradient parameter \mathcal{G} in accordance with the relationship:

$$\mathcal{G} = \frac{64}{3} Re \frac{\rho(2 - \omega)^2}{W^3 \omega^2} \quad (3.48)$$

derived for pipe flow [81], using equation 3.27 and the fact that the simulated pipe radius is $W/4$ (figure 3.1).

From equation 3.48 it is noteworthy that, whilst the lattice width W determines the pipe diameter, it also, for constant Re , effectively determines the spatial resolution of the simulation.

The data presented in figure 3.3 are in three series: (I) for $0.3 \leq 1/\tau < 2.0$, $W = 50$ (+ points), (II) for $0.2 \leq 1/\tau \leq 0.3$ with substantially increased spatial resolution, $W = 302$ (x points) and (III) $0.0 < 1/\tau \leq 0.15$, $W = 102$ (* points). The measured departure from the analytic steady state pipe flow profile, $v_{P_{th}}(\mathbf{r})$:

$$\Delta = \sum_{\mathbf{r}} |v_{P_{th}}(\mathbf{r}) - v_x(\mathbf{r})|, \quad (3.49)$$

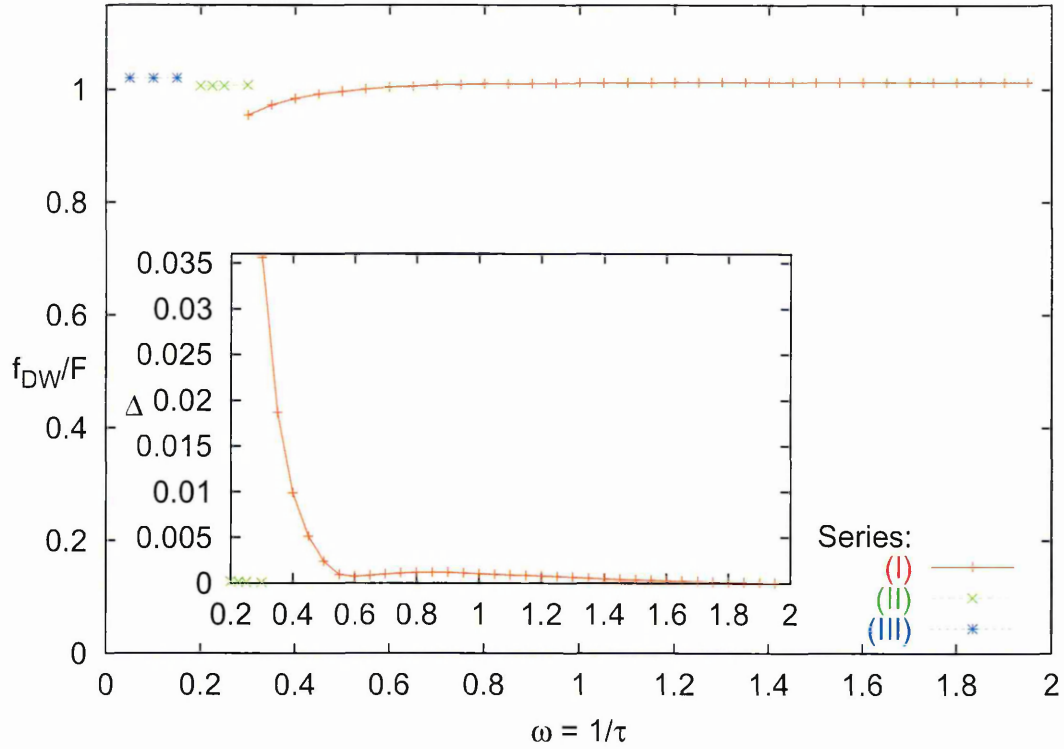


Figure 3.3: Measured value of Darcy–Weisbach friction factor expressed as a ratio with the analytic value. The data presented here is for constant Reynolds number $Re = 10$. The discontinuity in the region of $1/\tau = 0.3$ demonstrates the effect of an increase in spatial resolution between series (I) (+ points, $W = 50$) and series (II), (\times points, $W = 302$). The inset shows variation of simulation error, Δ , over the same range of $1/\tau$ as for series (I) and (II).

varies as $3 \times 10^{-5} < \Delta < 3.5 \times 10^{-2}$ over the data series (I). These data are presented in the inset to figure 3.3 over the same range of $1/\tau$ covered by series (I) and (II). However, it is clear from figure 3.3 that the increase in error as $1/\tau$ approaches the (arbitrary) value of 0.3, in series (I), can be combated by increasing the spatial resolution (value of W), as for series (II). So the accuracy of the numerical calculation (in terms of the velocity field) can be maintained at second order, even for small values of $1/\tau$, given sufficient spatial resolution. Below the value $1/\tau \approx 0.2$, an observed instability associated with the singularity of y (equations 3.45) means that the spatial resolution necessary for convergence greatly increases.

Data shown in series (III) of figure 3.3, for values of $1/\tau \leq 0.15$, were obtained using an analytic expression for the terms in equation 3.45 in our code. Note also that the convergence time, assessed in terms of time changes in the velocity field residual:

$$R = \sum_{\mathbf{r}} (v_x(\mathbf{r}, t+1) - v_x(\mathbf{r}, t))^2, \quad (3.50)$$

varies substantially over the range of data represented in figure 3.3, and also with

Reynolds number.

The factor $1/y$ which is attached to certain terms in expressions 3.45, for $h_i^{(1)}$ and $h_i^{(2)}$, is of course, peculiar to the chosen example problem of adjusting for cylindrical pipe flow, but its singularity clearly affects convergence behaviour.

In order to assess convergence time with varying spatial resolution, data were collected over a range of Reynolds number, for channels of width $W/2 = 25, 51, 101$ and 201 . In all cases, the correct laminar flow profile and friction factor were eventually obtained in good agreement with theory. The different convergence times for these checks are summarised in figure 3.4. Note that for all the data in figure 3.4 the lattice collision parameter was confined to the range $0.6 < 1/\tau < 1.85$.

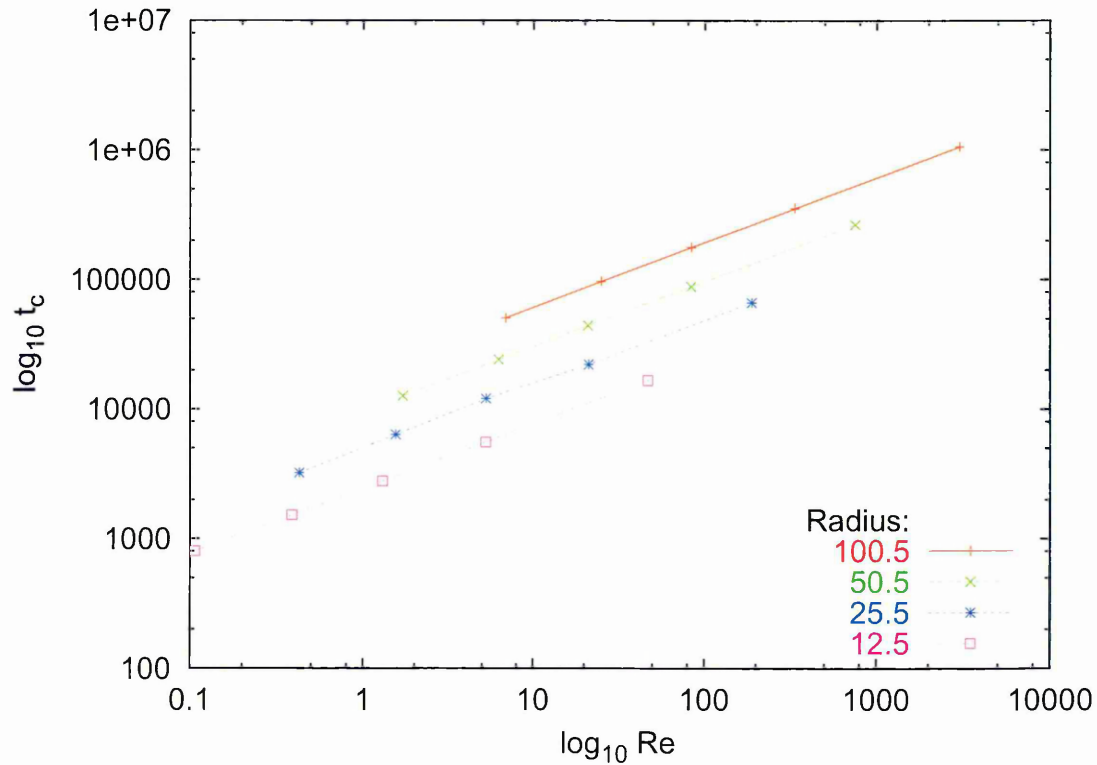


Figure 3.4: Convergence time data for four lattice sizes corresponding to channels of width, $W/2 = 25, 51, 101$ and 201 over a range of relaxation parameter, $0.6 \leq 1/\tau \leq 1.8$.

Figure 3.5 shows the convergence behaviour of the scheme in terms of the error (defined in equation 3.49) as a function of spatial resolution. The range of Reynolds numbers used in these simulations varied over the range $1 \leq Re \leq 100$ and the spatial resolution (measured by the value of W , the simulation width) over a range corresponding to channel radii $12.5 \leq R \leq 250.5$.

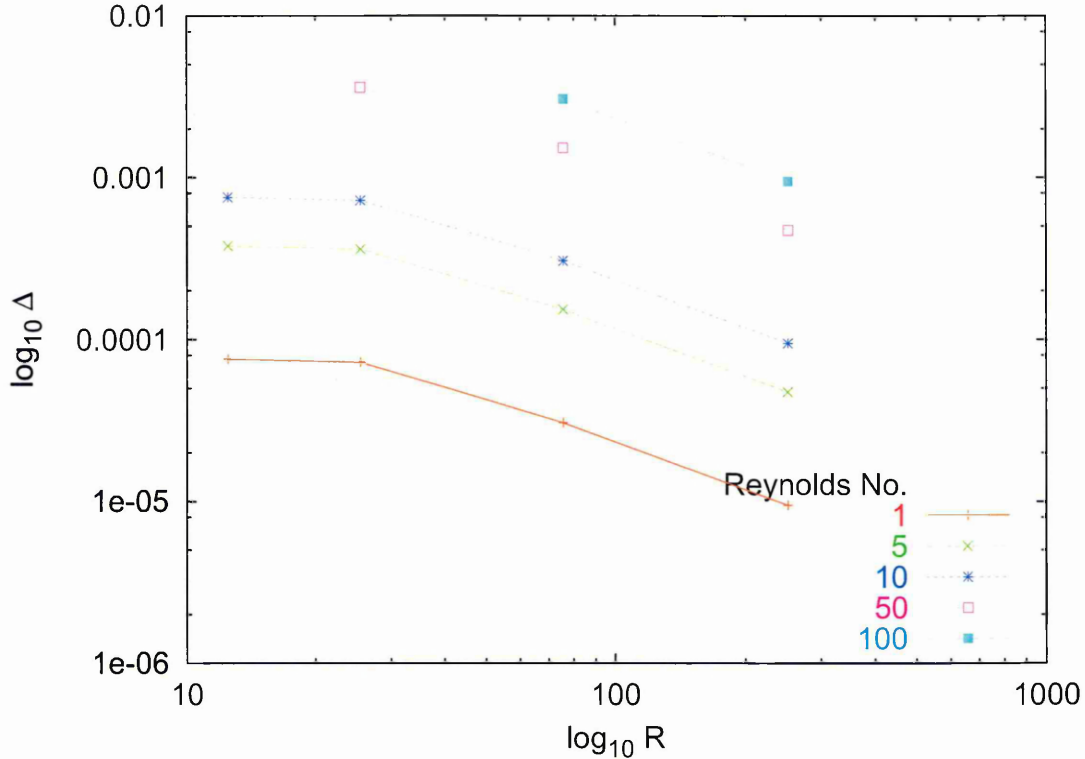


Figure 3.5: Convergence behaviour. Error, Δ , defined as departure from the analytic solution (equation 3.49), plotted as a function of spatial resolution. For the data shown here the range of Reynolds number is $1 \leq Re \leq 100$. The spatial resolution is measured by the value of $R = W/4$ (channel radius in lattice units) which varies over the range 12.5 to 250.5.

3.4 Discussion

Simulations employing the new forcing scheme demonstrate its effectiveness as is apparent from the previous section. It is in fact one of the primary results of the current work, that such a scheme has been successfully derived and implemented.

The aim is not, from a fundamental standpoint, to incorporate the effects of an external force upon the lattice fluid; rather, self-consistently to introduce extra terms in the lattice fluid's momentum equation, in this case terms characteristic of, for example, a different geometry.

It should be noted however, that any such momentum equation acceleration (body force) terms could be treated phenomenologically with the approach discussed in the next section. But, in a manner consistent with the analysis of reference [58] extended to apply to the Boltzmann equation with an acceleration term, Luo [89] has shown how external, conservative body forces can emerge from an LB scheme [89].

In the previous sections it has been shown how source terms inserted into the evolution equation can be used to adjust the final form of the lattice fluid's macrodynamics. At first sight it may seem that a forcing strategy which offers $2Q$ parameters $h_i^{(n)}$, $i = 1, \dots, Q$,

$n = 1, 2$ is flexible. However, one should sound a cautionary note. The strategy derived in section 3.2 is one example of the general considerations outlined in section 3.1.2. It is, moreover, somewhat sanitised, for in this example, the $h_i^{(1)}$ and $h_i^{(2)}$ in expressions 3.16 and 3.17 may be determined independently, and in a natural manner — the form of $h_i^{(1)}$ suggests itself and thus provides for determination of an appropriate form for $h_i^{(2)}$. This may not be possible in other applications and it may well be that, in such problems requiring more complicated source terms, constraints arise between the $h_i^{(n)}$, effectively reducing the number of independent $h_i^{(n)}$ available.

Clearly the particular forcing terms derived in section 3.2.1 and 3.2.2, against the example of pipe flow, contain gradient quantities. It may well be argued that explicit inclusion of gradients in this way is contrary to the philosophy of the lattice Boltzmann method, in that it undermines the distinction between lattice Boltzmann flow calculation and conventional finite difference Navier–Stokes solvers. However, derivative lattice Boltzmann simulations, already in the literature, rely upon forcing with gradient quantities to recover their target dynamics. Indeed, the philosophy of the approach in section 3.2 reflects the fact that forcing can be applied as a practical tool, to adjust the form of the macrodynamical equations of a lattice Boltzmann fluid. So, for such lattice Boltzmann schemes as do rely upon gradient forced macrodynamics, the way in which gradients quantities are incorporated, through the Chapman–Enskog expansion, is, hopefully, pertinent.

The strategy described in this work is envisaged as a resource for adjusting the dynamics of a *mono-phasic* lattice fluid. Whilst it can, in principle, modify the dynamics of a lattice Boltzmann scheme whatever the physical origin of the additional terms in the momentum and continuity equations (RHS of equations 3.5 and 3.6), the approach here still incorporates such terms carefully but phenomenologically. In particular, this work does not have the same fundamental basis in the full Boltzmann equation as the forcing strategies which have recently appeared [89].

The work reported in reference [89] formally addresses external acceleration terms $\mathbf{a} \cdot \nabla_{\xi} f_i$ in the LHS of a generalised Boltzmann equation and adopts a satisfying *a priori* approach to the problem of forcing lattice fluid flow. Probably it would be contrary to the philosophy of the work, but the analysis of reference [89] can obtain the effective forcing for the present problem of cylindrical pipe flow as follows.

In the notation of [89], corrections to the lattice continuity (momentum) equation in the RHS of equation 3.5 are obtained by generalising constraint equation 12a (12b) of reference [89] to:

$$\int d\xi \mathbf{a} \cdot \nabla_{\xi} f = F_0, \quad (3.51)$$

$$\int d\xi \xi \mathbf{a} \cdot \nabla_{\xi} f = \mathbf{F}_1, \quad (3.52)$$

with:

$$\begin{aligned} F_0 &= -\frac{1}{y} \rho v_y, \\ F_{1\alpha} &= -\frac{\nu}{y} \partial_y \rho v_{\alpha} - \frac{\nu \rho v_y}{y^2} \delta_{\alpha y}. \end{aligned} \quad (3.53)$$

Following reference [89] then, integrations in equations 3.51 and 3.52 work through a formal discretisation of the Boltzmann equation to generate summations in the emergent LBGK scheme, expressing the presence of forcing (strictly, for present purposes, an *effective* forcing) given by

$$\mathbf{a} \cdot \nabla_{\xi} f \rho w_i (c^{(0)} + c_i^{(1)} \xi_i + c_{ij}^{(2)} \xi_i \xi_j + \dots). \quad (3.54)$$

The coefficients $c^{(n)}$ depend on hydrodynamic variables and their gradients. By substituting the truncated series expansion of $\mathbf{a} \cdot \nabla_{\xi} f$ into the constraints of equations 3.51 and 3.52, one can obtain the coefficients $c^{(n)}$ up to certain order in \mathbf{u} consistent with the Chapman–Enskog analysis. It can be shown that the above analysis leads to the same results as were obtained here.

3.5 Synopsis and Conclusions

In this chapter, a forcing strategy is applied to the microscopic evolution equation of a lattice Boltzmann fluid. It is shown to correctly modify the emergent macroscopic equations toward a particular target form; specifically to recover cylindrical polar form of the macroscopic hydrodynamic equations. The reader is referred to the paper [52]. The work is demonstrably a practical realisation of a general theoretic result on forcing in the LB published earlier, [89].

For purposes of deriving the model’s macrodynamics (within the usual Chapman–Enskog expansion) the strategy treats any forcing terms (source terms) which are added into the microdynamical evolution equation in a manner consistent with the momentum densities. Forcing terms treated in this way occur, as it were, ‘recursively’ in the macrodynamics (see equations 3.16 and 3.17) and in consequence their inclusion into a lattice Boltzmann scheme is somewhat more involved than one might naively imagine. For the chosen application, in which there are no constraints on the forcing problem, it is straightforward systematically to determine a set of forcing terms.

Whilst the lattice Bhatnagar–Gross–Krook scheme is employed here and, for definite-

ness, the case of flow in a circular cross section duct is considered, the method can clearly generalise to any intentionally novel lattice Boltzmann scheme. In this respect the present work should be of interest to any worker attempting to adjust the macrodynamical equations of a lattice Boltzmann scheme; for example to applications in nematodynamics or viscoelasticity. In cases such as these however, any constraints on the forcing problem will reduce the number of independent forcing terms, with the possibility of rendering the proposed scheme unworkable.

Chapter 4

An improved lattice closure

A simple and adaptable closure algorithm for the edge nodes of a lattice Boltzmann fluid simulation space is developed. Its rules are designed to ensure that observed macroscopics are correct to second order at every instant. That is, to maintain local mass, to produce a specified fluid velocity and, crucially, the correct strain rate tensor at the resulting fluid boundary. Further, the algorithm models the fluid on boundary nodes to the same accuracy as on the bulk nodes and in a demonstrably equivalent manner, requiring only a specified boundary velocity; the fluid boundary pressure emerging.

Illustrative results for steady and time dependent flows, together with outline generalisations are presented in section 4.3. Following this, in section 4.4, space is devoted to an analysis and discussion of the efficacy and rectitude of the scheme, as compared to other similarly targeted strategies.

4.1 Improved lattice closure scheme: Introductory remarks

Accurate representation of the boundary is as essential and complicated in lattice Boltzmann simulations as it is in any other branch of computational fluid dynamics. If a distinction is drawn, between the two primary sub-sectors of any simulation domain (the bulk and the boundaries) and an investigation undertaken into the relative effect of each on defining the overall qualities and character of the solution, the significance of the boundaries will be apparent. The simulation domain boundary, in effect, ‘specifies’ the solution.

This may be obvious to one well versed in the extraction of solutions to problems posed mathematically: there, in the first instance, a *general* solution is obtained, from which a specific solution can only be selected by invoking an initial condition (IC). Boundary conditions (BCs) take an equivalent role as IC, but in specification of the original general solution.

So accurate implementation of boundary conditions is critical in simulations. Any seemingly minor errors in BC implementation leads to unpredictable, erroneous or widely variable results. During the process of developing a working code for the various simulations encapsulated in this work, numerous technical problems of this type were encountered. In this chapter a novel means to tackle such problems is presented and an attempt made to demonstrate the efficacy of the scheme in various scenarios. Later, in chapter 5, the scheme is utilised in earnest, in an otherwise impossible implementation of the wall layer in simulations of turbulent channel flow.

Particular problems encountered in simulations depend upon specific geometries of the

LB simulation lattice, the particular LB algorithm and the type of boundary required. In the literature therefore, a number of methods for closing a simulation lattice have been proposed, from which emerge various levels of effectiveness in bounding the lattice fluid. These are briefly discussed in the following paragraphs, to provide a context for discussions. After that, the focus moves to a detailed exposition of the method proposed here.

4.1.1 Existing LB closure schemes; a brief review

In application, the simplest closure strategy is the device of *equilibrium forcing*, which involves persistently over-writing LB boundary nodes with the appropriate equilibrium momentum density distribution. Whilst robust, this method at its simplest, is of first order accuracy. Again straightforward and robust, but only first order accurate, is the widely used *bounce-back* rule (see e.g. White, Halliday and Care [151]). Bounce-back enforces an equilibrium distribution function different from that of the core (bulk) scheme, resulting in a small slip velocity which varies with the value of the LB collision parameter [159]. These first order closure strategies are not designed to be correct at every instant but some of their other idiosyncrasies are understood. For example bounce-back has been carefully evaluated at steady state by a number of workers (e.g. [46,100]) and He, Zou *et al.* have shown how it is possible analytically to predict *boundary slip velocities* [59].

Higher order accuracy LB boundary algorithms involve, amongst other things: the ‘modified’ bounce back, of Ziegler [157]; the introduction of a counter slip velocity, by Inamuro *et al.* [70]; and second order bounce back of Kim, [72]. Skordos [124] has solved the problem of boundary closure by deriving auxiliary partial differential equations which may be solved for lattice boundary information.

Various verifiably *second order accurate* schemes have now been suggested, each with diverse origins and for differing lattice types. See for example Noble *et al.* [100] where the hexagonal FHP case is considered. Regarding the D2Q9 lattice specifically, there are two main schemes: Chen *et al.* [26] and Zou & He [159].

Chen *et al.* [26] carry out a simple link by link extrapolation of the density field, to arrive at values for densities on an augmented set of nodes, inserted one link ‘off lattice’. These are then used for generation of densities propagating onto lattice under the streaming operator.

Zou & He [159] employ a bounce back of the non-equilibrium part of the density distribution at the wall, thus providing information for the reconstruction of the set of f_i to be consistent with the BC constraints at the wall, namely the velocity vector.

Both approaches: Noble *et al.* and Chen *et al.*, achieve good second order space convergence at the wall, as has been demonstrated analytically in He *et al.* [59]. Zou & He demonstrate second order behaviour for the D2Q9 case separately.

With specific reference to this work: a novel scheme for implementing second order BC closure which ensures a correct and on lattice wall velocity condition, correct implementation of gradient information and ‘proper’ mass balance is proposed. At heart the work turns out to be similar to an earlier work of Ginzbourg and d’Humières [49], which is possibly the most overlooked and most general approach to simulation lattice closure. The locally second-order boundary method (LSOB) presented there, is more general and a little opaque to say the least. The discussion shall return to this in section 4.4, where differences between the two will be indicated. Before that, next, the scheme itself is developed and described.

4.2 Six equation system for lattice closure

Fluid pressure and velocity both emerge as solution to the Navier–Stokes equation upon, as minimum, specification of Dirichlet boundary conditions on fluid velocity. Such boundary information alone is sufficient to close a particular solution of the governing equations.

For LB simulations, the equivalent scenario consists of specifying appropriate boundary distribution functions. However, no systematic means is yet available for the general transcription of fluid dynamical BCs into their distributional counterparts, the LB method is not well developed enough. This necessitates implementation of other more ad hoc means.

The problem of terminating a 2D LB lattice resides in the fact that a given lattice fluid boundary node velocity provides only two conditions on moments of the f_i s (through equations 2.99) whilst there may be several unknown distribution components f_i . In information terms, the problem manifests itself as a lack of propagation mapping onto a certain set of wall node density components and their subsequent non-specification.

In general, it is easy to set values for these unknown lattice densities which merely conform to any specific Dirichlet BC, say

$$\mathbf{v}(\mathbf{x}, t)|_{\mathbf{x}^+} = \mathbf{u}_0(\mathbf{x}^+, t), \quad (4.1)$$

where \mathbf{x}^+ denotes points on the fluid domain boundary and $\mathbf{u}_0(\mathbf{x}^+, t)$ is a specified boundary velocity function. It is also relatively easy to ensure all mass is accounted for at such boundaries by implementing a mass balanced algorithm. Overall accuracy of the wall distribution, however, is not so easily implemented and the more hastily constructed closures introduce serious and persistent errors. Additional inconsistencies compound the problem, as wall nodes are not treated in an equivalent way as bulk nodes, especially in that they receive no collision. These matters must be addressed by any scheme intended to improve lattice closure.

4.2.1 Alternative closure scheme; conception and introduction

In attempting to make a wall node ‘like’ a bulk node, modifications to collision treatment at the wall were investigated in this work. It was found that traditional Boltzmann studies attempt to determine expressions or rules to dictate or describe a separate ‘wall (velocity) distribution’. Various more or less heuristic ideas have been proposed to develop this. In one, [18] pp 105-, molecules impinging on the wall are assumed to impart all of their kinetic energy in a process of adsorption, onto, or indeed into, the wall. This is followed by a ‘restitution’ process, whereby particles are returned to the bulk. When returned

in this way a random distribution, for the component of velocity parallel to the wall, is imparted. One characteristic of this process is that, in essence, fluid *at* the wall obeys the traditionally accepted no slip condition. Although *individual* particles do *not* generally conserve momentum in the process, nor ensure zero wall velocity, en mass they do. Another characteristic of this process is that to some extent it accounts for the fact that the wall itself cannot realistically be considered flat.

Such thinking encourages the idea of an adsorbed reservoir of fluid at the wall. On adapting the idea to the lattice Boltzmann formulation, it is found that the notion of reservoir is conveniently in keeping with the desire to give wall nodes attributes of the bulk. Further thought suggests the reservoir might consist of a zone of fluid just outside of the node centre, which is equivalent to removing the edge quality of the node.

Accordingly, it is henceforth proposed that in the new scheme, a designated boundary node lies infinitesimally *within* the lattice fluid and is supposed to be fully occupied by fluid moving at exactly the velocity specified of the wall itself. Moreover, the momentum densities, f_i , which comprise such a boundary, shall be constructed by requiring that they evolve according to rules equivalent to those operating on bulk nodes.

The suggestion that the wall node undergo a collision step, equivalent to that for the bulk, hints at the concluding part of the scheme. With respect to lattice evolution, collision is the step in which information and properties of the individual links (velocities) of the lattice mixes, or is allowed to combine. The inter-link movement of information occurs via the information content of the equilibrium distribution function, in that the non-equilibrium portion of the local link densities are ‘relaxed’ toward respective local equilibrium values. In that regard, collision operates on shear information of the node and suggests imposing a shear condition as a means to further specify unknown wall densities. This is what is proposed in the rest of the current chapter.

The idea of constructing the unknown momentum densities f_i by separately evaluating the individual contributions in the Chapman–Enskog expansion 2.104 is, apparently, used by Ginzbourg and d’Humières [49]. They consider a linearised lattice Boltzmann equation model, with flat or inclined Dirichlet boundaries, showing how and under what circumstances the first and second order terms $f_i^{(1)}$ and $f_i^{(2)}$ may be evaluated from a set of first and second order velocity derivatives.

By contrast here, a less general case is targeted in a more direct and practical way. The approach assigns values for equilibrium $f_i^{(0)}$ and non-equilibrium $f_i^{(1)}$ density contributions separately and, crucially, by differing means. This is done in such a way as to ensure consistency with BCs at the level of velocity field for one set, but also to leave unsolved a set for which other rules may be applied; primarily an unsolved set is cho-

sen which is soluble in a way consistent with the instantaneous local boundary stress environment.

The focus now turns to a detailed analysis of such a scheme and to its implementation. The analysis is made specific by arbitrarily concentrating on a ‘top’ boundary node; obviously, generalisation to other nodes, for purposes of final implementation, can be effected by simple rearrangement (transformation) of link references.

4.2.2 Lattice closure algorithm

Figure 4.1 represents the ‘top’, $y = N_y$ boundary site, for the D2Q9 lattice. The dotted line shows the supposed extent of the lattice fluid, so the node is now ‘bulk’ in that it is surrounded (albeit infinitesimally) by fluid and therefore undergoes a collision step. Links indexed $i = 1, 2, 3$ are ‘cut’ and the remaining links are taken to lie within the simulation domain. All the nodes other than the boundary nodes are evolved according to the standard evolution for a bulk node, equation 2.103. It therefore follows that at the end of a propagation step, a pre-collision value of lattice momentum density, f_i , exists on the boundary node shown, for all links except $i = 5, 6, 7$ (indicated by circles as opposed to arrows).

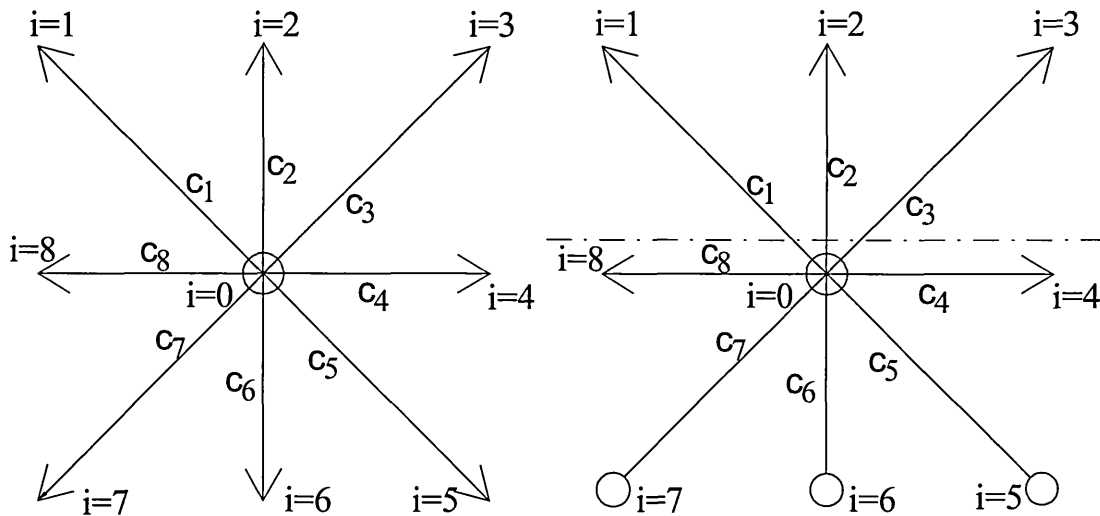


Figure 4.1: Schematic of a boundary node on the top wall, immediately prior to the collision step. Here the wall location is denoted by the dashed line, which makes the node ‘infinitesimally wet’. Propagated data is denoted by arrowheads, unknown link information (lack of data) is denoted by the open circles on links. The links are numbered as referred to in the text and link velocity vectors are numbered accordingly.

To produce a closure algorithm which recovers velocities and velocity gradients which are correct at very short time scales, whilst allowing the boundary density (pressure) to emerge from local information only, thus preserving an appropriate coupling between the

boundary nodes and the bulk, it is necessary to work with more than the three unknown densities f_5 , f_6 and f_7 .

Separate contributions to the f_i , where note, $f_i = f_i^{(0)} + f_i^{(1)} + f_i^{(2)} \dots$, the equilibrium contribution being denoted $f_i^{(0)}$, may be used for separate tasks in this regard. The $f_i^{(0)}$, calculated using the equilibrium distribution function, equation 2.100, also need to satisfy the three equations 2.101, essentially accounting for mass balance and velocity conditions. But there are separate conditions on the $f_i^{(1)}$ if velocity *gradient* information is to be correctly accounted for. Appropriate values for the full f_i may be constructed by summation of their respective contributions if calculated consistently.

Equilibrium contribution conditions arise from the definitions and requirements of the standard LB scheme, namely equations 2.101. This is in direct analogy to usual approaches, where f_i must satisfy similar constraints of equations 2.99. The $f_i^{(1)}$ however, are not so simply addressed.

With reference to section 2.5.2 and the standard features of the LBGK scheme, it is apparent that the definition of macroscopic variables of equation 2.99, coupled with the choice of equilibrium distribution function, 2.100, which satisfies the optional model constraints of equations 2.101, means that:

$$\sum_i f_i^{(n)} \Delta_i = 0 \quad n > 0, \quad (4.2)$$

where $\Delta_i = 1, c_{ix}, c_{iy}$.

Second velocity moments of the $f_i^{(n)}$ are not necessarily zero, however. In particular, for $n = 1$, that is, the first deviation from equilibrium, the Chapman–Enskog analysis demonstrates that:

$$\Pi_{\alpha\beta}^{(1)} = \sum_i f_i^{(1)} c_{i\alpha} c_{i\beta} = -2c_s^2 \rho \tau S_{\alpha\beta}, \quad (4.3)$$

where $S_{\alpha\beta}$ is the rate of strain.

Taking the case $n = 1$ in equations 4.2 generates three summations in the $f_i^{(1)}$ (one for each value of Δ_i). Similarly, since $S_{\alpha\beta}$ is symmetric in equation 4.3, three additional summations in $f_i^{(1)}$ are generated. In all therefore, six equations constrain the $f_i^{(1)}$, giving a system of six equations in nine unknowns (4.2 for $n = 1$ and 4.3). These are central to the method described in the next section; the system is exemplified for the top boundary in equation 4.7.

Accordingly, construction of second order correct f_i , is achieved by determining the value of the $f_i^{(1)}$ on a *chosen* set of six links at a boundary node (not just links $i = 5, 6, 7$) and forming the sum $f_i = f_i^{(0)} + f_i^{(1)}$. The remaining three $f_i^{(1)}$ are determined by other means.

The pre-collision boundary node densities thus constructed may then be collided and propagated in the usual way. This boundary node evolution thus involves the collision of second order accurate f_i , which are consistent with the target boundary velocity *and* the implicit wall stress.

In summary then, this boundary scheme has the following principal steps:

1. Determine the wall node density, $\rho(\mathbf{x}^+, t)$, and hence the equilibrium momentum density distribution $f_i^{(0)}$, $i = 0 \dots 8$ corresponding to the chosen boundary velocity, using 2.100, for all LBE schemes, $f_i^{(0)}$ is a function of velocity and density alone, note.
2. Construct the appropriate pre-collision $f_i^{(1)}$ to recover the measured boundary node strain rates. It is actually necessary to determine at least six of the pre-collision $f_i^{(1)}$ (see below) in order to respect all the necessary conditions on the $f_i^{(1)}$. Three (almost) arbitrarily chosen are calculated the usual way.
3. Collide and propagate the boundary sites according to equation 2.103

Steps 1 to 3 above are now detailed. In step (1), the problem in determining the node density ρ is that the momentum densities, f_i , in the directions $i = 5, 6, 7$ are each unknown. However, expression for their sum can be obtained by considering the y -momentum, using 2.99:

$$f'_1 + f'_2 + f'_3 - f_5 - f_6 - f_7 = \rho u_{0y} \quad (4.4)$$

where u_{0y} is the known target wall velocity¹.

The target density at the site can likewise be expressed as a sum of known and unknown momentum densities:

$$f'_0 + f'_1 + f'_2 + f'_3 + f'_4 + f_5 + f_6 + f_7 + f'_8 = \rho. \quad (4.5)$$

Now, it is possible to eliminate the term $(f_5 + f_6 + f_7)$ in the unknown densities between 4.4 and 4.5 to obtain an expression for ρ in terms of the *known* momentum densities:

$$\rho = \frac{1}{1 - u_{0y}} [f'_0 + f'_4 + f'_8 + 2(f'_1 + f'_2 + f'_3)]. \quad (4.6)$$

So, whilst the unspecified momentum densities f_5 , f_6 and f_7 cannot be determined individually from a given boundary velocity, their sum, and hence the node density

¹Notationally, primed momentum densities, such as f'_i , are hitherto used to indicate *known* values, streamed from adjacent lattice sites at the previous time step.

(pressure) *can*. With a value for the boundary node density, ρ , and the given boundary velocity it is then possible directly to determine $f_i^{(0)}$ on all links using equation 2.100 and the velocity condition, hence the first stage in the solution process is complete.

Step (2). To recover the required density, momentum and stress on the boundary nodes, the $f_i^{(1)}$ are chosen to recover a local rate of strain tensor, $S_{\alpha\beta}$, (see below). Hence the nine $f_i^{(1)}$, $i = 0 \dots 8$ are chosen to satisfy the six equations given by 4.2 and 4.3:

$$\begin{aligned}
 f_0^{(1)} + f_1^{(1)} + f_2^{(1)} + f_3^{(1)} + f_4^{(1)} + f_5^{(1)} + f_6^{(1)} + f_7^{(1)} + f_8^{(1)} &= 0, \\
 -f_1^{(1)} + f_3^{(1)} + f_4^{(1)} + f_5^{(1)} - f_7^{(1)} - f_8^{(1)} &= 0, \\
 f_1^{(1)} + f_2^{(1)} + f_3^{(1)} - f_5^{(1)} - f_6^{(1)} - f_7^{(1)} &= 0, \\
 f_1^{(1)} + f_3^{(1)} + f_4^{(1)} + f_5^{(1)} + f_7^{(1)} + f_8^{(1)} &= -2\rho\tau/3 S_{xx}, \\
 f_1^{(1)} + f_2^{(1)} + f_3^{(1)} + f_5^{(1)} + f_6^{(1)} + f_7^{(1)} &= -2\rho\tau/3 S_{yy}, \\
 -f_1^{(1)} + f_3^{(1)} - f_5^{(1)} + f_7^{(1)} &= -2\rho\tau/3 S_{xy}.
 \end{aligned}
 \tag{4.7}$$

Note that the velocity gradients (rate of strain tensor) which appear in the right hand side of the last three of equations 4.7 above, may be selected or determined in more than one way. The various approaches to this are discussed in in detail at a later stage, section 4.4.

The solution of the above system of simultaneous equations for the $f_i^{(1)}$, 4.7, is complicated by the fact that it is under-determined. It is necessary to select three $f_i^{(1)}$ to be *free* variables whose value may be calculated in other ways and which are used to fix the values of the remaining six *basic* variables consistently. It transpires that the choice of the free variables is restricted. This can be seen since the determinant of the matrix of coefficients of the basic variables vanishes for certain choices of the free $f_i^{(1)}$.

Column 1 of table 4.1 lists what are designated *forbidden combinations* of the free variables, the origin of which is discussed at a later stage, 4.4. These have been determined by consideration of the determinant arising from all possible choices of free variables. The table also includes a diagrammatic interpretation, relative to figure 4.1, of the forbidden sets of free variables, for purposes of illustration.

In order to solve the system of equations 4.7, three free $f_i^{(1)}$ are *chosen* which: (i) are not a forbidden set (in the sense of the discussion above) and; (ii) have accessible values corresponding to the f_i streamed onto the boundary node at the previous time step. Thus in figure 4.1, pre-collision values of $f_i^{\prime(1)} = f_i - f_i^{(0)}$, for $i = 0, 1$ and 2 are taken as free quantities, where note, the prime denotes they are designated ‘known’ by utilising the usual method. Accordingly the solution to equations 4.7, for the particular

case represented in figure 4.1 is:

$$\begin{aligned}
f_3^{(1)} &= \frac{1}{2}kS_{yy} - f_1'^{(1)} - f_2'^{(1)}, \\
f_4^{(1)} &= \frac{1}{2}kS_{xy} - kS_{yy} - \frac{1}{2}f_0'^{(1)} + 2f_1'^{(1)} + f_2'^{(1)}, \\
f_5^{(1)} &= \frac{1}{2}k(S_{xx} + S_{yy}) - \frac{1}{2}kS_{xy} + \frac{1}{2}f_0'^{(1)} - f_1'^{(1)} = -\frac{1}{2}kS_{xy} + \frac{1}{2}f_0'^{(1)} - f_1'^{(1)}, \\
f_6^{(1)} &= -kS_{xx} - f_0'^{(1)} - f_2'^{(1)}, \\
f_7^{(1)} &= \frac{1}{2}kS_{xx} + \frac{1}{2}kS_{xy} + \frac{1}{2}f_0'^{(1)} + f_1'^{(1)} + f_2'^{(1)}, \\
f_8^{(1)} &= -\frac{1}{2}kS_{xy} - \frac{1}{2}f_0'^{(1)} - 2f_1'^{(1)} - f_2'^{(1)}
\end{aligned} \tag{4.8}$$

where $k = -2c_s^2\rho\tau$.

Step (3). The pre-collision values of $f_i^{(1)}$ may now be added to $f_i^{(0)}$ as calculated in equations 4.8 above, then collided and propagated, to complete the evolution of the boundary site.

Forbidden combinations	Link representation
$f_1^{(1)}, f_2^{(1)}, f_3^{(1)}$	
$f_3^{(1)}, f_4^{(1)}, f_5^{(1)}$	
$f_5^{(1)}, f_6^{(1)}, f_7^{(1)}$	
$f_1^{(1)}, f_7^{(1)}, f_8^{(1)}$	
$f_0^{(1)}, f_4^{(1)}, f_8^{(1)}$	
$f_0^{(1)}, f_2^{(1)}, f_6^{(1)}$	
$f_0^{(1)}, f_1^{(1)}, f_5^{(1)}$	
$f_0^{(1)}, f_3^{(1)}, f_7^{(1)}$	

Table 4.1: Diagrammatic representation of the forbidden $f_i^{(1)}$ combinations.

4.3 Simulation results for improved BC scheme

The boundary algorithm described in the last section, is herein applied to the following flow configurations:

- Simple channel flow, of the kind described in section 2.6.1, page 85 and illustrated in figure 2.8 part i). The purpose here is to investigate accuracy of the solution in a well known geometry for which a simple analytical solution exists, thus facilitating quantification of accuracy.
- Impulsively driven plane Couette flow. This geometry is described in more detail in section 2.6.1, page 92. The purpose here is to investigate behaviour of the solution in an unsteady shear flow and its time dependence.

Firstly, the computational domain for a simple channel geometry was arranged as follows. Rest boundaries $U_{0x} = U_{0y} = 0$ are located at $y = 0^-$ and $y = W^+$ and the width of the channel, W , is taken arbitrarily to be 20. Periodic boundaries were applied in the x -direction and simulation flow is forced by a uniform pressure gradient in the x -direction [52]. See figure 4.2, part i). Results are compared to those arising under a bounce back closure, which are generated first.

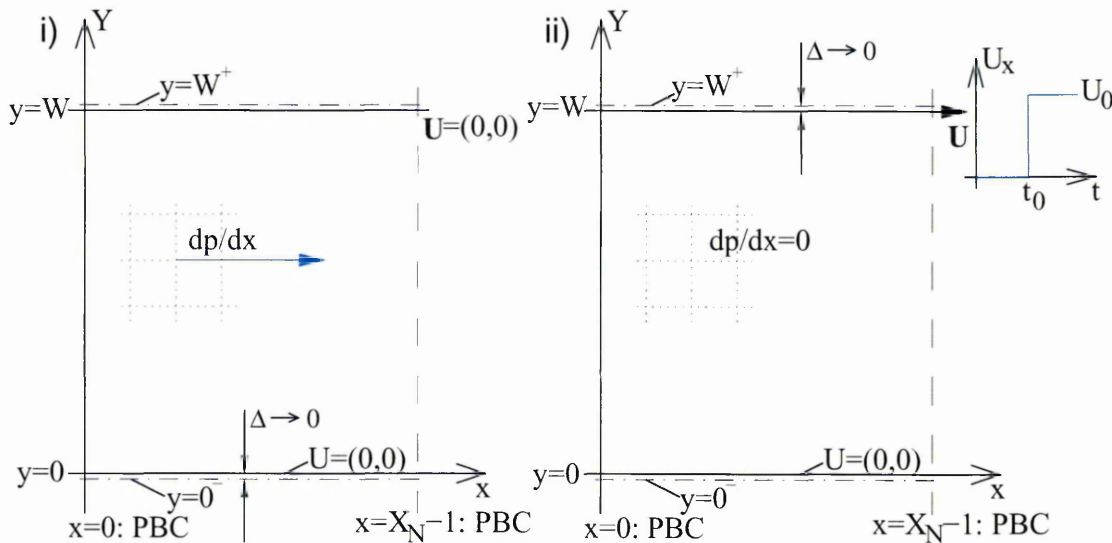


Figure 4.2: Two simulation domains to demonstrate improved boundary condition algorithm of section 4.2.2. Part i) represents simple channel flow — periodic with x , static walls along y and body forcing on all bulk nodes. Part ii) represents impulsively started Couette flow — periodic with x , static wall at $y = 0$, moving wall at $y = W$, with velocity as shown in plot; no body forcing.

Accuracy is discussed with respect to the normalised difference (error), ε_r , between the measured steady state flow profile $v_m(y)$ and the corresponding parabolic analytic

solution $v_{P_{th}}(y)$:

$$\varepsilon_r = \left| \frac{v_m(y) - v_{P_{th}}(y)}{v_{P_{th}}(y)} \right|, \quad y \neq 0. \quad (4.9)$$

Analytic solution, $v_{P_{th}}(y)$, is given by equation 2.121.

Simulations were carried out over a range of collision parameter: $1/\tau = 0.37, 0.5, 1.0, 1.5$ and 1.8 . For purposes of comparison, figure 4.3 shows the error ε_r as a function of y , as obtained using first order accurate bounce back BCs (solid lines). Figure 4.4 shows the result of an equivalent set of simulations using the new lattice closure algorithm developed in the last section (dashed lines).

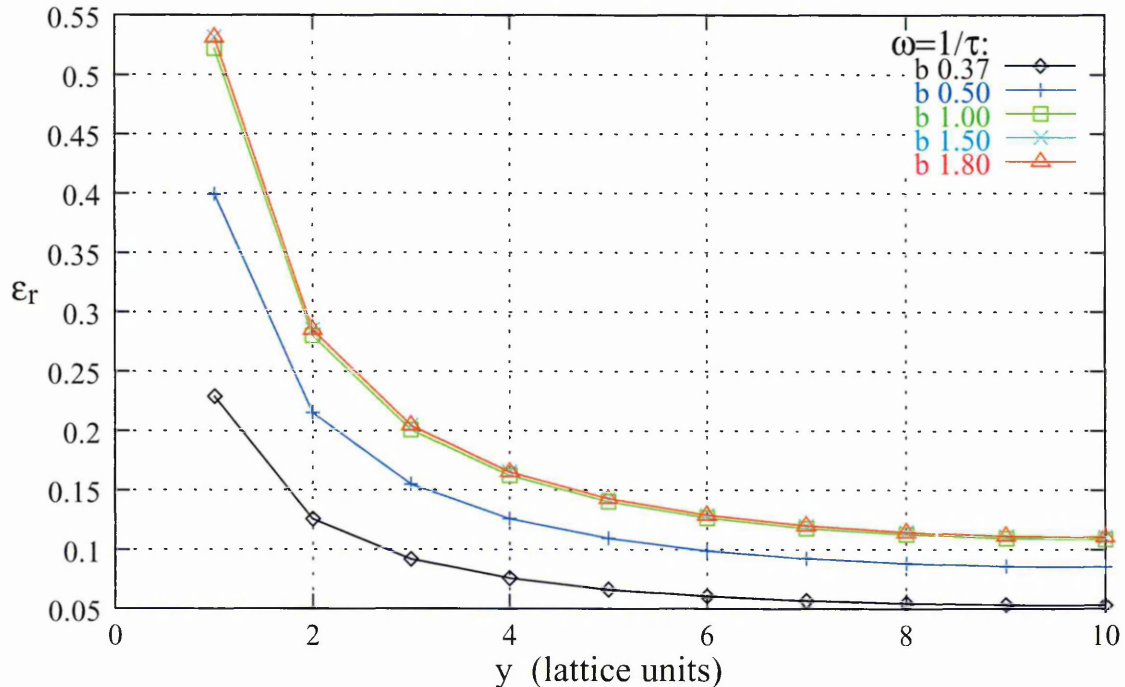


Figure 4.3: Normalised error (difference between measured and analytical parabolic profiles) at steady state, for traditional bounce back boundary conditions (solid lines). The data represents a range of collision parameter: $1/\tau = 0.37, 0.5, 1.0, 1.5$ and 1.8 denoted by \diamond , $+$, \square , \times and \triangle respectively. The duct width (resolution) was 20. Bounce back boundary accuracy varies significantly, both with Reynolds number (value of τ) and with channel position. To compare with data of new closure introduced here, shown in figure 4.4.

The data of figures 4.3 and 4.4 were obtained for constant lattice resolution, constant forcing and, therefore, variable Reynolds number. Run parameterisations are summarised in table 4.2. The Reynolds number given therein was calculated using analytic expression 2.123 for mean velocity V and the usual $Re = \ell V/\nu$, where in this case ℓ , the size parameter, is taken to be W , the channel width. Note that values for Reynolds number calculated from simulation profiles will disagree very slightly, in part due to the discrete nature of the integration (sum) to find the mean velocity V .

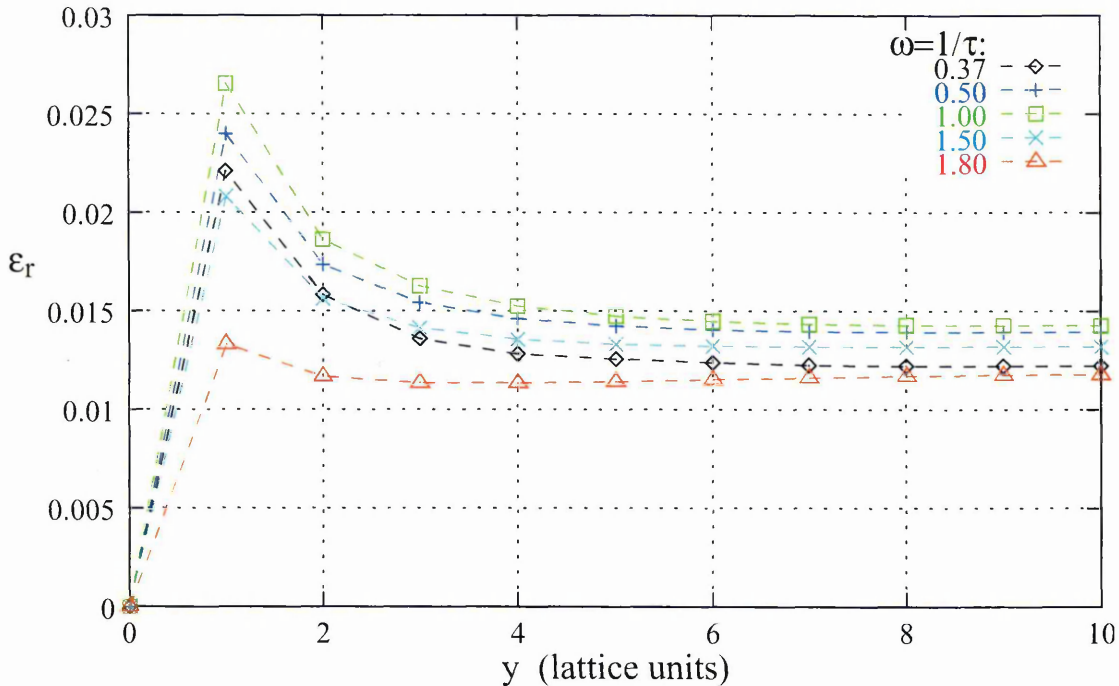


Figure 4.4: Normalised error (difference between measured and analytical parabolic profiles) at steady state, for the closure algorithm introduced here (dashed lines). Compare with data of figure 4.3, for bounce back case. Again, the duct width (resolution) was 20 and collision parameter takes the same values: $1/\tau = 0.37, 0.5, 1.0, 1.5$ and 1.8 , denoted $\diamond, +, \square, \times$ and \triangle respectively. Relative error, ε_r , associated with the new lattice closure, is at least an order of magnitude smaller compared to bounce back scheme. It also shows significantly less variation.

Symbol	ω	ν	$\mathcal{G} = 3 dp/dx$	W	Re
\diamond	0.37	0.7342	5×10^{-4}	20	2.4735
$+$	0.50	0.5000	5×10^{-4}	20	5.3334
\square	1.00	0.1667	5×10^{-4}	20	47.982
\times	1.50	0.0556	5×10^{-4}	20	431.32
\triangle	1.80	0.0185	5×10^{-4}	20	3895.9

Table 4.2: Table showing simulation parameters for the runs used to generate figures 4.3 and 4.4. Note that values for Reynolds number are calculated; see text.

Results presented in figure 4.4 clearly reveal the shortcomings of the first-order accurate technique. Foremost, as a reduction in the accuracy of the solution which increases toward the lattice boundaries; but also as a similar reduction, occurring for high Reynolds number (high relaxation parameter, ω). Accuracy of the solution obtained using the closure algorithm of section 4.2.2 is, by contrast: relatively uniform with channel position y and with Reynolds number; demonstrably second order accurate (at least an order of magnitude lower than bounce back), across the whole width of the simulation and over the range of Reynolds number; better behaved at extremes of relaxation parameter (approaching 0 or 2). Note also that *relative* error is undefined at the wall for the case of bounce back boundary conditions (it is effectively infinite because the analytic solution is

zero), whereas results for the bounding scheme of section 4.2 give, to machine accuracy, exactly zero relative error.

Results will now be considered, for simulations in the second geometry of interest here, demonstrating that the new boundary closure is instantaneously second order accurate. Refer to the second simulation domain of figure 4.2, ii).

A lattice fluid confined: in y-direction by two planes, top at $Y = W^+$ and bottom at $Y = 0^-$; and by periodic BCs in the x-direction. The fluid is initially at rest (momentum densities set to $f_i^{(0)}(\rho, \mathbf{0})$), but at some time, $t = 0^+$, the upper plate is impulsively started to velocity $\mathbf{U} = (U_0, 0)$ (in lattice units). This is done by first calculating ρ through equation 4.6, with $u_{0y} = 0$, then after substitution of this into the equilibrium distribution function, equation 2.100, with \mathbf{u} given by wall velocity \mathbf{U} , values for on propagating densities, consistent with the driven wall, may be ascribed.

For this situation the Navier–Stokes equation may be reduced to a one (spatial) dimensional diffusion equation with inhomogeneous boundary conditions. Seeking the (v_x only) solution, in the form of a steady state with separable transient, yields:

$$v_{\text{Cth}}(y, t) = \frac{U_0}{W} y + \frac{2U_0}{\pi} \sum_m \frac{(-1)^m}{m} \sin\left(\frac{m\pi y}{W}\right) \exp(-m^2 \pi^2 \bar{t}), \quad \bar{t} = \frac{\nu t}{W^2}. \quad (4.10)$$

Here \bar{t} represents a *dimensionless* time parameter allowing direct comparison between analytic and measured profiles.

Snapshots of the developing flow, across the width of the duct, are shown in figure 4.5, for both simulation and analytic data. Simulation data, denoted by symbols, are obtained for three values of discrete time, $t = 10, 100, 1000$ and for three values of collision parameter, $1/\tau = 0.6, 1.0, 1.6$, making nine sample profiles in all. This is presented alongside nine corresponding analytical solutions, generated using equation 4.10, shown as smooth lines. Pairs of data in figure 4.5 — symbols (simulation data) and lines (analytic profiles) — are characterised by the same value of \bar{t} . Parameterisations for \bar{t} are summarised in table 4.3. The data of figure 4.5 were obtained with the lattice resolution W and Reynolds number fixed, the latter being conserved by adjusting the moving plate velocity.

Clearly the agreement between the two is excellent, even down to a very small number (10) of simulation time steps. Note, moreover, that the lattice edge velocity (velocity measured on the lattice boundary nodes) is exactly the assigned velocity. This point however, is more apparent in the context of error data, discussed next.

\bar{t}	ω	ν	t	W	U_0	Re
0.00104	0.6	0.3889	10	20	4.67×10^{-4}	0.024
0.00417	1.0	0.1667	10	20	2.00×10^{-4}	0.024
0.00972	1.6	0.0417	10	20	5.00×10^{-5}	0.024
0.01042	0.6	0.3889	100	20	4.67×10^{-4}	0.024
0.04167	1.0	0.1667	100	20	2.00×10^{-4}	0.024
0.09722	1.6	0.0417	100	20	5.00×10^{-5}	0.024
0.10417	0.6	0.3889	1000	20	4.67×10^{-4}	0.024
0.41667	1.0	0.1667	1000	20	2.00×10^{-4}	0.024
0.97222	1.6	0.0417	1000	20	5.00×10^{-5}	0.024

Table 4.3: Table showing simulation parameters for the runs presented in figures 4.5 and 4.6. Dimensionless time, \bar{t} , is calculated according to equation 4.10, viscosity ν according to the standard LB formula, 2.114. All other parameters are input, including the (driving) wall velocity U_0 , which is adjusted in such a way as to keep constant Reynolds number; as calculated the usual way: $Re = WU_0/\nu$.

Relative error for the case of Couette flow, here denoted ε_C , is calculated according to:

$$\varepsilon_C = \frac{v_m(y) - v_{Cth}(y)}{U_0}, \quad (4.11)$$

not an absolute value, note. This is evaluated at different cross channel positions, y , for the profiles of figure 4.5, to form the data for figure 4.6. Such data reveals that the relative error generally increases as the dimensionless time \bar{t} decreases. Even ignoring the fact that, at $t = 0$, the measured lattice velocity y gradient cannot be infinite (its analytical value), the profiles of figure 4.5, show encouraging agreement with the analytical result, down to very short times. Naturally for low viscosities, ($1/\tau$ approaching 2), the diffusion of velocity from the upper (driven) plate is slower. Accordingly the finite difference approximation for the velocity y gradient at the boundary is poor, as is the convergence of the analytical solution 4.10 (due to the Gibbs phenomenon), both of which considerations affect the agreement at very small values of $\bar{t} = \nu t/W^2$, that is in the high flow gradient regime.

Nevertheless in all cases the velocity gradients do not change discontinuously, either near the lattice-edge or further in. Moreover, the relative error associated with the boundary, whilst higher than that associated with the bulk scheme, is still demonstrably an order of magnitude lower (more even) than that of simpler closures — bounce back for instance, shows discontinuities in the profile gradient one node in, for all time except at steady state.

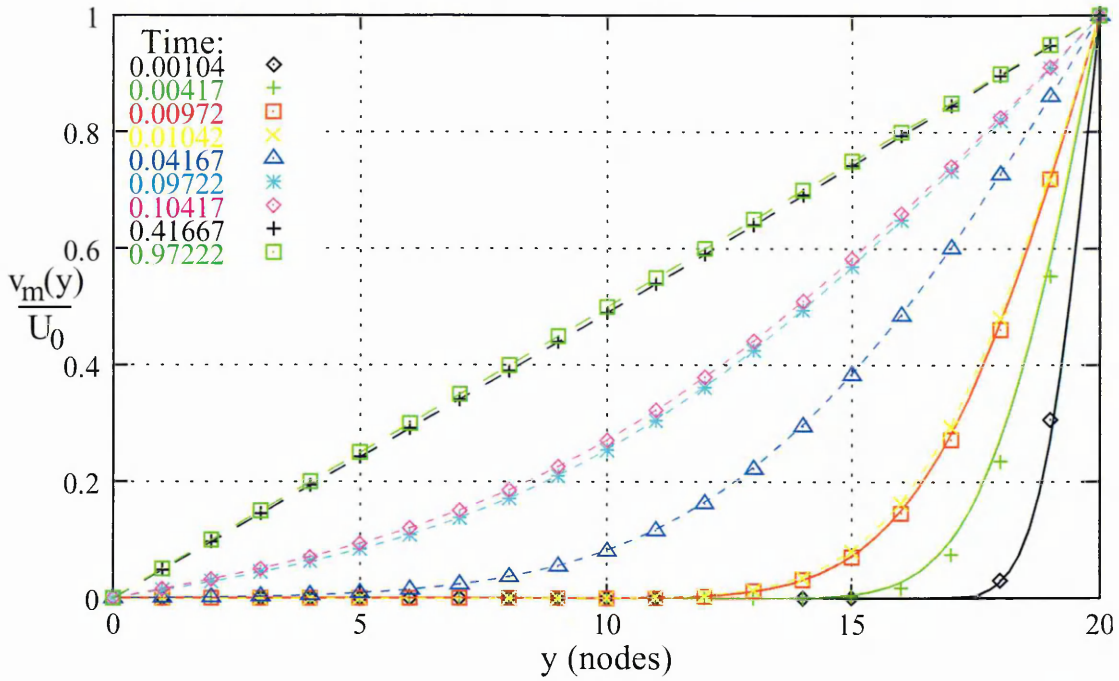


Figure 4.5: Impulsively started Couette flow profiles obtained for $Re = 0.024$ and simulation width (resolution) $W = 20$. The Reynolds number was maintained constant by adjusting the moving plate velocity, U_0 . Symbols show the normalised, measured profile v_m/U_0 , lines show the corresponding normalised analytic profiles, $v_{C_{th}}/U_0$, calculated for and characterised by the same range of \bar{t} values.

4.4 Discussion

It is obvious, in consideration of the results presented, that the new scheme fulfills its initial criteria, providing an improvement in: accuracy, both spatial and time dependent; simplicity, of analysis and implementation; and, most importantly, *consistency* of treatment between the various types of simulation node. However, some important aspects of the scheme warrant further discussion and these follow. Subsequently, the chapter is rounded off with a brief synopsis.

The main issues for discussion here concern: time dependence; improved accuracy; the means to determine $S_{\alpha\beta}$; primary applications; and interesting characteristics that arise. These are briefly expanded upon next.

As regards time aspects, the restitution model in the continuous Boltzmann formalism, introduces an unspecified time period between adsorption of a molecule and its subsequent return to the fluid. Over this period, conservations are not strictly met. In fact conservation only occurs over a time long compared to the process and, in a sense, en mass. Individual particle behaviour is therefore not captured in a restitution based model, nor is the intent to capture such. However, it is apparent that by using the previous time step's lattice data to calculate values for $S_{\alpha\beta}$ locally (for use in calculation of the

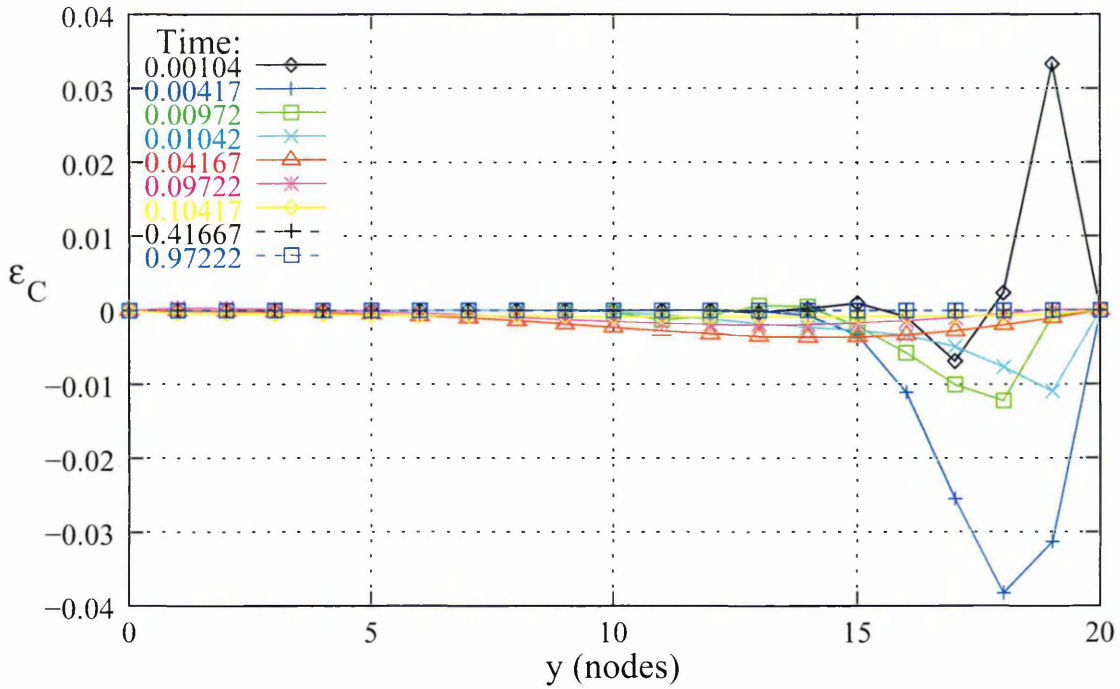


Figure 4.6: Relative error for the data of figure 4.5 as a function of distance y across the duct; as given by equation 4.11. Note the overall low error (second order accurate), even at very small time scales; also the extremely low error toward the static wall $y = 0$. Error data seem to approximate an underlying smooth nature — underlying curves and their derivatives are continuous. Importantly, note zero error, to machine accuracy, at both boundaries.

$f_i^{(1)}$), a similar ‘computational’ time delay is inadvertently introduced to the *model*. The nature of this may be benign or beneficial, it not being clear as to which is applicable. However it is clear that this may account for, or be suitably modified so as to account for, any physics that might arise in the restitution process.

It is also in fact possible, to calculate gradient information at the *current* time step, if information on sites adjacent to the boundary are used and the macroscopics thus generated are extrapolated. This has obvious consequences for the algorithm complexity, but these are not here considered to be too dire. Hence, an investigation of the relative efficacy of this mode of calculation of $S_{\alpha\beta}$ might be considered in further work.

The actual *formalism* within which determination of $S_{\alpha\beta}$ is made, is itself open to alternatives. Specifically for the LB, values may be calculated in a *self-consistent* manner: by interpolating f_i from neighbouring values, $S_{\alpha\beta}$ may be calculated directly using equation 4.3, a quality of the LB itself. Alternatively, simple finite difference schemes may be used. Both cases offer individual nuances, the comparative rectitude of each being open to debate.

In each case, the particular *method* of determination of $S_{\alpha\beta}$ is optional too. Note that equation 4.3 may be applied at either time step. For the case of finite differences, values

for local strain, $S_{\alpha\beta}$, may also be calculated using data at the previous or current time step, but in addition, by various interpolation or extrapolation schemes. Importantly (for other work herein, chapter 5), $S_{\alpha\beta}$ values may even be *set*, by invoking some other criteria emerging with the modelling problem in mind. This is of utmost significance as regards novel utility of the scheme. It was in this way investigations leading to its development were initiated; similarly, it is here that the true value of the new scheme emerges.

On that point, it is apparent that, since gradient qualities of the wall region attain some significance in implementing closure, herein might lie an efficient way in which to investigate effects of wall regions on flow solutions. This fact is utilised in full in the main section of the work, chapter 5, where a ‘law of the wall’ is to be implemented for turbulent channel flow. Summarising, the new scheme offers a hitherto impossible facility for incorporating stress as a parameter in simulations.

For the purposes of evaluating $S_{\alpha\beta}$ in this chapter, values were extrapolated to the boundary using second-order accurate finite difference expressions, on *measured* macroscopics, calculated one node in from the boundary at the previous time step. Some mileage might obviously be gained in investigating the efficacy and quality of other methods; but this is left for further work.

In addition to such implementation issues, interesting points arise as a consequence of the scheme itself. In particular, the seemingly arbitrary selection of three $f_i^{(1)}$ from the set of ‘known’ values and the fact that, with respect to obtaining a solution, some of these should turn out to be forbidden.

The physical origin of the forbidden combinations may be understood upon considering the variable set:

$$\begin{aligned}
g_1 &\equiv f_1^{(1)} + f_2^{(1)} + f_3^{(1)} \\
g_2 &\equiv f_5^{(1)} + f_6^{(1)} + f_7^{(1)} \\
g_3 &\equiv f_3^{(1)} + f_4^{(1)} + f_5^{(1)} \\
g_4 &\equiv f_1^{(1)} + f_7^{(1)} + f_8^{(1)} \\
g_5 &\equiv f_0^{(1)} + f_4^{(1)} + f_8^{(1)} \\
g_6 &\equiv f_0^{(1)} + f_2^{(1)} + f_6^{(1)} \\
g_7 &\equiv -f_0^{(1)} + f_1^{(1)} + f_5^{(1)} \\
g_8 &\equiv -f_0^{(1)} + f_3^{(1)} + f_7^{(1)}, \tag{4.12}
\end{aligned}$$

whereupon, the system of equations, 4.7, may be written in the simplified form:

$$\begin{aligned}
g_1 + g_2 & & + g_5 & & = 0 \\
& & g_3 - g_4 & & = 0 \\
g_1 - g_2 & & & & = 0 \\
& & g_3 + g_4 & & = -2\rho\tau/3 S_{xx} \\
g_1 + g_2 & & & & = -2\rho\tau/3 S_{yy} \\
& & & & g_7 - g_8 = -2\rho\tau/3 S_{xy}. \tag{4.13}
\end{aligned}$$

Here it is important to note that this reduction of the equations is not unique. Using the equations 4.13 it is possible to find expressions for the set of variables g_i in terms of the boundary density, velocity and strain rate. It is therefore clear that the combination of $f_i^{(1)}$ in each g_i cannot be independent and therefore the $f_i^{(1)}$ in that combination cannot all be chosen as ‘free’ variables, *that is*, they form forbidden combinations of link densities.

Some interesting questions arise with the occurrence of sets of forbidden $f_i^{(1)}$ selections, perhaps most intriguingly, in that among the remaining ‘available’ sets, selection *does* appear to be arbitrary. This leaves the question as to whether any difference exists entirely open. Additionally, if differences do exist, do they persist to have an effect on the final solution? Differences between choices of $f_i^{(1)}$ sets, might therefore, be investigated in further work.

4.5 Synopsis and conclusions

In summary, an adaptable method for closing a lattice Boltzmann simulation lattice, by calculating appropriate values for the set of missing momentum densities, has herein been set out and validated. The algorithm has demonstrably improved accuracy and is flexible. In particular, the new lattice closure strategy is accurate over a very small number of simulation time steps and is an improvement with respect to time development of a flow. Thereby it supersedes schemes aimed only at improving the spatial order of accuracy. Moreover, the method extends the scope of the LB by permitting use of the rate of strain tensor as a parameter in wall layer models.

Furthermore, as Ginzbourg and d’Humières have effectively demonstrated with their LSOB method, [49], the essential idea used will generalise to any linearised LB scheme and boundary orientation, provided one is prepared, in the language of the present work, to extrapolate the fluid density onto the Dirichlet boundary. Without similar modification, the present approach would generalise only to a boundary orientation for which the sum of

the missing momentum densities can be determined through an identity like equation 4.6 above. At present, the scheme is applicable to all normally oriented and flat boundaries, over which there is a target distribution of velocity. Therefore in principle, the method can be used to represent open or closed fluid boundaries, not just the usual ‘no slip’ condition.

Finally, the method could, in future, be further generalised to allow the simulator the freedom to place a boundary with known velocity distribution at any distance $y = h(x)$, $0 < h(x) < |c|$ off-lattice, thus bringing precise control of the simulation boundary within the scope of the LB method.

The bulk of the material presented in this chapter has since been published, see [51].

Chapter 5

Application of eddy viscosity model in LBM simulation of turbulent channel flow

A mixing length extension is described, to the lattice Boltzmann approach to simulation of an incompressible liquid in turbulent flow. The method uses a simple, adaptable, closure algorithm to bound the lattice fluid and incorporate a law of the wall. The test application, of an internal, pressure driven and smooth duct flow, recovers correct velocity profiles up to Reynolds number 20,000. In addition, the Reynolds number dependence of the friction factor, in the smooth wall branch of the Moody chart, is correctly recovered. A complete analysis is made on the effect of allowing LB relaxation parameter to vary both spatially and temporally. Matters arising are discussed in some detail. The method promises straightforward extension to other curves of the Moody chart(and to cylindrical pipe flow).

5.1 Introductory remarks and preview

This chapter presents material on the primary goal of the work carried out. The lattice Boltzmann scheme is applied, with suitable modification, to the problem of reproducing characteristics of turbulent flow in internal geometries; simple pipes, ducts and the like. In the introductory chapter, 1.2, the motivation and context for this investigation has been discussed in some detail and the great importance of such flow realisations, is made apparent. In background section 2.4, the nature of turbulence is described in some detail; in section 2.7 issues specific to turbulence in internal channel flow are explored and the motivation for this chapter is further expanded.

A prime interest lies in obtaining representation and quantification of pressure driven turbulent flow and from an engineering perspective certain qualities and properties stand out as being of greater relevance. Any attempt to model such flows then, must aim to reproduce these in order to prove worthwhile. Primarily, it is expected that properties such as: a ‘broadening and flattening’ in the *mean* velocity flow profile; an increase in the pressure drop (over the equivalent laminar case); increased mixing, or higher transport characteristics; and a greater friction coefficient, should be observed in the modelled flow. Changes such as these are highly significant in defining overall system behaviour and consequently attain the pinnacle of relevance in system design. They are described in greater depth in the background material of section 2.7, where causative factors are also discussed.

The investigations carried out here focus on one characteristic which summarises various aspects of this behaviour — the mean velocity profile — along with character that is derived from it, such as friction coefficients and Moody curves. They, again, are described in earlier background sections 2.7. As a basis for appraisal of the work carried out in this

chapter however, it is necessary to clarify the salient features of flow behaviour. A precise framework within which this work will be evaluated must be specified; equivalently, a mode by which the method is to be compared and judged. To these aims, section 5.1.2 provides a detailed basis for evaluation of the work. The first section, page 184 precisely defines how turbulence affects the nature of channel flow. To do this, some of the background material is summarised; characteristics to be recovered are then itemised. These consist of clear qualitative and some quantitative flow features. The latter section, page 187, resolves the issue of what means must be used for comparison, to form a basis for subsequent appraisal of modelled results with respect to standard or 'known' results of previous workers. It consists of sources, citations and reviews of various prior works in the field. Also detailed there are further quantitative features of previous research, with which to compare and contrast results generated here.

Subsequent sections begin with a detailed description, review and specification of the strategy employed in these studies and its implementation details, 5.2. This forms the primary technical content of the chapter. Having set out the basis for the studies, the discourse then moves to presentation of results, section 5.3 and their discussion with respect to the literature and proposed further work, section 5.4. Finally section 5.5 rounds off with a synopsis of the content of this chapter; its aims, objectives, successes and failures. Concluding remarks are made at that point. [But t/T]o begin with, a summary of the primary developments made and the nature of the novel contribution so generated, is now provided as preview.

5.1.1 Nature of the novel contribution and synopsis

Although turbulence modelling studies have been carried out within the framework the Bhatnagar–Gross–Krook lattice Boltzmann method and reported in the literature previously, see [72, 127, 132, 138], such work amounts to fundamental initiation of the field; it is very much intended to be built upon. The work presented here aims to contribute in precisely that way. Developments made are achieved as follows:

Firstly, in part as a validity exercise, novel results are generated utilising the unaltered original modelling strategy, [138], but applied to further specific geometries. The value of such data is improved by extracting new derived data sets from the raw output and carefully evaluating the validity and rectitude of these, along with the raw data. This is done in the light of accepted results of alternative approaches. These new results are consolidated by: investigating weak areas; probing other aspects of simulation output; and objectively analysing and discussing the model's relative effectiveness for the purpose. All of these are omitted in the founding material.

Building on the aforementioned, the current work then contributes by further novel augmentation of the model in such a way as to incorporating other behaviours associated with internal pressure driven turbulent flow. Specifically, a model is implemented to represent sub-grid scale (otherwise unresolvable) boundary layer features, namely a ‘law of the wall’.

New results thus generated are again used to extend the scope, validity and utility of the core scheme. Value is similarly added to these by deriving secondary data and results are further consolidated through additional analysis. In particular, observations are made of the effect of the specific changes that underlie the main extension of the core scheme — the effect of invoking spatio-temporal variation in LB relaxation parameter.

5.1.2 A basis for evaluation of model effectiveness

An idea of which behaviours are considered of practical importance must thus far be apparent. For purposes of analysis contained in the rest of this work, it is necessary to provide more detailed information in that regard. The two aspects of this information are treated separately. Firstly, (next) a detailed summary is given, of the main flow features which the simulations must recover; this in part consists of a review (and instantiation) of some background. As previously mentioned there are two primary types of data to be analysed, flow profiles and Moody charts. A description of these follows and in addition, aspects of how they are changed, under the transition from laminar to turbulent flow, are detailed. After that, page 187, exemplary data with which to compare, generated by earlier alternative work of other groups, is sourced, cited and acknowledged.

Important flow characteristics to be recovered

The effect of turbulence on the flow and hence mean flow is complex, though heuristically understood to some extent. Broad changes occur in the mean velocity profile, these being the primary attributes that the modelling scheme is required to recover. In addition significant changes occur in volumetric flow and friction parameters.

An example of the kind of turbulent velocity profile that arises is provided in figure 2.15 of section 2.7. The geometry of that example is a pipe, having cylindrical cross sectional shape. Note that, whilst superficially similar, subtle differences exist between turbulent pipe profiles and turbulent duct profiles, as for the laminar case. This character is not represented in figure 2.15, but is discussed there. It is further addressed in the next section, page 187 and in section 5.3. Later, in the discussion 5.4, specific examples of flow profile data are presented to illustrate this and for purposes of relatively quantitative comparison. Qualitative detail on how profiles and other data sets are altered, or

quantitative detail applicable in both cases are as follows:

- Qualitatively there is a ‘flattening’ of the profile, consisting of a reduction of central peak velocity hand in hand with development of a large region of fluid, central to the geometry, where profile gradient varies slowly. This is necessarily accompanied by the converse *increase* in flow profile gradient near the wall.
- The above could also be described as a ‘broadening’ of the profile in that there appears shoulder-like regions in the profile; increased mean flow located at mid to outer distances from channel centre line. This also leads to the emergence of two new regions of high curvature in the velocity profile — the ‘shoulders’. Notably the central one remains to some extent.
- In the vicinity of transition, between laminar and turbulent states, some complexity may arise in observed flow characteristics which may be intermittent, unstable or irregular, but are not representative of developed turbulence. Flow transits randomly between various ‘metastable’ states which may coexist. These are characterised by differing friction coefficients and therefore mean velocities. Observed global variables in such cases vary over a range encompassing those for laminar and turbulent states.
- At Reynolds number above the critical value associated with transition behaviour, Re_{cr} , there is a clear increase in friction coefficient. Moreover, the change in this friction coefficient with Reynolds number, as quantified in the so called Moody curves, is reduced here too, i.e. there is a reduction in gradient of the Moody curves.
- Also above the critical Reynolds number for turbulence, there is reduced volumetric flow rate, concomitant with the increased friction and reduced mean flow.
- The above features can be associated with a higher energy loss due to friction than is possible via viscous mechanisms alone. This may in turn be related to increased mean shear in fluid boundary regions which is known to ‘stretch’ vortices. Vortex stretching is a well understood mechanism whereby energy is redistributed amongst turbulent scales (toward smaller scales and on to dissipation).

Assessment of modelled flow profiles is a significant aspect of this work. Note however that it will not be an entirely quantitative exercise. For example, comparison between laminar and turbulent states will be relatively qualitative as it concerns the shape of the profile. Summary properties of the profile may be treated quantitatively; by this is

meant, statistics derived upon treating the profile, or part of it, as if it were a distribution of some sort. These include parameters such as mean velocities, ratios of peak to mean and other ‘statistical’ properties. Profile shape, being the velocity distribution across channel, is exactly quantitative but must be put into context, by comparison either to experiment or to theory.

Comparison of simulation profiles to experimentally observed ones will also here be qualitative in nature. This is because true quantitative assessment may only be made when flow is simulated under conditions precisely matching those pertaining to an experimental case. In order to be precise, tables of raw data are then required, if only to put the two side by side on the same plot, certainly if any statistical analysis is to be performed. Since little original data is available for this — sources of raw data are only readily available for the pipe geometry, as will be seen — the approach is not followed.

Comparisons to theory might be regarded as the most productive approach to quantitative appraisal. Theoretical models may be used to derive data for plots, for direct, visual comparison. Alternatively, statistical tests might be carried out on deviations of simulation data from analytic predictions. These are discussed at length 2.7.3 and, especially relevantly, in the following, at page 187. Many of these relations relate to the near wall region, or pertain to behaviour dependent on distance from the wall.

Comparison between turbulent states at differing levels of forcing or Reynolds number is very important and may be done quantitatively. The parameters involved in such analyses are best viewed in plots such as Moody curves, which relate retardation effects to driving; more specifically, coefficient of friction to Reynolds number, see section 2.7 of the background. For qualitative illustration only, an exemplary Moody chart is given there, figure 2.18. Differences between laminar and turbulent flow states are summarised by the discontinuity or transition zone in the region of the critical Reynolds number, Re_{cr} . Features such as an overall increase in friction coefficient, along with a reduction in variation of friction coefficient with Reynolds number, should be apparent above the transition region.

Transition behaviour itself is poorly understood, except either generally or in quite specific instances. Note that this work does *not* attempt to capture transition behaviour — by its very nature the model, when applied, introduces behaviours attributable only to the ‘fully developed’ turbulent state. It is expected however, that the model recover an appropriate *differential* relationship between the laminar and turbulent realms of validity. In other words, Moody charts for each case are expected to show an *idealised* form of transition region. Moody chart data will therefore be central derived data in these investigations, hence detailed and quantitatively accurate representations are provided

next, page 187 and as yardsticks in appraisal of results, sections 5.3.

Sources of data for comparison and evaluation

All initial investigations in this chapter treat the infinitely deep duct channel geometry. Experimental data on such however, turns out to be relatively scarce. This is due primarily to practical difficulties experienced in approximating plane flow experimentally, but also arises with the fact that pipes are practically important, whereas ‘infinitely deep’ ducts are just technically interesting; they are practically almost irrelevant! Data therefore, appropriate for validation and comparison purposes here, is difficult to come by.

Knudsen and Katz (hereafter often just K&K), [73], refer to studies carried out on the case of flow ‘between planes’, see pages 206/7. This is equivalent to our infinitely deep channel but it is likely, though not stated, that what is meant is strictly a *duct* geometry. Note that a duct in this sense is just a rectangular channel and only in the limit of high aspect ratio does such approximate our infinitely deep channel. In the absence of original papers, which are effectively unavailable, it is difficult to be clear what aspect ratios are applicable. However, it is clear that such works must be at least *adequate* as a basis for comparisons. They cite six works, reviewed in brief next for the aforementioned reasons.

Early investigations were carried out around the late twenties. Donch measured point velocities in turbulent air in 1926, [34]. Nikuradse seems to have pre-empted his extensive and well known studies on pipes, by a study in deep ducts in 1929, [98]; he measured the same but in turbulent water. These works, being quite similar studies, were further and separately analysed a decade later by Goldstein [50]. He established the ‘velocity defect’ (in the sense of equation 2.156) relationship:

$$\frac{v_{pk} - v}{v_\tau} = -3.385 \left[\ln \left(1 - \sqrt{\frac{y_c}{W/2}} \right) + \sqrt{\frac{y_c}{W/2}} \right] - 0.172, \quad (5.1)$$

strictly quoted for the core region of a duct flow, but practically for say $y^+ \geq 30$, using their results. Note v_τ , the friction velocity, is as defined in equation 2.154 of the background herein, W is the usual channel width and y_c is the distance from geometric centre line between the planes; that is $W/2 + y$.

As mentioned, the above works are supposed applicable to the idealised case of infinitely deep channel geometry, however it is obvious that their experimental results could not have been obtained in this way and so presumably noticeable differences existed between apparatus. Despite this their data agree well however. Plotted in the commonly encountered way, v^+ as a function of y^+ , in the sense of section 2.7.3 (page 127), an

empirically derived fit is found for the data as follows:

$$v^+ = 6.2 \log y^+ + 3.6. \quad (5.2)$$

This is to be contrasted with equation 2.184 of section 2.7.3 and coefficients for which, as derived for the pipe case. Hence differences between the two cases are therein summarised, arising purely through the geometry.

Empirical relations such as these, despite being a relied upon means to solve practical problems or for validation, are not to be considered precise. This is demonstrated by the results of Laufer [80], which show strong disagreement over the value of at least one constant, despite targeting equivalent experimental systems. Laufer's data were obtained with a hot wire anemometer and were found to be much higher than Nikuradse's and Donch's, presumably with a derived intercept constant say 4 to 10, although this is not directly stated. The data is valid to much lower dimensionless distance y^+ — in fact to $y^+ = 2$ — on account of the measurement system employed. This is well into the laminar sub-layer, where the data validate the applicability of equation 2.174 to the viscous sub-layer of a duct.

Results for y^+ this low however, are not testable with the simulation technique employed here, on account of the fact that it is at sub-grid scale. Even our law of the wall *model*, is in this respect a relative 'sledge hammer' method of imposing a correct BC on the bulk scheme, in that it sets a velocity for the first node in, at say $30 \leq y^+ \leq \mathcal{O}(10^3)$.

Other works cited in K&K include Schlinger and Sage, [122], whose data agree well with that of Nikuradse and Donch's over the range collected, that is for y^+ values up to 750. Importantly, over that range their data also match relations derived for turbulent flow in *pipes*. In particular, equation 2.184 of background section 2.7.3 and the following:

$$v^+ = 2.78 \ln y^+ + 3.8, \quad (5.3)$$

which was derived by Deissler [32], for turbulent air in a smooth tube. Deissler's data, being valid for a smaller range of y^+ (up to 5000), is not considered as reliable for the pipe case as that of Nikuradse [99]. It does, however, indicate that laws derived for pipe flow profiles might fairly be applied in duct flow analyses, when presented in dimensionless form.

Furthermore, Pai [101] derived an equivalent relation:

$$\frac{v}{v_{pk}} = 1 - 0.3293 \left(\frac{y_c}{W/2} \right)^2 - 0.6707 \left(\frac{y_c}{W/2} \right)^{32}, \quad (5.4)$$

but worked analytically from the Reynolds averaged Navier–Stokes equation to achieve this. Exponents in equation 5.4 were specified in a way dependent on Laufer’s earlier work, note.

A modern search on the web reveals a multitude of interesting, though not particularly relevant works. This method of search is only good for the period of say three decades and misses important works from outside that period. It can’t therefore be deemed comprehensive and the need to include review of such is not justifiable. In fact, it is apparent that amongst those works so far cited, there is sufficient content to form a fair and complete appraisal of results expected to be generated here.

Just a few modern citations generated from a ‘Web of Science’ search include, for instance S. Chen *et al.* [23] (and subsequent papers by the same authors [21, 25]); where analytic solutions are proposed for flow in a duct geometry. Their work generates results sufficiently at odds with other analyses (in direct equivalence to those produced here) that their introduction as a yardstick is not warranted.

It is handy, if not rigorously correct, to use pipe data in place of duct data. Many studies such as Deissler’s [32] and Schlinger and Sage, [122] allude to the fact that differences between turbulent flow profiles for pipe and duct geometries are practically slight. There is good availability of data for cylindrical or pipe geometries, in contrast to ducts. These are discussed in the earlier background section 2.7.3, again basing the review on the text of K&K. Here, owing to the relatively dubious nature of assuming equivalence, such data are used for relatively qualitative comparisons.

One other work is of note, primarily because of its availability as a direct data resource on the web, that being the rather grandiosely named Princeton ‘super-pipe’ data. This is the work primarily of Zagarola, see the PhD thesis [153], generated under the auspices of the well known turbulence specialist S.A. Orszag. Because the data are comprehensive, cover a wide range of Reynolds number and readily available in the raw form, it will be a primary qualitative resource used for comparative work in this study, both for pipes and for ducts; see acknowledgments 6.3.

Discussion in the previous paragraphs is centered upon turbulent velocity profiles, which form the crude data of these investigations and from which other, more refined data sets are extracted. Of the derived data, as previously mentioned, friction data are perhaps most useful. In particular, Moody curve results, whether derived for turbulent flow in pipes or ducts.

The most crucial of these arises from, and is valid under, two perspectives and is attributable to various sources on account of this. It is relation 2.193 of the background (see section 2.7.4). As mentioned there, Nikuradse derived relation 2.193 semi-empirically

from a compilation of various extensive data sets. However, the result is strengthened by the fact that von Kármán derived a very similar form:

$$\frac{1}{\sqrt{f_B}} = 4.06 \log(Re \sqrt{f_B}) - 0.6, \quad (5.5)$$

from a *theoretical* perspective, [142]. He used the universal velocity distribution for the turbulent core, equation 2.184. Its validity extends over the range for which data were available at the time.

Compare equation 5.5 to that derived by Nikuradse for his results on the circular channel, equation 2.193. Their close similarity is obvious. Hence this result provides a good link between experimental and theoretical approaches, possibly even providing guidance for yet to be initiated analyses on channel flow.

The relevance of this equation is further enhanced from the perspective of this work, in light of the fact that it is supposed applicable to the case of *duct* flow also. Knudsen and Katz state in [73] that both relations are valid for the case of flow between parallel planes (page 207). Although they give no basis for this statement, or evidence that it is true — such amounting to a very slight omission on their behalf — it is likely that its truth may readily be demonstrated. That at least is the point of view taken here. Hence relations 2.193 and 5.5 form the second most important tool for purposes of assessing efficacy of the LB turbulence model.

Before moving on to details of such an appraisal, as found in section 5.3, the following section now details the way in which the scheme utilised for the purpose is to be implemented. After reducing the geometric dimensionality and by inserting a model of the effects of turbulence into the LB evolution equation, mean flow profile across a turbulent channel is derived. A model based on the logarithmic wall law is used to incorporate the effect of a sub-grid scale boundary layer. The effect of such on the global friction behaviour of the flow is then studied.

5.2 Models and implementation

In previous sections, the eddy viscosity concept, page 58, and mixing length hypothesis (MLH), page 59, are introduced in some detail. In this work these are the primary tools with which the problem of internal turbulence modelling is to be tackled. In a following section, 5.2.2, implementation details for such ‘mixing length models’, specific to the LB framework, are reviewed and presented.

The nature of the mixing length itself is such that, in (mixing length) modelling, its specification is largely an empirically guided and ad hoc matter. For investigations carried out in this chapter, an appropriate algebraic form is simply chosen from the set available. The particular choice is reviewed at page 197; its specification is fundamentally ‘geometric’ in nature.

Earlier sections also review the nature of boundary layers, 2.7.2, the ‘wall law’, 2.7.3 and its implications for turbulent channel flow, 2.7.4. In a following section, 5.2.3, details are presented on how a ‘law of the wall’ may be implemented in the LB, so that near wall flow character may be appropriately and adequately modelled.

Implementational issues arising with other considerations in the turbulent channel geometry, for example forcing, streamwise closure, invariance and the like, are common with channel simulations of earlier chapters. They may therefore be dealt with by means established earlier in this work, to which the reader is referred. In particular see section 2.6 for the background and the simulation section 5.3.1 for specific details.

Before moving on to cover the above matters in earnest, a brief aside is firstly taken to look at the chosen modelling strategy in the context of the literature.

5.2.1 Eddy viscosity and mixing length in the LBM: a review

In an eddy viscosity model, the contribution of turbulent fluctuations to transport of mean momentum in the Reynolds averaged, or space filtered momentum equation, is postulated to be analogous to that effected by molecular viscosity — that is, the mean deformation tensor $S_{\alpha\beta}$ is supposed to mediate further effect on the mean flow via an additional contribution to viscosity, ν_T , to augment that of the raw molecular viscosity, ν_0 . See earlier background sections 2.4.4 and 2.7. In other words, the Reynolds stress tensor is *modelled* by an ‘effective’ viscosity term. Generation of interesting and valid output arises as a consequence of prescribed variation in the augmented viscosity, which, by defining properties of the eddy viscosity, is dependent on the deformation tensor itself. Invoking the mixing length model means that further dependence arises in the defining variation of mixing length, ℓ_{mix} .

Traditional CFD addresses the issue of molecular viscosity directly, as it appears in the modelled equations. For the case of the LB however, viscosity is not a ‘natural’ variable of the scheme in that it appears only upon identification of terms arising in the Chapman–Enskog expansion, see equation 2.114 of section 2.5.2 (pages 76 on). Since molecular viscosity does not directly appear in the LBM and since: constraints exist on the values it may take; its identification with BGK relaxation parameter makes it strongly related to numerical stability; further, it is assumed invariant in the Chapman–Enskog expansion analysis, implementation of an *eddy viscosity* based LB turbulence model is somewhat complicated. This does not prove in any way insurmountable, however, as evinced in the following sections, which detail the exact nature of an LB mixing length model. The strategy to be utilised is now reviewed in the context of the current literature.

There is comparatively little work on this subject in the public domain at present; in fact only three closely related papers were available at the initiation of this project: Succi, Amati & Benzi [132]; Hou, Sterling, Chen & Doolen [68] and Teixeira [138]. The former two of these seem to have appeared independently and at about the same time.

Before these appeared however, Somers, in [127]¹, used a three dimensional linearised LB scheme to simulate turbulent pipe flow. Note that the linearised LB is significantly more complex than the BGK counterpart which is the subject of this study. Whilst they attempt also to incorporate transition and despite the fact that their cylindrical BCs are implemented in a very crude rectilinear form, they achieve good results for some values of their basic parameters (C_s and C_n). Unfortunately, no method arose to derive proper ‘calibrated’ values for such and the work was not directly followed.

Succi *et al.* [132], seems to be the first paper containing a discussion of turbulence modelling in LBGK, a very simple form for the eddy viscosity is suggested using the so called Smagorinsky model. The paper by Smagorinsky [125], referred to in [132]², is in fact a huge work focusing on the modelling of atmospheric flow and other meteorological issues. The turbulence model therein, only a small part of the work, may readily be seen as belonging to the general class of models essentially of the mixing length form, (although with a alternative value for the empirical constant: $k^2 \equiv C_S$ (C_S being the Smagorinsky constant)). Succi then goes on to describe prospective scheme for k - ϵ turbulence model using two new populations. No simulation results are published for either however.

At about the same time, Eggels and Somers [37], whilst considering the case of free convective flow in a two dimensional square cavity, also hint at how a sub-grid scale (SGS)

¹Also / equivalently: *Proceedings of the Fourth European Turbulence Conference* ECT-IV, Delft, June 30th 1992.

²All the early papers refer to Smagorinsky’s paper, note; the reason for this appears to be the slightly greater simplicity of ‘plain eddy viscosity’ over strict mixing length models.

model might be affected in the LBM. Their proposed method seems to be implemented in two stages; firstly by changing the form of the LB equilibrium distribution function (to incorporate Reynolds stress generating terms), then by deriving a new form of linearised collision operator so endowed as to recover the required macroscopics in a way consistent to the new equilibrium. Whilst their *model basis* is in essence of the Smagorinsky class, their model *implementation* pertains strictly to the linearised LB case, hence it is not applicable to the simpler single relaxation time (BGK) form employed here. Their method is sufficiently at odds with subsequent works, including this, to warrant no further consideration herein. However, the relative merits or potential of such an approach are discussed in a later section 6.1.

In a later paper [38], Eggels performs direct numerical simulations (DNS) of *channel* flow as a means to check performance of their solver. They then use SGS model based on the previous paper [37], to perform large eddy simulation (LES) of flow in a baffled stirred tank reactor. Note that in this case no SGS model is applied to the channel simulation and the work is not of direct relevance here.

Hou *et al.* [68] give a very full description of eddy viscosity and mixing length in the LBGK and they detail specifics of implementation. The scheme developed is applied to the driven cavity (LDC) problem, with Reynolds number over a wide range: $100 \leq Re \leq 10^6$. There is no treatment of channel flow turbulence. Their treatment is concise however and makes clear the relation between CFD and lattice Boltzmann instances; especially with respect to scales. For this reason it will frequently be cited in later discussions. They too work in terms of the Smagorinsky model, drawing attention to its weaknesses.

Teixeira [138] builds on the earlier works and is first to apply an LBGK turbulence model to the problem of channel flow. Both an algebraic mixing length model and a k - ϵ model are applied, in LBM form, to two geometries: one is pipe flow, the other a back-facing step. The emphasis of their investigations seem to be to compare, within the LB framework, between the various modelling approaches mentioned, especially in the context of their existing (commercial) code and BCs. Further to demonstrate that, of these, the two k - ϵ forms (standard and renormalisation group (RNG)) are most accurate. In so doing they generate 3D LBGK mixing length model data for *pipe* flow which are in good agreement with experimental observation. This is encouraging with respect to the current work, but their data pertain only to two Reynolds number, which leaves much more to be done.

Finally the subject of turbulence models in LBM is again brought up in a recent book by Succi, [135]. The content is largely a reiteration of points made in his earlier paper, [132]. However, there are some additional comments of interest, especially regarding

a non-local BGK collision integral which will be discussed later, section 6.1.

So, with respect to the suitability of lattice BGK in particular, for modelling turbulent channel flow, there is comparatively little in the literature; largely because of the relatively early stage that the LBM has evolved to. It is this point which the present chapter attempts to address; the presentation continuing now with the mixing length model implementation.

5.2.2 LB Mixing length model: implementation

Now moving on to implementation of the eddy viscosity idea and mixing length model within the LBGK framework. In the paper by Teixeira [138], the form of eddy viscosity is in essence the same as that given in equation 2.85. It is proposed that this turbulent contribution augments the effect of the molecular viscosity under simple addition:

$$\nu = \nu_0 + \nu_T. \quad (5.6)$$

However, as previously stated, in the lattice Boltzmann method, viscosity is not a parameter that appears directly. Instead control is effected over viscosity by varying the relaxation parameter, the two being related in a simple way by the following identification:

$$\nu = \frac{\rho}{6} \left(\frac{2}{\omega} - 1 \right). \quad (5.7)$$

This identification is made between, the viscous Navier–Stokes terms that are *required* to appear during derivation of the lattice fluids macrodynamics, under the Chapman–Enskog expansion, and those that *actually* appear. So, it is not trivially apparent exactly how the augmentation into two elements should be carried out.

As a means to suggest a way round this which might otherwise be guessed at and to justify the next steps, a short aside is now made to ascertain the essence of the identification 5.7. Upon inspection it is apparent that the mapping of ω consists of: a ‘rationalisation’ $\omega \mapsto 2/\omega$, which gives rise to a number in the range $[0, 1]$; a coordinate or origin shift $2/\omega \mapsto 2/\omega - 1$; followed by a ‘calibration’ under the coefficient $\rho/6$. This means that, over the domain of ω acceptable to a relaxation scheme $0 \leq \omega \leq 2$, there is a bijection to the viscosity ν which ranges over the interval $[0, \infty)$ as required. It is vital that the approach leaves this structure ‘effectively’ intact.

In the light of this reciprocity between ν and ω , it is fair to assume that the relaxation parameter must ‘add in parallel’, to draw analogy for instance, with parallel resistive networks in electronics. Under this assumption the lattice Boltzmann equiva-

lent to equation 5.6 is:

$$\frac{1}{\omega} = \frac{1}{\omega_0} + \frac{1}{\omega_T}, \quad (5.8)$$

which usefully gives rise to $\omega = \omega_0\omega_T/(\omega_T + \omega_0)$, and an alternative statement of equation 5.7 for the turbulent case, which becomes:

$$\nu_0 + \nu_T = \frac{\rho}{6} \left(\frac{2}{\omega_0} + \frac{2}{\omega_T} - 1 \right). \quad (5.9)$$

To continue, we now need to specify the exact form that the eddy viscosity ν_T , will take. Taking into account the various presentations in Succi *et al.*, Smagorinsky and Hou *et al.* (mainly ‘plain’ eddy viscosity, in the sense of Smagorinsky), along with those appearing in standard turbulence modelling texts such as Tennekes and Lumley [139] and Launder and Spalding [82] (mainly Prandtl mixing length forms), the following ‘standard’ mixing length based form is assumed for the eddy viscosity:

$$\nu_T = \kappa^2 \ell_m^2 \| S \| . \quad (5.10)$$

Here ℓ_m is the mixing length in lattice units, κ is the undefined von Kármán constant and $\| S \|$ is the magnitude of the large-scale strain rate tensor as follows:

$$\| S \| = (S_{\alpha\beta} S_{\alpha\beta})^{\frac{1}{2}}, \quad (5.11)$$

with

$$S_{\alpha\beta} = \frac{1}{2}(\partial_\alpha U_\beta + \partial_\beta U_\alpha). \quad (5.12)$$

Then it would appear that we have a workable turbulence modelling scheme.

Note that this model is *not* of the Smagorinsky form, as are most of the early papers; no direct mixing length factor is contained therein as it pertains strictly to external flow. Henceforth, the treatment is most likened to that of Teixeira [138].

In practice however, the calculation of $\| S \|$ in the case of a lattice Boltzmann method need *not* be made in terms of spatial gradients of velocities as in equation 5.12, in fact to do so would seriously detriment the very LB advantages it is intended be exploited; instead the following form for $S_{\alpha\beta}$ is utilised, as arises during the Chapman-Enskog expansion:

$$S_{\alpha\beta} = -\frac{3\omega}{2\rho} \sum_i (\bar{f}_i - f_i) c_{i\alpha} c_{i\beta}. \quad (5.13)$$

The RHS of equation 5.13 can be thought of as the second raw moment of the *non-equilibrium* portion, $\bar{f}_i - f_i = f_i^{(1)}$, of the instantaneous density distribution function at that point. This quantity, has the distinct advantage over the traditional CFD finite

difference form 5.12, of being calculable entirely from *local* density values. This facilitates parallelisation of the algorithm and keeps more in tune with the spirit of the LBM. The term $\sum_i f_i^{(1)} c_{i\alpha} c_{i\beta}$ is usually denoted by $\Pi_{\alpha\beta}^{(1)}$, in analogy with the momentum flux tensor, additionally upon inspection of equation 5.13, it is apparent that³

$$\| S_{\alpha\beta} \| = \frac{3\omega}{2\rho} \| \Pi_{\alpha\beta}^{(1)} \| . \quad (5.14)$$

Combining equations 5.9, 5.10 and 5.14, and defining the molecular viscosity ν_0 in the same way as originally done for ν , that is: $\nu_0 = \rho(2/\omega_0 - 1)/6$ now, it can be seen that equation 5.10 is essentially a quadratic in $1/\omega_T$:

$$\frac{1}{\omega_T^2} + \frac{1}{\omega_0} \cdot \frac{1}{\omega_T} - \kappa^2 \ell_m^2 \frac{9}{2\rho} \| \Pi_{\alpha\beta}^{(1)} \| = 0 , \quad (5.15)$$

the roots of which and hence a solution for ω_T , may be found in the usual way; see appendix B.1. Taking the positive discriminant only, and defining a new constant Q as follows:

$$Q = \kappa^2 \ell_m^2 \frac{9}{2\rho} \| \Pi_{\alpha\beta}^{(1)} \| , \quad (5.16)$$

the solution for ω_T is found to be

$$\omega_T = \frac{2\omega_0}{\sqrt{1 + 4\omega_0^2 Q} - 1} . \quad (5.17)$$

The above expression for ω_T may either be added to the molecular relaxation parameter, ω_0 , or used to re-calculate an expression for ω , the total relaxation parameter, using 5.8. In this work the latter method is chosen, they being directly equivalent, which in summary means that the equation for the locally varying viscosity is as follows:

$$\omega = \frac{2\omega_0}{1 + \sqrt{1 + 4\omega_0^2 Q}} . \quad (5.18)$$

This simple expression is the one used in this work to affect control over the lattice fluid viscosity and thereby model unresolvable, or sub-grid scale turbulence character in the flow.

In a following discussion, section, 5.4.2, an analysis is made of the consequences of introducing the specific model proposed here. This involves determining the mathematical terms generated through implementation of this scheme under the Chapman–Enskog expansion. Also there, behaviour of the variable components to the viscosity and relation

³Note that for a general rank two tensor, \mathcal{T} , $\| T_{\alpha\beta} \| = (T_{\alpha\beta} T_{\alpha\beta})^{1/2}$; for which the Einstein summation convention applies, and under which any constants become positive but remain unaltered in value.

of these to underlying flow state variables, is plotted and discussed.

Specification of the mixing length

Once established in this way, one other aspect remains to be dealt with, specifically, the exact way in which the mixing length ℓ_m — an integral part the eddy viscosity scheme — is designated. Despite the fact that an ‘impression’ of its form is required in advance of mixing length model derivation, an exact form and mixing length specification has not yet been made.

Prandtl’s original discourse on the mixing length hypothesis was made within a gas kinetic context, where the formulation depended on fluid particle velocity correlation distances and derived length scales, see earlier sections, page 59. Modern perspectives, in the light of improved understanding, adopt a different view point. For channels and boundary layers in particular, the mixing length becomes an almost geometric quantity, simply related to the proximity of walls. Such is the stance taken here.

There are in fact various possible formulations for this essentially empirical parameter. They all incorporate similar general features and typically centre on an algebraic relationship. One such feature, in the presence of boundaries, is an approximate proportionality between mixing length and distances to solid objects in the flow such as walls.

Direct proportionality (linear), may be implemented using say: $\ell_m = c(R - r)$ where c is any constant, R is the channel radius and r is the radial coordinate of the point in question: $R, r \in \mathcal{R}^+$, $r = |y - R|$, see figure 2.14. Piece-wise linear formulations are common for their simplicity, however they contain unwanted gradient discontinuities.

More complex quadratic formulations exist however, which do not suffer the problem of discontinuities. For *pipe* geometries in particular a fourth power law has been derived empirically:

$$\ell_{m4} = R \left[0.14 - 0.08 \left(1 - \frac{y}{R} \right)^2 - 0.06 \left(1 - \frac{y}{R} \right)^4 \right], \quad (5.19)$$

which fills all the basic criteria and has been observed to exhibit a close match to experimentally derived inferences. Its shape is depicted in figure 5.1.

Specification of the mixing length is not a highly exacting issue, and simulations are relatively insensitive to it. For these and the above reasons, formula 5.19 is the one adopted for calculation of ℓ_m in the present work. Its strict validity to the *duct* geometry is not known, however. Note that coefficients in formula 5.19 have values which incorporate the von Kármán constant, as occurs as a constant of proportionality in mixing length analyses.

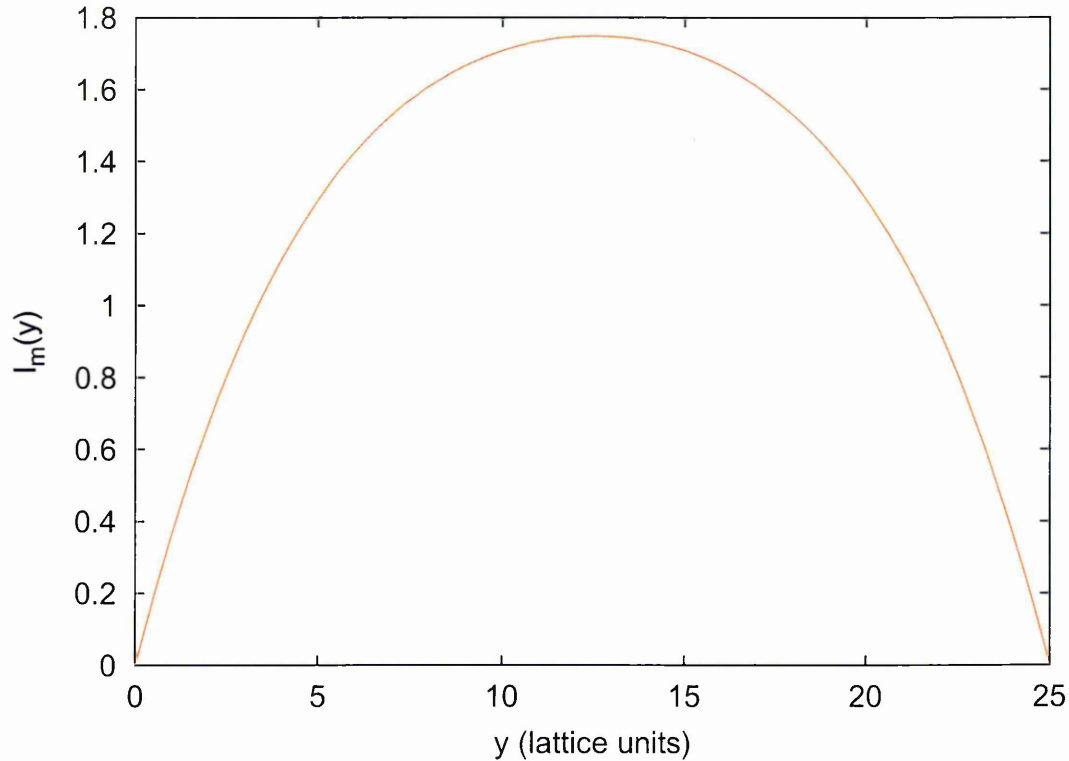


Figure 5.1: Cross channel profile of the traditionally accepted fourth power mixing length, see [148]. Note that an appropriate value for the von Kármán constant is subsumed into the definition, 5.19, for ℓ_{m4} as the coefficients.

5.2.3 Turbulent boundary layer implementation

In the following, investigations are carried out on flow in channel geometries, with an LB scheme modified so as to invoke properties of turbulence. It is well known that properties of such *wall bounded* turbulence are to a great extent determined by the fluid behaviour at or near the walls. Section 2.7 of the background discusses this in greater detail. Moreover, the processes at work in the buffer layer and viscous sub-layer are manifestly different to those at work in the flow bulk. Such matters therefore, ought to be addressed in investigations, if possible.

Incorporation of a sub-lattice scheme to model the boundary layers of a flow amounts to doing more science, but is in perfect keeping with the aims and objectives of this work and the interests of the sponsors. Efforts are therefore directed to this area in this work.

Regarding wall implementation for LB fluids, that is, solid boundaries with no slip condition, traditional methods range from first order schemes, such as the ubiquitous bounce back, to second order schemes such as that presented in chapter 4. General lattice closure issues are reviewed in section 2.6.3, page 101. In fact, later studies herein apply the second order scheme of chapter 4 in channel turbulence simulations. Such simulations however, take only ‘global’ account of aforementioned flow intricacies at or

near the boundary — behaviour which is known to be of great practical relevance.

Great interest lies therefore, in finding an accurate representation, within the LB fluid model, of turbulent boundary layers. In particular, it is desirable to build an LB *wall model* and to ‘match’ behaviour of such with experimentally verified theories valid in the boundary region. This might be regarded, not so much as science, as essential calibration of simulation boundary conditions.

The prime candidate here, with which to match results, is the logarithmic law of the wall; reference to section 2.7.3, page 125 reminds one of the nature of this. In addition, the model might be expected, on appropriate scales, to display characteristics reminiscent of the seventh power law, page 122. Section 2.7 explains how these are arrived at and their scope and validity.

On appeal to the fact that CFD methods often invoke a slip velocity at the edge node to account for the boundary layer, it becomes obvious that the improved lattice closure scheme of chapter 4 is eminently suitable for LB implementation of such. Indeed that is how motivation for the scheme arose, and hence it is adopted for that purpose in the following.

Wall models for boundary layer effects at sub-grid level

Incompressible, turbulent flow in pipes and ducts is a complicated problem. Different parts of the flow reside in different flow regimes: near the boundary (wall) there is a narrow but important *viscous sub-layer* in which the velocity varies rapidly, but flow is, for smooth walls at least, nearly laminar [118, 148]. Around the centre of the duct, in the so called *core* flow, there is fully developed turbulence. Between these two regimes there are at least two identifiable interstices, namely the overlap or buffer layer and the turbulent logarithmic layer. Some background science on boundary layers is provided in section 2.7.2.

Important features of the boundary layer exist on a scale smaller than that which the lattice spacing in a typical LB simulation would permit resolution. Conventionally, the viscous layers are deemed to extend out to say $y^+ \approx 30$ from the wall and the viscous sub-layer to $y^+ \approx 5$. For a typical turbulent pipe flow at say $Re = 10^5$, the latter amounts to about 0.1 percent of the channel width, [118]. In comparison, a typical cross flow number of lattice nodes would be of the order 100, implying that viscous dominated boundary features are typically an order of magnitude smaller than the inter-node spacing.

Means are therefore required to incorporate the effect of a turbulent boundary layer at sub-grid level; thus following traditional CFD, where explicit resolution of flow in the laminar viscous sub-layer is not commonly attempted, see e.g. [148]. Instead the

lattice fluid domain is closed by specifying that fluid on boundary sites has velocity in keeping with a *wall law*; that is, an appropriate *slip* velocity, U_s , is specified for the lattice boundary, which also implies an axial rate of strain S_{xy} . Correct matching of the slip velocity U_s to that of its equivalent regions in the wall layers is essential.

The simulations described in the next section take the explicitly modelled boundary to lie parallel with the x -axis and periodic boundary conditions are imposed, to form flow domain boundaries along y . Clearly then the solution must be translationally invariant and, accordingly, flow can be safely induced by a uniform body force, sections 2.6.3 and 2.6.4. Hence an additive constant is introduced into the evolution equation 2.103, since this is the exact equivalent of a uniform pressure gradient in the chosen geometry.

The purely axial time average velocity is assumed to fall linearly to zero over a sub-lattice distance at the wall, consistent with Prandtl's mixing length assumptions. Thus, in a practical calculation of pipe flow, a slip velocity U_s may be determined, in terms of the friction velocity u_τ (sometimes called the *stress velocity* [148]), which in turn depends upon the average shear stress on the wall, τ_{wall} [118]:

$$\rho(u_\tau)^2 = \tau_{\text{wall}} = \frac{(p_1 - p_2)A}{A_w}. \quad (5.20)$$

Here p_1, p_2 are the pressures at flow stations 1 and 2, assumed to lie a streamwise distance L apart. Also, $A = Wd$ is the cross sectional area of the duct (W being the duct width and d its (unspecified) depth) and $A_w = 2Ld$ is the area of the wetted perimeter. Accordingly:

$$u_\tau = \sqrt{\frac{\mathcal{G}W}{6\rho}}, \quad (5.21)$$

in which $\mathcal{G} = 3dp/dx$ is the pressure gradient. With a value of u_τ given by equation 5.21 a slip velocity may be obtained from any of the various relations of section 2.7.3.

Practically this may be done by first transcribing the LB lattice spacing D , to dimensionless off wall distance $y^+ = yu_\tau/\nu_0$ form, that is to $y^+(y = D)$. From there, an appropriate wall law can be chosen from those available, in accordance with their ranges of validity. Alternatively, but less likely, the *edge* lattice spacing Δ , may be so engineered as to put location of the slip boundary, at a y^+ location consistent with the chosen wall law model.

Note that for the law of the wall to be valid, the edge node spacing Δ must ensure that: $5 \leq y^+(y = \Delta) \leq \mathcal{O}(10^3)$. In particular here, the 'universal' mean velocity distribution

for the range $30 \leq y^+ \leq \mathcal{O}(10^3)$ is used, see equation 2.184 and references [73, 148, 150]:

$$U_s = u_\tau \left(\frac{1}{\kappa} \ln y^+ + B \right). \quad (5.22)$$

Therein, $\kappa = 0.41$ is the von Kármán constant and B , a constant of integration, which may be taken as 5.5. Hence, for this (logarithmic) law model to be valid, the edge lattice spacing Δ must satisfy⁴: $30 \leq y^+(y = \Delta) \leq \mathcal{O}(10^3)$. This may be achieved by various means, based around the relation:

$$u_\tau, \Delta, \nu_0, \text{ are such that: } 30 \leq \frac{u_\tau \Delta}{\nu_0} \leq \mathcal{O}(10^3) \quad (5.23)$$

where $u_\tau = \sqrt{\tau_{\text{wall}}/\rho} = \sqrt{\mathcal{G}W/6\rho}$ (equation 5.21); according to $\tau_{\text{wall}} = -\varnothing_{\text{h}} dP/4dx$ (equation 2.140) and $dp/dx = \mathcal{G}/3$. Also where, note, in terms of the lattice relaxation parameter, τ : $1/\nu_0 = 6/(2\tau - 1)$ from equation 2.114 for molecular viscosity.

This choice of a log law model is motivated by practical size constraints related to the geometry and the lattice size; it is by no means the only possibility however. The reader is referred to the general literature for alternatives.

Hence the slip velocity U_s , for use in bounding the lattice fluid domain, may be derived from consistent values for lattice fluid relaxation parameter, forcing, fluid density and duct width, as follows:

$$U_s = \sqrt{\frac{\mathcal{G}W}{6\rho}} \left[\frac{1}{\kappa} \ln \left(\sqrt{\frac{\mathcal{G}W}{6\rho}} \frac{6\Delta}{2\tau - 1} \right) + 5.5 \right]. \quad (5.24)$$

For these simulations Δ is chosen to be 0.99 lattice units; to ensure that whilst being less than a lattice spacing, it nevertheless appears as a normal inter-nodal spacing — not a necessity, but aesthetically pleasing. (Later some simulations are performed using $\Delta = 1$).

Corresponding velocity gradient at the unmodelled (off lattice) boundary now follow from the slip velocity 5.22 and the modelled depth Δ of the boundary layer:

$$S_{xy} = S_{yx} = \pm \frac{U_s}{\Delta} \quad S_{xx} = S_{yy} = 0. \quad (5.25)$$

This is of use where the second order boundary scheme of chapter 4 is employed. There, a method is developed for closing an LB simulation lattice with verifiably correct hydrodynamic behaviour to second order accuracy; i.e. of setting densities, f_i , on the undefined links with values consistent with those populating bulk lattice node at the lattice edge.

⁴Note that in the recent paper by the authors [53], this point is made erroneously.

According to that, values for the strain rate tensor S_{xy} , at the edge nodes, must be specified in some way as part of the closure. In contrast to chapter 4, where *measured* values are used for this, calculated from the local non-equilibrium densities by 4.3, here appropriate values are specified by the above wall law model, which are then assigned directly.

Thus, the lattice fluid domain is effectively bounded by a sub-lattice turbulent boundary layer of specified depth Δ ; that is, the lattice outer edge moves with a slip velocity U_s , consistent with the law of the wall, which ensures the correct average shear stress at the unmodelled (physical) wall.

Detailed presentation of simulation results for these models now follow.

5.3 Turbulent channel simulations and results

In this section, the LB model described in the last section is applied to simulate internal, pressure driven flow in a uniform cross section, infinite aspect ratio duct, with smooth walls and over a range of turbulent Reynolds number.

In particular, the intent is to investigate:

- Mean turbulent velocity flow profiles. Their shape, magnitude, gradient continuity, dependence on simulation parameters: (viscosity) relaxation parameter, forcing, and turbulence and wall model coefficients.
- Variation of friction factor with Re . The relation of our derived Moody curves data to theory and experiment.
- Boundaries. How these affect the flow via the turbulence algorithm and how they might be utilised as means to invoke wall laws.
- The wall law. How effectively it captures the sub-grid near wall behaviour and what errors it introduces to the result sets.
- The turbulent component of the collision parameter, $\omega_0(\mathbf{x}, t)$. Its variation, range of values and dynamic behaviour.

As regards description of the flow there are only a few basic data sets of relevance. Since the aim here is to quantify characteristics of the *mean* velocity field only, a very great reduction is affected in complexity of investigations and the amount of results generated. It will become apparent that most of the discussion and analysis of results, may be carried out within the context of just two types of data set — equivalently two types of plot. One is the mean velocity profile across channel. The other, which is derived from the former, quantifies both the retardation of mean velocity by friction induced shear and the dependence of coefficient of friction on the flow environment, i.e. with Reynolds number. Of these, the latter forms the substance of ‘derived’ results; that is, those not arising as raw output of the simulations. Visualisation of this data is presented in a Moody chart, which effectively summarises behaviour of these simple flows.

Other derived data sets are limited in number, though of high practical importance. They consist of channel averaged mean velocities and associated volumetric fluxes. Also the mean strain rate tensor. All derived data however, stem from raw data consisting of profiles of mean velocity, for this reason such profiles form the ‘nuts and bolts’ of simulation output.

Throughout, our *observed* or modelled mean profiles will be compared to either theoretical or experimental ones. These are discussed in some detail in preceding sections: 2.7 for the pipe geometry and 5.1.2 for ducts (of infinite aspect ratio, i.e. two dimensional geometry). All data correspond to that which emerges after some kind of statistical averaging of the turbulence.

5.3.1 Standard simulation domains implementation of channel geometry

Simulations were considered for various simulation domains, each with slightly differing qualities. Representations of the first order accurate boundary scheme can be found in previous chapters. For a discussion of those employed, see earlier chapters 2.6.3 and 2.6.4. First order accurate data is not presented here on account of space limitations.

Representations of the second order accurate boundary scheme are provided in figure 5.2; parts i) and ii) describe first and second order closures respectively. They have some features in common:

- they are infinitely deep with z and translationally invariant with x , in the sense of their detailed description in section 2.6, pages 85 and 108.
- Translational invariance is implemented using periodic BCs in the x direction (page 108).
- As a consequence of translational invariance, the driving pressure gradient is replaced by a uniform body force term in the lattice evolution equation; in the usual way, $\mathcal{G} = 3 dp/dx$ (section 2.6.4). The fluid is thus forced parallel to the x -direction: $F_i = 3\mathcal{G}w_i\rho c_{ix}$.

For both second order closures of figure 5.2, lattice boundaries (walls) occur at at $y = 0$ and W (implied), each having zero velocity imposed by the closure. First and last *on lattice nodes* occur at $y = \Delta$ and $y = W - \Delta$ respectively, denoted in the figure by blue lines, to highlight their evolution consistent with bulk nodes. This is in contrast to the first order closure where either the last lattice site is (not bulk); also to contra-forcing where all nodes may be considered bulk (their density field undergoes collision process).

Throughout, V denotes the *cross duct* average velocity, W the physical width of the duct and ν_0 the *molecular* viscosity of the lattice. The density of the lattice fluid was chosen to be 1.8.

Forcing must be small to maintain stability when the lattice fluid has the small viscosity necessary to access large Reynolds numbers; as characterise turbulent flow. Accord-

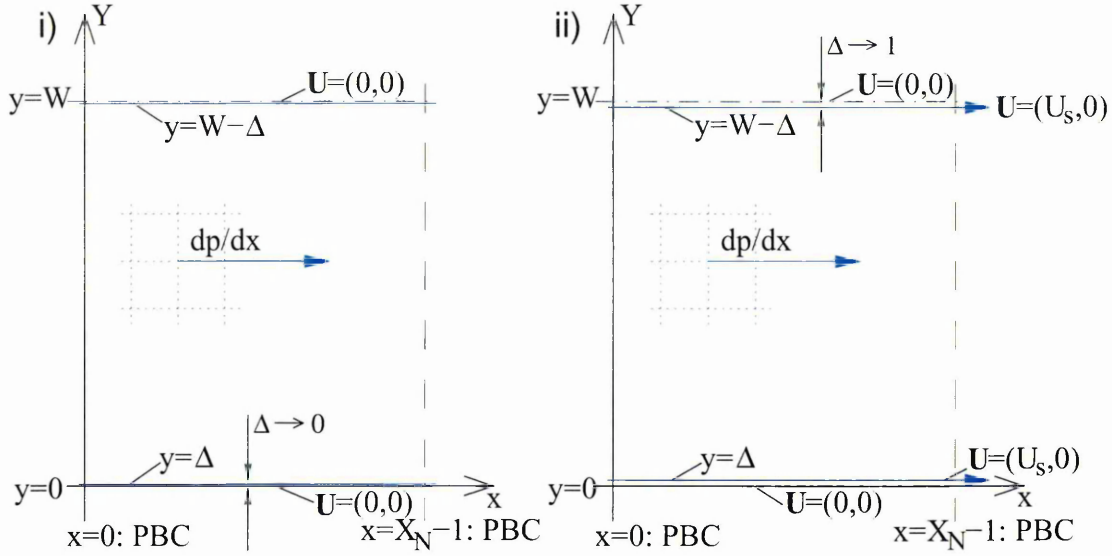


Figure 5.2: Computational domains for second order closure of turbulent channel simulations; these are described further in the text. Differences are as follows: Part i), has edge nodes which are ‘just inside’ the fluid (infinitesimally wet) and a zero velocity condition there. It describes initial simulations with the second order closure, but no law of the wall. Part ii) in contrast, has edge nodes which are significantly inside the bulk of fluid — Δ is the order of a lattice spacing — and, moreover, they have finite slip velocity U_s imposed, in accordance with the wall law.

ingly, for all the results presented here, $\mathcal{G} = 1.5 \times 10^{-5}$ (which is very small) was chosen. This, alongside a set of lattice resolutions, corresponding to widths of $W = 15, 40$ and 60 lattice units. The physical width of the simulated duct is actually $W = YN + 2\Delta$ where Δ is the width of the lattice sub-layer. The simulations correspond to constant spatial resolution.

The von Kármán constant at $K = 0.41$, is implied by the choice of mixing length function, 5.19; this has implications in calculating slip velocities on the first bulk node, in accordance with the chosen log wall model, as U_s is here set using equation 5.24. Note that the value B of equation 5.22 evident in equation 5.24 is 5.5, which is consistent with smooth walls [148].

In order to ensure sufficiently large Reynolds numbers:

$$Re = \frac{2WV}{\nu_0}, \quad (5.26)$$

consistent with turbulent duct flow, the molecular component of the collision parameter was varied in a range $1.991 \leq \omega_0 \leq 1.999$, close to its maximum value of 2 (where the corresponding variation in the molecular viscosity is rapid). The resulting variation in the measured Reynolds number was found to be $10^4 < Re < 10^5$: well into the turbulent regime. Convergence of the data was slow (several tens of thousand of time steps) on account of the very small molecular viscosities in use. All the data presented derive from

steady state velocity fields which have evolved for many thousands of time steps, without fluctuation; as determined by studying convergence in velocity ‘residuals’.

To implement a law of the wall, a second order closure scheme is required for the LB lattice in which it is possible to take shear as an input parameter. For this purpose, developments described in chapter 4 are built upon and utilised. In particular, for a discussion and basis of this requirement, see sections 4.2 and 5.2.3.

5.3.2 Results for wall law bounded channel: flow profiles

Mean flow profile results are now presented for turbulent duct flow; these have the ‘law of the wall’ of section 5.2.3 invoked to model the effect of the viscous sub-layer. Profile results for such begin in figure 5.3. A first appraisal of such then is very encouraging; qualitatively excellent profiles emerge for this particular case of channel simulation.

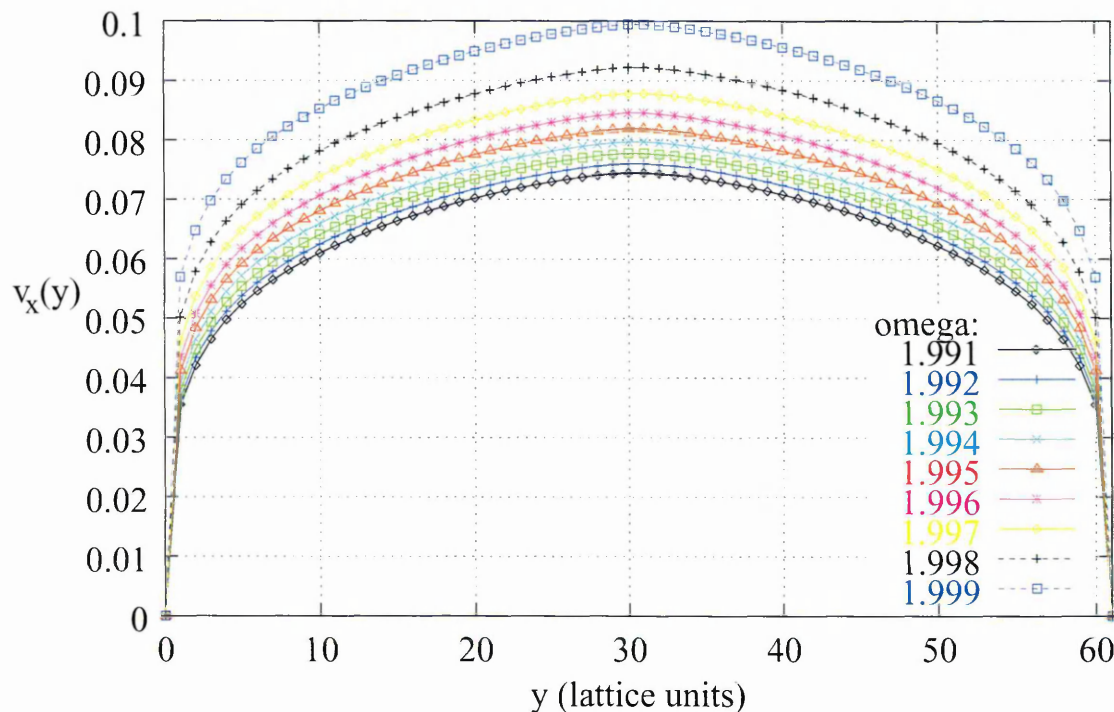


Figure 5.3: Nine steady state velocity profiles, measured after 7×10^5 time steps, for $1.991 \leq \omega_0 \leq 1.999$ at increments of 0.001. Average velocities, V , calculated by use of the trapezium rule and corrected for the viscous sub-layer are summarised in the table 5.1 (page 207) along with resulting Reynolds numbers.

Figure 5.4 shows a normalised steady state velocity profile. This is obtained from data measured after 7×10^5 time steps, for $\omega_0 = 1.995$, resulting in an average velocity (calculated by use of the trapezium rule and corrected for the viscous sub-layer) of $V = 0.069722$, which yields a Reynolds number of 20,357. The velocity profile shown in figure 5.4, into which the unmodelled sub-layer data has been inserted, clearly exhibits

all the expected characteristics of a turbulent profile [118,148]. Moreover, it does across the whole width of the duct, without any spurious slip velocities at the boundary, either at the wet boundary of the viscous sub-layer or the wall.

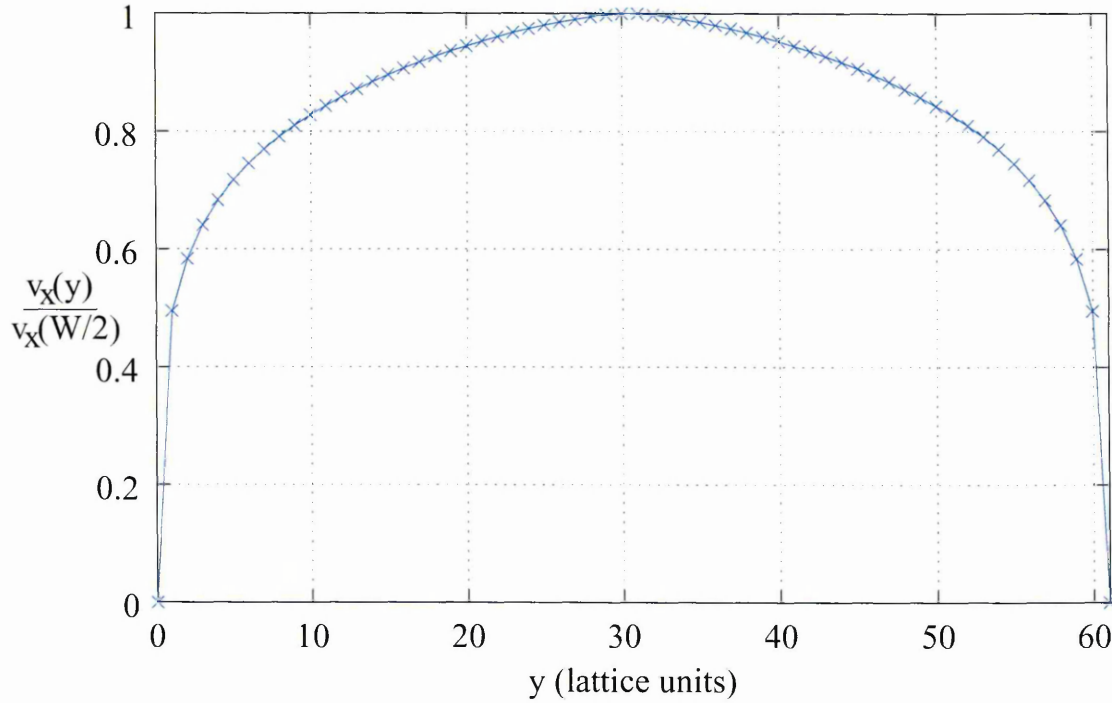


Figure 5.4: A normalised steady state velocity profile selected from those of figure 5.3, corresponding to $\omega_0 = 1.995$. The data result in an average velocity, V , of 0.069722 which yields Reynolds number $Re = 20357$.

ω_0	ν_0	\bar{v}	Re	f_{DW}
1.991	0.009457	0.062706	10151	0.031017
1.992	0.008210	0.064172	11693	0.029616
1.993	0.007003	0.065794	13708	0.028173
1.994	0.005838	0.067620	16444	0.026673
1.995	0.004716	0.069722	20357	0.025089
1.996	0.003640	0.072220	26371	0.023383
1.997	0.002616	0.075344	36701	0.021484
1.998	0.001650	0.079605	58193	0.019246
1.999	0.000758	0.086633	126726	0.01625

Table 5.1: Table of measured simulation parameters for the profiles presented in figure 5.3. These are provided to give a feel for the parameter range within which a standard LB can easily simulate.

Are these profiles *quantitatively* good? To investigate this, theoretical results such as equation 5.2 and 5.3, for flow in ducts, along with equation 2.184 for flow in pipes, must be used as yardsticks. Each of these require simulation data to be recast in terms of dimensionless variables. Whilst this is not a problem and is carried out in the following, it is important to note that this introduces an element of ambiguity to results via the

empirical scaling parameters (here u_τ and f_F in particular). The ambiguity arises in the fact that, depending on the perspective adopted, u_τ and f_F may be considered either as emergent variables of the simulations (in real experiments or CFD), or ones which are effectively input (into the LB sub-layer model). This matter is discussed later.

Two established or theoretical velocity profiles are now introduced as the latter two data sets of figure 5.5, which, to be concise, show only the left half of the channel domain. The lower, short dash, being equation 5.2 for turbulent flow in a duct whereas the upper, long dash, corresponds to the universal velocity distribution in a pipe. Also shown are plots of two simulation profiles which were obtained for a channel width of 16 (these simulations had an axially central node, the point for which is not shown) and at two values of molecular viscosity $\omega_0 = 1.991$ and 1.999.

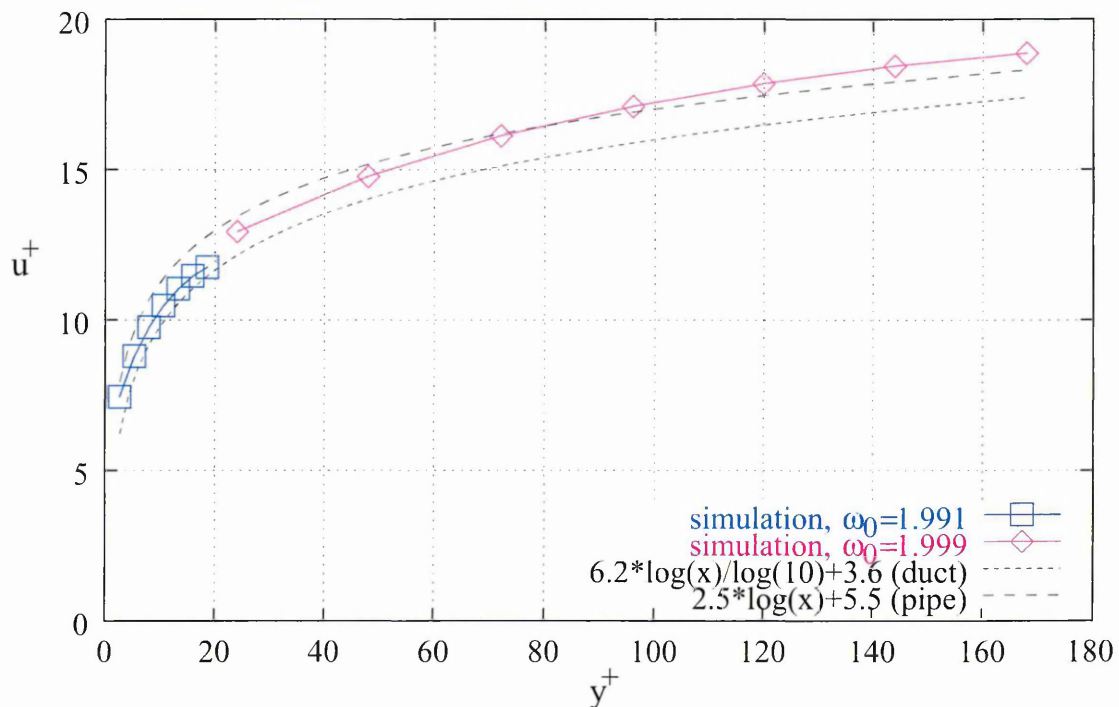


Figure 5.5: Dimensionless plot of mean turbulent velocity profiles generated with turbulent LB algorithm and law of the wall incorporated. Two simulation data sets are included (in blue and magenta, boxes), representing the upper and lower investigated extremities in relaxation parameter, ω_0 . Also included are theoretic profiles of earlier sections, equations 5.2 and 2.184, for the duct and pipe respectively (in black, dashed).

Obviously, the duct data at this stage appear qualitatively acceptable, although both profiles seem to fall somewhere between established data for pipes and that for finite rectangular pipes (i.e. ducts). To get a better qualitative feel, it is necessary to plot on semi-logarithmic axes; this is done in figure 5.6 which shows the same data.

Some minor deviations from the straight line are therein evident, one of which appears consistently: a small wall defect appears (as a slightly reduced profile gradient) on the

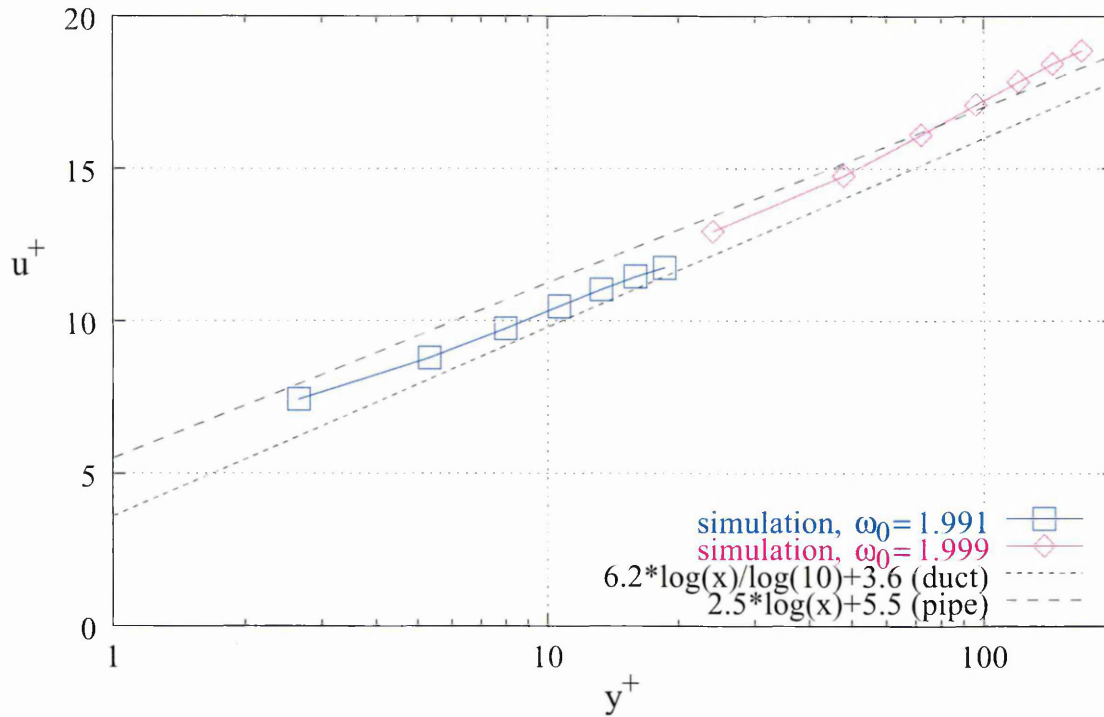


Figure 5.6: Semi-logarithmic representation of the dimensionless profiles in figure 5.5. This form is supposed to bring out the logarithmic nature of the profile around the overlap region — the profiles should appear as straight lines, ideally coincident with that for the duct (the lower of the two theoretic ones (black, short dashes)).

first explicitly resolved node. It may be due to systematic error; the location corresponds to the Dirichlet BC slip node. In addition, a further and similar defect appears at channel centre. There is also a slight difference in gradient between the two plots, which corresponds to an apparent, marginal viscosity differential. These results are, however, very encouraging. The need arises, however, to investigate whether such subtle characteristics in the data are universal — to these models and simulations.

Originally it was envisaged that, upon establishing good fit to straight line (on the log plot) and therefore clear values for the $Re = 1$ ordinate intercept and plot gradient (B and κ parameters respectively, which effectively describe the modelling strategy), then two logical continuations would emerge. One relates to the fact that B and κ and their ‘fit’ indicate the quality of our approach. Hence, improvements could be made in results by altering certain input parameters and monitoring variation in B and / or κ . Thereby optimisation of the input parameters is enabled. The other relates to the fact that B and κ might themselves provide a means to refine the simulation data, in that using updated or calibrated values for input variables in the log layer model (to calculate slip velocity in the $\mathcal{O}(2)$ boundary scheme, note), might ensure that wall conditions more closely resemble the nature of the bulk — as it emerges under a LB simulation.

Either process, if carried out recursively, potentially forms a basis for optimisation or

calibration of simulation data. However, in view of the initial quality of fit to straight line, which at first glance seems a little delicate, the potential is eroded somewhat.

It becomes of interest to see how the profiles vary over the range of relaxation parameter set out in figures 5.5 and 5.6. The full set of profiles so derived are provided in figure 5.7, which shows data obtained for $1.991 \leq \omega_0 \leq 1.999$ in intervals of 0.001. Figure 5.7 makes it apparent, however that, due to plot overlap, it is very difficult visually to pick out any repeating or consistent features.

The figure does hint, however, at the prospect of collecting all profile points on one plot, to obtain a fit to the data and thereby to glean an idea of possible revised values for $1/\kappa$ and B . This might be done to give a feel for how the bulk scheme would dictate these parameters. Figure 5.8 shows this; a straight line is fitted to the data, generated using gnuplot's standard fit routine. The fit line is shown to guide the eye.

This data might be interpreted as good evidence for a tendency toward overall logarithmic behaviour of the bulk LB model; the 'scatter' is quite low (standard deviation $\sigma = 1.2$ and 2.57 in gradient and intercept respectively) and a straight line fit seems relatively obvious; although there is some visible curvature. Values for B and $1/\kappa$ derived from this data are $B = 4.13 \pm 0.1$ and $1/\kappa = 2.82 \pm 0.03$ respectively. Both the value for B and that for κ (at 0.36) lie outside ranges expected by considering other pipe analyses: $[4.40, 5.85]$ and $[0.38, 0.41]$ respectively (see page 128); such might be expected.

This picture is misleading however, as the gradient value ($1/\kappa$) that is expected should be appropriate for *duct* geometry, as provided by an equation such as 5.2. That is, 2.82 should⁵ be compared against $6.2/\ln 10$, which evaluates to 2.69 . This means the fit is better than at first appears; unfortunately however, no spread of values is available to the author for a duct geometry.

The value for $1/\kappa$ appears closer to the upper limit of its accepted range when one considers relation 5.3, derived by Deissler [32]. As previously stated, that result arises from an accepted experimental study of air in pipes, even if one that differs from other result sets quite markedly. Values for B and $1/\kappa$ determined therein are 3.8 and 2.78 respectively which improves the perspective on results generated here — they appear much better.

Uncertainty in κ itself gives rise to the range: $0.3509 \geq \kappa \geq 0.3584$, which lies just outside the new range permitted by Deissler's data $[0.38, 0.41]$. The value for B is brought within acceptable limits in the same way: $4.13 \in [3.8, 5.85]$.

On another vein, there is the matter of slight observed discrepancies in all the profiles at each end; wall and mid-channel. It is of interest to see if these exist under differing

⁵As an aside, note that natural or Napierian logarithms $\ln(\cdot)$ appear as $\log(\cdot)$ in gnuplot plots.

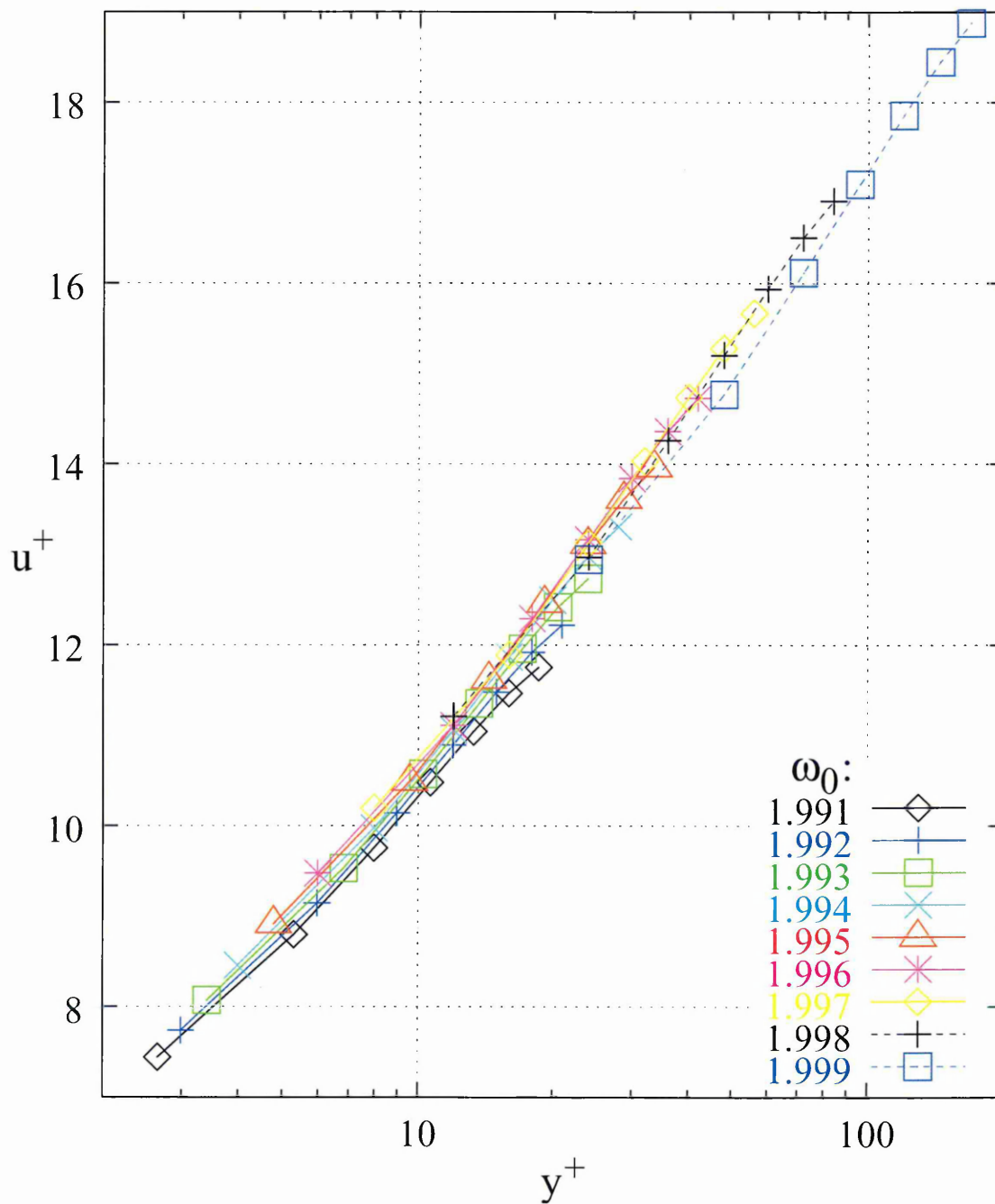


Figure 5.7: Semi-log dimensionless profiles derived at nine relaxation parameter values for channel width of 16 lattice units. As can be seen (just!), the profiles are almost straight, but they have slight though consistent discontinuities in gradient adjacent to the boundary. Gradients tend to increase with ω_0 and with y^+ .

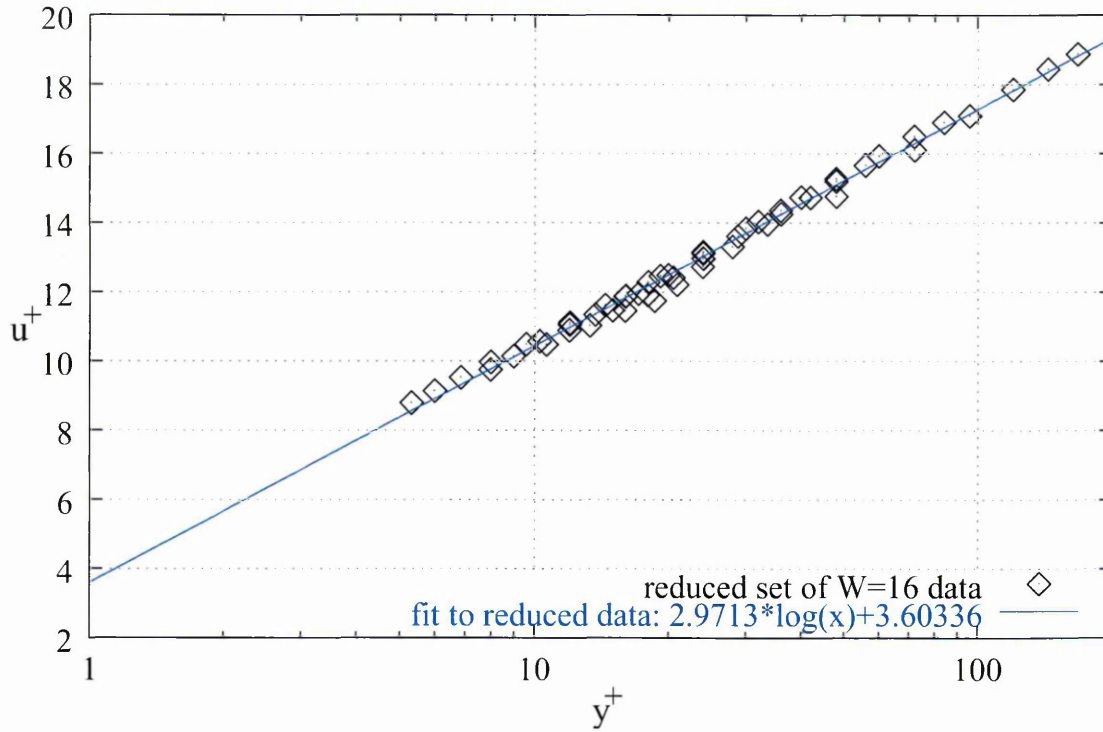


Figure 5.9: Plot as for figure 5.8 but with data corresponding to the first (boundary) LB node removed to aid the fit. The effect of removing this data results, however, in worsened values for B and κ .

better spatial resolutions.

Figure 5.10 shows two profiles generated for a channel of width 61 (60 explicitly resolved LB nodes). The curves pertain to two values of relaxation parameter. As for figure 5.6, these are $\omega_0 = 1.991$ and 1.999 respectively. The following characteristics and corollaries are therein evident:

- The profile shape is relatively consistent across relaxation parameter values (viscosities) and, to some extent, channel widths.
- The profile shape has a vague ‘wave back face’ S-like reflex curvature. It consists of:
 - A near wall region of lower gradient. This portion most closely resembles established predictions for pipes and ducts; it lies somewhere between the two.
 - A channel medial region which has high mean velocity with respect to predicted values for both pipes and ducts and which has higher gradient.
 - A channel central region with mean velocity much too high with respect to predicted values for finite systems. This region has a falling gradient.

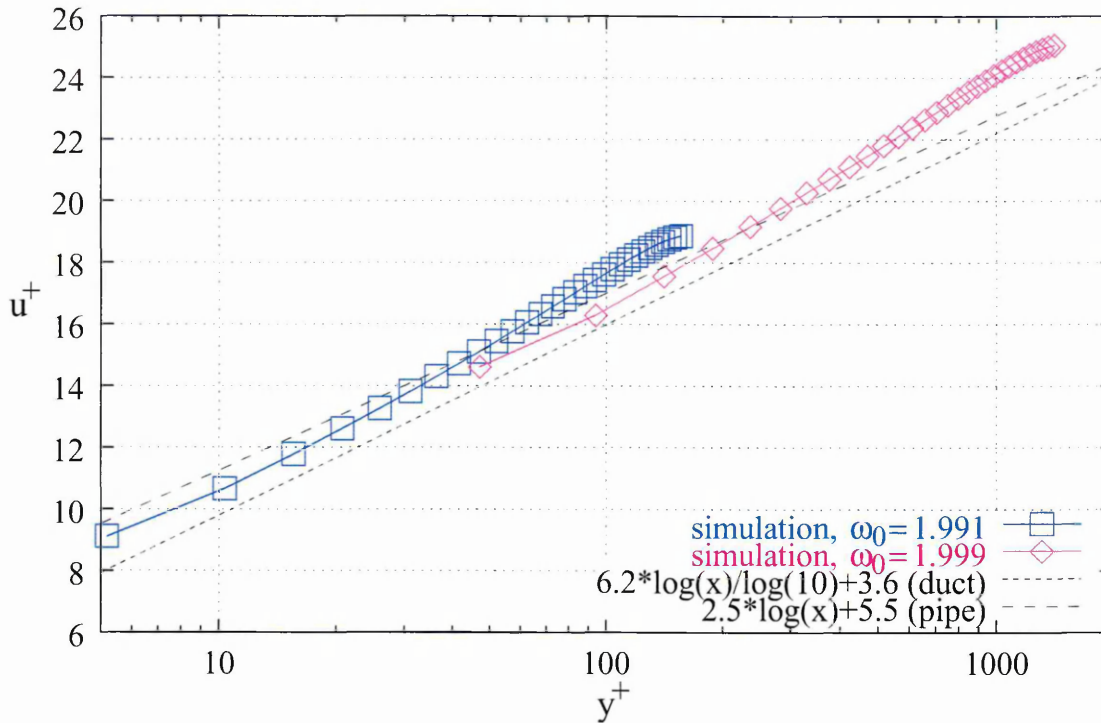


Figure 5.10: Equivalent (semi-log, dimensionless velocity profile) data to figure 5.6 but for a wider channel (channel width $W = 61$; that is 60 explicitly resolved LB nodes). The better resolved profiles show greater consistency, though still significant quantitative departure from what might be regarded as desirable (the duct data in black, short dashes).

- Interestingly, the inner portions (channel central) of the profiles qualitatively resemble *defect law* predictions rather well.
- There is still evidence of a slight boundary induced gradient discontinuity adjacent to the LB boundary node; this must be considered erroneous.
- Straight line fits to the profiles, whilst possible, will be systematically inappropriate in the light of their consistent ‘S’ shape.
- Fits to selective portions of the profiles might prove of interest, despite their lack of physical validity.
- It is obvious that descriptive parameters such as B and κ values derived from any straight line fit, whatever its basis, will be incapable of matching those predicted or determined by other means (the two dashed lines included amongst others).
- Crudely combining data from profiles with differing relaxation parameter values (as was done for figures 5.7 to 5.9) is not appropriate and is therefore not attempted.

It should be noted that the general form of data presented in figure 5.10 is entirely similar to that generated by Teixeira in [138].

Bearing in mind that in physical (channel) space each data point in the figure represents an equivalently sized portion of the channel (for the duct case at least) it is apparent that average velocities calculated from such data will be consistently high with respect to theoretical and experimental predictions. This adversely affects derived data, namely friction factors and Reynolds number values. Friction factors in particular are affected, as their dependency on the mean is inverse square, see equation 5.38; they will be too low by a significant margin. Reynolds number values scale proportionately with the mean velocity and hence will be too high, though not by the same margin. The net effect of such should be to steepen Moody curves, pushing them at the same time to the right on the chart and down below that required. Such ‘predictions’ are tested in the next section.

Two approaches to matching these wider profiles to theory might be considered as a last resort; they are to: determine appropriate criteria by which profiles may be consistently broken down and to subject remaining portions to straight line fitting procedures. The variation by profile of fit parameters for such may then be viewed in the light of predicted values. Alternatively, points which display minimal defect law character may be selected (from all profile points) and a fit applied to these. The latter is tantamount to getting a feel for the regime over which our model produces results that are consistent with predictions of other methods.

At this point it is not clear what lines of investigation should be followed to improve the quantitative validity of these results. One possibility is outstanding however, being suggested by the variation in observed B value (intercept) that occurs with simulation relaxation parameter ω_0 . Such behaviour suggests that — the model being highly ω_0 dependent — differing relaxation parameter values might in effect denote differing levels, or ‘intensities’, of turbulence, (on top its understood determination of Reynolds number variation). If that were the case then ideally profiles should only be compared between simulations with equal ω_0 values and that Reynolds variation should only be invoked using the channel width (or forcing, an issue which is ignored for the moment at least).

To investigate this point, simulation data is collected for a set of channels of various widths, but each having consistent relaxation parameter. When two such profiles are compared, however, as is shown in the next figure 5.11, it is apparent that no progress will be made, as again the possibility of finding a globally consistent fit seems low. The usefulness of performing this analysis is therefore limited and is not pursued further.

On a further line of investigation, equation 5.1 can be used to generate a set of specific profiles against which simulation results may be compared. This permits our simulations to be assessed with respect to other established works of Donch [34] and Nikuradse [98] (via Goldstein [50]). The profiles are specific in that they depend upon (are scaled by) a

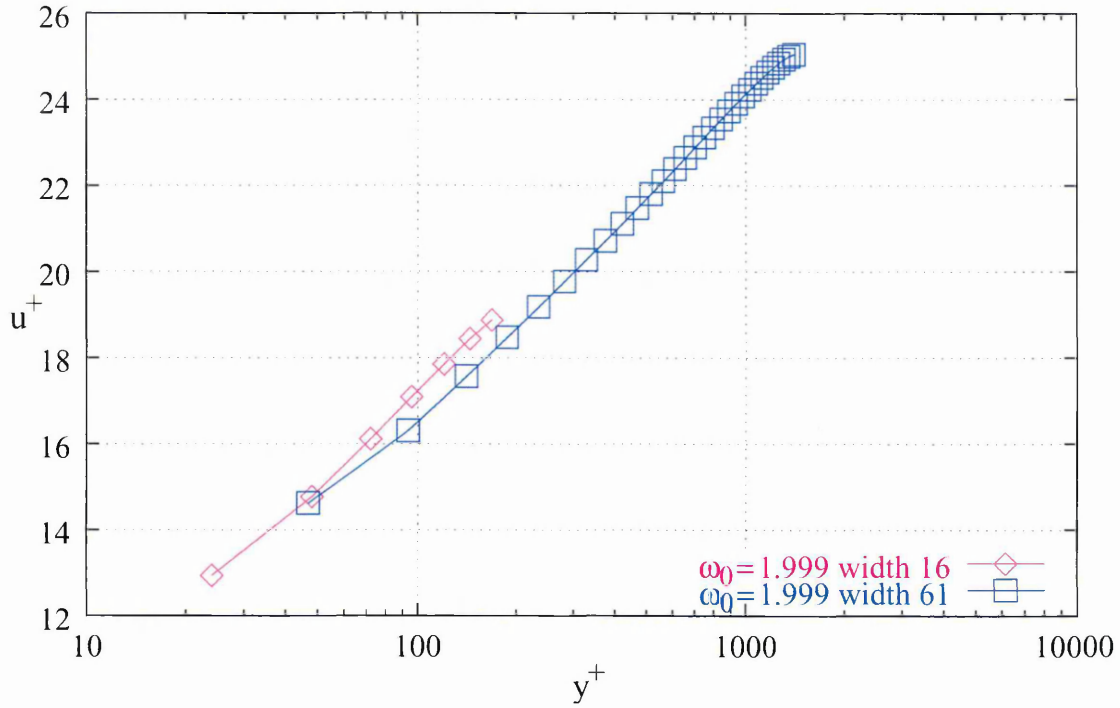


Figure 5.11: Comparison between turbulent velocity profiles for LB fluids with matching relaxation parameter ($\omega_0 = 1.999$). The two data sets are for channels of width $W = 16$ and 61 . The intention behind the plot is to investigate the possibility of obtaining values for $1/\kappa$ and B which are consistent between simulations. It is herein evident however, that such is not possible; whilst for sections of each profile, gradient parameters are similar, the same is not true for intercept parameters (hence B in particular is not consistent).

measured peak mean velocity, as can be seen once rearranged:

$$v = 3.385v_\tau \left[\ln \left(1 - \sqrt{1 - \frac{2y}{W}} \right) + \sqrt{1 - \frac{2y}{W}} \right] + 0.172v_\tau + v_{\text{pk}}, \quad (5.27)$$

where y_c has been replaced by $W/2 - y$.

Data corresponding to solution of this equation, for specific duct realisations, have been calculated using peak velocities (and mean velocities for v_τ) obtained using the LB simulation data. Figure 5.12 shows these for two relaxation parameter values of 1.991 and 1.999 alongside actual simulation data for direct comparison. Note that owing to the non-universal character of the relation 5.27, axes in the plot are linear and are expressed in lattice units.

Therein, (figure 5.12) it is again apparent that the current model's results show a slight departure, in a quantitative sense, from those suggested by tried and tested means. No simple form is, as yet, apparent by which this departure may be classified and thereby addressed.

Adopting a similar approach, Pai's relation, equation 5.4, might also be employed for

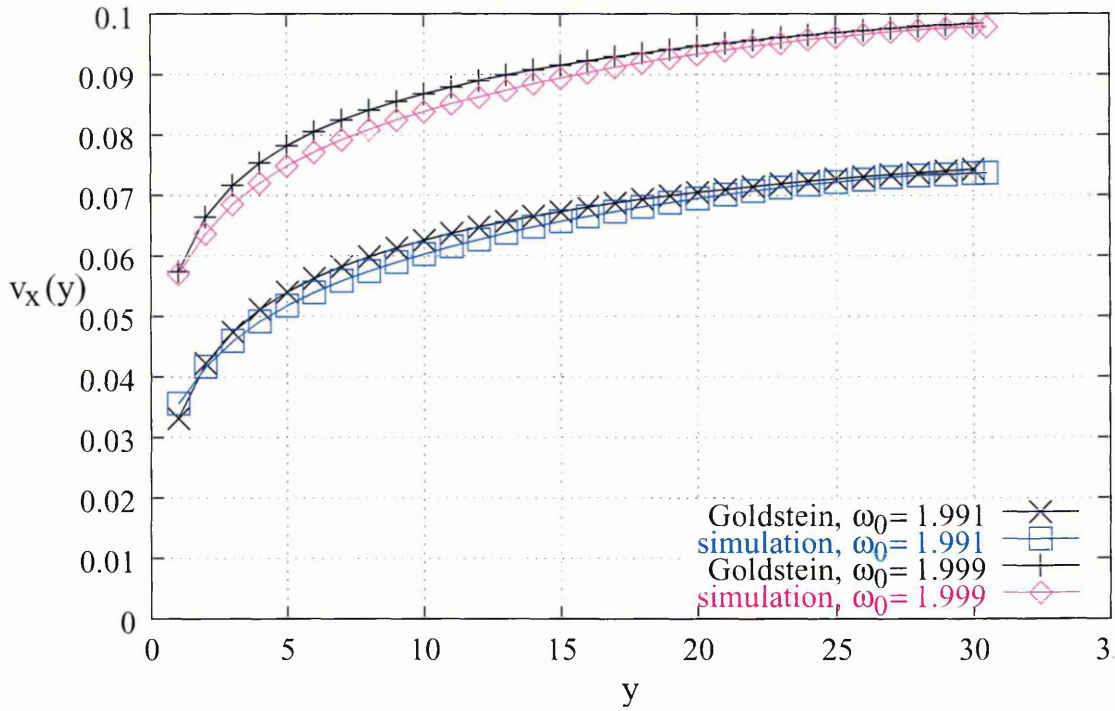


Figure 5.12: Comparison, in the physical domain (lattice units), between LB turbulent flow profiles and those derived using the relation 5.27, which is based on experimental data collated by Goldstein. Results are for a channel of width 61 lattice units and for two molecular relaxation parameters, corresponding to viscosities: 7.53×10^{-4} and 8.34×10^{-5} (ω_0 being 1.991 and 1.999 respectively).

the same purpose as above. This is valid over the entire channel, though data for only half a channel are needed here. They are presented in figure 5.13, which is of the same form as 5.12.

As can be seen, data generated using the LB turbulence model perhaps matches Pai's relation more closely than all others considered. This is particularly true at high relaxation parameter values where at least one curve is a very good match. This is encouraging, as Pai derived relation 5.4 by considering the Reynolds momentum equation 2.67.

It is perhaps not surprising that some discrepancy exists, however, as discrepancies exist between those results which here are deemed 'established'. To emphasise, Pai's results don't match Goldstein's relation all that well. In the light of such then, it is of some value to determine a form of quantification for relative similarities between the data sets. This is briefly covered next.

To do this, results generated using the various means must first be normalised, then an arbitrary differential quantification applied. Here it is sufficient to use a simple cross channel sum of absolute difference between profile values, like:

$$\Delta_c = \sum_{Y=1}^{Y \leq W/2} \Delta_p, \quad (5.28)$$

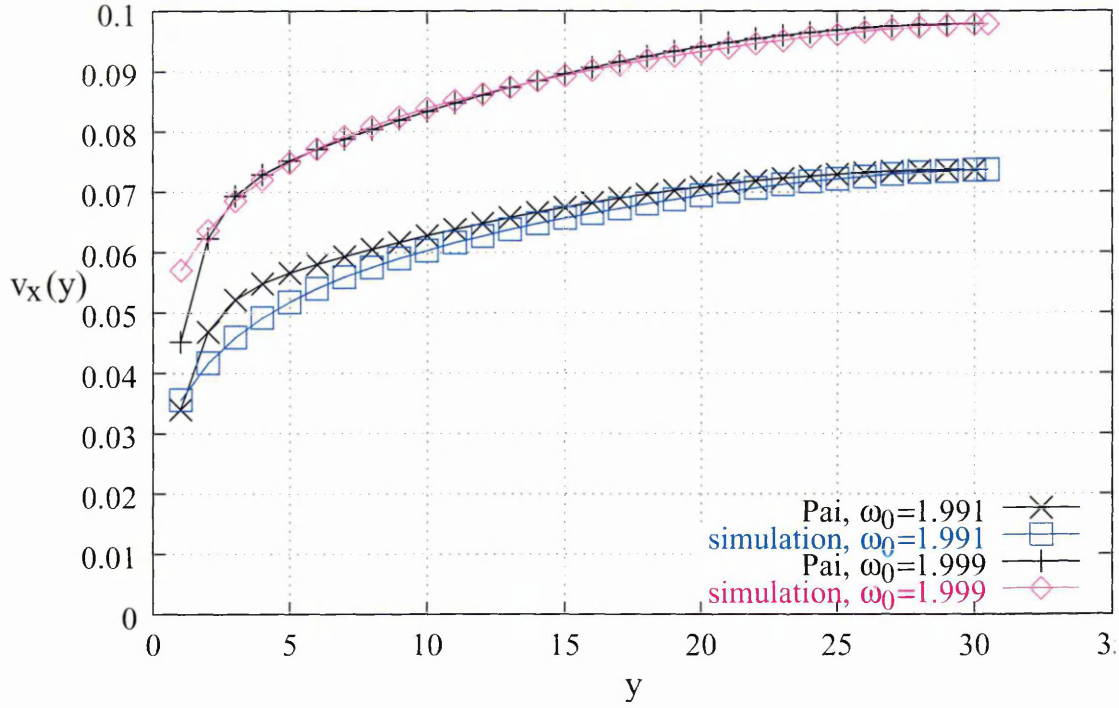


Figure 5.13: As for figure 5.12 but for semi-empirical result of Pai, 5.4; a comparison, in the physical domain (lattice units), between LB turbulence profiles and those derived using Pai's relation 5.4. Profiles are for a channel of width 61 lattice units and for two molecular relaxation parameters, corresponding to viscosities: 7.53×10^{-4} and 8.34×10^{-5} (ω_0 being 1.991 and 1.999 respectively).

where, Δ_c is a cross channel sum of absolute profile difference, Δ_p :

$$\Delta_p = \sqrt{(v_{\text{profile A}} - v_{\text{profile B}})^2}. \quad (5.29)$$

It is possible to determine this function for each binary comparison between result sets, A to B . For the three sets of results: Goldstein, Pai and the LB turbulence model, only three non-degenerate cases need be considered.

Data collected for this purpose are presented in figure 5.14 (as it varies with relaxation parameter, ω_0). Figure 5.14 considers only duct data. LB turbulence model data is therein denoted 'simulation'. It is also possible to simultaneously compare against dimensionless equations such as that for the duct (e.g. equation 5.2). Results for the three extra two way comparisons so generated are also shown in figure 5.14. Data generated using the dimensionless relation 5.2 are denoted 'Donch-Nikuradse'.

As is evident, the two data sets which most closely resemble each other are those from Goldstein's relation, 5.27, and those from Pai, 5.4. For these, the cross channel sum of absolute differences varies around 0.01. Other comparisons are all substantially worse than this. Significantly, comparisons against equation 5.2 (Donch-Nikuradse) reveal some

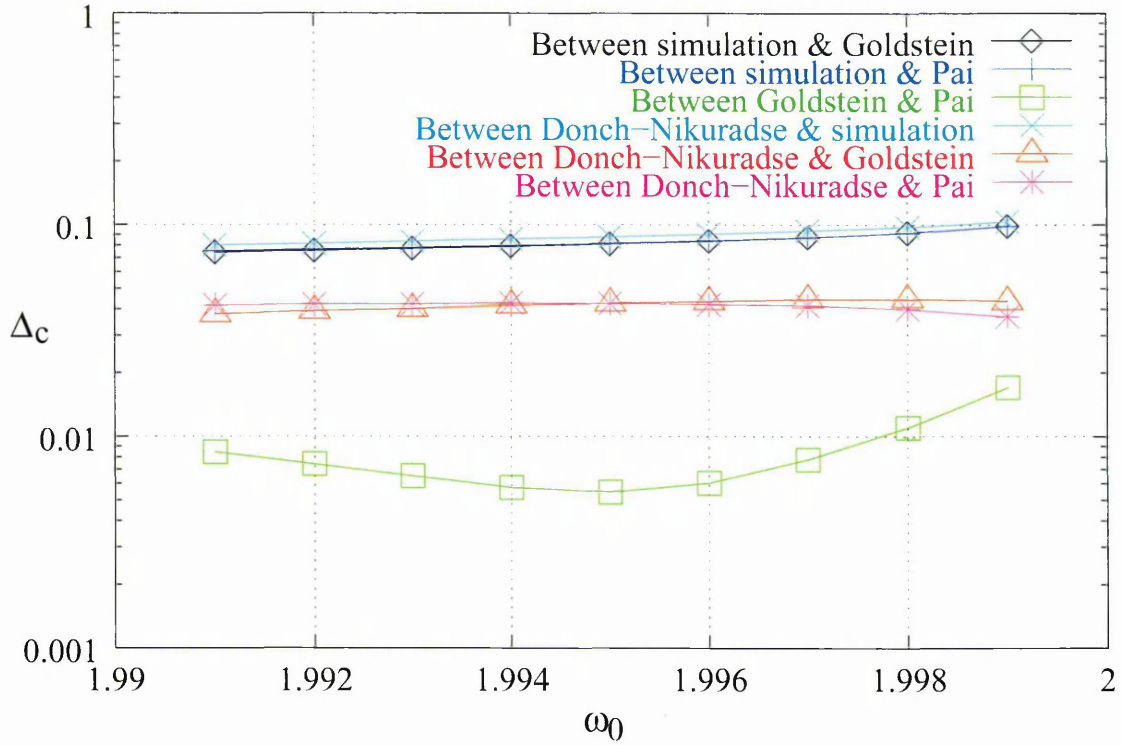


Figure 5.14: Variation of Δ_c , the cross channel sum of absolute profile difference parameter Δ_p , with simulation relaxation parameter ω_0 (see equation 5.29). There are six binary profile comparisons, as suggested in the key. The data congregate into three main bundles. The highest difference parameter occurs in the uppermost bundles, which unfortunately pertain to differences with LB simulation results. Progressively lower differences occur, the lowest of which is between results of Goldstein and Pai.

discrepancy against Goldstein and Pai (the other two ‘established results’). However, the most serious departure occurs for the comparison between equation 5.2 and LB simulation results. This demonstrates the relative inaccuracy of of simulations.

On a similar line of attack, it is also of interest to be able to visualise how such a difference parameter, Δ , varies in accordance with channel location, y .

An attempt is made in figure 5.15 to shed light on the nature of such data, in a similar way to figure 5.14. Here the difference parameter used is referred to by Δ_{rp} , as it is appropriate to sum over omega values in contrast to the previous analysis. Explicitly, Δ_{rp} is defined as follows:

$$\Delta_{rp} = \sum_{\omega_0=1.991}^{\omega_0=1.999} \Delta_p. \quad (5.30)$$

Such an approach to condensing the data is, however, not revealing on this occasion; the summation seems to erase any clear or discernible features of interest from the data. It must therefore be concluded that no obvious functional dependence of difference parameter exists with respect to channel location; the contributions at various relaxation

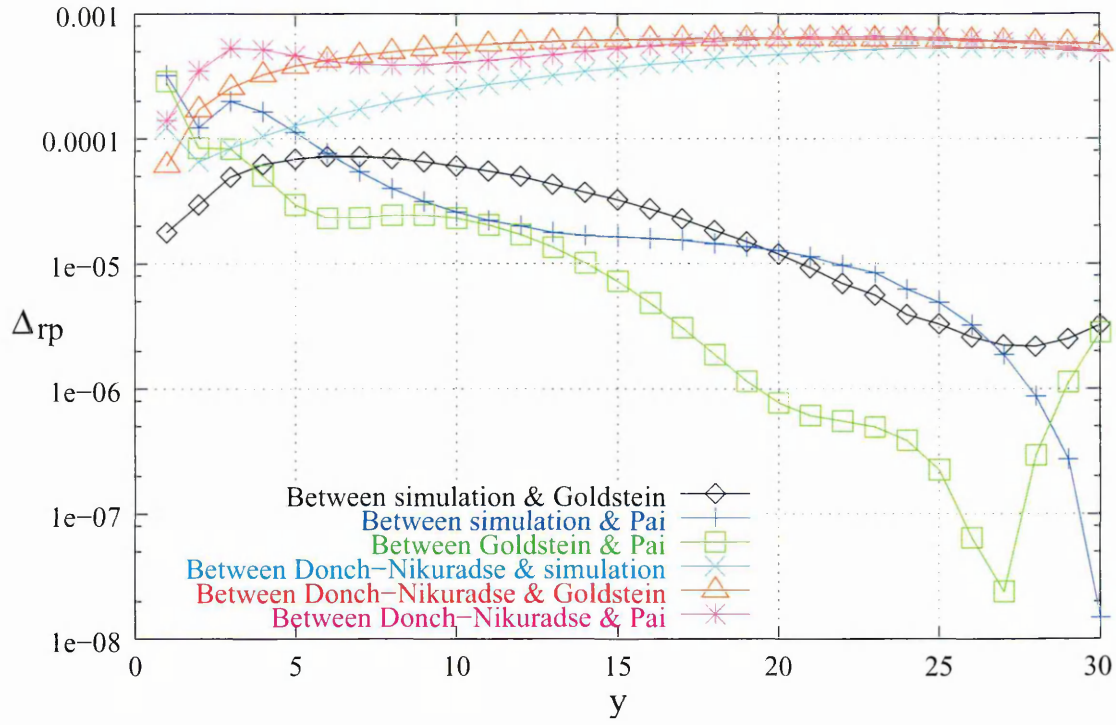


Figure 5.15: Variation of absolute profile difference parameter Δ_{rp} with cross channel location (equation 5.30), for the profile differences suggested in the key. It is clear that no systematic features in the data will be made visible in this way, the plot is included for completeness only.

parameter values essentially interfere.

The above, relatively inconclusive analyses, are not the only way to look at profile quality as a function of channel location. Indeed, the fact that our profiles qualitatively resemble experimental *velocity defect law profiles*, alludes to one other serious means to clarify the nature of the results generated.

The defect law (not described in any detail in the background) arises analogously to the wall law, when a dimensional analysis of channel flow is carried out. It is another well established aspect of turbulent channel flow theory. In summary, upon observing physical dependencies in the core flow, a universal form for the core profile may be derived, which appears as follows:

$$\frac{v - v_{pk}}{v_\tau} = G(\eta). \quad (5.31)$$

This is in direct analogy with equation 2.169 of section 2.7.3. Note that equation 5.31 simply instantiates equation 2.171 of the background (the velocity defect law) by taking half the channel width $R \equiv W/2$, to parameterise the boundary layer thickness δ and, wherein, η is then defined as dimensionless channel location:

$$\eta = \frac{y}{W/2}, \quad (5.32)$$

which is normalised to 1 at mid-channel. See for example [128, 139, 148, 150]. Note no confusion should arise between η defined here and the Newtonian coefficient of fluid viscosity defined elsewhere.

The precise form of $G(\eta)$ will be of interest here; unfortunately some inconsistencies arise in the literature, both on this subject and on the ‘wake function’ which follows. Moreover, some ambiguity is frequently communicated of the meaning of the velocity defect function, as it pertains to the ‘duality’ between expected and measured values. These points are discussed in the following.

To fill in some background details, instances of velocity defect behaviour are derived by integration of specific forms of the governing fluid dynamical equations. Section 2.7 does this explicitly for laminar flow. For turbulent flow the arguments are more convoluted, but the principle remains the same. In that case the start point is the turbulent ‘energy budget’, a differential equation derived considering turbulent versions of the fluid energy equations, 2.25.

The process will not be entered into here. Suffice to say that this is how the likes of Prandtl, von Kármán [141] and Millikan [95] first derived analytic forms for turbulent flow in a pipe (and thereby instantiated the more general wall and defect laws). The arguments of von Kármán are known as similarity law and, owing to the very concise overview of this presented in Tennekes and Lumley [139], these are what the following material is based upon.

As an alternative, which is to some extent equivalent for the channel, it is possible to assume that the law of the wall (logarithmic overlap region) extends its validity to channel centre, which permits some simple rearrangements. See in particular Tennekes and Lumley and Spurk [128]. This amounts to the implicit assumption that the velocity defect law in a channel is coincident with the wall law, in that if the flow is fully developed, the channel width (or half this) fully and solely characterises inertial length scales; a point which is obviously only relevant to channel flow.

An established form for this expression is available in Tennekes and Lumley:

$$\frac{v - v_{pk}}{v_\tau} = 2.5 \ln \eta - 1, \quad (5.33)$$

which, whilst strictly only valid for pipe geometries, is of some relevance here. However, if one assumes the universal logarithmic overlap velocity distribution, equation 2.184, to hold at channel centre $y = W/2$, and that the mean x -wise turbulent velocity is v_{pk} there,

as is done in Spurk [128], then

$$\frac{v_{pk}}{v_\tau} = 2.5 \ln \frac{v_\tau W}{2\nu_0} + 5.5. \quad (5.34)$$

Whereupon back substitution into equation 2.184 gives

$$\frac{v - v_{pk}}{v_\tau} = 2.5 \ln \eta, \quad (5.35)$$

which is to be contrasted with equation 5.33.

The main reason this is important is in order to derive an equivalent velocity defect relation for the duct geometry case, to which our simulation data pertain. Also because any discussion of how measured or simulation profiles differ from logarithmic, depend critically on a precise specification. Derivations for the duct case are not carried out in this work, see further work 6.1.

It is presumably instructive to look at how profiles derived using the LB turbulence model with law of the wall boundaries differ from a velocity defect law derived for pipes, as a check to the idea at least. To continue (with the pipe formulation), simulation data must firstly be converted to ‘defect form’, by subtracting the peak velocity, as occurs at channel centre, and normalising with respect to the friction velocity, u_τ . Similarly, channel position is normalised to the half width to give η values. The difference is then sought between the aforementioned and values derived using a theoretic defect law; this is often known as a ‘wake function’, denoted $W(\eta)$.

In Tennekes and Lumley [139] a specific wake function is defined as follows:

$$W(\eta) = G(\eta) - 2.5 \ln \eta + 1. \quad (5.36)$$

This is the functional difference between the observed point mean velocities and the defect law derived from a logarithmic law assumption. Note that what is meant by $G(\eta)$ seems here to be *measured* $G(\eta)$ (from simulation), hence meaning $(v - v_{pk})/v_\tau$ by equation 5.31.

It is suggested in [139], that the wake function is typically approximated by a sinusoidal form:

$$W(\eta) = \frac{1}{2} \left[\sin \pi \left(\eta - \frac{1}{2} \right) + 1 \right]. \quad (5.37)$$

(Working through this analysis and a preview of the following plot 5.16, makes it apparent that with this form (equation 5.37), the -1 term of equation 5.33 is essential). The equivalence of using equation 5.35 instead, along with a suitably adjusted sine term in the wake function 5.37 is not investigated.

Function 5.37 is plotted in figure 5.16, alongside consistent curves generated for our

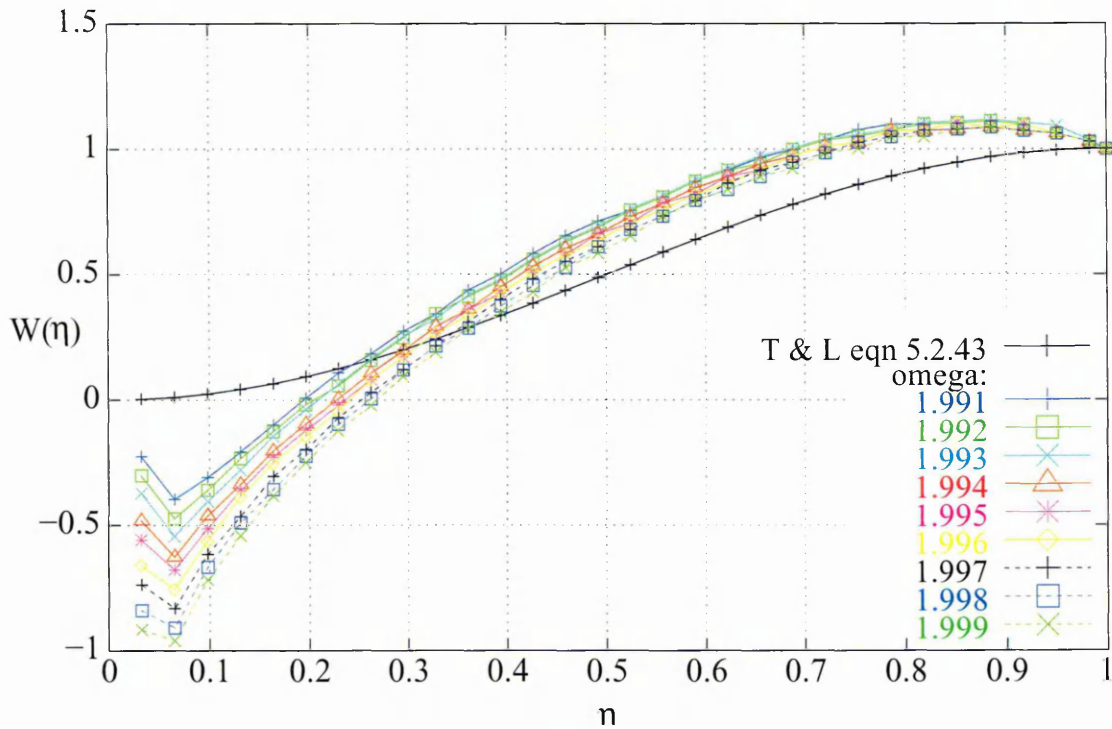


Figure 5.16: Wake function as derived using the universal logarithmic profile for flow in a pipe. The abscissa η is dimensionless location into channel given by $\eta = y/W/2$. The line marked ‘T & L eqn 5.2.43’ (black, with pluses +) refers to equation 5.37, that is the sinusoidal wake function mentioned in Tennekes and Lumley [139].

data.

This is perhaps the most revealing and interesting graph concerning results for the LB turbulence model thus far generated. It reveals the typical departure of real experimental data for the core flow, from fits and theory on data applicable in the logarithmic overlap layer.

The ‘Tennekes and Lumley equation 5.2.43’ data is seen to reach maximum at channel centre, falling gradually to zero at the wall region. Note that on a logarithmic plot such as figure 2.17 of the background (which was drawn up for purposes of illustration) the region of departure (most of the domain of figure 5.16) appears compressed into the high y^+ region. But importantly, the two plots are not inconsistent; this characteristic is simply due to the logarithmic scaling.

Our data display features not attributable to the wake function, differing quite substantially and revealingly. Whilst the form is approximately sinusoidal as expected, the various parameters which might be used to describe this (amplitude, phase and ‘origin’) are at variance. Moreover, our wake function data changes sign at one point (around $0.2 \leq \eta \leq 0.27$) and shows a serious discontinuity adjacent to the boundary node.

The latter might be assumed to arise as a consequence of the BC implementation (or law of the wall). Whatever the view, figure 5.16 is valuable because, in no other plot

are these departures so visible. On that basis, further investigations might be based on inferences so derived.

As regards the *quality* of defect style profiles generated with the LB turbulence model and wall law, there is creditable resemblance to expected defect behaviour, but this is relatively superficial. The most obvious problem, wake data which cross the $W(\eta) = 0$ ordinate, is probably attributable to the fact that figure 5.16 compares duct data to pipe theory; a matter to be resolved by further work. Secondly, there is the very pronounced inflection that occurs adjacent to the boundary node. Again, a treatment of which is left to further work.

As a redeeming feature, it is still quite remarkable that features such as a qualitatively correct wake function emerge from our data, especially when not explicitly incorporated. A thorough investigation of this aspect of the simulation data must, be based upon data derived from consistent flow geometries. Equivalent relations to 5.36 and 5.37, for duct flow, should really therefore be found before a continuation is considered.

5.3.3 Results for wall law bounded channel: Moody curves

A much more stringent test of the model (core and boundary algorithm together) resides in its ability correctly to recover stresses at the duct wall and thereby correctly model friction effects on the flow. Assessments of such matters are commonly addressed using friction factors as a probe parameter. As mentioned in the introductory material, such data are most often analysed with respect to Reynolds number variation, which is the basis of the Moody chart.

The Darcy–Weisbach friction factor, which was defined earlier 3.46 but is restated here:

$$f_{\text{DW}} = \frac{\mathcal{G}W}{\frac{1}{2}\rho V^2}, \quad (5.38)$$

where \mathcal{G} represents the driving force, or pressure gradient, will be used in the following discussions.

The friction factor, like the Reynolds number against which its variation is to be investigated, is *derived* data in that it is calculated from summary aspects of an entire profile — namely the profile mean velocity. In that respect a profile generates a single point on a Moody curve. The fact that the data are ‘derived’ introduces a further level of detail which might either: form a cause of error, obscure correct interpretation, or introduce extra factors to the analysis; this must be borne in mind.

A good example demonstrating such, which has relevance in the following, is the fact that differing methods of arriving at a mean velocity for a profile will produce slight,

but consistent, differences in mean values and therefore change the appearance of Moody data.

Luckily, during the course of the study, various alternatives to averaging were utilised and such was found to have relatively insignificant bearing on interpretation.

The method used for data presented here was a simple trapezium rule, which is very commonly utilised in all numerical studies of discrete data. Possibly importantly, in the context of flow profiles, this method *consistently underestimates the mean velocity value*. This matter will be returned to shortly. Before that some example Moody data, as derived from LB simulations with the specified mixing length model and law of the wall, are presented for discussion.

Figure 5.17 shows, on a logarithmic scale, the variation of friction factor for the data (and range of Reynolds number) specified by table 5.1. This branch of the Moody curves of course corresponds to smooth duct walls (reflected in the choice of $B = 5.0$ in equation 5.22). Incidentally, wall roughness can be successfully modelled in the traditional way, by changing the value of the constant B . The data of figure 5.17 is in excellent agreement with experimental data, [153].

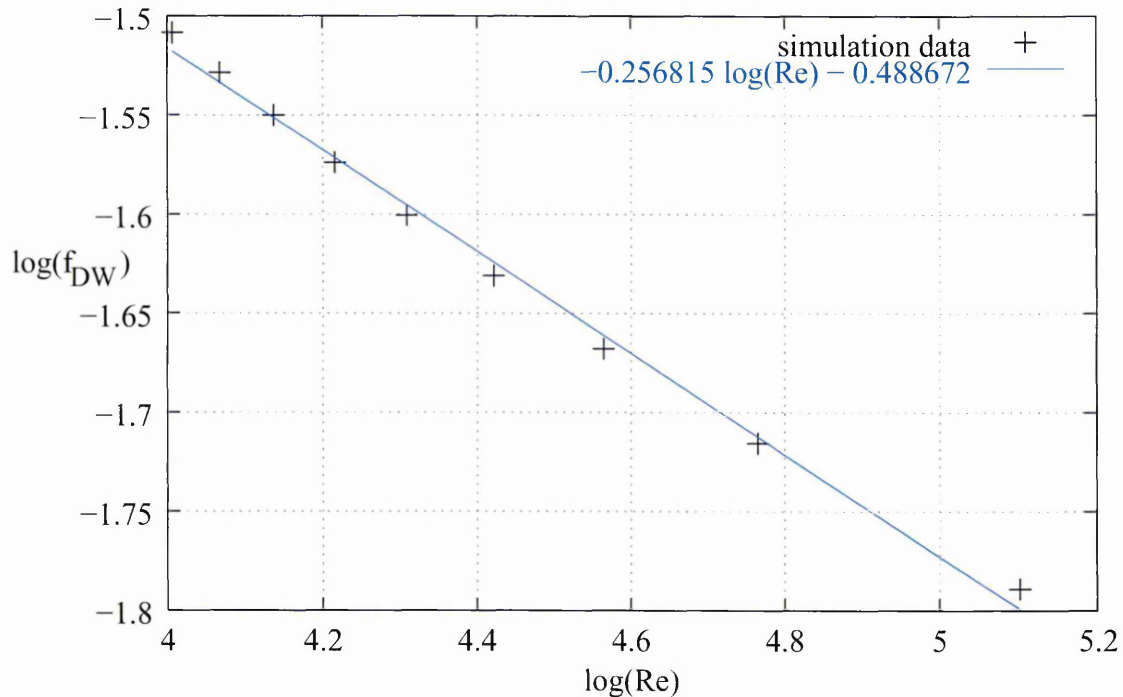


Figure 5.17: Moody curve from earlier simulation data; see tabulated values 5.1 and figure 5.4. The (logarithmic) variation of measured Darcy–Weisbach friction factor, f_{DW} , for Reynolds number Re in the range $10^4 < Re < 10^5$.

As the range of Reynolds number over which there is data is relatively small, little variation in gradient is expected between each end of the curve. This is indeed observed in our data. The precise amount of curvature may be qualitatively ascertained when the

data are compared to that of other sources. Such is presented in figure 5.18; which shows LB simulation data, adjacent to data generated using those benchmark methods that were included in earlier sections for comparison.

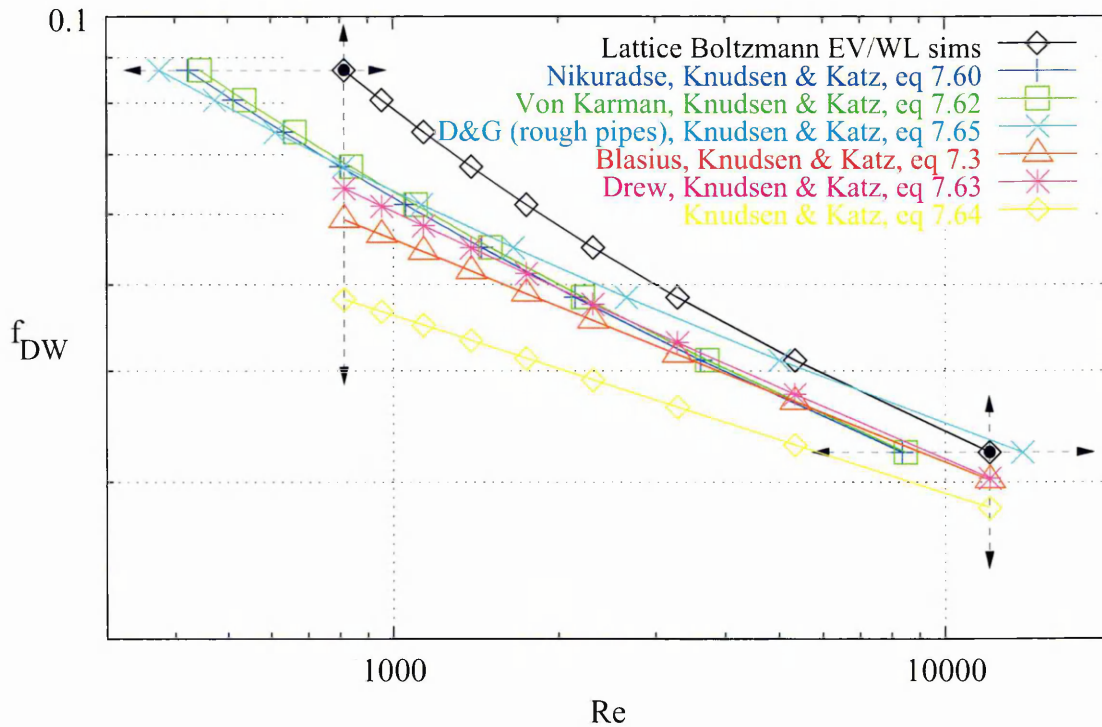


Figure 5.18: Moody data gathered for a set of friction factor / Reynolds number relationships. All calculated data stem from equations taken from Knudsen and Katz [73]; these are variously analytic or semi-empirical. The data correspond to quite low Re values (relatively, with respect to the range for which experimental data exist). At this point, the curves are widely spread, but there is some indication of a trend to become closer for higher Re .

In particular, relations 2.193, 5.5, [K&K 7.65], 2.192, 2.194 and 2.195 respectively, of section 2.7.4, are used for the purpose; a reminder of the details for which are indicated in the key. Note that some data relate to a forcing regime which, in an equivalent physical system, would not normally lead to a manifestation of turbulence. This is indicative of the ‘global’ influence of the LB turbulence algorithm. When the model is invoked, all areas of the relaxation parameter space (and hence Reynolds number) exhibit characteristics of turbulence. Such is not physically realistic, a matter discussed later.

The LB data of figure 5.18 are very well placed amongst the alternatives, especially at higher Re , and thus can be considered in excellent agreement with established data. The LB data is peculiar in that it shows the highest level of curvature of the set; an interesting point to which the discussion returns.

Note that curves fall into two distinct groups, those with horizontal sets of points and those with vertical sets of points; the various ‘displaced’ data sets meet at the LB data and are indicated by dashed arrows. Such does not indicate any special treatment for

the LB data. It is merely an artifact of the ‘mapping direction’ for the K & K relations — equations 7.60, 7.62 and 7.65 are ‘inverse’ in that they only solve for Re using f_{DW} and not vice versa. To illustrate the point see equation 5.5 herein.

As it happened, new data had to be generated for figure 5.18, as a (minor) error was discovered in the original coding. The number of nodes across channel was arbitrarily chosen to be 15 LB nodes. This corresponds to a channel width of $15 - 1 + 2\Delta$, where, from this point on Δ is taken as 1 — the earlier supposed necessity for it to be less than 1 was recognised as incorrect. Hence these ‘comparative’ results relate to a channel width of $W = 16$ lattice units.

As indicated, it appears that LB data converge on the accepted solution in the limit of high Reynolds number. This can be checked by plotting data over a wider Re range. Figure 5.19 does just that, wherein the quality of the derived LB data becomes apparent.

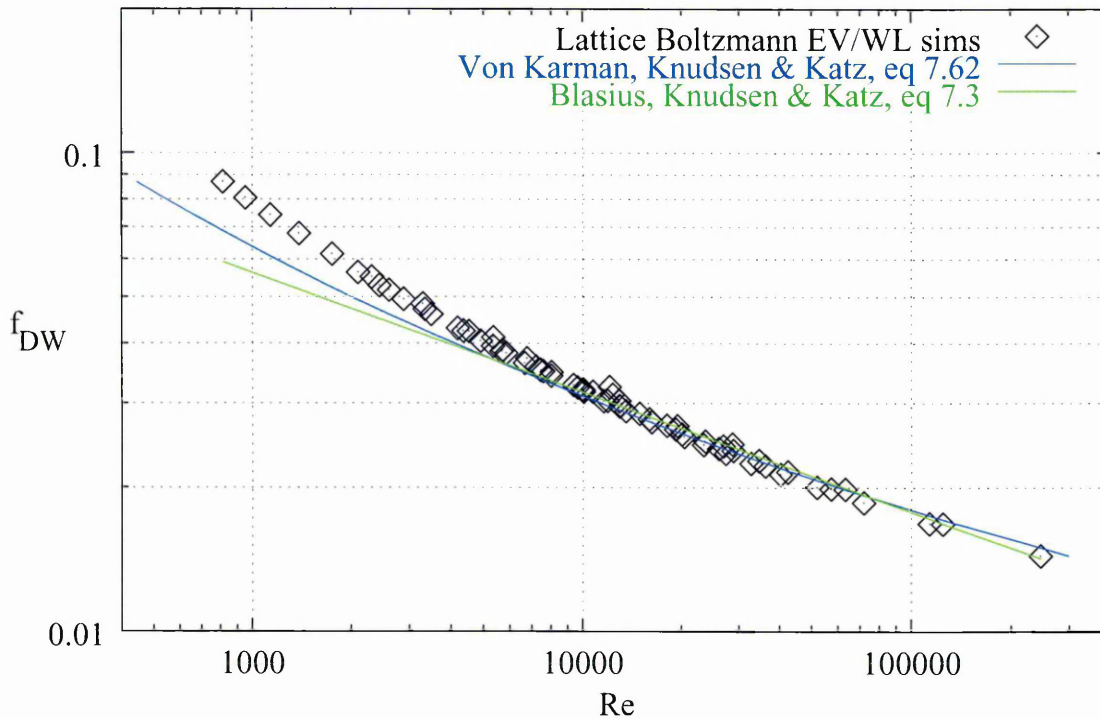


Figure 5.19: Moody data gathered for a subset of the friction factor / Reynolds number relationships (von Kármán’s and Blasius’ results, obviously alongside LB data). All calculated data stem from equations taken from Knudsen and Katz [73]. The data correspond to medial Re values. Convergence of LB data to the accepted solution is obvious. Not all relations of figure 5.18 are hereafter shown, as there are considerable similarities between them.

Attention turns to the cause of deviation from norm in the LB data of figures 5.18 and 5.19 — that is at lower Reynolds number. Various possibilities emerge, all based upon the fact that Moody data depend crucially on cross channel averaged velocities — from here on conveniently referred to simply as the mean.

The mean is influenced by velocity profile shape, magnitude and its accuracy. It

is known from the earlier study, that some discrepancy exists in a quantitative sense between the LB derived profiles and expected data. However, no consistently applicable features were observed. In contrast, the Moody data do show a consistent feature, in that for low Re , the Moody curve is a little too high. Possibilities for the cause of this are now discussed.

In the previous section 5.3.2, profile inaccuracies are alluded to which might be responsible for inaccurate mean data. They centre on boundary introduced anomalies and consequent error propagated into the bulk. It is expected that in this way, boundary error — whilst reduced here by the methods of chapter 4 — is expected to have a knock on effect on the Moody domain.

In an effort to reduce said error various actions were taken, targeting local velocity calculations, derived mean values and mean velocity shear. Shear, or in particular the strain rate tensor S_{xy} at LB bounding nodes, is a prime error source candidate, because it is both a derived quantity of the lattice data (densities or macroscopics) *and* a quantity used as input — in that way it provides a feedback mechanism for error.

Various improved methods to calculate shear velocity were tried, all of which were eventually ruled out as possible means to reduce error. They included: implementing different schemes for extrapolating S_{xy} at $y = \Delta$ and $y = W - \Delta$, mainly consisting of improved approximation forms to differing orders of accuracy, up to third.

The *formalism* used to calculate shear, which in the LB can also be achieved by a lattice density summation (equation 5.13 of section 4.2), may also be changed in an attempt to reduce errors. This too was found to have little effect; or at least the changes caused are of negligible magnitude if they exist.

In addition, the *moment* at which shear values are calculated in evolution (when done using either method) may have proved to be significant. But this too was ruled out on account of the fact that the second order scheme utilised (of section 4.2) is exacting with respect to timing and leaves no scope for adjusted application.

So what possibilities are left? As previously mentioned, the mode of averaging has some effect: utilising a trapezium type scheme to calculate the mean velocity from a set of discrete values will consistently, though slightly, underestimate the true mean. The questions arise, to what extent does this affect Moody data and in what ways can such error be reduced?

Some deeper understanding of the nature of this averaging scheme is warranted in order to clarify. It is instructive to consider, by way of an analogy, a set of chords⁶ under the profile whose ends meet and are congruent with a retaining curve (here the

⁶Strictly, straight lines joining two points on the inside of a circle.

velocity profile) much like a polygon inside a semicircle, with vertices of the polygon — analogous to our data set — lying on the circle. The area of any such faceted shape inside the a curved one will always be lower than that defined by the curve. A little further consideration of the analogy reveals that the said area discrepancy must fall as the number of vertices is increased (the lattice resolution in these simulations). Hence increasing the cross channel number of nodes should reduce averaging errors and should be considered as an approach to improve results.

Bearing in mind that averaging error would manifest itself more obviously at low Reynolds number it is expected that the deviation be worse at the left of the plot — and this is indeed observed to be the case. Such suggests that a truer picture of the macroscopics of the LB turbulence model is provided by the high Re tail and that further data should be collected for this region.

Figure 5.20 shows this high Reynolds number data, plotted alongside just a representative selection of data collected in other ways. As can be seen therein, LB data for high resolution simulations close increasingly onto the accepted solution, until which point as they all begin to diverge. Moreover, the deviation of LB data from other methods is, for forcing above $Re \approx 20,000$ and below $\approx 3 \times 10^6$, of comparable magnitude or lower, to the spread in values amongst other means.

All means to arrive at Moody data diverge above Re around 3×10^6 ; this is on account of experimental difficulties in obtaining data against which to calibrate empirical relations. Figure 5.20 therefore, is taken as clear and unambiguous evidence of the effectiveness of the current LB turbulence model for simulating turbulent duct flow.

It is now possible to set aside the low Reynolds number error of figures 5.18 and 5.19 as most likely due to errors in the cross channel mean. These are caused either by the averaging procedure or the profile inaccuracy at the first explicitly resolved LB node (boundary inaccuracy). One could proceed to analyse deviation from the accepted curve in a quantitative sense, but in the light of differences amongst the LB rivals this is not deemed necessary or justifiable.

It was decided that the way in which errors in calculated means affect Moody data should really be investigated further. The approach taken to this involved (firstly) estimating an order of magnitude figure for V error, as introduced by the trapezium approximation employed. This, it is expected, is resolution dependent. For a lattice size of 15, i.e. channel width $W = 16$ a ball park figure of 2×10^{-3} seemed appropriate. Hence the code and data output routine was manipulated directly to return mean values 1.002 times the original and runs were carried out.

Simulation data for such adjusted velocity data were collected, but they remained

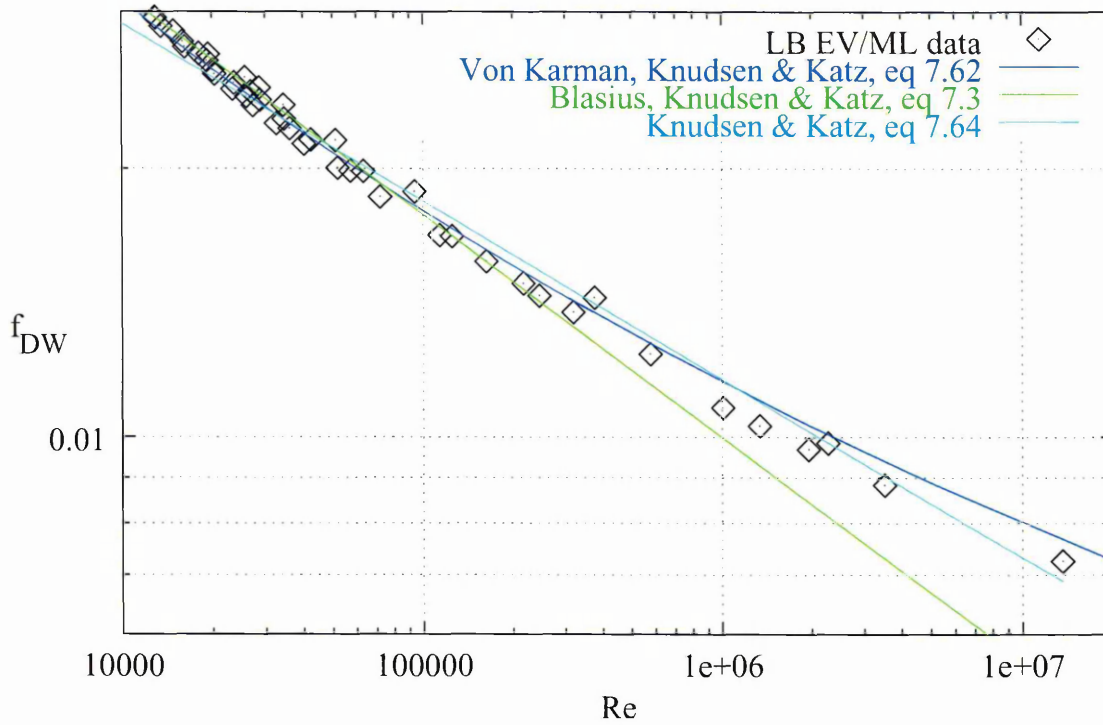


Figure 5.20: Moody data gathered for the high Re limit. Results for von Kármán's and Blasius' results are also shown as an illustration of their relative applicability to high Reynolds numbers. Data from relation [7.64] of reference [73] are also included, as these closely match the LB data. One of the better matches is with that of von Kármán, which is very encouraging as von Kármán based his expression 5.5 on the universal velocity distribution for the turbulent core — a semi-empirical relation.

so close to normal output that the effect was hardly visible. Instead, to illustrate the dependency of mean on an error parameter, data were then generated for much higher velocity coefficients (which will hereafter be denoted V_c). These are compared against normal output in figure 5.21.

From the definitions of friction factor and Reynolds number respectively, friction factor scales as V^{-2} , whereas Reynolds number scales linearly with V . This implies that there will be significant dependency of dimensionless parameters Re and f_F on V . Hence the effect of, say artificially increasing the observed mean values, should be to shift the Moody curves down and to the right; the latter more so.

Having clarified the displacement of Moody curves with mean velocity data and, upon observing that such is both non-linear and twofold, it is reasonable to expect that accuracy of results in the Moody domain might depend heavily on cross channel mean velocity calculation accuracy.

As the trapezium rule average is expected to *underestimate* cross channel means, the above reiterates that plot points will in turn appear higher and to the left. For most of the LB curve in figure 5.18 the data do indeed appear to be a little high which indicates

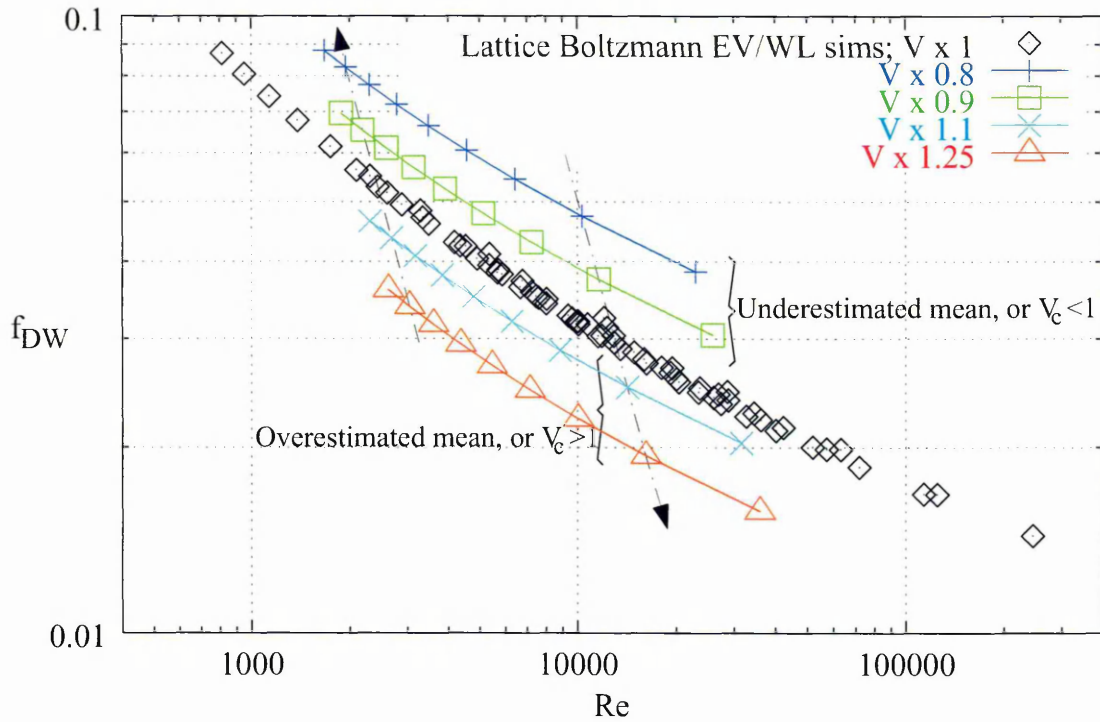


Figure 5.21: Moody curves showing the effect of directly manipulating cross channel mean velocities by introducing a multiplicative factor, V_c . Curves for four V_c factors are shown juxtaposed against the actual simulation output. The aim is to indicate how any errors that occur in calculated mean velocities manifest themselves on the Moody chart. The four ‘outer’ data sets are neither real data nor physically valid, they are for illustration only. The factors are, from top to bottom: 0.8, 0.9, [1.0], 1.1, 1.25. In that no real calculation or simulation error is likely to be of this magnitude, the values are obviously very high, however, in this way they make the point better — errors which overestimate the mean move plot points *down* and to the right, the latter to a greater extent.

that an averaging error of this kind — or an equivalent artifact — exists.

5.4 Discussion

It will be of some value to anyone preparing to continue this work (either with studies of their own, or those ideas suggested in section 6.1) to gain an insight into some of the more misleading aspects of the field. For this reason, I have taken the opportunity in the following, to indicate some of the pitfalls and challenges that were overcome during the development of these studies; they help reveal the progression of the project too. Prospects for further work and recommended continuations are left to a later point, 6.1.

Also discussed in this section are: some descriptive results on the behaviour of our dynamic relaxation parameter; for illustrative and informational purposes only. Also, a description and appraisal of the parameter space within which this work is framed.

Finally, a brief discussion is initiated on theoretic aspects of the specific modelling

strategy employed for the work. Only after that, in section 6.1.3, are the more fundamental and speculative points raised during the work formally addressed. Prospects for future work forms part of that summary.

5.4.1 Problems solved and lesson learned

Application of a lattice Boltzmann Prandtl mixing length model in an x -periodic translationally invariant channel proved to be a tricky objective. Initial studies led to unclear and inconclusive results, though most, if not all, obscurities were eventually ironed out.

This section constitutes a mini ‘manual’; advice for anyone wishing to continue the work, or who contemplates building upon it. The hope is that, in briefly describing the problems encountered and their solutions, a great reduction is effected on the possibility of wasting effort. Various types of problems might and, for us did, arise; they are categorised as: those related to core model implementation, some boundary and forcing implementation issues, coding errors, interpretational errors and visualisation problems. Specific problems encountered are now mentioned.

In the early stages, obtained velocity profiles were either very similar to the parabolic one of plane Poiseuille flow, or were unphysically distorted, often containing extreme discontinuities, depending on the values taken by the free parameters of the model. Careful analysis of the local update to the relaxation parameter field demonstrated efficacy of the algorithm and code in that regard, so an early impasse was reached.

One anomaly appeared consistently; a discontinuity in the gradient of the observed velocity profile exactly one node into the channel. A similar observation had been made during work of a previous chapter (3), in the light of which this occurrence was readily attributable to the chosen bounce back boundary condition. The bounce back scheme is known to be only first order in accuracy [59,157], so these initial observations suggested that an improved form of lattice closure would be required, before any meaningful results for the turbulent channel could be generated. Hence the motivation for and commencement of concurrent work on second order BCs, the subject of the previous chapter, 4. Once an appropriate second order closure was established, work on the turbulent channel began in earnest.

Unfortunately, it transpires that the profile of velocity derived from an inadequately converged simulation is qualitatively very similar to that expected for flow incorporating modelled turbulence. Owing to the large Reynolds number required for turbulence simulations, which in LB is usually achieved by increasing the relaxation parameter toward its limit of 2, relaxation processes in the fluid were, as a consequence, slow. Under these circumstances, an inadequate criterion for convergence led to the erroneous conclusion

that the simulation output displayed turbulence. Future workers should be aware of the need to ensure adequate convergence.

In order to disregard lack of convergence as a cause of anomalies, a consistent method was invoked to ensure that flow profiles under scrutiny were indeed fully converged to their steady state form. Here this was achieved by implementing a ratio metric criteria, based on the decay of velocity ‘residuals’ that occurs with time. Algorithmically, a comparison is made at each time step, between the current residual and the original ‘peak’ residual, as occurs after forcing is initiated. Convergence is defined by the ratio falling to an appropriate fractional limit, usually of the order 10^{-5} .

Another ‘anomaly’ was observed, which became referred to as the ‘shoulder and peak’ profile. It consisted of the expected ‘shoulders’ in the velocity profile (see previous descriptions, section 5.1.2), but also an *unexpected* high curvature ‘peak’ occurring at mid-channel. The lack of expectation for this feature turned out to be a most unfortunate interpretational error, as will be seen.

In fact, various subtle factors were inhibiting progression and certain clarifications were in order. They were quite diverse in nature. One consisted of complete removal of the effect of any boundary conditions on the core scheme and turbulence model. This was achieved by implementing the contra-forced fully periodic channel, in which all nodes are assigned as ‘bulk’. It was carried out in parallel to work already begun on formulating appropriate second order accurate boundary condition schemes as a means to achieve a fix.

The main clarification occurred with the realisation of the aforementioned interpretational error. The ‘shoulder and peak’ profile, which in the early stages had confusingly been regarded as incorrect, was finally recognised for its true value. Turbulent flow in a channel *does* indeed display such a feature — the profile gradient does not change evenly throughout the core, as had been expected. This unfortunate misinterpretation arose with poor qualitative descriptions of channel turbulence and was compounded by inadequate communication within the research team. It significantly and adversely affected progress because it gave rise to all kinds of suspicions regarding the model, the algorithm and its coding.

In addition to the above, certain minor computational issues warrant mention: Both ‘gnuplot’ and ‘C’ use the name `log` to denote what is in fact the natural (Naperian) logarithm `ln`. This matter causes some considerable scope for confusion. It is of relevance here in that the graphical output of gnuplot prints `ln` as `log`; be warned.

After all such interpretational errors were removed and manifold checks had been made, the situation arose to re-evaluate in the light of new results. Qualitatively correct

flow features, *do* indeed emerge in the data for high ω_0 values. This fact was greeted with some relief, owing to the relatively late stage in the project timetable that this element of work had reached. Subsequent quantitative analyses of the data were deemed encouraging too and the impasse was finally broken.

5.4.2 Dynamics of the turbulence model

It is of great interest to consider the precise mechanism by which the turbulence model affects such significant change over the flow profile. During many analyses in this project, an understanding of this emerged as critical for ascertaining how the model might be failing, how it might be working or how it might be improved.

More than one perspective can be adopted on this subject and it is helpful, when working, to exploit one or the other effectively. In one, the process can be viewed from an informational stance; adopting the view of a computational scientist. Alternatively, a purely physical view can be taken. Here, since the matter was usually considered during attempts to validate the algorithm, an informational view was generally taken, the merits of which will become apparent.

Either way, a little consideration makes certain attributes of the mechanism clear. The effect of the turbulent aspect of the algorithm is *incremental* in that, boundary conditions *don't* impose a state on the variable viscosity which is then fixed and, toward which the solution converges. Instead, they impose an 'incremental change' on the relaxation parameter — an adjustment, which is dynamically updated at each time step and, which, through the effect it has on the collision operator, constitutes a kind of 'numerical force'. This force in turn imposes an incremental change on the macroscopic variables, thereby altering the equilibrium solution.

The process of reaching a solution is unchanged in that it involves a continual, or, in discrete time incremental, competitive process between each evolutionary mechanism. Particular mechanisms include: the pressure to 'relax' implemented by the collision, the tendency to advect implemented by streaming operator, the pressure to accelerate implemented by the forcing, the inhomogeneous retardative effect of the boundary conditions and the internal redistributive, or dissipative effect of the turbulence.

The net effect is highly complex; but interestingly, at the level of a node and its immediate environment, individual working processes may be followed in detail.

In fact, it became apparent during investigations that, for the highly idealised case of a translationally invariant channel, a solution to the profile might be possible analytically. A direct corollary of this is that plane Poiseuille flow might also be analytically soluble within the LB framework. Indeed, further investigation of such revealed it to be true;

though unfortunately for us, work establishing this beyond doubt had, it turned out, already been done [59].

The realisation led however, to some digressional work toward an analytic solution for the turbulent case. It was deduced that, for LBGK only, the scenario reduced to a system of *linear* simultaneous equations, for which it was needed to know if a certain 12×12 matrix was invertible. This appeared to not be the case however; though the studies did not verify this beyond doubt and solution of the system might actually be possible.

5.4.3 Analysis of the effect of variable viscosity

A mathematical analysis was made of the consequences of introducing the specific model proposed here. This involved determining extra terms generated under the model implementation, that appear under application of the Chapman–Enskog expansion. The analysis proceeded to develop a categorisation for these in order to identify means by which they might be simplified. The aim was to identify how the dynamics differed from the desired turbulent dynamics and subsequently identify error terms. Means to correct for these might then come to light.

However, in the light of new reading on the matter, this work was rendered unnecessary: Hou, Sterling, Chen and Doolen, in [68], state that: “it can be easily proved that neither the Chapman–Enskog expansion procedure nor the derivation of Navier–Stokes equations will be changed by the spatial dependence of the relaxation time if the filtered density and velocity are defined as $\bar{n} = \sum_i \bar{f}_i$ and $\bar{n}\bar{\mathbf{u}} = \sum_i \bar{f}_i \bar{\mathbf{e}}_i$, respectively”⁷.

Figure 5.22 shows a typical variation with cross duct distance y of the full and turbulent component, ω and ω_T respectively, of the LB collision parameter. The variation in the effective value of ω is notably small, as one might expect, considering that values of ω close to 2.0 accommodate a large range of kinematic viscosities. The simulation data and Reynolds number are as in figure 5.4.

Consistency of effect across the range of relaxation parameter: With the LB turbulence model invoked, it is implicit that representative systems of interest are driven in such a way as to be regarded inside the turbulent regime, that is, driven beyond the ‘critical Reynolds number’. As mentioned, initially it was expected that the turbulence model, being in operation over the entire range of values of relaxation parameter, must

⁷The filtered density to which they refer emerges from their decision to explicitly filter out of sub-grid flow features by use of an averaging procedure against a function with characteristic size related to the lattice spacing. Their velocities are denoted by \mathbf{e}_i in contrast to our \mathbf{c}_i and density by n in contrast to f ; but all else remains identical.

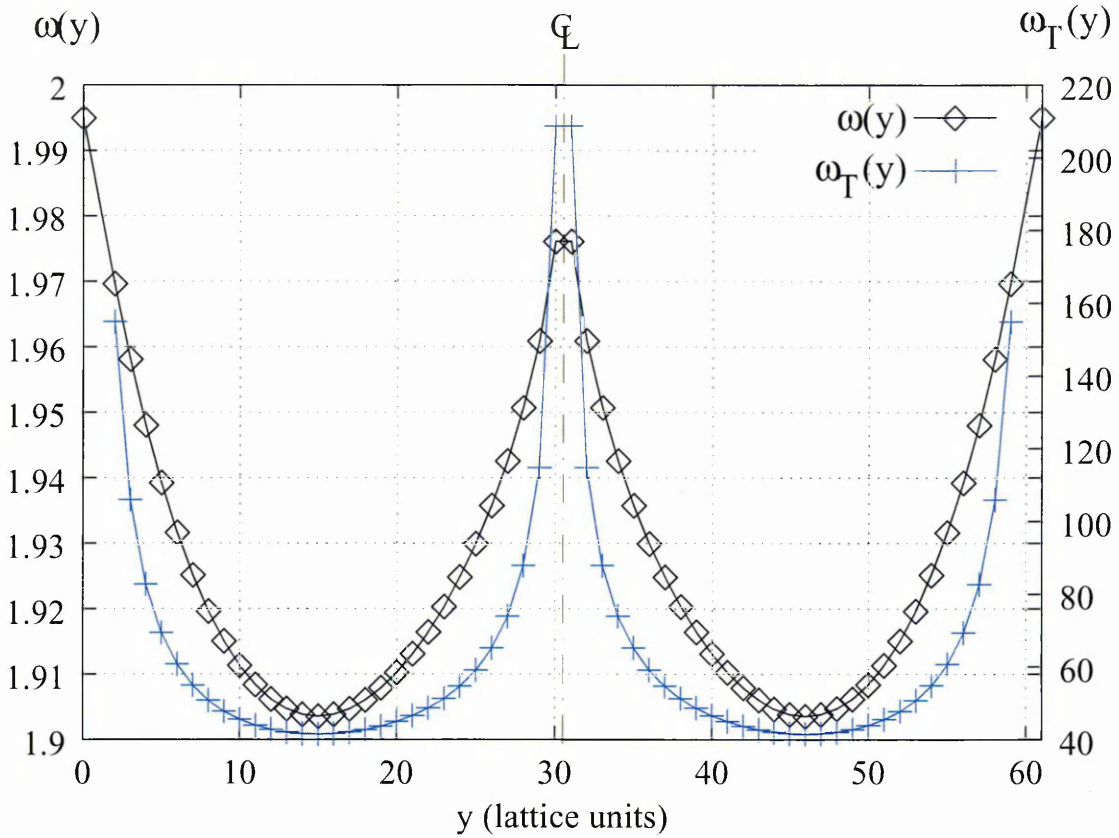


Figure 5.22: Left axis (diamonds \diamond): Typical emergent variation, with cross duct distance y , of the LB collision parameter ω . Variation is notably small, as one might expect considering that values of ω close to 2.0 accommodate a large range of kinematic viscosities. Right axis (pluses $+$): Corresponding variation in the turbulent component of collision parameter, ω_T . Data stem from the simulation of figure 5.4.

have an effect which also visible at any value of relaxation parameter. This is a somewhat unphysical aspect of the model, but acceptable nevertheless.

In the confusing results of initial simulations this was indeed observed to be true, for the varied effects seen, which included those originally interpreted as incorrect. However, to derive the strongest turbulent features it was realised that correspondingly high Reynolds number must be obtained — somewhat in contradiction to the proposition above. As with many things, this can be understood by moving away from such a ‘black and white’ viewpoint. It is essential to consider the effect of the dynamically updated relaxation field on its physical equivalent the viscosity, more importantly, the gradient function must be analysed.

Discussion of variation of viscosity, whether it be with relaxation parameter, or Q , or both, is facilitated in the *relaxation time* framework — that is with respect to τ as opposed to ω . This is because the viscosity is simply linear with τ , whereas an inverse

relationship is introduced by ω . Note that

$$\nu = \frac{2\tau - 1}{6}, \quad (5.39)$$

or, after introducing the turbulent eddy viscosity, $\nu = \nu_0 + \nu_T$:

$$\nu_0 + \nu_T = \frac{2(\tau_0 + \tau_T) - 1}{6} = \frac{2\tau_0 - 1}{6} + \frac{\tau_T}{3}, \quad (5.40)$$

which, were it not for τ_T 's dependence on τ_0 , would be a simple straight line. Expressing equation B.8 for ω_T , equivalently in terms of the reciprocal relaxation parameter, τ , either by solving the quadratic equivalent to B.1 in terms of τ , or by direct substitution, gives:

$$\tau_T = \frac{-\tau_0 + \sqrt{\tau_0^2 + 4Q}}{2} \quad (5.41)$$

which by the relation 5.40 and by $\nu = \nu_0 + \nu_T$ gives a variation of viscosity with τ_0 and Q as follows:

$$\nu(\tau_0, Q) = \frac{\tau_0 - 1 + \sqrt{\tau_0^2 + 4Q}}{6}. \quad (5.42)$$

A simple plot of this function reveals its essential planar nature, see figure 5.23. Also, it

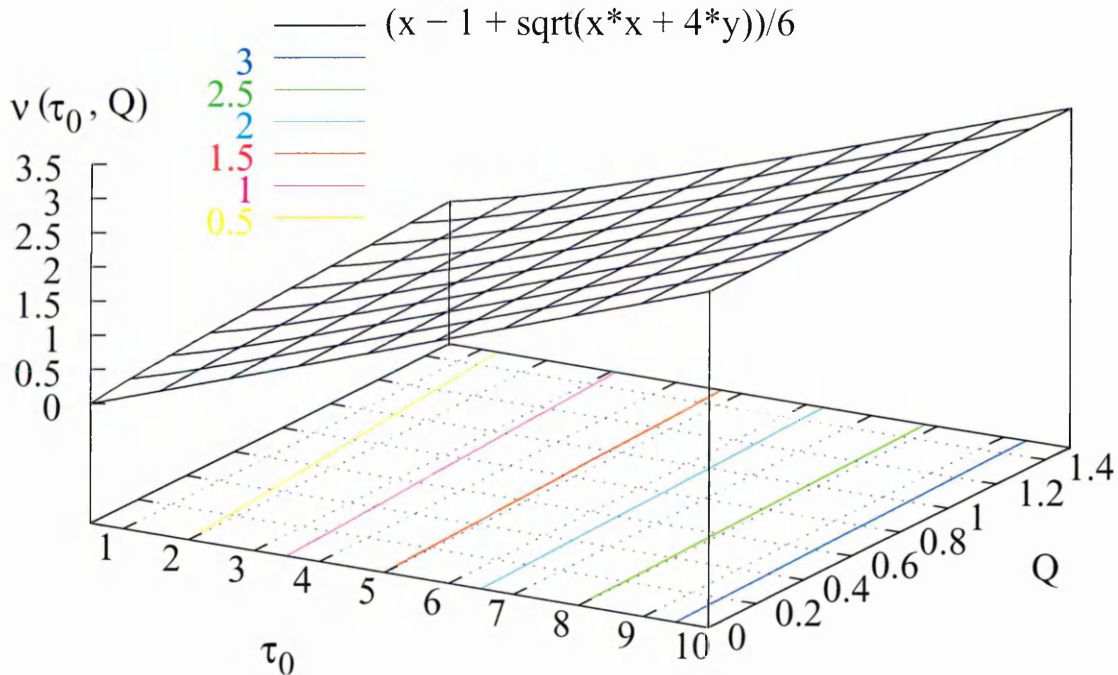


Figure 5.23: Variation of dynamic viscosity with molecular relaxation parameter τ_0 and with Q , the parameter which quantifies the effect of shear on the flow as implemented by the mixing length model. Note that both are always positive; closer inspection verifies that $0.5 \leq \tau_0$. The surface 'appears' planar.

reveals that the viscosity is expected to increase as the effect of flow shear increases with

$\|\Pi_{\alpha\beta}^{(0)}\|$. However part of the picture is hidden therein, as the point of greatest variation in viscosity occurs for low Q value and low relaxation parameter. This can be seen if the gradient of the viscosity surface of figure 5.23 is plotted; see figure 5.24 (gradient function derived in section B.1.1, page 268, equation B.17). The gradient peaks at -1 for

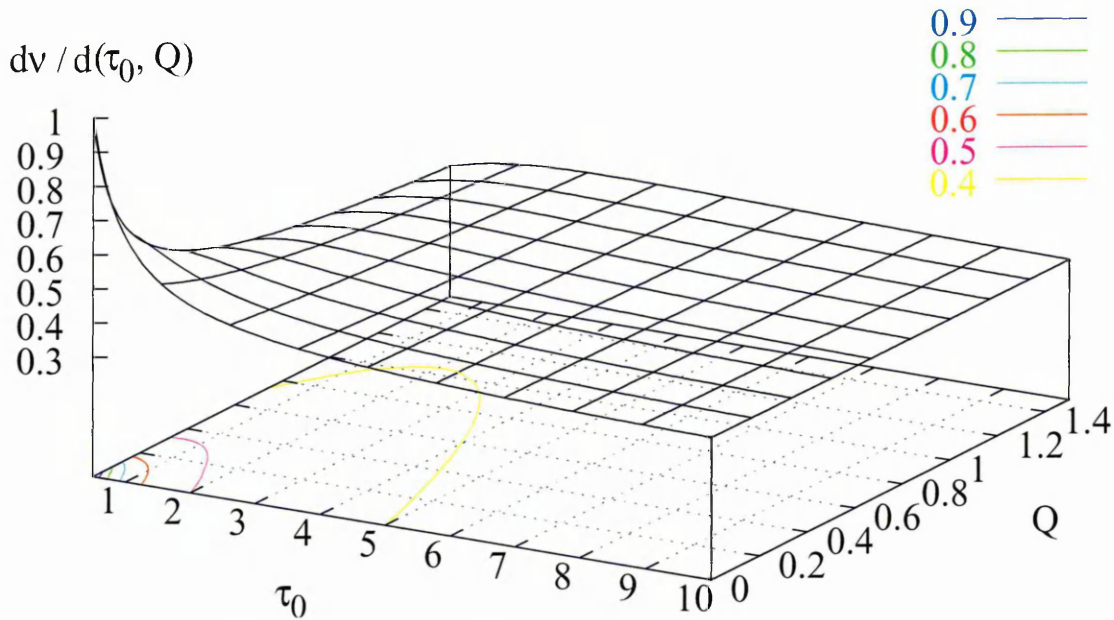


Figure 5.24: Variation of *gradient* of dynamic viscosity with molecular relaxation parameter τ_0 and with Q , over the same parameter ranges as in figure 5.23. This surface reveals the non-planar nature of figure 5.23 by the sharp increase of gradient at low τ_0 and Q values.

ultra low viscosities and low shear influence.

Observe however, figure 5.25 which focuses on a region close to the minima for both τ_0 and Q . Zooming in on the origin region, by observing viscosity variation over the range of relaxation parameter consistent with previous data $1.99 \leq \omega_0 \leq 2$ (equivalent to $0.5025 \geq \tau_0 \geq 0.5$, the minimum physical value for τ_0 being 0.5 note, from positivity requirement, $\nu \geq 0$), reveals that the dynamic viscosity is virtually invariant of the molecular relaxation parameter over the small range of values typically employed.

This indicates and reiterates that the macroscopics and strain rate tensor calculation are critical for determining the dynamic evolution of the lattice densities.

5.4.4 Other critical points

Finally, this section is rounds matters off by mention of a small selection of other points which might, to some, warrant discussion.

With respect to the work of J.A. Somers: check the way he calculates S , his coefficients C_s, C_n the construction of ν_T . Also the relative quality of our fit to Blasius

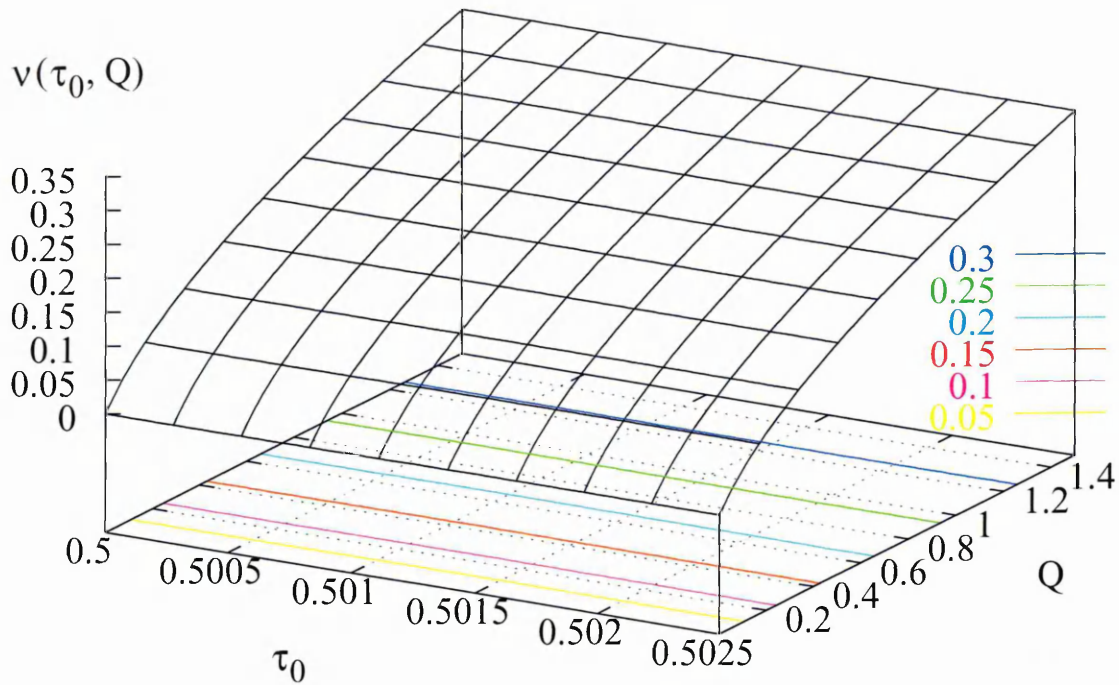


Figure 5.25: Variation of dynamic viscosity over the parameter range relevant to turbulence simulations carried out in earlier sections. As is evident, the variation caused by the initial choice of (molecular) relaxation parameter, is virtually negligible, so it is the introduction of strain rate tensor qualities which largely determines the dynamics of the model.

$f_B = 0.3164Re^{0.25}$. Discuss his transition idea and his notes on efficiency. see little notes attached.

Comparison between this work and that of C.M. Teixeira: Various contrasts exist between the current work and that of Teixeira. The main differences are here listed, for brevity:

- Their mixing length is of a piecewise linear form
- They perform simulations at only two values of Reynolds number
- They use a three dimensional code
- They have flow BCs at either end of the pipe which introduces compressibility error; this then has to be compensated for.
- Their law of the wall is based on a ‘pressure gradient extended law of the wall’ (PGE-LW) which in turn is based a rather overly complex scheme of another paper. See [28] for details of their ‘arbitrary boundary condition’ implementation.
- The specific boundary implementation is known to posses flaws, [28].

Teixeira’s work, whilst thorough and interesting is, it is probably fair to say, partly defined by his relation the Exa Corporation, for whom it will no doubt incrementally improve their commercial LB / turbulence codes.

Comparison of mixing length formulae: Various algebraic forms for the mixing length were investigated, see section 2.7.2, page 197. On account of discontinuities in gradient of piecewise linear forms and in the light of observed continuity problems in flow profiles (not to mention the non-physical nature of a piecewise linear ℓ_{mix}) only results for the fourth power mixing length form are reported here.

Input parameters (primarily ℓ_{mix}) might be ‘engineering’ the correct output: A criticism could be raised that by choosing the fourth power form for mixing length simulations that qualitatively correct forms for flow profiles are in some way ‘engineered’, by virtue of similarity in form between the two functions. That is, one could argue that qualitatively correct results were generated, simply because qualitatively consistent parameterisations were *input*.

This argument implies that the model somehow boils down to a simple linear relationship between input and output. Whilst such a criticism is difficult to refute rigorously, the following points are cited in an effort to suppress related reservations.

Primarily, it has been observed in this work that, discontinuities aside, the effect of variable relaxation parameter on the solution flow profile has low dependence upon the type of mixing length utilised. Relative invariance through equation 5.42 (essentially, the differential in effect between $\|\Pi_{\alpha\beta}^{(0)}\|$ terms in equation 5.15 and that of ℓ_{mix}).

The weight of this point is augmented by the fact that the mixing length employed could just as legally have its form defined through its (original) gas kinetic basis. Under that perspective the mixing length is interpreted as say the distance an average fluid ‘particle’ travels before losing some dynamic quality of its originating environment. In which case, there are few constraints to govern its profile, other than the simple linear proportionality with distance to the bounding walls and it would be unlikely that any such criticism would arise.

The reason a fourth power form for mixing length is employed here, is that it is the simplest empirically derived form which is proven to be appropriate in theoretical and CFD studies of channel flow, and that has continuous derivative. See [148].

5.5 Synopsis and conclusions

Possibly the most interesting theoretical point, arises from the treatment, in section 5.2.1, of Teixeira's method [138] of 'turbulent modification' to the basic LB algorithm, through what is essentially a shear dependent relaxation parameter. This shows that derivation of the macrodynamics of an LB model via the Chapman–Enskog expansion (the traditional way of deriving the model's dynamics) exactly yields the (time averaged) influence of turbulence as additional, modelled stresses. This precise correspondence, with a form of the Reynolds averaged Navier–Stokes equations, without additional error, is not necessarily accidental and may be regarded as a consequence of the essential LB algorithm: the momentum densities interact in this (and most other LB) schemes at a point; i.e. through a 'zero ranged' potential. Mathematically, the position of the viscosity terms in the right hand side of the Navier–Stokes equation (in the 'right' position, sandwiched between differential operators) arises out of the structure of the Chapman–Enskog derivation of the dynamics, in which time scales associated with particular processes are effectively separated; which fact may also be significant.

In practical terms, a method has been implemented, after Teixeira, to simulate turbulent flow, using a lattice Boltzmann equation solver, adapted to the Prandtl mixing length model of the Reynolds averaged Navier–Stokes equations. The method has been validated for internal, incompressible flow in an infinite aspect ratio duct. The method relies upon the imposition of a second order accurate boundary strategy to enable law of the wall closure of the simulation lattice. The stringent test of Reynolds number variation of Darcy–Weisbach friction factor (equation 5.38), shown in figure 5.17, decisively supports the observation that our implementation is capable of representing smooth walled duct flow. Moreover, results for walls of variable roughness can be recovered from the model straightforwardly, using the usual device of varying the law of the wall parameter B , equation 5.22.

Of course, in applications, cylindrical pipe flow is far more common than duct flow. The method presented here could be adapted, to the simulation of cylindrical pipe flow, using the method [52] of expressing a lattice Boltzmann fluid flow problem with axial symmetry in a one coordinate system. The encouraging nature of the results recovered from this rather simpler problem certainly indicate that to do so would be a worthwhile undertaking, especially as there is a larger body of data for this type of turbulent flow [153].

6.1 Alternatives and future work

Further work in this field should centre on the geometrical issue of translating the turbulence algorithm of chapter 5 into cylindrical form, so that the model is thereby capable of representing pipes.

This is an equivalent task to that carried out in chapter 3 where the simple *Cartesian* LBGK scheme is extended to cylindrical form by use of carefully derived forcing terms. The work of chapter 3 is therefore a logical and effective start point from which to diversify to include the turbulence model. This forms an ideal way of bringing developments of two primary chapters herein together. Issues relating to such an undertaking are discussed further in the following subsection 6.1.1; to include some details of how this might be approached, technical issues that might be encountered and discussions of its value, scope and extensibility.

In addition to this most pressing aspect to further work and, perhaps to some, of similar importance is the prospect of improving, changing, or otherwise diversifying attributes of the models employed. The diverse ways that this can be achieved are briefly reviewed in section 6.1.2.

The prospect of modelling turbulence by an approach more closely befitting the LB, of which the introduction of new populations is a good example, is perhaps more interesting and certainly provides some hope of significant advances to the field generally. The diversity and novelty of ways by which this may be achieved brings them under the scope of a further subsection here, 6.1.3. The material of this last section perhaps constitutes the most speculative aspect of findings presented herein.

6.1.1 Turbulence in pipes: bringing our developments together

As is alluded to throughout earlier sections of this work, the applicability of the proposed mixing length / eddy viscosity turbulence model to the problem of flow in internal geometries is, unfortunately, not practically as high as one might desire. The reason for this lies in the model's Cartesian geometric basis.

There is a relatively low abundance of planar flow configurations amongst existing studies — those based on cylindrical elements (pipes) are far more frequently seen. Moreover, rectilinear ducts, whilst common are still more regularly studied than idealised flows such as the infinitely deep duct of this work.

It is possible to interpret some overlap between result sets, by utilising the fact that when rectangular aspect ratio is increased to the infinite limit, such a configuration resembles the flat two dimensional one of these studies; but this is of little consolation.

Such matters constitute the primary reduction of validity of the main chapter's results. As such, it is also the most important aspect of the work that should be addressed in any continuation.

In direct analogy with the work of chapter 3, it is desirable for the coordinate basis of the active lattice Boltzmann and turbulence modelling scheme to be transformed; from the Cartesian representation, to an equivalent cylindrical form. Technical issues involved in such are now reviewed.

Analysis of implementation

The means by which a coordinate transformation is invoked in chapter 3 — without actually changing the underlying lattice — is by the introduction of forcing terms. These are so engineered as to influence the flow in a way which is of direct numerical equivalence to extra terms which arise in the cylindrical formulation. Implementing the equivalent coordinate change, but for turbulent flow simulations, in the sense of chapter 3, amounts to deriving a soluble set of relations suggesting appropriate forcing terms.

The sense of the approach must be borne in mind in these discussions, as it is likely that other means exist to achieve the same result — though none are known to the author.

So various questions arise. Is it expected that simply adding the forcing terms of chapter 3 (equation 3.45), will *not* produce the desired geometric transformation? And if so, in what ways does the turbulence model differ from plain LB such that physically correct behaviour will fail to emerge?

Briefly reviewing the turbulence algorithm, it is apparent that the most significant difference between the two scenarios arises with variation in viscosity (via the locally updated relaxation parameter). Any analysis attempting to answer the aforementioned questions, must condense mathematically or quantitatively how the introduced (artificial) forcing terms 3.45 interact with a dynamically varying LB collision operator. Vice versa, what new forcing terms have the desired geometric effect, but do not adversely affect an inhomogeneous and dynamic LB collision?

The relative effect of such newly quantified terms is a central issue to be resolved before a numerical continuation of this work is pursued. In answering such, the contributor will implicitly further the field, in addition to enabling new continuations.

Discussion

The value of extending work of earlier chapters in this way centers on the fact that it permits a simple and practical utilisation of the scheme. Crucially, the cylindrical

geometry, whilst modelled here using only two dimensions and which after symmetries consists of two or less dimensions, is in fact a practical solid object. This is in contrast with the (rectangular) infinitely deep duct, which can never amount to any real object in any respect other than similarity in the limit of high aspect ratio.

Hence, real application of the scheme, albeit still to a very small set of scenarios, becomes possible. Moreover, the breadth of corresponding data against which to compare or calibrate is vastly increased.

In addition, the scope of the model would be very significantly enhanced by this development, as any adaptations to the rectangular case would likely be valid for the cylindrical case without necessitating further transformational changes.

6.1.2 Progression to improved overall scheme

Progression of this work may be achieved on various fronts and these are discussed in the following. A little consideration reveals that each possibility can be classified as belonging to one of four main categories; which are discussed separately under the separate sub-headings:

- **Extending to other CFD derived turbulence models**
- **Improving the scheme by using other LB variants**
- **Implementing other wall models or boundary schemes**
- **Newly proposed significantly modified LB schemes**

Specific possibilities from the last category are discussed further in a subsequent section, 6.1.3 on ‘self consistent / energetics based’ approaches.

Three papers to date discuss the possibility of invoking turbulence models other than a mixing length within the LB formalism. They are Succi *et al.* [132], Eggels and Somers [37] and Teixeira [138]. Each discuss LB extensions which implement alternative traditional models such as k - ϵ . Succi *et al.* and Eggels & Somers, also discuss specific and novel ‘LB variant’ approaches. These works form the reference material around which the following discussions, on extensions and improvements to the model, are based.

Extending to other CFD derived turbulence models:

The prospects for invoking other continuum CFD turbulence models in an LB context, including the well known and accepted k - ϵ model, are good. As mentioned previously, the matter of invoking standard turbulence models within the LB framework has been

discussed before by the likes of Succi *et al.* and Teixeira. Other than these works, however, the matter has not seriously been addressed to date in any rigorous manner.

Here the various possibilities are reviewed. Owing to the great variety of bases for extension or improvement of the scheme, detail provided in the discussions is necessarily sparse.

In Teixeira [138] the focus, other than its mixing length treatment, is on two versions of the well established k - ϵ ‘two equation’ model; they being the standard and renormalisation group forms. Two equation models in general are denoted such because they involve solving for two additional physical quantities in parallel with the usual flow variables. In the k - ϵ model these are the turbulent kinetic energy and energy dissipation rate, k and ϵ respectively. Together these are supposed to describe the effects of turbulence.

The question of how k and ϵ are solved for remains independent to the model, however. In traditional CFD they are solved for the usual way, by use of discretised versions of the governing PDEs. But the possibility exists for solution via some LB based physical arguments.

In the earlier paper by Succi, Amati and Benzi, [132], a means is proposed whereby quantities k and ϵ are represented by lattice populations, in much the same way as density is in plain LB. Their solution is thereby enabled using LB based arguments. Such an approach is rigorously quite tenuous, however, and amounts to a complete and heuristic technical generalisation. In that respect, that aspect of reference [132] might here best be categorised along with the other more tentative schemes suggested in section 6.1.3. In fact, it will again be discussed there.

In contrast, Teixeira approaches the issue of solving for k and ϵ by use of a completely traditional means. Specifically, he uses extra and non-congruent computational lattices for the purpose. The contrast between Teixeira’s approach and that of Succi *et al.*, highlights the broad range of ways individual turbulence models can be invoked — as applicable to just one fluid model.

Many other traditional turbulence models exist, from which anyone wishing to extend the current work can chose which they deem the most appropriate. Other two equation models exist and, needless to say, three equations and so on. These are all possibilities for extending what has been done here.

A particularly good reference detailing possible alternative models from the CFD field, is Launder and Spalding [82], which is very practically oriented and comes highly recommended.

Improving the scheme by using other LB variants:

The possibility of moving away from LBGK turbulence model implementations, by utilising other lattice Boltzmann schemes — or even going back to the newly improved lattice gas models — is tempting. One such approach is discussed in some detail in [132], though the possible variations on this theme are manifold. For instance, the single relaxation time (BGK) approximation could be dropped in preference of the (still simple) linearised LB. Lattice Boltzmann variants which might be utilised in preference to the single relaxation time (BGK) form include its *predecessors*. In reverse chronology these include:

- The LBE ‘with enhanced collisions’; first suggested in Higuera, Succi and Benzi [64]. Advantages afforded by changing to this model relate to the fact that there is *no single parameter* characterising relaxation speed. This might seem innocuous, but the step to single relaxation parameter is well documented as that (of the steps undertaken to from LGCA to LBGK) which trades off the most crucial physics. Stability is adversely affected, especially for thermal models.

In fact a thermodynamically consistent LBGK scheme seems, at present, to be unrealisable and, bearing in mind that turbulence is inherently an energetically constrained phenomenon — see next section, 6.1.3 — loss of energetic consistency might be critical. For those interested, the LBE with enhanced collisions receives an excellent treatment in the recent text by S. Succi, [135].

- Prior to that, the ‘quasi-linear’ LB scheme, first implemented in 1989 by F. Higuera and J. Jiménez [62] might hold benefits. These would be derived from the fact that the quasilinear LB has a collision operator which retains significant, though not overly complex, relation to the microdynamical particulate basis of the LGCA. If it were deemed necessary to ‘get inside’ the collision and relaxation process in order to adequately implement a new turbulence model, then quasi-linear LB would likely be the most appropriate choice.
- Next, the original *non-linear* LB of G.R. McNamara and G. Zanetti [92]. This scheme might confer advantages in a similar way to the quasi-linear LB; as afforded by detail in the collision operator. Such are likely to be eroded in this case, however, by additional levels of computational complexity.
- Then, ultimately, one could consider the LGCA as holding promise; though it is fair to say that the LGCA community as a whole has become relatively pessimistic

about the possibility of doing valuable high Reynolds number hydrodynamical science. Concomitant advantages in this case would most probably relate to the renewed numerical exactness; by going back to bit state representation, floating point round off error would be removed.

By way of alternatives to LBGK predecessors, one could consider picking a *successor*. These now come in a myriad of guises, which it is not appropriate to discuss further here. Similarly, hopefully not labouring the point to much, a successor to a BGK predecessor could be utilised. Finally, one of the ‘derived’ LB forms could be employed. These include: ‘exactly incompressible’; ‘integer’; ‘interpolation supplemented’; and finite volume / difference / element LB sub-classes.

From any perspective, the options are many and considerable knowledge of the field is desirable for the most appropriate choices to be identified.

Implementing other wall models or boundary schemes:

Some useful science could be carried out here, related to the traditional use of B as a parameter for wall roughness. Recall that B is the universal velocity distribution’s intercept with the $Re = 1$ ordinate, but that it can also be used to describe bounding wall roughness. This means to further develop the model would lead to some useful science, but this would be specific to the character of the LB scheme and not generally applicable.

‘True’ science, of application and prediction in physically valid systems, is unlikely to be achieved by refining the wall laws, however. This is because of the meso-scopic nature of the LB itself means that all the important physics at the wall occurs on a sub-lattice unit spatial scale and thus can not, in detail, be modelled.

Potential exists for improvement of the existing law of the wall, to other models, but this is limited. Similarly, work on better boundary schemes (in the sense of lattice information) is an obvious possibility which is not discussed further.

Instead, it is believed that emphasis should fall on finding wall / boundary schemes for which the boundary induced error to the bulk scheme is minimised; as it is this which most seriously detracts the efficacy of the bulk LB scheme itself. Once this is achieved the various lattice parameters involved could be ‘tweaked’ as a form of model calibration, so as to ensure that bulk simulation output is as accurate as possible.

Newly proposed significantly modified LB schemes:

One paper which crops up in section 6.1.2 is the by now well known one of Succi *et al.*, [132]. In that paper there is some discussion of model extensions which are of the

kind suggested in previous paragraphs; but the authors also allude to a less conventional means to implement algorithmic changes. They suggest the introduction of an extra density function on an additional lattice, which carries with it the possibility of modelling new and desirable physics.

Since the material of following sections instantiates this approach rather well, further consideration is left until then.

Finally, in addition to the four categorisations of extension suggested in the previous paragraphs, the interested reader might like to consider geometric or practical generalisations, for instance to annuli, jets wakes and boundary layers. Annuli in particular are discussed in K&K [73] whereas various other geometries are alluded to in section 2.6 herein.

6.1.3 Alternatives: self consistent energetics approach

The previous sections detail in what logical and appropriate way the work presented earlier in the thesis should be built upon and further developed. The material discussed there, arguably indicates the possibility of another few years research, which might sufficiently occupy a student (or students as the field develops) to form the basis of further PhD projects. It is not possible to justify the stance however, that adopting such a sequential and visibly logical approach in science is either the best or the only approach to progression. Significant advances almost always involve some element of ‘lateral’ development; that is, a leap of faith to another line of reasoning, or the adoption of a new direction. In the current context therefore — a preview of scientific continuations — it is, not only important and interesting, but essential that other potential lines of attack be highlighted.

Obviously there exists greater potential for subjectivity and guesswork in respective arguments, moreover, erroneous conclusions may possibly be drawn. Such material then comprises the most speculative aspect of that which is here presented; it is primarily composed of the views and opinions of the author, in the current state to which they have evolved over the period of research.

There is in fact *only one* fundamental point which will be expanded here, it being I believe at the heart of a collection of others which are more readily apparent, but which are just superficial manifestations of the same thing. Opinion on the issue was nurtured during the author’s wide and quite general reading on turbulence itself, it being a relatively obvious and certainly not exclusive resolution. It is, simply, that because turbulence is (arguably, most) usefully described in the context of energy and energetics, then taking an energetics approach to turbulence modelling in LB must surely prove very

(most) fruitful.

Such is the subject of the following final pages of this thesis, where the various issues are elaborated in some detail. The proposition implicit in the above however, is not further discussed, as the utility exists, whatever its perceived influence or value.

The utility and benefits of adopting an energetics point of view is demonstrated, quite generally, in all fields of physics, from dynamical systems to quantum mechanics. This scarcely needs highlighting. However, despite the LB possessing ‘working’ energy equations, this in no way means that energetics are easily incorporated into practical simulations in a generally acceptable way. Moreover, though quite diverse energy based models are widely incorporated into adaptations of plain LB and many papers discuss implementation of energy quantified processes, see e.g. [2,28,89,103,136] and many others, very little has been done as regards in particular turbulence. Reasons for this centre on subtle but crucial inadequacies of the LB method in the context of energy — see the first bullet point of page 247.

Much work has been done on the aforementioned inadequacies, occupying the time and efforts of some of the leading players in the field; much therefore could be said on the subject. Here, in the light of constraints on ‘scope’, discussion of such is narrowly condensed. Over the following paragraphs, a careful selection of work is picked out for discussion, targeting what appear to be the most pertinent factors.

The main problem with the model developed herein, is its inability to incorporate an explicit dissipation mechanism for the turbulent kinetic energy. Moreover, to include such would necessitate that energy be a standard variable of the scheme with an appropriate and simple definition.

Naturally, all models which address the issue of energetics have to resolve to some extent the concept of temperature; this in LBGK is not simple. Insertion of an energy dissipation mechanism which correctly handles the fluid temperature could be a necessary prerequisite for self consistent LB turbulence models.

Should conventional (non-dynamical) energy variables not be required for the proposed turbulence model, then ideas such as Succi *et al.* proposing extra density populations will probably produce good simulation results and quickly. However, the prospect is unlikely and probably the model will need to reference the fluid temperature somewhere along the way.

Despite the aforementioned range of ways in which LB simulations can adequately involve other energies; examples being surface tensions in multi-phase, stored energy in nematodynamic fluids or relaxation forces in anisotropic fluids such as liquid crystals, temperature is notoriously difficult for the simple LBGK model to deal with. This is

associated with the loss of a global H-Theorem for lattice densities which seems to accompany the single relaxation time approximation [27, 90].

Discussion of H-theorem arises in various contexts, that of stability and that of the thermal models (and with respect to the LGCA basis of LB, for which an H-theorem is proved, [27, 90, 135]). Again the two are likely related and it is commonly heard that lack of an adequate H-theorem is *the reason* for instability in, especially thermal LB [27, 90].

Hence if a rigorous energetics model is to be pursued in LB, it might be necessary to go ‘back down’ the simplification ladder to more complex LB forms — those which retain better or more realistic physics (note the various LB predecessors are itemised and discussed around page 247).

Whether or not this is done, it might prove necessary for the new models to be based upon ‘new’ additional LB variables — new populations as opposed to new quantities derived from the simple density f (as would be rigorously desirable to stay in keeping with the LB basis).

These extra variables could either be ‘flow’ or ‘fundamental’ formulations, roughly corresponding to macroscopic or microscopic. In the sense of Succi *et al.*, they propose additional populations for both the mean turbulent kinetic energy κ and the energy dissipation ϵ .

An alternative line of attack consists of confidently imposing a new element to the algorithm, the basis for which need be no more than an educated guess, and simply to observe what results subsequent simulations return. This is not such a bad idea as it might seem, though it depends upon the particular algorithmic change one wants to achieve. This approach is perfectly respectable as one can worry about rigorous basis of any results later.

A myriad of possibilities exist for such an approach, but one thing must obviously apply, that is that the choices made are based on a sound understanding of turbulence and the specific context of the LB flow simulations.

For instance, as energy is of the form mv^2 , which is roughly equivalent to LB lattice summations like $\sum_i f_i c_{i\alpha} c_{i\beta}$, then all that is required is to find some two-way (balanced) mechanism for extracting some portion of this locally, dependent on local conditions and redistributing it. The mechanism can be inspired by for example the eddy viscosity hypothesis, a mixing length feature or something derived from vortex stretching ideas — so long as it is a known phenomenon of turbulence in channels.

Obviously any extracted quantity needs to go somewhere and needs to be accounted for in some way, which is where invoking additional variables might come into use. Again these could be inspired by densities (LB population based) or simple numerical values

(possibly summations) depending on whether the approach is macroscopic or microscopic. With regards to the balance aspect of the new model it is probably advisable that a return mechanism is in place, though on physical grounds (dissipation) this would need to be weaker overall.

One ‘quirky’ aspect of the LB scheme really ought to be investigated is the lack of incorporation of a whole set of degrees of freedom for the lattice fluid (in particular the underlying gas particles which the Boltzmann approach models). There are no degrees of freedom for the modelled particles which are equivalent to either vibration or rotation. This is odd because such are precisely the thermal modes required.

No structure exists for the introduction of such energetic variables to the LB as far as the author is aware. But to find one might prove highly illuminating as regards LB energetics and the notion ought to be pursued.

The physical attribute of vibration and rotation surely form an excellent model around which to base an extra variable or extra LB population argument in the LB framework. Specifically the following suggestion seems appropriate for further work:

An LB style population is used to account for some energy parameter in the model. Some two-way, balanced mechanism is devised whereby densities on lattice are redistributed (slightly) in accordance with a physically inspired model. A physically more realistic LB variant is used for the core scheme — that way, if the quantities are ever calibrated and found to represent a real quantity, this may be mapped onto the LB in a way which is parametrically appropriate. The LB scheme can be chosen so as to have the desired level of thermodynamic consistency.

To date this has not been attempted in any *direct* way. Although it could be said that some more general propositions, put forward in existing papers, might result in this desired effect.

This is a well motivated and logical approach which is well in keeping with the LB basis. Various good papers utilise similar strategies to great effect, see for instance [102, 103]. However, presently, it is in a serious way inconsistent: the LBM *already has* a ‘valid’ temperature variable. The nature of this apparent conflict and its eventual resolution is a matter I read with continued interest.

6.2 Conclusions

In this work, it has been demonstrated that the lattice Boltzmann scheme is, in its present state of development, an appropriate candidate for modelling investigations on the nature and quantification of single phase turbulent flows in simple internal geometries.

It is probably fair to say that, the method developed does not yet constitute a strong *practical* alternative to its more highly refined competitors. The model is quite capable of recovering quantitatively accurate summary data for certain scenarios of interest: single phase fluids constrained by very simple geometries for instance. But in the case of highly inhomogeneous geometries or ones of any complexity, some considerable development is still required.

The limit of applicability is probably to model piecewise sections of the turbulent flow — simple portions of otherwise complex geometries. Importantly, the two dimensional scheme still needs to be modified to incorporate three dimensional characteristics before any practical utilisation is possible. To do this requires further work.

However, much new material exists in the literature, which is poised to be properly developed and implemented. When eventually this occurs and the various attributes of the scheme are used in combination, then it really will emerge as a unique and useful addition to the CFD modeller's toolkit.

Such amounts merely to a maturation of the field. Perhaps more tellingly it also amounts to a jump in the confidence and familiarity of end users who might be interested to use it.

Whilst the results generated are not in themselves of immediate *practical* use, the clear demonstration of adequacy of the model for such purposes is highly significant, as it opens a new avenue for investigation which is both extensible and readily adaptable. Adaptability of the approach has been proved herein by the incorporation of subtle but influential boundary layer effects via a law of the wall. These may further and readily be adapted to incorporate factors such as bounding surface roughness or von Neumann BCs. Extensibility is made obvious by results of an earlier chapter (3), which describes an effective implementation of a coordinate system transformation for the entire scheme, via the use of simple additive body force terms in the lattice evolution equation. Further application of the methods proposed therein would greatly enhance practical utilisation possibilities.

Some valuable applications might be modelled directly and in the shorter term, but it is likely that these will be on an ad hoc basis, perhaps even then the method will only constitute a strong contender to other established schemes where those are particularly lacking by virtue of their own peculiarities and failings.

The most obvious extensions to this work are proposed and discussed in some detail in suggestions for further work, section 6.1. What is mentioned there forms the logical basis for at least one project at PhD or post-doctorate level. Results generated by application of any of the extended schemes referred to there, importantly, *would* be of great practical

use; hence the value of our efforts.

Moving to more specific points: Consistency of the turbulence model with theoretic results and simultaneous match to experimental data has been demonstrated for all developments herein. A detailed analysis of ‘error’ terms generated by the method turned out to be unnecessary, as these can be arranged to be zero by choice of a suitably redefined lattice density.

Finally, through the studies carried out in order to make our developments, some progress has been made in clarification of appropriate directions for general advancement in the field. This is described in our concluding section of further work, where a clear foundation is provided for the opening of a whole new line of attack on the subject. It is felt that this may, in the end, prove to be the most significant aspect of the work, in that it alludes what might be the most appropriate non-continuum approach to the problem of computational modelling of practical turbulence quite generally.

6.3 Acknowledgments

- Firstly, a very warm thank-you to the project supervisors, Dr. Ian Halliday and Prof. Chris M. Care, both of the Materials Research Institute Modelling Group at Sheffield Hallam University. Their help has been invaluable in my progress and development as a physicist. Thanks also for the ‘implementation’ of some much needed humour.
- Also thanks to Dr. Alan Stevens working at the sponsors, Rolls Royce Associates; primarily for acquiring the funding in the first place, but also for many a useful discussion.
- Thanks are due to Prof. D. d’Humières for comments on the original of our second manuscript [51].
- Thanks also to authors of the ‘Princeton super-pipe’ data, who very usefully have made their data available for comparative use on the web. These are, namely M.V. Zagarola under S.A. Orszag, [153].
- Many thanks also to friends and family for the general motivational support and humour they provided.
- Finally, my greatest appreciation goes out to Deborah, who provided endless support throughout, both inspirational, motivational and financial.

Appendix A

Some mathematical technicalities

A.1 General notation and nomenclature

It is worthwhile clarifying conventions followed regarding notation herein. In the main, frequently encountered notations are employed, which should require little explanation. For the purposes of removing any ambiguities however, the following paragraphs aim to clarify any aspects which might have been taken for granted in the work, or which might otherwise cause confusion. Where non-standard notations are employed, these are explained at the time.

Starting with the basic independent variables: as is traditional, time and time interval are denoted t and Δ_t respectively; spatial components are taken, for the Cartesian frame, as x, y, z . The latter, when in vector form, is conventionally denoted bold: \mathbf{x} . In general, as is commonly seen, bold font is utilised to denote the vector form of any quantity. Here, the idea is extended to include tensor quantities, where *sans serif* fonts are utilised; e.g. tensor pressure $\mathbf{P} = P_{\alpha\beta}$.

Other coordinate systems are introduced at the time. In particular, \mathbf{r} is used in place of \mathbf{x} to denote coordinates in a general non-Cartesian frame. For the cylindrical geometry (especially of chapter 3) $\mathbf{r} \equiv (\phi, r, z)$.

Velocity, being the one variable which crops up in many contexts, is referred to by differing notations to highlight the context. From a purely fluid dynamical perspective, especially in section 2.2 where the continuum nature of a fluid particle is to be emphasised, it is referred to as \mathbf{u} , or u_α in tensor form.

Where the measured nature of the quantity is to be emphasised, however, velocity appears as the more logical \mathbf{v} (v_α in tensor form). So, with respect to the LB, where velocity is *used* (from measured values on previous time step) to calculate equilibrium densities $f_i^{(0)}$, it appears as \mathbf{v} . The only exception to this is the notation used in the section on stability and transition to turbulence. There the \mathbf{v} form is employed to draw

attention to the fact that the velocity decomposition used there ($\mathbf{v} = \mathbf{v}_0 + \mathbf{v}'$), differs fundamentally from that employed in Reynolds' analysis ($\mathbf{u} = \mathbf{U} + \tilde{\mathbf{u}}$).

Differential terms, where they appear in vector or tensor relations, are indicated by the traditional abbreviated (suffix) form as follows:

$$\partial_x X \equiv \frac{\partial X}{\partial x}. \quad (\text{A.1})$$

Here x stands for any independent variable and X any differentiable quantity.

Macroscopic *differences* in contrast, are denoted by uppercase delta, Δ . Lowercase δ , where it occurs, implies small differences; limiting differentials, however, are d for the exact derivative and ∂ for partial derivatives, as is conventional.

Uppercase delta is also used as the rank four tensor specifier, e.g. $\Delta_{\alpha\beta\gamma\delta}$, whereas the rank two tensor 'identity', $\delta_{\alpha\beta} = 1$, which is 1 for $\alpha = \beta$ and 0 for $\alpha \neq \beta$.

Simulation parameters, being discrete, are differentiated from their continuous counterparts by using equivalent uppercase characters. So (2D) simulation space is conventionally (X, Y) , with X and Y domains as follows: $0 \leq X \leq L$, where L is along channel length, and $0 \leq Y \leq W$, W being the channel width. Note that r might be supposed to vary $0 \leq r \leq R$, but when mapped to or congruent to a simulation domain, it is convenient to say r varies over $-R \leq r \leq R$, R being the pipe radius. Other channel parameters include \varnothing_h , which is the hydraulic diameter, see page 97.

Averaging processes and notations are discussed in the following sections, but it is repeated for completeness: Mean quantities are conventionally indicated in uppercase. Stochastic quantities, in the sense of relations 1 to 3 of page 261, are indicated by the tilde, e.g. \tilde{u}_α , the fluctuating component of turbulent velocity. Averages of *measured* variables (usually velocities) are denoted by the over bar, for example \bar{V} is the cross channel mean of the temporal mean velocity, the averaging in these cases is explained at the time.

Suffices, where used to simply 'tag' a variable to a particular instance, appear in standard text form. So ℓ_{mix} is the instance of length ℓ applicable to the mixing length model and so on.

Superfixes, where intended as a label and not a power, are enclosed in parentheses. Hence, for example $f_i^{(1)}$ is the first (non-equilibrium) component of the i link lattice density; not f_i to the power 1.

Following Boltzmann, f is used for densities in the *lattice* Boltzmann; in contrast to the notation n which is often seen. On the lattice, \mathbf{c}_i is used for LB link velocity vectors, which are subscripted by i to denote the link. Hence, in tensor form these appear as $c_{i\alpha}$. Such link velocities often appear as \mathbf{e}_i .

Finally, ellipses: ‘...’, are used to represent a missing sequence of like, or consistent, terms. These may occur one or more times in any expression.

A.2 General mathematical prerequisites

Particular mathematical identities and relationships which are referred to or assumed known in the text are, for convenience, simply listed:

1. Representation of sets on the real line, ‘ranges and domains’. Boundaries of ‘open’ intervals are here denoted by standard parantheses: (and); the boundaries of ‘closed’ intervals are denoted by square parantheses: [and]. This is in keeping with conventions in analysis. An open set does not actually contain its boundary, closed sets do. E.g. the interval $[0,1)$ contains 0 but not 1. Infinity, as limit of real line can never be ‘in’ a closed set, hence: $\mathcal{R} = \{x : x \in (-\infty, \infty)\}$.
2. Differentiation rules: chain, product and inverses (e.g. integration by parts). Where $X(x)$ and $Y(x)$ for all x :

Product rule:

$$\partial_x XY = X \partial_x Y + Y \partial_x X. \quad (\text{A.2})$$

Chain rule:

$$\partial_x X(Y) = X \partial_X Y + Y \partial_x Y. \quad (\text{A.3})$$

Inverse of product rule

$$X \partial_x Y = Y \partial_x X - \partial_x XY, \quad (\text{A.4})$$

which, for generally well behaved integration, gives integration by parts formula:

$$\int_b^a X \partial_x Y dx = \int_b^a Y \partial_x X dx - [XY]_b^a, \quad (\text{A.5})$$

by integrating both sides (with respect to x).

3. Taylor expansion (various ways of expressing).

Basis:

$$f(x + \Delta x) = f(x) + \frac{\Delta x}{1!} \partial_x f + \frac{\Delta x^2}{2!} \partial_x^2 f + \frac{\Delta x^3}{3!} \partial_x^3 f + \dots \quad (\text{A.6})$$

Vector:

$$\mathbf{f}(\mathbf{x} + \Delta \mathbf{x}, t + \Delta t) = \mathbf{f}(\mathbf{x}, t) + \frac{1}{1!} (\nabla + \partial_t) \mathbf{f} + \frac{1}{2!} (\nabla + \partial_t)^2 \mathbf{f} + \frac{1}{3!} (\nabla + \partial_t)^3 \mathbf{f} + \dots, \quad (\text{A.7})$$

4. The infinitesimal volume element in the product space $d\mathbf{p}d\mathbf{q}$ is.

$$\begin{aligned} (p_x^{(1)}, p_x^{(1)} + dp_x^{(1)}) \times (p_y^{(1)}, p_y^{(1)} + dp_y^{(1)}) \times (p_z^{(1)}, p_z^{(1)} + dp_z^{(1)}) \times (q_x^{(1)}, q_x^{(1)} + dq_x^{(1)}) \times \\ \dots \times (p_x^{(2)}, p_x^{(2)} + dp_x^{(2)}) \times \\ \dots \times (p_\alpha^{(n)}, p_\alpha^{(n)} + dp_\alpha^{(n)}) \times (q_\alpha^{(n)}, q_\alpha^{(n)} + dq_\alpha^{(n)}) \times \\ \dots \times (q_z^{(N)}, q_z^{(N)} + dq_z^{(N)}) \end{aligned} \quad (\text{A.8})$$

5. Note that the particular way in which the phase space is created leads to differing mathematical notations. It may be decided to talk in terms of $N \times 6$ dimensional vectors and spaces, or $2 \times N \times 3$ dimensional vectors and spaces. Individual coordinates (i.e. ‘parts’ of the product) are often separated hierarchically, employing commas then semicolons in order of precedence. Alternatively it might be decided that the precedence is merely notational — in that case just commas are used. The distinction between each is practically irrelevant; for this reason the notation herein makes no attempt to reflect the detailed nature of the product space, hence the use of commas only.

6. Vector differential operators in Γ -space.

Phase space is often denoted by Γ and the point within it variously by, for instance, (\mathbf{p}, \mathbf{q}) in the momentum-position formalism. This is a condensed ‘vector-style’ notation; the bold type is used to highlight the two $3N$ dimensional sub-space vectors. Such generalised notation is fine until one adopts consistent generalised forms for the various vector differential operators; div, grad, curl and ∇^2 etc. Some care is then due. In Γ :

$$\mathbf{div} \equiv \nabla_\Gamma \equiv \sum_{n=1}^N \left(\sum_{i=1}^3 \frac{\partial}{\partial p_i^{(n)}} + \sum_{i=1}^3 \frac{\partial}{\partial q_i^{(n)}} \right). \quad (\text{A.9})$$

7. Other forms of the Liouville equation.

The Liouville equation is, in a concise form:

$$\frac{dP}{dt} + \nabla_\Gamma \cdot (P\mathbf{u}_\Gamma) = 0. \quad (\text{A.10})$$

There exist many ways of expressing this equation, each having specific advantages and disadvantages dependent on the context; see for instance [93] for the Hamiltonian form and the Liouville operator.

For the purposes of further development here observe that additional complexity

arises in the dot product $\nabla_{\Gamma} \cdot (P\mathbf{u}_{\Gamma})$ due to the fact that the operand is a product, $P\mathbf{u}_{\Gamma}$. Under the product rule (see item 2 of A.2) this means that:

$$\nabla_{\Gamma} \cdot (P\mathbf{u}_{\Gamma}) = P\nabla_{\Gamma} \cdot \mathbf{u}_{\Gamma} + \mathbf{u}_{\Gamma} \cdot \nabla_{\Gamma} P. \quad (\text{A.11})$$

8. For the generalised form of Gauss' theorem, see texts such as Arfken [4]. No further treatment is deemed necessary here.
9. Special tensors involved in this work are: The rank two identity

$$\mathbf{I} \equiv \delta_{\alpha\beta}, \quad (\text{A.12})$$

which has components $\{\{0, 1\}, \{1, 0\}\}$.

The Levi-Civita third rank tensor:

$$\varepsilon_{\alpha\beta\gamma} = \begin{cases} 0 & \text{for } \alpha = \beta, \beta = \gamma \text{ or } \gamma = \alpha, \\ +1 & \text{for } (\alpha, \beta, \gamma) \in \{(1, 2, 3), (2, 3, 1), (3, 1, 2)\}, \\ -1 & \text{for } (\alpha, \beta, \gamma) \in \{(1, 3, 2), (3, 2, 1), (2, 1, 3)\}. \end{cases} \quad (\text{A.13})$$

Similarly, the equivalent at fourth rank:

$$\Delta_{\alpha\beta\gamma\delta} = -(\Delta)^{\alpha\beta\gamma\delta} = \begin{cases} +1 & \text{where } \alpha\beta\gamma\delta \text{ is an odd permutation of } (1, 2, 3, 4), \\ -1 & \text{where } \alpha\beta\gamma\delta \text{ is an even permutation of } (1, 2, 3, 4), \\ 0 & \text{in other cases.} \end{cases} \quad (\text{A.14})$$

These are used primarily in simplifications of terms derived during Chapman-Enskog expansions, especially on higher dimensional lattices. Mostly they reduce to a coefficient of 1 or 0 dependent on the permutation of indices α, β, γ and δ .

A.3 Averaging: notation, relations and technicalities

A.3.1 Technical aspects

Averaging is a concept intuitively understood by most people. Unfortunately this very familiarity precipitates a slight tendency toward loose thinking, even amongst those to whom data analysis is most familiar. With respect to this study, the actual notion and

procedure of averaging must be made precise; moreover, some general concepts must be clarified so that discussions, especially of latter pages, are communicated effectively. Since theoretical and experimental approaches lend themselves to differing formulations, relevant issues of both perspectives will be considered.

Notation

In the following, two ‘generic’ dependent functions are referred to; these will be denoted arbitrarily f and g . In addition, physical realisations of such are of interest, which in the current context are well exemplified by fluid velocity \mathbf{u} . All topics discussed are equally applicable to vector and tensor quantities as to the simple scalars for which they are quoted.

Firstly, the mean of a fluctuating variable will be denoted by capitalisation (uppercase); for example f has mean F . The actual mathematical operation of averaging, ‘the averaging operator’, conventionally denoted by overbars (example \bar{f}), is here denoted by angled braces, $\langle f \rangle$. This is in a way similar to the bra and ket notation of quantum mechanics. The intention is to evoke the duality between *expectation* of a random variable and, in contrast, an *observed* average; the difference being subtle for sure.

From an analytic standpoint, any fluctuating variable may be taken as consisting of a sum of a mean component and a strictly stochastic one; definitions for which are to be clarified in the following. Hence it may be said that, say f , is ‘decomposed’ as follows:

$$f = F + \tilde{f}. \tag{A.15}$$

Therein, the stochastic part is denoted by the tilde, \tilde{f} . Decompositions such as this, whilst widely utilised and of great value, are not necessarily physically accurate however; though this is largely a moot point.

Averaging procedures

From an experimental perspective averaging is a seemingly clear concept. However, just a brief discussion illuminates intricacies. For instance it is possible to average measured data over both time and space domains, for long (wide) or short (small) intervals. For averages over finite intervals, especially time, the mean derived may be a *varying* quantity (for example a ‘moving average’ varies over scales longer than the integration interval). This is at odds with the idea of a mean being somehow invariant. In some cases, especially flows, it may seem apparent that there is some sort of equivalence between temporal and spatial averages — this is suggestive of the Taylor hypothesis, (see most texts for

references).

But again, formalising this idea requires care.

From a theoretical standpoint it is common to seek limiting averages; various aspects of a problem may thus be illuminated. Such quantities are invariant; however, their practical relevance or utility is limited. It is also possible to average over ‘states’, the (usually infinite in number) possibilities that a system may occupy. This leads to the important statistical mechanical notion of ensemble average, which is utilised in sections 2.3 and 2.5.

In particular, with respect to the *velocity* of a turbulent flow, a time average may be defined as:

$$\mathbf{U}(\mathbf{x}) = \langle \mathbf{u}(\mathbf{x}, t) \rangle \equiv \lim_{\Delta t \rightarrow \infty} \frac{1}{\Delta t} \int_{t_0}^{t_0 + \Delta t} \mathbf{u}(\mathbf{x}, t) dt. \quad (\text{A.16})$$

This describes the common notion of averaging, understood from an experimental perspective. Note that practically the limit of infinite time duration, Δt , may never be achieved. However, all that is required for practical validity is that the duration be long in comparison to that of turbulent fluctuations. Hence, taking the average of a variable velocity \mathbf{u} is shown as $\langle \mathbf{u} \rangle$, and the result denoted \mathbf{U} . Most fundamental fluid dynamical variables can be treated this way. Note that variation of the mean with respect to the space of integration is possible for finite intervals; but here the taking limit removes all t variation from \mathbf{U} .

Now going back to the idea of a variable f consisting of two components, equation A.15. The above definition for \mathbf{U} , A.16, is adequate to use for F in A.15, but the fluctuation term there remains to be specified. As the difference $f - F$ between the variable value and its mean, the following are conventionally postulated of \tilde{f} :

- It is as often positive as negative; i.e. has zero mean.
- It has finite variance.
- (Often implicit, but not necessary) It is normally distributed.

In fact f is decomposed so that its mean is essentially invariant and all the variation occurs within the fluctuating component \tilde{f} , for which there is no ‘DC part’.

As a consequence the following may be taken as defining properties of the random variable:

1. $\langle \tilde{f} \rangle = 0$. The expectation of the stochastic quantity is zero, by definition. This relates to the nature of our decomposition.
2. $\langle \tilde{f} X \rangle = 0$. Expectation of the product of stochastically variable quantity with any quantity X (except, see 3 below) is zero. The fluctuations are just as often

positive as negative and therefore ‘weigh’ X to zero in the expectation operator’s integration.

3. $\langle \tilde{f}\tilde{g} \rangle \neq 0$. An important exception to the previous is where the other quantity \tilde{g} (also a stochastically variable) is in some way correlated to \tilde{f} ; then the expectation of the product is not necessarily zero. In particular, \tilde{g} may in fact be \tilde{f} again, in which case the expectation is related to the correlation of f with itself, or between its own components if a vector. The Reynolds stresses are of this form.

These will be assumed known throughout the core of the work herein.

Equation A.16 defines averaging in accordance with its primary usage herein. Whilst other methods are common in experimental investigations, data of which being cited occasionally, there is little need to go into further detail so long as the intricacies described are borne in mind.

Other averaging is utilised, in particular spatial averages of velocity over (here across) the physical flow domain:

$$V_x(Y) = \frac{1}{W} \sum_{Y=0}^{Y=W} v(Y)|_{t \rightarrow \infty}, \quad (\text{A.17})$$

but it should be clear from the context what the particulars of each involve. Spatial averages are *not* shown using bra and ket notation; to do so would be misleading. Instead the traditional device of capitalisation is employed.

Other relations

In keeping with the previous definitions for fluctuating or random variables and what is meant here by taking the expectation, it is an easy exercise to derive identities useful for analytic manipulations herein. They are based upon more fundamental relations regarding commutation, distributivity etc. of underlying operators. Especially linearity of integration (due to its summation nature), which implies linearity of differentiation operators and, in particular, linearity of the expectation operator (which is an integral). Using O to denote *any* of the above operators and X, Y any unknowns, the following fundamental relations are relevant:

1. Operator on a sum of unknowns is the sum of operators on the unknowns:

$$O[X + Y] = O[X] + O[Y]. \quad (\text{A.18})$$

2. Importantly, the operator on a product of unknowns: $O[XY]$, may not be further

reduced, except when they are ‘decomposed variables’. In which case, the operator on a product is the sum of operators on products expanded over the decomposition:

$$O[fg] = O[(F + \tilde{f})(G + \tilde{g})] = O[FG] + O[F\tilde{g}] + O[G\tilde{f}] + O[\tilde{f}\tilde{g}], \quad (\text{A.19})$$

3. Finally, as regards nested operators, operator order may be reversed:

$$O_1[O_2[X]] = O_2[O_1[X]]. \quad (\text{A.20})$$

These, along with properties of the decomposition, give rise to a summary set of ‘secondary properties’ or relations, which for emphasis are here accompanied by their meaning in words:

1. $\langle f \rangle = F$. The expectation of a varying quantity, is its average.
2. $\langle F \rangle = F$. The expectation of an averaged quantity, is the averaged quantity itself.
3. $\langle f + g \rangle = \langle f \rangle + \langle g \rangle = F + G$. The expectation of a sum of terms, is the sum of the means of the terms.
4. $\langle Fg \rangle = F\langle g \rangle = FG$. The expectation of a product of mean and fluctuating terms, is the product of the means of the terms; the mean being a mere coefficient in the averaging.
5. $\langle \int f \cdot dx \rangle = \int \langle f \rangle \cdot dx = \int F \cdot dx$. The expectation of a integral of a variable, is the integral of the mean of that variable; via property 3 above, integration in essence being summation.
6. $\langle \partial_x f \rangle = \partial_x \langle f \rangle = \partial_x F$. The expectation of a derivative of a variable, is the derivative of the mean of that variable; an equivalent and inverse to the previous.

All these are assumed known in the body of the current work.

A.3.2 Specific case of Reynolds decomposition

Notation

Here the aforementioned ‘cap-tilde’ notation is adopted for the respective components of the full velocity variable. Capitalisation of the variable name is used to denote the averaged quantity, in the usual way; e.g. \mathbf{u} becomes \mathbf{U} under the averaging of relation A.16. In contrast however, to some works on the Reynolds decomposition, the purely stochastic,

fluctuating component of velocity, as occurs superimposed on the mean, is here denoted using the tilde, $\tilde{\mathbf{u}}$. Hence the decomposition appears as follows:

$$\mathbf{u} = \mathbf{U} + \tilde{\mathbf{u}}, \quad (\text{A.21})$$

where the meaning of averaging and fluctuating components follows definitions of section A.3.1. Adoption of this slightly naive picture for the decomposition of velocity implies:

$$\langle \tilde{\mathbf{u}} \rangle = \lim_{\Delta t \rightarrow \infty} \frac{1}{\Delta t} \int_{t_0}^{t_0 + \Delta t} (\mathbf{u} - \mathbf{U}) dt \equiv 0, \quad (\text{A.22})$$

by definition. This is by the linearity of integration and properties 1 and 2 of relations section, page 262.

Note that, for readers familiar with the treatment and notation of say Tennekes and Lumley [139], some confusion may arise owing to similarities between the above and their decomposition: $\tilde{\mathbf{u}} = \mathbf{U} + \mathbf{u}$. This is unfortunate in the light of the quality of their exposition, but the differential is deemed both desirable and justified on account of current context, also since the notation is equally illustrative either way.

The Reynolds averaging in detail

Following Reynolds, the substitutions described in equations 2.60 and 2.61 of section 2.4.3, allow the full momentum equation 2.20 to be rewritten as follows

$$\begin{aligned} & \partial_t U_\alpha + \partial_t \tilde{u}_\alpha + U_\beta \partial_\beta U_\alpha + U_\beta \partial_\beta \tilde{u}_\alpha + \tilde{u}_\beta \partial_\beta U_\alpha + \tilde{u}_\beta \partial_\beta \tilde{u}_\alpha \\ = & -\frac{1}{\rho} \partial_\alpha P - \frac{1}{\rho} \partial_\alpha \tilde{p} + \nu \partial_\beta \partial_\beta U_\alpha + \nu \partial_\beta \partial_\beta \tilde{u}_\alpha. \end{aligned} \quad (\text{A.23})$$

To this, an averaging procedure along the lines of that described in section A.3.1, may be applied. Under property A.18 of the previous section of this appendix, page 262, individual terms may then be treated separately and thus reduced in the following manner.

Firstly, the expectation of the time derivative of the average velocity field may take the following values

$$\langle \partial_t U_\alpha \rangle = 0 \text{ or } \partial_t U_\alpha, \text{ dependent on averaging scale.} \quad (\text{A.24})$$

The specific case of averaging duration taken here is discussed in the following. Then for

subsequent terms:

$$\begin{aligned}
\langle \partial_t \tilde{u}_\alpha \rangle &= 0 \text{ by operator order A.20 and defining property 1} \\
\langle U_\beta \partial_\beta \tilde{u}_\alpha \rangle &= 0 \text{ by summation convention, then A.18, A.20 and property 1} \\
\langle \tilde{u}_\beta \partial_\beta U_\alpha \rangle &= 0 \text{ by summation convention and defining property 2} \\
\langle \partial_\alpha \bar{p} \rangle &= 0 \text{ by A.20 and defining property 1} \\
\langle \nu \partial_\beta \partial_\beta \tilde{u}_\alpha \rangle &= 0 \text{ by A.20 and defining property 1}
\end{aligned} \tag{A.25}$$

These give rise to an averaged equation of the form:

$$\partial_t U_\alpha + U_\beta \partial_\beta U_\alpha + \partial_\beta \langle \tilde{u}_\alpha \tilde{u}_\beta \rangle = -\frac{1}{\rho} \partial_\alpha P + \nu \partial_\beta \partial_\beta U_\alpha. \tag{A.26}$$

Note that all terms in means of equation A.23 persist. Also note that term 6 in LHS of equation A.23 must stay on account of potential correlation between \tilde{u}_β and \tilde{u}_α (defining property 3). Moreover, using incompressibility condition $\partial_\beta \tilde{u}_\beta = 0$ and the product rule in reverse, this appears as $\partial_\beta \langle \tilde{u}_\alpha \tilde{u}_\beta \rangle$ in equation A.26 before being identified as the Reynolds stress in equation 2.73.

Referring back now to A.24, this time derivative does not appear in many texts, having been identified as zero in the idealised case where the averaging duration tends to, or is equivalent to, infinite. However, it is not essential to assume this; a time long on the scale of the turbulent velocity fluctuations is all that is required for further analysis to be valid. Assuming a finite duration means the $\partial_t U_\alpha$ term persists; its inclusion is advantageous in some circumstances.

In this work the $\partial_t U_\alpha$ term is retained; see equation 2.73 of section 2.4.3. This is to reduce the behaviour described by equation A.23, to a form very similar to the standard Navier–Stokes equation, see equation 2.67. That, as is likely now apparent, being the equation that the LB scheme models. So the lattice Boltzmann, as it models averaged particle velocities, might be considered more ‘at home’ with the Reynolds averaged Navier–Stokes.

Appendix B

Other snippets of analysis

B.1 Obtaining the formula for ω_T by solution of the quadratic, equation 5.15

A brief inspection of equation 5.15:

$$\frac{1}{\omega_T^2} + \frac{1}{\omega_0} \cdot \frac{1}{\omega_T} - \kappa^2 \ell_m^2 \frac{9}{2\rho} \|\Pi_{\alpha\beta}^{(1)}\| = 0, \quad (\text{B.1})$$

substituting the following Q parameter definition

$$Q = \kappa^2 \ell_m^2 \frac{9}{2\rho} \|\Pi_{\alpha\beta}^{(1)}\|, \quad (\text{B.2})$$

reveals that it is essentially a quadratic in $1/\omega_T$:

$$\frac{1}{\omega_T^2} + \frac{1}{\omega_0} \cdot \frac{1}{\omega_T} - Q = 0. \quad (\text{B.3})$$

The solution formula for the roots of such a quadratic, adopting the traditional notation for the generic quadratic: $ax^2 + bx + c = 0$, is

$$x = \frac{-b \pm \sqrt{b^2 - 4ac}}{2a}. \quad (\text{B.4})$$

With the following specific instances of constants a , b and c : $a = 1$, $b = 1/\omega_0$ and $c = -Q$, and with $x \equiv 1/\omega_T$, we find the following:

$$\frac{1}{\omega_T} = \frac{-1/\omega_0 \pm \sqrt{1/\omega_0^2 + 4Q}}{2}. \quad (\text{B.5})$$

Taking the reciprocal and multiplying top and bottom RHS by ω_0 then gives

$$\omega_T = \frac{2\omega_0}{-1 \pm \omega_0 \sqrt{1/\omega_0^2 + 4Q}}, \quad (\text{B.6})$$

which on recalling rules for combining powers, may be manipulated as follows:

$$\begin{aligned} \omega_T &= \frac{2\omega_0}{-1 \pm \omega_0^{1/2} \omega_0^{1/2} (\omega_0^{-2} + 4Q)^{1/2}} \\ \Rightarrow \omega_T &= \frac{2\omega_0}{-1 \pm (\omega_0 \omega_0 (\omega_0^{-2} + 4Q))^{1/2}} \\ \Rightarrow \omega_T &= \frac{2\omega_0}{-1 \pm \sqrt{1 + 4\omega_0^2 Q}}, \end{aligned} \quad (\text{B.7})$$

which, taking the positive discriminant only, is equivalently:

$$\omega_T = \frac{2\omega_0}{\sqrt{1 + 4\omega_0^2 Q} - 1}. \quad (\text{B.8})$$

Finally, to rearrange this expression for ω , simply substitute into

$$\omega = 1 / \left(\frac{1}{\omega_0} + \frac{1}{\omega_T} \right), \quad (\text{B.9})$$

to give:

$$\omega = \frac{2\omega_0}{1 + \sqrt{1 + 4\omega_0^2 Q}}, \quad (\text{B.10})$$

whereupon the consequent variation of viscosity may be found from substitution into the standard D2Q9 identity for viscosity 2.114. This is discussed in more detail in the relevant section 5.4.

Equivalents to equations B.8 and B.10 above, in terms of the reciprocal relaxation parameter τ may be derived; either by solution of the equivalent quadratic, or by simple substitution. They are:

$$\tau_T = \frac{-\tau_0 + \sqrt{\tau_0^2 + 4Q}}{2} \quad (\text{B.11})$$

and

$$\tau = \frac{\tau_0 + \sqrt{\tau_0^2 + 4Q}}{2} \quad (\text{B.12})$$

which are included for their suitability for discussing viscosity in relation to relaxation parameter.

B.1.1 Gradient of the viscosity with relaxation parameter and stress

The functional dependence of viscosity on relaxation parameter and stress parameter, here taken as Q by equation 5.16, is of interest as regards finding the region of fastest variation. This information is essentially the gradient function of viscosity. For purposes of discussion, the functional form of gradient of viscosity ν is derived here.

It is possible to work in terms of both molecular relaxation parameters, ω_0 and τ_0 , however, owing to the reciprocity between ω_0 and ν it is obviously better to work with τ_0 , which is done here.

Note that viscosity is dependent on two parameters τ_0 and Q and therefore the gradient required is not so simply arrived at. For functional dependence on two variables, the total change in ν is the sum of the changes with respect to each independent variable. Using Δ to denote the changes:

$$\Delta\nu = \frac{\partial\nu}{\partial\tau_0}\Delta\tau_0 + \frac{\partial\nu}{\partial Q}\Delta Q, \quad (\text{B.13})$$

where note, the two derivative terms are *partial*. These are found the usual way. Here the form of ν is

$$\nu(\tau_0, Q) = \frac{\tau_0 - 1 + \sqrt{\tau_0^2 + 4Q}}{6}. \quad (\text{B.14})$$

as of equation 5.42, and partial derivatives are found to be as follows:

$$\left. \frac{\partial\nu(\tau_0)}{\partial\tau_0} \right|_Q = \frac{1}{6} \left(1 + \frac{\tau_0}{\sqrt{\tau_0^2 + 4Q}} \right) \quad (\text{B.15})$$

$$\left. \frac{\partial\nu(Q)}{\partial Q} \right|_{\tau_0} = \frac{1}{3\sqrt{\tau_0^2 + 4Q}}. \quad (\text{B.16})$$

Hence the required gradient function may (loosely) be written

$$\frac{d^2\nu}{d(\tau_0, Q)} = \frac{1}{6} \left(1 + \frac{\tau_0 + 2}{\sqrt{\tau_0^2 + 4Q}} \right) \quad (\text{B.17})$$

where it must be noted that this does not mean a cross derivative (in the sense of $\partial_{\tau_0, Q}$), but the full variation of viscosity as a function of both τ_0 and Q . The RHS expression is obtained as the limit of small changes is considered: $\Delta\tau_0, \Delta Q \rightarrow 0$. This loose notation for derivative with respect to two variables at once, non-rigorously indicates division through by Δ on both sides (implies $\Delta\tau_0$ and ΔQ are set equal).

Bibliography

- [1] T. Abe, *J. Comp. Phys*, **131** 241 (1997).
- [2] F.J. Alexander, S.Y. Chen, J.D. Sterling, *Phys. Rev. E*, **47** R2249 (1993).
- [3] J.D. Anderson, *Computational Fluid Dynamics*, 1995, McGraw-Hill.
- [4] G.B. Arfken and H.J. Weber, *Mathematical Methods for Physicists*, 1995, Academic Press.
- [5] V.I. Arnold, *Mathematical Methods of Classical Mechanics*, 1978, Springer-Verlag.
- [6] V.I. Arnold, V.V. Kozlov and A.I. Neishtadt, *Mathematical Aspects of Classical and Celestial Mechanics*, 1996, Springer-Verlag.
- [7] Sunday Times article, 4th August 2002; author not known.
- [8] D.J. Bell, *Mathematics of Linear and Non-Linear Systems*, 1990, Oxford.
- [9] R. Benzi, S. Succi and M. Vergassola, *Phys. Reports*, **222** 145 (1992).
- [10] P. Bhatnagar, E.P. Gross and M.K. Krook, *Phys. Rev.* **94** 511 (1954).
- [11] H. Blasius, *Mitt. Forschungsarb*, **131** 1 (1913).
- [12] H. Blasius, *Z. Math. u Phys.* **56** 1 (1908).
- [13] B.M. Boghosian and P.V. Coveney, *Int. J. Mod. Phys. C*, **9** 1231 (1998).
- [14] L. Boltzmann, *Lectures On Gas Theory* (Translated by S.G. Brush), 1995, Dover. Originally 1964 University of California Press.
- [15] J. Boussinesq, *Mém. prés. par div. savant à l'acad. sci. Paris*, **23** 46 (1877).
- [16] E. Buckingham, *Phys. Rev.* **4** 345 (1914).
- [17] C.M. Care, I. Halliday and K. Good. *J. Phys.: Condens. Matter*, **12** L665 (2000).

- [18] C. Cercignani, *Theory and Application of the Boltzmann Equation*, 1975, Scottish Academic Press.
- [19] S. Chapman and T.G. Cowling, *The Mathematical Theory Of Non-uniform Gases*, 1952, Cambridge.
- [20] S. Chen, H. Chen, D. Martinez and W.H. Matthaeus, *Phys. Rev. Lett.* **67** 3776 (1991).
- [21] H. Chen, S. Chen and W.H. Matthaeus, *Phys. Rev. A*, **45** R5339 (1992).
- [22] S. Chen, G.D. Doolen, *Ann. Rev. Fluid. Mech.* **30** 329 (1998).
- [23] S. Chen, C. Foias, D.D. Holm, E. Olson, E.S. Titi and S. Wynne, *Phys. Rev. Lett.* **81** 5338 (1998).
- [24] S. Chen, C. Foias, D.D. Holm, E. Olson, E.S. Titi and S. Wynne, *Phys. Fluids*, **11** 2343 (1999).
- [25] S. Chen, C. Foias, D.D. Holm, E. Olson, E.S. Titi and S. Wynne, *Physica D*, **133** 49 (1999).
- [26] S. Chen, D. Martinez and R. Mei, *Phys. Fluids*, **8** 2527 (1996).
- [27] H. Chen and C. Teixeira, *Comp. Phys. Comm.* **129** 21 (2000).
- [28] S. Chen, C. Teixeira and K. Molvig, *Int. J. Mod. Phys. C*, **9** 1281 (1998).
- [29] CornubertDL91pd
- [30] H. Darcy, *Recherches Experimentales Relatives au Mouvement de L'Eau dans les Tuyaux* 'Experimental Research Relating to the Movement of Water in Pipes', 1857, Mallet-Bachelier, Paris.
- [31] R.G. Deissler, *NACA TN*, 2138 (1950).
- [32] R.G. Deissler, *Trans. ASME*, **73** 101 (1951).
- [33] R.G. Deissler, *NACA TN*, 3145 (1954).
- [34] F. Donch, *V.D.I. Forschungsheft*, 282 (1926).
- [35] D. d'Humières, P. Lallemand, U. Frisch, *Europhys. Lett.* **2** 291 (1986).
- [36] T.B. Drew, E.C. Koo and W.H. McAdams, *Trans. AICHE*, **28** 56 (1932).

- [37] J.G.M. Eggels and J.A. Somers, *Int. J. Heat Fluid Flow*, **16** 357 (1995).
- [38] J.G.M. Eggels, *Int. J. Heat Fluid Flow*, **17** 307 (1996).
- [39] P. Ehrenfest and T. Ehrenfest, *The Conceptual Foundations of the Statistical Approach in Mechanics*, 1959, Cornell University Press.
- [40] www.exa.com
- [41] M. Farge, *Annu. Rev. Fluid Mech.* **24** 395 (1992).
- [42] O. Filippova, S. Succi, F. Mazzacco, C. Arrighetti, G. Bella and D. Hanel, *J. Comp. Phys*, **170** 812 (2001).
- [43] U. Frisch, D. d'Humières, B. Hasslacher, P. Lallemand, Y. Pomeau and J.P. Rivet, *Complex Systems*, **1** 649 (1987).
- [44] U. Frisch, B. Hasslacher and Y. Pomeau, *Phys. Rev. Lett.* **56** 1505 (1986).
- [45] U. Frisch, *Turbulence*, 1995, Cambridge University Press.
- [46] M.A. Gallivan, D.R. Noble, J.G. Georgiadis, R.O. Buckius, *Int. J. Num. Meth. Fluids* **25**, 249 (1997).
- [47] J.W. Gibbs, *Elementary Principles in Statistical Mechanics*, 1960, Dover.
- [48] I. Ginzbourg and P.M. Adler, *J. Phys. II*, **4** 191 (1994).
- [49] I. Ginzbourg and D. d'Humières, *J. Stat. Phys.* **84** 927 (1996).
- [50] S. Goldstein, *Proc. R. Soc. Lond. A*, **159** 473 (1937).
- [51] I. Halliday, L.A. Hammond and C.M. Care, *J. Phys. A*, **35** L1 (2002).
- [52] I. Halliday, L.A. Hammond, C.M. Care, K. Good and A. Stevens, *Phys. Rev. E*, **64** 011208 (2001).
- [53] L.A. Hammond, I. Halliday C.M. Care and A. Stevens, *J. Phys. A*, **35** 1 (2002).
- [54] L.A. Hammond. PhD Thesis. Sheffield Hallam University, 2003.
- [55] J. Hardy, Y. Pomeau, *J. Math. Phys.* **13** 1042 (1972).
- [56] J. Hardy, Y. Pomeau, O. de Pazzis, *J. Math. Phys.* **14** 1746 (1973).
- [57] J. Hardy, O. de Pazzis, Y. Pomeau, *Phys. Rev. A*, **13** 1949 (1976).

- [58] X. He and L.S. Luo, *Phys. Rev. E*, **56** 6811 (1997).
- [59] X.Y. He, Q. Zou, L.S. Luo and M. Dembo, *J. Stat. Phys.* **87** 115 (1997).
- [60] M. Hénon, *Complex Systems*, **1** 475 (1987).
- [61] F. Higuera, *Phys. Fluids*, **2** 1049 (1990).
- [62] F. Higuera and J. Jiménez, *Europhys. Lett.* **9** 663 (1989).
- [63] F. Higuera and S. Succi, *Europhys. Lett.* **8** 517 (1989).
- [64] F. Higuera S. Succi and R. Benzi, *Europhys. Lett.* **9** 345 (1989).
- [65] J.O. Hinze, *Turbulence*, 1975, McGraw-Hill.
- [66] J.O. Hirschfelder, C.F. Curtiss and R.B. Bird, *Molecular Theory of Gases and Liquids*, 1954, Wiley.
- [67] D.J. Holdych, D.R. Noble, J.G. Georgiadis and R.O. Buckius, *Submitted to J. Comp. Phys.* 2002.
- [68] S. Hou, J.D. Sterling, S. Chen and G.D. Doolen, *Fields Inst. Comm.* **6** 151 (1996).
- [69] S. Hou, Q. Zou, S. Chen, G.D. Doolen and A.C. Cogley, *J. Comp. Phys.* **118** 329 (1995).
- [70] T. Inamuro, M. Yoshino, F. Ogino, *Phys. Fluids* **7**, 2928 (1995).
- [71] L.P. Kadanoff, G.R. McNamara, G. Zanetti, *Complex Systems*, **1** 791 (1987).
- [72] I.C. Kim, *K.S.M.E. Int. J.* **14**, 84 (2000).
- [73] J.G. Knudsen and D.L. Katz, *Fluid Dynamics and Heat Transfer*, 1958, McGraw-Hill.
- [74] J.M.V.A. Koelman, *Europhys. Lett.* **15** 603 (1991).
- [75] A.N. Kolmogorov, *Dokl. Akad. Nauk SSSR*, **30** 9 (1941) (reprinted: *Proc. R. Soc. Lond. A*, **434** 9 (1991)).
- [76] A.N. Kolmogorov, *Dokl. Akad. Nauk SSSR*, **31** 538 (1941).
- [77] A.N. Kolmogorov, *Dokl. Akad. Nauk SSSR*, **32** 16 (1941) (reprinted: *Proc. R. Soc. Lond. A*, **434** 15 (1991)).

- [78] A. Koponen, M. Kataja, J. Timonen and D. Kandhai, *Int. J. Mod. Phys. C*, **9** 1505 (1998).
- [79] P. Lallemand and L.S. Luo, *Phys. Rev. E*, **61** 6546 (2000).
- [80] J. Laufer, *N.A.C.A. Rept.* 1053 (1951).
- [81] L.D. Landau and E.M. Lifschitz, *Fluid Mechanics*, 2nd ed. 1987, Pergamon, Oxford.
- [82] B.E. Launder and D.B. Spalding, *Lectures in Mathematical Models of Turbulence*, 1972, Academic Press.
- [83] LavalleeBN91pd
- [84] R.L. Liboff, *Kinetic Theory. Classical, Quantum and Relativistic Descriptions*, 1998, John Wiley and Sons.
- [85] J. Loschmidt, *Wein. Ber.* **73** 128, 366 (1876).
- [86] J. Loschmidt, *Wein. Ber.* **75** 287 (1877).
- [87] J. Loschmidt, *Wein. Ber.* **76** 209 (1877).
- [88] L.S. Luo, *J. Stat. Phys.* **88** 913 (1997).
- [89] L.S. Luo, *Phys. Rev. Lett.*, **81** 1618 (1998).
- [90] L.S. Luo, *Comp. Phys. Comm.* **129** 63 (2000).
- [91] L.S. Luo, *Phys. Rev. E*, **62** 4982 (2000).
- [92] G.R. McNamara and G. Zanetti, *Phys. Rev. Lett.* **61** 2332 (1988).
- [93] D.A. McQuarrie, *Statistical Mechanics*, 1976, Harper and Row.
- [94] W. Miller, *Phys. Rev. E*, **51** 3659 (1995).
- [95] C.B. Millikan, *Proceedings of the Fifth International Congress on Applied Mechanics (Cambridge Mass. 1938)*, 386, (1938) Wiley, New York.
- [96] L.F. Moody, *Trans. A.S.M.E.* **66** 671 (1944).
- [97] C.L.M.H. Navier, *Mém. Acad. Roy. Sci.* **6** 389 (1823).
- [98] J. Nikuradse, *V.D.I. Forschungsheft*, 289 (1929).
- [99] J. Nikuradse, *V.D.I. Forschungsheft*, 356 (1932).

- [100] D.R. Noble, S. Chen, J.G. Georgiadis and R.O. Buckius, *Phys. Fluids*, **7** 203 (1995).
- [101] S.I. Pai, *J. Appl. Mech.* **20** 109 (1953).
- [102] B.J. Palmer and D.R. Rector, *J. Comp. Phys*, **161** 1 (2000).
- [103] B.J. Palmer and D.R. Rector, *Phys. Rev. E*, **61** 5295 (2000).
- [104] P. Pavlo, G. Vahala, L. Vahala and M. Soe, *J. Comp. Phys*, **139** 79 (1998).
- [105] H. Poincaré, *Acta Math.* **13** 1 (1890).
- [106] L. Prandtl, *Z. angew. Math. u. Mech.* **1** 431 (1921)
- [107] L. Prandtl, *Z. angew. Math. u. Mech.* **5** 136 (1925). See also L. Prandtl, NACA TM 1231, (1949). Also S. Goldstein, *Modern Developments in Fluid Dynamics*, vol.1, 1938, p.205, Oxford University Press.
- [108] L. Prandtl, *Ergeb. Aerodyn. Versuchsanstalt Göttingen* 3, 1 (1927).
- [109] L. Prandtl, *Z. angew. Math. u. Mech.* **5** 136 (1930). See also L. Prandtl, NACA TM 1231, (1949). Also S. Goldstein, *Modern Developments in Fluid Dynamics*, vol.1, 1938, p.205, Oxford University Press.
- [110] L. Prandtl, *Z. Ver. deut. Ing.* **77** 105 (1933). See also L. Prandtl, NACA TM 720, (1933).
- [111] L. Prandtl, *Z. angew. Math. u. Mech.* **22** 241 (1942).
- [112] Y.H. Qian, D. d'Humières and P. Lallemand, *Europhys. Lett.* **17** 479 (1992).
- [113] Y.H. Qian and Y. Zhou, *Europhys. Lett.* **42** 359 (1998).
- [114] H. Reichardt, *NACA TM*, 1047 (1943).
- [115] O. Reynolds, *Trans. R. Soc. Lond. A*, **174** 935 (1883).
- [116] O. Reynolds, *Philosophical Transactions of the Royal Society of London, Series A*, **186** 123 (1894).
- [117] L.E. Reichl, *A Modern Course in Statistical Physics*, 1998, John Wiley & Sons.
- [118] A.J. Reynolds, *Turbulent Flows in Engineering*, 1972, Wiley.
- [119] J.P. Rivet and J.P. Boon, *Lattice Gas Hydrodynamics*, 2000, Cambridge University Press.

- [120] J.P. Rivet, M. Hénon, U. Frisch and D. d’Humières, *Europhys. Lett.* **7** 231 (1988).
- [121] D.H. Rothman, S. Zaleski, *Lattice Gas Automata*, 1997, Cambridge University Press.
- [122] W.G. Schlinger and B.H. Sage, *Ind. Eng. Chem.* **45** 2636 (1953).
- [123] M.R. Spiegel, *Vector Analysis*, 1974, McGraw-Hill.
- [124] P.A. Skordos, *Phys. Rev. E* **48**, 4823 (1993).
- [125] J. Smagorinsky, *Monthly Weather Review*, **91** 99 (1963).
- [126] M.V. Smoluchowski, *Pisma Marjana Smoluchowskiego*, 1924, Krakowie.
- [127] J.A. Somers, *Appl. Sci. Res.* **51**, 127 (1993).
- [128] J.H. Spurk, *Fluid Mechanics*, 1997, Springer.
- [129] J.D. Sterling, S. Chen, *J. Comp. Phys*, **123** 196 (1996).
- [130] G.G. Stokes, *Trans. Camb. Phil. Soc.* **8** 105 (1843).
- [131] G.G. Stokes, *Mathematical and Physical Papers by G.G. Stokes*, **1** 17 (1880), Cambridge University Press. Republished by Johnson Reprint Corporation, New York, 1966.
- [132] S. Succi, G. Amati, R. Benzi, *J. Stat. Phys.* **81** 5 (1995).
- [133] S. Succi, R. Benzi, F.J. Higuera, *Physica D*, **47** 219 (1991).
- [134] SucciFH89el TO FIX
- [135] S. Succi, *The Lattice Boltzmann Equation*, 2001, Clarendon Press.
- [136] M.R. Swift, E. Orlandini, W.R. Osborn and J.M. Yeomans, *Phys. Rev. E*, **54** 5041 (1996).
- [137] G.I. Taylor, *Philosophical Transactions of the Royal Society of London, Series A*, **215** 1 (1915).
- [138] C.M. Teixeira, *Int. J. Mod. Phys. C*, **9** 1159 (1998).
- [139] H. Tennekes and J.L. Lumley, *A First Course In Turbulence*, 1972, MIT Press.
- [140] T.H. von Kármán, *Proc. 3rd Int. Congress Appl. Mech.* Part 1, 85 (1930).

- [141] T.H. von Kármán, *Mechanische Ähnlichkeit und Turbulenz*. Math. Phys. Klasse, **58** (1930).
- [142] T.H. von Kármán, *NACA TM*, 611 (1931).
- [143] T.H. von Kármán, *J. Aeronaut. Sci.* **1** 1 (1934).
- [144] T.H. von Kármán, *Proc. R. Soc. Lond. A*, **164** 192 (1938).
- [145] T.H. von Kármán, *Trans. ASME*, **61** 705 (1939).
- [146] G. Vahala, P. Pavlo, L. Vahala and N.S. Martys, *Int. J. Mod. Phys. C*, **9** 1247 (1998).
- [147] R. Verberg and A.J.C. Ladd, *Phys. Rev. Lett.* **84** 2148 (2000).
- [148] H.K. Versteeg and W. Malalasekera, *An Introduction to Computational Fluid Dynamics*, 1995, Longman.
- [149] C. Wang, *J. Appl. Mech. A* **68** 85 (1946).
- [150] F.M. White, *Fluid Mechanics*, 1999, McGraw-Hill.
- [151] D.M. White, I. Halliday, C.M. Care and A. Stevens, *Physica D*, **129** 68 (1999).
- [152] S. Wolfram, *J. Stat. Phys.* **45** 471 (1986).
- [153] M.V. Zagarola, Ph.D. Thesis, Princeton University, June 1996.
- [154] E. Zermelo, *Ann. Physik* [3], **57** 485 (1896).
- [155] E. Zermelo, *Ann. Physik* [3], **59** 793 (1896).
- [156] E. Zermelo, *Investigations in the foundations of set theory I*, 1908, (translated in van Heijenoort, *From Frege to Gödel*, 1971, Harvard University Press.).
- [157] D.P. Ziegler, *J. Stat. Phys.* **71** 1171 (1993).
- [158] Q. Zou, S. Hou, S. Chen and G.D. Doolen, *J. Stat. Phys.* **81** 319 (1995).2
- [159] Q. Zou, X.Y. He, *Phys. Fluids* **9**, 1591 (1997).
- [160] Q. Zou, S. Hou, S. Chen and G.D. Doolen, *J. Stat. Phys.* **81**, 319 (1995).
- [161] Q. Zou, S. Hou and G.D. Doolen, *J. Stat. Phys.* **81** 319 (1995).